Anchorage of Shear Reinforcement in Prestressed Concrete Bridge Girders

A THESIS

SUBMITTED TO THE FACULTY OF

UNIVERSITY OF MINNESOTA

BY

Brian Thomas Mathys

IN PARTIAL FULFILLMENT OF THE REQUIREMENTS

FOR THE DEGREE OF

MASTER OF SCIENCE

Catherine W. French Carol K. Shield

June 2014

Acknowledgements

I would like to thank the many individuals and local companies who have invested their time, expertise, and finances into the completion of this research project. I would specifically like to thank MnDOT for sponsoring the project, ABC Coating for donating materials, Graham Construction for providing expertise, and Cretex Concrete Products for providing both materials and expertise. I would like to individually thank Paul Bergson and Rachel Gaulke for spending countless hours assisting me in the lab and ensuring I performed work safely. I would also like to thank Catherine French and Carol Shield for giving me guidance and helping me grow as a thinker and writer. I am truly grateful to have had you both as advisors.

Last, I would like to thank my friends and family for their unending support, timely advice, and for the help they have given throughout the years.

Abstract

The Minnesota Department of Transportation has typically used epoxy coated straight legged stirrups anchored in the tension zone as transverse reinforcement in prestressed concrete bridge girders. With the straight legs of the U-shaped stirrups anchored into the bottom flange of the girders, this configuration is readily placed after stressing the prestressing strands. American Concrete Institute (ACI) and American Association of State Highway and Transportation Officials (AASHTO) specifications require stirrups with bent legs that encompass the longitudinal reinforcement to properly anchor the stirrups. Such a configuration is specified to provide mechanical anchorage to the stirrup, ensuring that it will be able to develop its yield strength with a short anchorage length to resist shear within the web of the girder. AASHTO specifications for anchoring transverse reinforcement are the same for reinforced and prestressed concrete; however, in the case of prestressed concrete bridge girders, there are a number of differences that serve to enhance the anchorage of the transverse reinforcement, thereby enabling the straight bar detail. These include the precompression in the bottom flange of the girder in regions of web-shear cracking. In addition, the stirrup legs are usually embedded within a bottom flange that contains longitudinal strands outside of the stirrups. The increased concrete cover over the stirrups provided by the bottom flange and the resistance to vertical splitting cracks along the legs of the stirrups provided by the longitudinal prestressing reinforcement outside of the stirrups help to enhance the straight-legged anchorage in both regions of web-shear cracking and flexure-shear

cracking. A two-phase experimental program was conducted to investigate the anchorage of straight legged epoxy coated stirrups that included bar pullout tests performed on 13 subassemblage specimens which represented the bottom flanges of prestressed concrete girders in a number of configurations to determine the effectiveness of straight legged stirrup anchorage in developing yield strains. Additionally, four girder ends were cast with straight legged stirrup anchorage details and tested in flexure-shear and web-shear. The straight leg stirrup anchorage detail was determined to be acceptable for Minnesota Department of Transportation M and MN shaped girders as nominal shear capacities were exceeded and yield strains were measured in the stirrups prior to failure during each of the tests.

Table of Contents

List of Tables

List of Figures

1 Introduction

1.1 Background

Prestressed concrete girder design includes consideration of the shear limit state. The two types of shear failure modes considered are web-shear and flexure-shear failures. Web-shear failures typically initiate with cracking in the web region of the girders at the location of the maximum principal tensile stress near the critical section. Flexure-shear failures initiate with flexural cracks generated in the bottom flange that turn into inclined cracks as they penetrate into the web and form flexure-shear cracks in regions of high shear. The flexural cracks usually occur at discontinuities in the girder (e.g., at locations of stirrups).

Prior to cracking, principal tensile stresses in the web caused by shear forces are resisted by the tensile strength of the concrete. Following cracking, the shear resistance is provided by the concrete in the form of aggregate interlock and shear resistance in the concrete compressive zone, the vertical component of the draped prestressing steel, dowel action of the longitudinal prestressing steel, and by the transverse reinforcement (Lin and Burns 1981).

The shear resistance can also be idealized by a truss model, where vertical tensile forces are resisted by the transverse reinforcement. These forces are equilibrated by horizontal forces at the top and bottom of the stirrups, where the concrete provides the resistance to the compressive forces, and the longitudinal reinforcement provides the resistance to the tensile forces. Diagonal compressive struts in the concrete transfer the forces across the girder to the supports (AASHTO 2010).

In both of these models, the transverse reinforcement is required to be adequately anchored to achieve yield stress in the stirrups. The largest stresses in the stirrups are achieved in the vicinity of the shear cracks. Achieving the yield stress is important regardless of the crack location in the web relative to the stirrup anchorage.

Current recommended design details specify that all web reinforcement be anchored into the bottom flange with a standard hook around longitudinal reinforcement (AASHTO 2010). Such a configuration is specified to provide mechanical anchorage to the stirrup, ensuring that it will be able to develop its yield strength with a short anchorage length to resist shear within the web of the girder. Additionally, the presence of the longitudinal bar reduces crack widths at stirrup locations, helping to retain concrete confinement in the anchorage zone following flexural cracking (ACI Committee 318 1989).

MnDOT has routinely used epoxy-coated straight legged U-shaped stirrups, with the straight portion of the bar terminating in the bottom flange of the girder. When straight bars are used, reinforcement cages can be prefabricated and dropped into place within the already stressed prestressing strands on the precast bed. The use of this detail has not resulted in any known web reinforcement anchorage problems for the girders in MnDOT's bridge inventory.

The AASHTO specifications for anchoring transverse reinforcement are the same for reinforced and prestressed concrete; however, in the case of prestressed concrete bridge girders, there are a number of differences that serve to enhance the anchorage of the transverse reinforcement, thereby enabling the straight bar detail. These include the precompression in the bottom flange of the girder in regions of web-shear cracking. In addition, the stirrup legs are embedded within a bottom flange that contains longitudinal strands outside of the stirrups. The increased concrete cover over the stirrups provided by the bottom flange and the resistance to vertical splitting cracks along the legs of the stirrups provided by the longitudinal prestressing reinforcement outside of the stirrups help to enhance the straight-legged anchorage in both regions of web-shear cracking and flexure-shear cracking.

1.2 Motivation and Objectives

The shear capacity of MnDOT prestressed concrete girders has been studied in the past; however, the transverse reinforcement was not instrumented and the impact of lift hooks on capacity was not known Runzel et al. (2007). Additionally, literature regarding the development of straight-legged stirrups is limited and investigations have been primarily centered on the effects of corrosion on stirrup anchorage (Varney, et al. 2011). Due to the current lack of understanding of the anchorage of shear reinforcement in prestressed concrete bridge girders, further research was warranted.

The objective of the research documented in this report was to investigate the effectiveness of the straight legged stirrup anchorage detail which has been commonly used in MnDOT prestressed concrete bridge girders. The investigation consisted of a two-phase experimental program that included bar pullout tests on 13 subassemblage specimens that represented the anchorage of the straight-legged stirrups into the bottom flange and tests of four girder ends subjected to either web shear or flexure shear demands.

Several design specifications are referenced in this report, as the effectiveness of the straight legged anchorage is of value for both existing girders and newly constructed girders. The application and implementation of the various design specifications are explained in greater detail in the body of the report.

1.3 Literature Review

1.3.1 Development of Web Reinforcement in ACI 318

Design specifications adopted by the American Concrete Institute (ACI) as late as the 1983 (ACI 318-83) edition allowed the use of straight legged anchorage for web reinforcement as long as the straight legs were anchored in the compression region of the member. For deformed bar, U-shaped stirrups, code provision 12.13.2.2 required an embedment length on the compression side of the member of at least the full

development length or 12 in. from *d/2* where *d* is the depth to the centroid of tension reinforcement (ACI Committee 318 1983).

Requirements for anchorage of both ends of web reinforcement with a standard hook were first stated in ACI 318-89 (ACI Committee 318 1989) and continue through ACI 318-11 (ACI Committe 318 2011). In addition to the benefit of having mechanical anchorage between the stirrups and the longitudinal bars, the commentary in ACI 318-89 provided additional insight as to why a standard hook was specified for the development of web reinforcement. "A longitudinal bar within a stirrup hook limits the width of any flexural cracks, even in a tensile zone," (ACI Committee 318 1989). This statement indicated the widths of flexural cracks, which act to debond the stirrups from the concrete, were limited by longitudinal reinforcement. Thus, concrete anchorage was enhanced by hooking the web reinforcement around the longitudinal bars.

1.3.2 Development of Shear Reinforcement in AASHTO

The design specifications adopted by the American Association of State Highway and Transportation Officials (AASHTO) follows ACI 318 closely in regards to the development of shear reinforcement. The guidance provided on the development of shear reinforcement in the 1989 AASHTO Standard Design Specification with 1991 Interim, referred to as the 1989/91 AASHTO STD in this report, was equivalent to that of the provisions in ACI 318-83 which allowed straight legged stirrup anchorage in the compressive zone of a member given that proper development lengths were provided (AASHTO 1991). As is the case for current ACI design specifications, current AASHTO LRFD Bridge Design Specifications require all web reinforcement be anchored with standard hooks around longitudinal reinforcement (AASHTO 2010).

1.3.3 Anderson and Ramirez

Anderson and Ramirez (1989) investigated various stirrup configurations to determine the effect of web reinforcement details on stirrup anchorage and overall girder

behavior in non-prestressed, reinforced concrete beams. The stirrup anchorage, girder behavior, and ultimate strength of 12 reinforced concrete beams were evaluated under high shear stresses.

The primary variable between the 8x20 in. deep, rectangular specimens was the detailing of the shear stirrups. The stirrups were uncoated Grade 60 No. 3 bars. The stirrup details included U-shaped stirrups with straight legged embedment anchored in the compression flange, U shaped stirrups with hooked legged embedment, and closed rectangular hoops. The girder capacity was predicted with the guidance of ACI 318-83. The *a/d* ratios, longitudinal reinforcement ratios, and stirrup reinforcement indices were held constant in the study. The concrete strength of the specimens ranged from 4 to 6 ksi.

The stirrups were instrumented with strain gages located at mid-height of the girders in order to capture crack induced stirrup strains. Crack and strain observations from the tests showed that adequate stirrup anchorage was required to develop yield throughout the height of the stirrup due to the inclined nature of shear cracks. Thus, the use of hooked stirrup anchorage was recommended to facilitate development.

Anderson and Ramirez stated that in practice, the benefit of hooking a stirrup around a longitudinal bar is only achieved if direct contact between the bars exists. Because this was not easily achieved in construction with Grade 60 steel, the researchers believed stirrup anchorage depended primarily on the hook and effective straight anchorage length.

The stirrups with straight legs anchored in the flexural compression region failed prematurely, as the ratio of predicted to measured shear capacities only reached 0.97. It was observed that a crack crossed the stirrup above mid height, near the free end of the stirrup. This resulted in an anchorage failure and yield strains were not measured for this stirrup.

The premature failure of the specimen with straight legged stirrup anchorage led to the recommendation that this detail be avoided. It is likely, however, that the rectangular shape of the girder contributed to the loss of anchorage as the stirrup was not embedded into a flange which would help to confine the stirrup leg. An additional recommendation was to anchor the stirrup hooks into the concrete core to improve stirrup behavior.

1.3.4 Minor and Jirsa

Minor and Jirsa (1970) investigated the influence of parameters on the anchorage of bent deformed reinforcing bars cast in concrete blocks. The concrete blocks ranged from 8x12 in. to 12x16 in. and were large enough to prevent concrete splitting cracks during testing. The parameters investigated were bar diameter, bond length, bend angle, and inside bend radius. Load-slip relationships among the various anchorage details were compared. Additionally, ultimate bar stress and failure modes were recorded for each test.

Three different bar sizes were used for the pull tests including No. 5, No. 7, and No. 9 bars. Each of the bars were uncoated, Grade 60 deformed bars except for one of the No. 9 bars which had a smaller yield stress equal to 44 ksi in order to achieve a 3 in. bend radius. Bar bond length was designated as the distance from the face of the concrete to the beginning of the bar bend, or the end of the bar in the case of straight bars. The ratio of bond length to bar diameter ranged from 2.4 to 9.6 for the tests. The bend angles investigated ranged from 0 to 180 degrees with inside radius to bar diameter ratios ranging from 1.6 to 4.6.

The nominal concrete compressive strength at time of test ranged from 2.7 to 6.6 ksi; however, because concrete strength was not an intended test parameter, the results were normalized to a common compressive strength of 4.5 ksi to reduce the impact of concrete strength on load-slip relationships.

Slip measurements during testing were significantly higher for bars anchored with bends. This was due to the fact that the bent bars tended to crush the concrete on the inside of the bends, allowing them to straighten out. Additionally, the bars were pulled away from the concrete on the outside of the bends, reducing the contact surface between the developing bar and the concrete.

For the specimens detailed with No. 5 stirrups without bent anchorages, measured ultimate bar stress varied significantly in relation to bond length. The tests for the specimens with 6 in. bond lengths were terminated prior to failure due to stresses exceeding 80 ksi being measured. The average ultimate stresses measured for specimens with bond lengths equal to 4.5, 3.0, and 1.5 in. were 64.5, 26.8, and 20 ksi, respectively. The presence of a 90 degree hook increased the ultimate stresses measured for the specimens with bond lengths equal to 4.5 and 3.0 in. by 20 and 90%, respectively (Minor and Jirsa 1970). These results show that yield stresses can be achieved in bars with straight embedment given sufficient bond length; however, a sharp decrease in the ability of the straight anchorage to develop yield stresses exists for short bond lengths. The results from the tests for No. 5 bars without bent anchorage were representative of the No. 7 and No. 9 bars tested.

The researchers presented a few key findings based on the results from this study. First, assuming equal embedment length, bars anchored with hooks had greater slip than those without, with higher measured slips correlating to greater hook angles and tighter hook radii. Second, ultimate anchorage strength was unaffected by hooked anchorage except for very short bond lengths.

1.3.5 Kuchma, Kim, Nagle, Sun, and Hawkins

Kuchma et al. (2008) studied the shear behavior of high strength concrete prestressed girders. A total of 20 tests were conducted to provide experimental evidence justifying the use of high strength concrete (HSC) in LRFD Sectional Design Models.

The 20 tests consisted of shear tests on both ends of ten 42 ft long, 73 in. deep prestressed concrete bridge girders. The primary test variables were concrete strength, maximum design shear stress, strand anchorage details, and end reinforcement detailing. An unintended test variable included in the tests was a straight legged transverse reinforcement anchorage detail.

The first two girders tested (G1 and G2) experienced a fabrication error in the transverse reinforcement which resulted in the use of straight legged stirrup anchorage rather than hooked stirrup anchors as was originally intended. The straight legged stirrup anchorage detail was similar to that commonly used in MnDOT prestressed concrete bridge girder design. None of the transverse reinforcement used in the bulb-tee girders was epoxy coated. The stirrup size and spacing for the first girder (G1) and second girder (G2) consisted of No. 4 stirrups spaced at 12 in. and No. 5 stirrups spaced at 11 in., respectively.

The stirrups located in the girder ends were each instrumented with 4 strain gages placed at different heights. Stirrup strains exceeding yield strain were measured in each of the girder end tests. The girder ends were denoted by east (E) and west (W). Most of the stirrups yielded during the G1E, G1W, and G2W tests prior to failure. During the G2E test, only some of the stirrups measured yield strains prior to failure while most other gages measured strains close to yielding under the peak load.

Ultimate shear capacities were compared to the nominal shear capacities predicted by five different design standards including the 1996 AASHTO Standard Specifications with 2002 Interim Revisions, which will be referred to as the 1996/02 AASHTO STD (AASHTO 2002). The nominal shear capacities predicted using the 1996/02 AASHTO STD were evaluated at the critical section of *h/2* from the face of the support as specified in the 1996/02 AASHTO STD. Using the predicted nominal shear capacities, the ratios of the measured and calculated shear strengths for the G1E, G1W, G2E, and G2W tests

were 1.31, 1.30, 1.28, and 1.31, respectively. The average of the measured to calculated shear strength ratios (under guidance from the 1996/02 AASHTO STD) for all of the girder tests in the program was 1.36 with a coefficient of variation equal to 0.07. The use of straight legged stirrup anchorage details in G1 and G2 showed no clear signs of reducing girder capacity in comparison to the girders fabricated with hooked stirrup anchorage details (Kuchma, et al. 2008).

There were differences between the transverse reinforcement used in the first two girders tested by Kuchma et al. (2008) and MnDOT standard practice. The differences included the use of black bars rather than epoxy coated bars, bar size (use of No. 5 bars in G2 rather than No. 4 bars, as was used in G1 and in MnDOT girders), and anchorage depth. Development lengths for epoxy coated bars are longer than those for the same size black bar. The No. 5 bars in G2 would be expected to require additional development length when compared to smaller sized bars. The anchorage depth, which appeared to be 8-½ in. for the girders tested by Kuchma et al., was based on a stirrup length of 68 in., a section height of 63 in., a projection of the stirrup out of the top flange of 7 in., and a bottom flange height of 10-½ in. Typical nominal anchorage depths used in MnDOT bridge girders were 8 and 10 in. for MnDOT M- and MN-shaped girders, respectively, though acceptable fabrication tolerances can reduce the as-built anchorage depths in these MnDOT sections to 6-¾ and 8-¾ in., respectively. Although some design variables affecting stirrup anchorage used in the girders studied by Kuchma et al. (2008) varied from typical details used in MnDOT girder design, it was clear that anchoring straight-legged stirrups in the bottom flange within prestressed longitudinal strands can result in acceptable anchorage conditions.

1.3.6 Varney, Brown, Bayrak, and Poston

Varney et al. (2011) investigated the shear capacity of four ends of two reinforced concrete beams with “improperly” anchored stirrups. The girders were 16 ft. long with a 13x24 in. cross section. Transverse reinforcement included three legged stirrups. Two of

the stirrup legs were provided by rectangular closed stirrups and the third stirrup leg was provided by a single vertical stirrup located in the middle of the cross section. Each of the four girder ends had different anchorage details which included properly anchored stirrups, "improperly" anchored middle stirrups (i.e. the bar was not hooked around the longitudinal bar in the tension face), and two details with reduced longitudinal reinforcement in the corners of the transverse reinforcement stirrups; one of which used No. 3 corner bars rather than No. 10 bars and the other detail did not include any corner longitudinal bars.

The transverse reinforcement in each of the girders consisted of No. 3 bars spaced at 10 in. The stirrups were not epoxy coated and had a 1 in. clear cover on all sides. Strain gages were attached at mid-height of all three stirrup legs at three stirrup locations near the middle of the shear spans.

The report only included strain gage measurements for the middle stirrup leg without hooks during the second girder test at one stirrup location. All three gages measured yielding prior to failure.

The shear capacities predicted with measured material properties for the girders using the ACI 318-08 simplified method, ACI 318-08 detailed method, 2007 AASHTO LRFD Bridge Design Specifications with 2008 Interim Revisions, and the 2007 AASHTO LRFD Bridge Design Specification were 79.2, 96.6, 100.2, and 92.5 kip with ratios of V_c to V_s equal to 0.71, 1.08, 0.58, and 0.54, respectively. The measured applied shear at failure for the control, unanchored center leg, reduced corner bar area, and no corner bar girder ends were 130, 125, 128, and 149 kip, respectively. The observed shear capacities exceeded the nominal shear capacities in each of the girder end tests (Varney, et al. 2011).

There were many differences between the girder ends and transverse reinforcement details in this study and typical MnDOT prestressed concrete bridge

girders. Those differences include girder shape (rectangular rather than flanged shape), the use of black bars rather than epoxy coated bars, hooked stirrup anchorage rather than straight legged anchorage, bar size (No.3 rather than No. 4 stirrups), and the sections in the study were not prestressed. The presence of the flange and prestress in MnDOT prestressed concrete bridge girders likely improves the anchorage between the transverse reinforcement and the concrete. In addition, MnDOT sections have the stirrups anchored within longitudinal prestressed reinforcement that likely improves the anchorage condition of the MnDOT configuration.

1.3.7 Regan and Kennedy Reid

Regan and Kennedy Reid (2004) investigated the effect of corrosion on stirrup anchorage by replacing up to 75% of the shear reinforcement in the beams with straight legged stirrups. Four of the girders were tested with deformed mild steel bars for the transverse reinforcement. Each of these girders were approximately 118 in. long with 5x15-¾ in. cross sections. The main variable between different girders tested was the number of closed stirrups replaced with straight bars representing corroded stirrups.

The transverse reinforcement in the girder tests consisted of deformed bars with up to 75% of the closed hoops replaced by bars without end anchorages. The girders were designed using the British Highways Agency's 1995 code (BD) in order to have slightly higher shear capacity than flexural capacity for a girder fabricated with properly anchored stirrups across the entire span length. The ultimate shear capacity measured varied by only 1% between girders tested with 0, 50, and 75% of the closed hoop stirrups replaced with straight bars. Flexural failures controlled in each of the tests with deformed bar stirrups (Regan and Kennedy Reid 2004).

Excluding girder shape, size, and the use of prestressing steel, the main differences between the girders investigated by the researchers in this study and bridge girders typically designed by MnDOT were the bar sizes (No. 2 rather than No. 4) and the

use of black bars rather than epoxy coated bars. The expected development length of stirrups used in this study was shorter than for typical MnDOT girder reinforcement, as the bars in this study were uncoated No. 2 deformed bars.

2 Subassemblage Tests

2.1 Introduction

Subassemblage tests that replicated the anchorage of stirrups in the bottom flange of prestressed concrete girders were used to quickly examine the effect of embedment length, flange shape, concrete compressive strength, presence/absence of confinement steel, and level of prestress on stirrup anchorage. This chapter presents the design, fabrication, testing and results from the thirteen subassemblage tests.

2.2 Test Specimen Design

Because of the large number of variables that may affect the anchorage of straight legged stirrups, a simple test was needed to determine the most important parameters. The critical location for stirrup anchorage was at the bottom flange-web intersection, the lowest point in the girder web that can experience shear cracking. If a stirrup is crossed by a crack at this location, the anchorage length below that point is the shortest anchorage length possible that needs to be considered. To investigate this critical case, subassemblage specimens representing a portion (3 ft. 4 in. long section) of the bottom girder flange were constructed which anchored a pair of straight bars, representing the anchorage of the straight legged portion of an inverted U-shaped stirrup embedded in the bottom flange. The bars protruding from the bottom flange were subjected to pullout tests to investigate their respective anchorage conditions.

Variables included flange shape/embedment depth, nominal 28-day concrete compressive strength, applied nominal precompression, and presence/absence of confinement steel at the location of the stirrup. A universal testing system (i.e., 600 kip MTS Model 311 Material Test frame) was used to simulate the precompression forces in the bottom flange. Other than corner reinforcement, there was no longitudinal reinforcement in the test specimens. This was believed to be conservative, as longitudinal reinforcement could control potential splitting cracks that could develop while investigating the stirrup anchorage. The specimen length was chosen such that the

bearing of the test apparatus on the specimens would have minimal interference with the stirrup anchorage during testing. Additionally, the length of the specimens had to be short enough such that flexural cracking associated with bending would not occur in the specimens prior to stirrup yielding.

The straight legged stirrup anchorage detail has been used by MnDOT for many years, during which time design parameters, such as typical concrete strengths and design specifications, have changed. Considering this, conservative values were selected for parameters such as design 28-day concrete compressive strength, while a range of prestress levels were investigated in order to capture the extreme bounds of prestress experienced in typical MnDOT bridge girders.

Two levels of nominal 28-day concrete compressive strength were targeted for the subassemblage tests, 5 and 7.5 ksi. Higher concrete tensile strengths associated with higher concrete compressive strengths were thought to increase the bond strength. Older prestressed girders in the MnDOT bridge inventory had specified 28-day compressive strengths as low as 5 ksi. More typically these girders were cast with concrete that reached compressive strengths in excess of 6 to 7 ksi at 28 days (Dereli, et al. 2010) and likely 8 ksi after several years (Wood 1991).

Two different levels of precompression were investigated with the subassemblage test specimens. The precompression force applied by the universal testing system was chosen based on the assumption that the design 28-day compressive strength of a typical M- and MN-shaped girder was 5 and 6 ksi, respectively. Although the realized 28-day concrete strength of a MnDOT prestressed concrete bridge girder in the field is likely higher than these values, the 5 and 6 ksi strengths represented reasonable lower bounds for concrete strengths used to determine girder prestressing in design. Precompression varies along the length of the girder, from no precompression at the start of the transfer zone to full precompression at the end of the transfer zone. Precompression is also

affected at service and ultimate by the level of moment in the girders. Using the 5 and 6 ksi design concrete strengths, a minimal level of precompression equal to $0.015f_c'$ was applied to the sections representing a near zero precompression level. This precompression was obtained by applying 20 and 30 kips of precompression to the M- and MN-shaped subassemblages, respectively. Using the same nominal 28-day compressive concrete strength of 5 ksi for the M-shaped girder, a maximum precompression level of $0.45f_c'$ (575 kips) was applied to subassemblage specimens representing the upper limit for the compressive stress in the bottom compression fiber of a prestressed concrete girder at service (AASHTO 2010). The 2010 AASHTO LRFD specifications were selected to represent the greatest maximum bottom fiber compressive stress at service used by MnDOT in current girder design.

The use of confinement hoops in the bottom flange of prestressed concrete girders to surround and confine the prestressing strand was a typical design detail in MnDOT bridge girders. In older girders in the MnDOT inventory, bottom flange confining hoops were only placed at every other stirrup location, resulting in some stirrups being anchored without the presence of confinement hoops. Because there was the potential for the confining hoop to improve stirrup anchorage, the presence or absence of these confining hoops was chosen as a test parameter. Figures 2-1 and 2-2 show the confining hoop detail in the M and MN shapes, respectively. Figure 2-3 shows the locations of the confinement hoops for a typical subassemblage specimen. Confinement hoops were included at the ends of each of the specimens in order to provide support to the longitudinal steel. This placement was assumed to have a negligible impact on the test results as the hoops were located outside of the failure region. The critical confinement hoop location was at the base of the stirrup which was only included in specific specimens. This was the only longitudinal reinforcement in the test specimens.

Each of the subassemblage specimens included No. 4 Grade 60 epoxy coated bars located at the corners of the confinement hoops as show in Figure 2-1.

2.3 Fabrication of Subassemblage Specimens

The specimens were cast in three batches on October 26, 2012 and April 24, 2013 at Cretex Concrete in Elk River, MN. The first batch cast in October 2012 consisted of both M- and MN-shaped specimens with target 28-day compressive strengths between 5 and 7.5 ksi. The measured 28-day strength at 8 ksi was higher than anticipated, and at the time of testing, the strengths were as high as 9.4 ksi. To investigate a lower range of concrete strengths, additional M-shaped test specimens were cast in April 2013 in two batches with targeted concrete strengths of 5 ksi and 7.5 ksi, respectively. Concrete placement was performed by Cretex staff in order to ensure safety and quality control were maintained. Concrete cylinders were cast from each concrete batch in order to monitor concrete compressive strengths throughout the specimen tests, starting at 28 days.

2.4 Material Tests

2.4.1 Subassemblage Concrete Properties

Companion 4x8 in. concrete cylinders were used to measure the 28-day concrete compressive strengths (ASTM Standard C39 2012), the concrete compressive strengths at the time of testing, and the split tensile strengths (ASTM Standard C496 2011) of the concrete near the time of testing. The average strength of three cylinder tests were used to determine each of the aforementioned concrete properties given in Table 2-1. The table shows that the split tensile strengths of the concrete cast in October 2012 was similar to that of the 7.5 ksi target concrete cast in April 2013 (786.2 vs. 728.1 psi) whereas the split-cylinder tensile strength of the 5 ksi target strength concrete cast in April 2013 was 576.9 psi.

2.4.2 Subassemblage Reinforcement Properties

The yield strength of the straight-legged stirrups in the subassemblage specimens was 66.4 ksi, based on the average of three direct tension tests (ASTM A370). The results from the tension tests are shown in Figure 2-4.

2.5 As-built Specimen Descriptions

Figures 2-5 and 2-6 show the bottom flange subassemblage parameters tested. Specimens were named based on the concrete strength, girder shape, presence/absence of confinement, and value of precompression load. The specimen names are in the form A.AB_CC_DDDE, where A.A is the measured 28-day compressive strength (6.4, 8.2, or 8.0), B is the flange shape (M or MN), CC is the confinement indicator (WC with confinement, NC without confinement), DDD is the precompression load applied by the universal testing system in kips (020, 030, or 575), and E, when present, is the repetition indicator (A for the first test, B for the repeat test). For example, the second test of the M-shaped specimen with 8.0 ksi measured 28-day compressive strength and confinement hoops with 575 kips of compressive force applied would be named 8.0M_WC_575B. All of the tests were duplicated except for 8.2M_NC_20.

2.6 Test Configuration

During testing, each subassemblage test specimen was rotated 90 degrees, oriented with the flange in the vertical direction such that the universal testing system could apply the precompression force along the longitudinal axis of the test specimens, which would normally be applied by prestressing strands. After application of the precompression, a 77-kip actuator was used to apply the pullout tension forces to the straight legged stirrup bars protruding out of the girder flange (into what would be the web direction). The test setup for an M-shaped subassemblage specimen is shown in Figure 2-7 which was typical for all tests. Potential bending introduced into the load setup was anticipated to cause tension on the face of the specimens from which the stirrups protruded and potential splitting, and thus was considered to provide a conservative evaluation of bond.

A steel test frame was designed to minimize the shear force transfer from the test specimen to the 600 kip test machine using grouted bearing pads which were nominally 2 in. wide and ½ in. thick. The bearing pads were located to accommodate a 35 degree

concrete breakout cone between the stirrup and the center of the bearing pads for each of the subassemblage specimens. It was also likely that a failure cone would occur at the face of the bearing pads, resulting in failure cone angles of 38 degrees and 37 degrees as shown Figures 2-8 and 2-9 for the M and MN shaped subassemblages, respectively.

Shims were placed underneath the test specimens in order to level the stirrups which reduced the bending strains associated with out-of-plane loading from the 77 kip actuator. The specimens were placed in the 600 kip machine such that any stress gradient caused by eccentric application of the precompressive force would not produce an increased compressive stress near the stirrups which could artificially increase stirrup anchorage. Additionally, the compressive stress near the face of the flange (where the web would be) was further reduced due to specimen bending initiated by the applied pullout tensile force.

The 77 kip actuator was attached to the straight reinforcement extending out of the bottom flange using the assembly shown in Figure 2-10. The bars were passed through a steel plate which was bolted to the actuator head. Lenton LOCK B-Series mechanical rebar couplers specified for No. 4 bars were fastened to the ends of the stirrups which then bore against the steel plate. The locks were cut in half giving the same rebar development length as was originally intended for rebar splices. Although the couplers were fastened to reduce uneven bearing, the actuator head was also allowed to swivel in order to maintain even loading of the two stirrup legs.

The rebar couplers were tested prior to the subassemblage tests to ensure the rebar could develop ultimate stress when the coupler bolts were only tensioned to 50% of the recommended value in order to allow reuse of the couplers and ensure removal of the subassemblages without the need for cutting the stirrups.

2.7 Instrumentation

All subassemblage specimens were instrumented with stirrup strain gages, and linear variable differential transformers in order to measure strains developed in the stirrups, detect any stirrup slippage, and to monitor specimen movement due to the application of the tensile force. The first specimens were also instrumented with strain gages applied to the surface of the concrete to assess potential eccentricity of the axial precompression in the subassemblages. Figure 2-11 shows a rear view of the specimen including LVDT placement and locations of the concrete strain gages while Figure 2-12 shows plan and elevation schematics of a typical instrumentation layout for a subassemblage specimen. The instrumentation details are specified in the subsequent sections.

2.7.1 Yielding of Transverse Reinforcement

Texas Measurements FLA-3-11-5LT strain gages were applied to the straight bars protruding from the top of the flange in order to measure strains in these bars while they were pulled. An electric grinder was used to flatten the bar deformations or ribs prior to sanding the bars smooth. Subsequently, the gages were epoxied to the bar. This method resulted in a slight decrease in stirrup area concentrated at the gage locations. Each bar had two strain gages attached on opposite sides in order to measure both the axial strain and the bending strain about the horizontal axis. The strain gages were attached approximately 7 in. from the face of the concrete. The bar fractures that were observed to occur in the bar pullout tests were always observed at the location of the strain gage attachments.

2.7.2 Reinforcement Slip

Linear Variable Differential Transformers (LVDTs) were used to monitor slip of the reinforcement as shown in Figure 2-13. The displacements associated with the strain gage measurements over the gage length of the LVDTs were subtracted from the displacements measured by the LVDTs in order to determine if slip occurred between the

stirrups and the concrete face. A pair of $\pm$ 0.5 in. and a pair of $\pm$ 1.0 in. LVDTs were typically attached approximately 3 in. from the face of the specimen, one set on each stirrup leg.

2.7.3 Eccentricity of Prestressing Force

Strain gages were attached to the surface of the concrete in the longitudinal direction of six of the flange subassemblages at the nominal height of the stirrups. The gages were attached on the east and west faces of 8.0M_NC_575 and 8.0M_NC_020 and on all four faces of 8.0M_WC_575 subassemblage tests, in both the A and B duplicate specimens. The Texas Measurements PL-60-11-3LT concrete strain gages were used to investigate potential eccentricity of the applied compressive force.

2.8 Test Procedure

Prior to applying the pullout force to the stirrups, the precompression force was applied to the subassemblages by the universal testing system (i.e., 600 kip MTS Model 311 Material Test frame). A load pin was attached to the piston as shown in Figure 2-14 which allowed for rotation of the specimen during the test due to the lateral load applied by the 77 kip actuator introducing the axial tensile force to the stirrup legs. The 600 kip testing machine was controlled with an MTS FlexTest IIM Digital Controller operated in force control. The load rate for application of the precompression force was set to 190 k/min for each of the $0.45f_c$' tests and 15 k/min for the $0.015f_c$' tests. Once applied, the compressive force was held constant throughout each subassemblage tests

Tension was applied to the straight bars protruding from the flange (in the web direction) using a Model 244.40S 77 kip actuator. The 77 kip actuator was also controlled with the MTS FlexTest IIM Digital Controller set to displacement control. The displacement rate was equal to 0.025 in./min until yielding was indicated by the strain gages attached to the bars; at which point the load rate was increased to 0.10 in./min to

expedite the test conclusion. The tests were stopped once a clear pullout failure was achieved or bar fracture occurred.

2.9 Results

In all thirteen subassemblage tests performed, strain gages located on the transverse reinforcement clearly indicated strain hardening occurred, exceeding the measured yield stress by a minimum of 28%. The results of all subassemblage tests are summarized in Table 2-2. All of the M-shaped specimens with $0.015f_c$' applied nominal prestress pulled out after strain hardening was measured except for the 8.0M_WC_020B test. During this test, the stirrups began to pull out, but ultimately fractured. Each of the stirrups in the M-shaped subassemblage test specimens with $0.45f_c$' applied nominal prestress as well as the MN-shaped subassemblage test specimens with $0.015f_c$' applied nominal prestress reached the ultimate strength of the rebar and fractured during testing.

Concrete strain gages attached to the faces of six of the subassemblage specimens tested indicated only minor eccentricity of precompression force, with maximum eccentricities of 1 in., causing more compression on the flange bottom side of the specimen. Moments in this direction were thought to have the potential to reduce the effectiveness of the bond because of the decreased compression due to the eccentricity of the axial (longitudinal) compressive load and the tensile force on the bar applied by the 77 kip actuator on the face of expected splitting. There was only one test out of the first six tests instrumented in this way that indicated bending causing compression on the face of expected splitting. In this case, the measured eccentricity was -0.64 in. and thought to be insignificant. Given the low values of eccentricity measured in the first six specimens, these measurements were not made for the remainder of the specimens.

Stirrup slip was monitored visually as well as by using the measurements obtained by the LVDTs and the strain gages attached to the stirrups. Figure 2-15 shows the measured slip for the south bar during the 8.0MN_WC_030A test. This figure shows a

slip of less than 0.03 in. occurred prior to the bar yielding. The rate of measured slip began to increase dramatically at an average bar stress of 87.5 ksi until bar fracture occurred. This figure represents a typical force-slip curve measured during tests which resulted in bar fracture. Figure 2-16 shows the force-slip curve for the north bar of the 8.0M_NC_020A test which represents a typical curve measured during tests which resulted in pullout. This figure shows that a similar slip (less than 0.03 in.) occurred prior to stirrup yielding followed by an increased rate of slip until bar pullout was achieved, signaled by a drop in load as the slip continued to increase.

A typical bar stress-strain curve recorded during a subassemblage test is shown in Figure 2-17. The bar stress was calculated assuming the force from the actuator was distributed evenly between the two stirrups. The strains shown in Figure 2-17 are equal to the average of the strains measured by the gages applied to opposite sides of the stirrup. This figure shows a clear yield plateau followed by strain hardening, which was typical for all subassemblage tests.

As noted above, strain hardening was observed in all subassemblage tests prior to failure; and bar fracture was observed in seven of the 13 tests. Of the six tests which did not ultimately exhibit bar fracture, two types of pullout failures were observed: stirrup pullout following concrete splitting and concrete cone breakout. The splitting concrete failure mode was most common and was observed in the 8.2M_NC_020 (test specimen without a duplicate), 8.0M_WC_020A, and both 8.0M_NC_020 tests. The 8.0M_WC_020B test also exhibited initial concrete splitting and pullout, but ultimately bar fracture was experienced. Figure 2-18 shows the cracking pattern after completion of the 8.0M_WC_020A test. The figure shows an overview of the concrete splitting cracks which occurred prior to stirrup pullout which began at the base of the stirrup, progressed across the face of the bottom flange, and down the side of the flange as shown in Figure 2-19. These splitting cracks were expected to diminish the integrity of the stirrup anchorage and allow pullout to occur. Splitting cracks were also observed during the

8.0MN subassemblage tests as shown in Figure 2-20; however, the ultimate failure mode was stirrup fracture in both tests. The second pullout failure mode observed was a cone breakout failure. Figure 2-21 shows a cone breakout failure for the 6.4M_NC_020A failure which was observed in both of the 6.4M test specimens, though the cone size was much smaller for the second test. The failure cones were 4-½ in. deep and 2-½ in. deep for the 6.4M_NC_020A and 6.4M_NC_020B tests, respectively.

The coupler on the north stirrup slipped during testing of the 8.0M_NC_020A specimen. Figure 2-22 shows that a yield plateau and strain hardening were still measured during testing and that the slip did not occur until the average strain measured was in excess of 15,000 microstrains. Following the coupler slip, the south bar pulled out of the specimen. Figure 2-23 shows improper application of the coupler caused the slip to occur. Three bolts were used to clamp the stirrup to a ribbed sleeve inside the couplers, two pointed, and one flat tipped. The coupler which slipped was bolted with one pointed tip and two flat tip bolts, reducing the coupler capacity and allowing slip to occur.

All of the specimens that had 575 kips of precompression failed by bar fracture at the strain gage location; however, these specimens also had the highest concrete compressive strength. Figure 2-24 shows a typical stirrup fracture failure mode which occurred at the gage location during the 8.0M_WC_020B, 8.0M_NC_575, 8.0M_WC_575, and 8.0MN_WC_030 tests. Concrete splitting cracks were not observed during the testing of the 8.0M subassemblage specimens with 575 kips of precompression. The only M shaped specimen with 20 kips of applied precompression which resulted in bar fracture was the 8.0M_WC_020B. Confinement hoops were present in the specimen at the stirrup location; however, it was not clear that the presence of confinement hoops increased stirrup anchorage as the 8.0M_WC_020A test resulted in a concrete splitting failure. Significant bond deterioration at the concrete face prior to bar fracture was observed during 8.0M_WC_020B test as shown in Figure 2-25.

Regardless of the presence of prestressing strand confinement hoops, level of precompression, concrete strength, and flange shape/embedment depth, all stirrup bars yielded prior to loss of anchorage. As was expected, in general, the specimens with larger precompression, embedment depths, and concrete strengths at testing were able to develop significantly more stress than yield, failing by bar fracture. Additionally, the specimens with larger precompression did not exhibit splitting cracks prior to failure.

3 Girder Tests

3.1 Introduction

The anchorage of shear reinforcement in prestressed concrete girders was investigated by testing four girder ends in shear. The girders were designed to investigate the ability of U-stirrups to yield when the girders were subjected to large shear. The U-stirrups had straight legs anchored in the bottom flange of the girders. Both web-shear failure and flexure-shear failure modes were of interest. This chapter describes the design, fabrication, instrumentation, testing, and results of these shear tests.

3.2 Design

Two girders (four girder ends) were designed to study the anchorage of transverse reinforcement in areas of high flexure shear and high web shear. Parameters investigated included the girder section depth, anchorage depth of the stirrup legs into the bottom flange, and stirrup spacing. Girder lengths were dictated by targeting an *a/d* ratio between 2.5 and 3 for each web-shear test. A single point load was applied by the universal testing system (i.e., 600 kip MTS Model 311 Material Test frame) to the girder ends for the web-shear tests and two point loads were applied by 110 and 220 kip actuators spaced 40 in. apart to the girder end being tested in flexure-shear. Additionally, strand patterns that would allow for both girders to be cast on the same bed at the same time were favorable for economic reasons.

The shear and flexural capacities of the girders used in design were based on the 1989 AASHTO Standard Design Specification with 1991 Interim Revisions, which will be referred to as the 1989/91 AASHTO STD (AASHTO 1991). To ensure that the girder ends failed in shear and not in flexure, the flexural reinforcement was selected such that the moment capacity, assumed to be 10% less than the nominal code value, exceeded the shear capacity of the girders, assumed to be 30% higher than the nominal code specified

value, as discussed in section 3.2.5. An iterative design process was used in order to determine the number of longitudinal strands required to resist the flexural demand associated with the expected shear capacities of the girders. Subsequently, the resulting strand prestress levels were determined as detailed in section 3.2.2.

A nominal concrete compressive strength of 7.5 ksi was chosen for the girders as it represented a reasonable lower bound for girders in the MnDOT inventory. Older MnDOT girders, fabricated in the 1970s had specified 28-day nominal concrete compressive strengths of 5 ksi. Dereli et al. (2010) reported that the average increase between specified 28-day concrete compressive strength and measured 28-day concrete compressive strength for MnDOT prestressed concrete girders cast at the Elk River Plant was 38% for girders with a specified 28-day concrete strength between 4.75 and 5.25 ksi. Additionally, Wood (1991) documented a 20% increase in concrete strength over the 28-day measured strength after a period of 20 years. Thus a girder with a 5 ksi 28-day design strength could be expected to have a realized concrete strength of 6.9 ksi at 28 days and 8.2 ksi after 20 years in service.

3.2.1 Girder Sizes

Girder shapes and depths were selected to give conservative results for investigating the anchorage of straight legged stirrups in MnDOT bridge girders. The two most common girder shapes used by MnDOT were M- and MN-shaped girders. M-shapes were selected for both girders in the study because these sections have narrower webs and shorter stirrup anchorage depths than MN shaped girders as previously described in Chapter 2.

Girder depths commonly associated with M-shaped bridge girders used by MnDOT ranged from 27 to 81 in. in increments of 9 in. In selecting the girder depths to be included in the study, it was thought that if the stirrups were spaced at the maximum spacing (i.e., where the potential shear crack would intercept one stirrup at approximately

midheight), the deeper webs in deep girders would provide greater effective anchorage lengths for stirrups crossed by shear cracks. A concern in choosing very shallow girders was that they were likely to have significantly more shear capacity than predicted by the AASHTO design equations because of the neglected concrete contribution of the flanges, which take up a relatively large portion of the cross section in shallow girders. Additionally, very shallow girders may have no stirrups cross a web-shear crack in the web because of the small web heights. If the stirrups were closely spaced, it is likely that shear cracks would cross some of the stirrups near bottom flange-web interface in both shallow and deep girders. At such locations, stirrup anchorage would be exclusively provided in the bottom flange which was independent of girder depth.

Based on these reasons, girder depths of 45 and 36 in. were chosen for the study. The 45M girder ends were used to investigate web-shear with two different stirrup spacings, 24 and 8 in., respectively. The 36M girder ends were used for a flexure-shear and a web-shear test with stirrup spacings of 18 and 8 in., respectively. A 27M prestressed girder was considered for study, but a stirrup spacing of at least 18 in. was required to fail the girder in flexure-shear and it was unlikely for a shear crack to cross a stirrup in the 27M girder web with stirrup spacing wider than 16 in.

3.2.2 Prestressing

The prestressing strands used in the girders were 0.6 in. diameter, 270 ksi, 7-wire low relaxation strands with a nominal strand area equal to 0.22 in^2. The targeted precompression level in the 45M was the maximum compressive stress limit at service of $0.4f_c'$ (AASHTO 1991). The bottom fiber compressive stress in the 36M was limited to $0.14f_c'$ at service to facilitate a flexure-shear failure. To achieve the required precompression in the girders and to avoid problems with overstressing at the hold down points, three different levels of prestress were applied to the strands. The number of strands selected for each girder was the result of an iterative design process which promoted adequate flexural capacity based on the expected applied load to initiate a shear

failure. To achieve the required flexural capacities, a total of 18 and 20 strands were required in the 36M and 45M girders, respectively. Because the two girders were cast on the same bed, some of the strands in the 45M section had to be debonded completely through the 36M girder.

A cross-sectional view of the prestressing strand layout and stress levels for the 45M girder is shown in Figure 3-1. As shown in the figure, the 20 straight strands present in the bottom flange of the 45M girder used one of two prestressing levels. The highest level of prestressing of $0.60f_{pu}$ (162 ksi) was applied to 14 of the straight strands. The lowest level of prestressing of $0.1f_{pu}$ (27 ksi) was applied to the remaining six straight strands (to lift them off the bed). Each of the six draped strands was prestressed to $0.43f_{pu}$ (116 ksi), which was limited by the hold down capacity of the prestressing bed.

Because the 36M and 45M girders were cast on the same bed, all of the prestressing strands present in the 45M girder ran through the 36M girder. In order to achieve a flexure-shear failure in the 36M, full length debonding sheaths were used to reduce the prestressing force applied to the 36M girder. Figure 3-2 shows the sheaths used to debond the strands from the girder. Duct tape was wrapped around the sheaths in order to ensure no concrete could bond with the strands. Figure 3-3 shows a cross-sectional view of the prestressing strand layout and stress levels for the 36M girder including the eight strands which were debonded the full length of the girder. The 36M had only six of the 14 prestressed strands which were stressed to $0.60f_{pu}$ (36 kip) bonded to the girder. The remaining six straight strands were stressed to $0.1f_{pu}$ and the draped strands were stressed to $0.43f_{pu}$ as mentioned above.

This procedure resulted in expected bottom fiber compressive stress levels at service in the 36M and 45M girders of $0.15f_c'$ and $0.26f_c'$, respectively. It was not possible to achieve the target $0.4f_c'$ in the 45M girder without introducing a different fourth prestress force level in the strands that were debonded in the 36M girder or

without requiring even more longitudinal steel in the 45M section, which could further complicate the fabrication process. The lower levels of bottom fiber compression stress in the sections were considered to be conservative in investigating the anchorage of the stirrups. Estimates of measured concrete prestress levels at time of test are discussed in Section 3.6.4.

The heights of the draped strands at the girder ends and hold down points were controlled independently in each girder. Figure 3-4 shows that the nominal heights of the draped strand centroids for the 45M and 36M girders were 40 in. and 29 in. at the girder ends and 7 in. and 5 in. at the hold down points, respectively. The hold down points were nominally spaced 4 ft. apart and centered on both girders. With the given prestressing strand layout, Table 3-1 summarizes the prestressing steel centroids for the draped and straight strands of the 45M and 36M prestressed concrete girders.

3.2.3 Transverse Reinforcement

Stirrup spacing was the primary parameter varied among the four girder ends. The stirrups were No.4 epoxy-coated Grade 60, inverted U-shaped bars with straight legs embedded into the bottom flange of the girder. This reinforcement detail is designated as G1302E in accordance with the naming convention used by MnDOT, where the "13" stands for the bar diameter in metric units and the "E" stands for epoxy-coated reinforcement. The other mild reinforcement details and their designations in accordance with MnDOT convention are given in Appendix A. The G1302E stirrups were spaced such that one end of the 45M girder had 6 spaces at 24 in. and 36 spaces at 8 in. on the other end. The 36M girder had 23 G1302E stirrups spaced at 6 in. followed by 6 spaces at 18 in. on the flexure-shear end. The 6 in. stirrup spacing provided near the support of the flexure-shear end was intended to prevent a web-shear failure from occurring prior to a flexure-shear failure at that end. The web-shear end of the 36M girder had 15 G1302E stirrups spaced at 8 in. followed by 20 spaces at 6 in.

Girder ends were named using their depth and shape name followed by the stirrup spacing and type of shear test (i.e., F for flexure shear and W for web shear) such that the web-shear tested end of the 45M girder with 24 in. stirrup spacing would be called 45M_24W. Figures 3-5 to 3-8 show the stirrup layouts for the 45M_24W, 45M_8W, 36M_18F, and 36M_8W, respectively. These figures show the size and spacing of the primary transverse shear reinforcement which included G1605E and G1608E (No. 5) stirrups at the girder ends to protect the concrete from bursting due to the high prestressing forces and G1302E stirrups throughout the rest of the girder as the primary shear reinforcement. Lift hooks were purposely excluded from the girders, as their contribution to shear capacity would be unknown. Figure 3-9 shows a cross-sectional view of the prestressing confinement reinforcement for the 45M girder which was typical for M-shaped prestressed girders. The G1607E prestressing strand confinement hoops were placed at each stirrup within a distance of 1.5 times the girder depth from the end and G1303E confinement hoops were placed in the bottom flange at every other stirrup with a maximum spacing of 24 in.

Because the lowest tips of the shear cracks in the webs were expected to reach the bottom flange-web interface, the stirrup leg anchorage depth was assumed to be the distance between the bottom flange-web interface and the bottom of the stirrup leg. Two different anchorage depths were chosen to investigate their impact on the ability of the stirrups to achieve yield strains. One anchorage depth was based on a 3 in. nominal clear distance between the bottom of the flange and the bottom of the stirrup, which was typical of current M-shaped girder designs, and one anchorage depth represented the worst case anchorage depth within acceptable fabrication tolerances. Figure 3-10 shows the nominal dimensions of a 45M prestressed concrete girder including typical fabrication tolerances for the stirrup length, girder height, and stirrup projection from the top flange. The worst case tolerance for bar fabrication for the out-to-out stirrup length is given by ACI 315 and the CRSI Manual of Standard Practice as minus ½ in. The worst

case tolerance for the girder height and stirrup projection is plus ½ in. and ¼ in., respectively. The anchorage depths were investigated by shortening one of the stirrup legs by 1-¼ in. to account for worst case tolerances giving an anchorage depth of 6-¾ in. and 8 in. for the short and long stirrup legs, respectively, as shown in Figure 3-11.

3.2.4 Girder Deck

A concrete deck designed assuming a 28-day concrete compressive strength of 4300 psi was cast compositely on each girder in order to anchor the tops of the stirrups as well as provide a smooth surface to apply point loads. The deck width was designed narrower than the flange width to facilitate girder construction, as the forms could rest on the edge of the girder flanges. The total concrete thickness over the girders was 9 in. which included an 8 in. thick deck with a 1 in. thick stool. The reinforcement layout of a 9 in. thick deck is shown in Figure 3-12 which shows the typical cover distances for a deck system with no wearing course. In the figure, the midspan top and bottom primary reinforcement cover distances were taken as 3 in. and 1 in., respectively. This scheme led to a clear distance from the bottom layer of deck reinforcement to the top girder flange of 2 in. to account for the 1 in. clear cover, as shown in the figure, and the 1 in. deck stool. The bar size and spacing for the shrinkage and temperature reinforcement and primary (transverse) reinforcement was selected using the guidance of Table 3-2 which gives standard deck reinforcement layouts based on girder spacing and deck thickness. For the purpose of using the MnDOT design table to provide a reasonable amount of steel in the decks of the test girders, the assumptions of no wearing course, a girder spacing of 8.5 ft., and a deck thickness of 9 in. were used, as 9 in. was the minimum deck thickness available in the tables.

A cross-sectional view of the final deck geometry and reinforcement is shown in Figure 3-13. The nominal width of the 9 in. thick slab (8 in. deck plus 1 in. stool) was 28-½ in. The figure also shows the shrinkage and temperature steel and primary reinforcement used in the deck. The primary (transverse) reinforcement was epoxy coated

No. 4 bar spaced at 5 in. and 6 in. for the top and bottom mats, respectively. The longitudinal steel in the top mat consisted of two No. 4 bars spaced at 18 in. and the bottom mat used three No. 5 bars spaced at 10 in.

3.2.5 Girder Capacities

In order to ensure a shear failure would precede a flexural failure in the tests, the flexural capacity, reduced by 10%, was required to exceed the nominal shear capacity amplified by 30%. The 10% reduction in flexural capacity accounted for an undercapacity factor of 0.9. The 30% increase in shear capacity was based on the findings of Hawkins, et al. (2005), who found in the tests of 64 reinforced concrete girders and 83 prestressed concrete girders, that the web shear capacity was typically 30% greater than the capacity predicted by the 1996/02 AASHTO STD. The shear design provisions presented in the 1996/02 AASHTO STD were nearly identical to those in the 1989/91 AASHTO STD, resulting in a similar expected increase in web-shear capacity.

Nominal capacities were calculated using the 1989/91 AASHTO STD; however, a more refined design (i.e., strain compatibility) was required to determine moment capacity as a consequence of the relatively high number of strands required to promote a shear failure and the low levels of prestress required to initiate a flexure-shear failure.

The nominal shear capacities were based on the contributions of concrete, prestressing strand, and transverse reinforcement. The concrete contribution was determined as the minimum of V_{cw} and V_{ci} which represented the web-shear and flexure-shear capacities of the concrete, respectively. The shear resistance due to the prestressing strand was included in the concrete shear strength equations in the 1989/91 AASHTO STD. The contribution from the transverse reinforcement was determined assuming shear cracks occurred at 45 degrees. This assumption was conservative as the prestressing force typically produces shear cracks at shallower angles. All stirrups expected to cross shear cracks were assumed to be sufficiently anchored to yield.

The nominal shear capacities increased by 30% (i.e., $1.3V_n$), and applied shears required to reach those capacities at the critical sections of 36M_18F, 45M_24W, 45M_8W, and 36M_8W tests are shown in Figures 3-14 through 3-17. The critical sections for the web-shear failures were taken at $h/2$ from the face of the supports as recommended by the 1989/91 AASHTO STD. In the case of the flexure-shear failure identified in Figure 3-14 for the 36M_18F test, the critical section was assumed to be at Stirrup #22, which was the last stirrup spaced at 6 in. in the flexure-shear controlled region of the girder. The shear failure capacity was assumed at this location as it had the highest flexure-shear capacity in the failure region which ensured adequate testing capacity. Figure 3-14 also shows the shear capacity was increased with the tight 6 in. stirrup spacing near the reaction, which promoted the shear failure in the flexure-shear controlled region of the girder.

The nominal moment capacities were predicted following the 1989/91 AASHTO STD with recommendations from the Precast/Prestressed Concrete Bridge Design Manual (1997). The PCI manual was used for guidance on calculating prestressing strand stresses due to the fact that the simplifications given in the 1989/91 AASHTO STD were not permitted for prestress levels lower than $0.5f_{pu}$. Strain compatibility was assumed in predicting the nominal moment capacities for each of the girders as summarized in Table 3-3. The table shows comparisons between the reduced nominal moment capacities (i.e., $0.9M_n$) and the expected ultimate moment (i.e., termed "M_u") for each of the girder tests. The ultimate moment was associated with the applied load required to cause a shear failure at the critical sections given that the nominal shear capacity was increased by 30%. The girders were designed to achieve an intended $0.9M_n/M_u$ ratio of greater than 1.0 for all four girder ends; however, a calculation error resulted in an over prediction of the girder nominal moment capacities. The correctly calculated ratios of the 36M_18F and 36M_8W girder ends fell to 0.82 and 0.98, respectively. In the case of the 45M tests, the correctly calculated nominal moment capacities were sufficient to resist the expected

moment despite the calculation error because of the additional capacity provided by the strands added to increase the bottom fiber compressive stress, resulting in $0.9M_n/M_u$ ratios of 1.56 and 1.10 for the 45M girder ends.

3.3 Fabrication

The two prestressed concrete girders were cast on the same bed at Cretex Concrete Products in Elk River, MN during August 2013. The prestressing strands were tensioned using a hydraulic jack on August 19, girder concrete was poured on August 20, and the prestressing strands were detensioned on August 22. The girders were transported to the University of Minnesota where each of the four ends were tested in the Galambos Structures Laboratory. The majority of the girder fabrication was performed by Cretex professionals in order to ensure MnDOT fabrication quality standards were met. The concrete was poured in five batches with approximately two batches placed in each girder starting with the 45M_8W girder end and finishing with the 36M_18F girder end. Figure 3-18 shows that a couple of inches of formwork on the 36M_18F end needed to be filled following the placement of the fourth batch of concrete which was filled with concrete from Batch 5.

A total of 38 4x8 in. cylinders were made with ten cylinders from Batches 1 and 3 each and nine cylinders from Batches 2 and 4 each. The cylinders were tested to obtain material properties for concrete compressive strength, split tensile strength, and modulus of elasticity. Cretex also cast 4x8 in. cylinders used to determine when the girders achieved their release strength. A total of three modulus of rupture beams were cast for the 36M girder, one came from Batch 3 and two came from Batch 4.

The 36M and 45M decks were cast in the Galambos Structures Laboratory with the help of Graham Construction on October 8 and 29, 2013, respectively. The concrete mix design used for the decks (3YHP-1) was consistent with current MnDOT standards for bridge decks. The mix had a 28-day nominal design compressive strength of 4300 psi.

Figure 3-19 shows the completed formwork and deck casting for the 45M girder. Cylinders were cast from each deck in order to determine the concrete compressive strength in each deck at the time of testing.

3.4 Instrumentation

Both girders were instrumented with strain gages on the prestressing strands and transverse reinforcement, vibrating wire strain gages embedded in the concrete, and with linear variable differential transformers (LVDTs) to capture girder deflections during testing.

3.4.1 Initial Prestressing Force

Texas Measurement FLK-1-11-5LT strain gages were attached to the prestressing strands during girder fabrication in order to measure the initial prestressing force and the losses due to elastic shortening. Figures 3-20 and 3-21 show the location of these strain gages. The gages shown in the figures were named numerically from 1 to 30 starting at the dead end of the 45M girder. Gages 1 through 5 were attached to the unstressed strands outside of the girder on the dead end prior to tensioning. After an initial prestress of 6 kips was applied to the strands required for additional flexure capacity and 4 kips for all remaining strands, the remaining gages were attached at their respective locations. These forces were enough to lift the strands off the precasting bed and untangle them. Both girders had ten gages located at midspan, two of which were attached to the draped strands. Of the remaining five gages, four of them were located outside of the 36M girder on the live end and Gage 30 was placed on a debonded strand 10 ft. from the outside face of the girder on the live end. A total of 13, five, seven, and five gages were put on the fully bonded straight strands, fully bonded draped strands, lightly prestressed straight strands, and debonded straight strands, respectively. The strain gages were monitored from tensioning through detensioning.

3.4.2 Prestress Losses

Geokon Model 4200 Series VWGs were used to monitor prestress losses due to elastic shortening, creep, and shrinkage. One vibrating wire strain gage (VWG) was placed near the resultant of the prestressing force near midspan of each of the concrete girders prior to casting. Figure 3-22 shows the VWG placement in the 36M girder which was typical for both girders. The gage was zip tied to two short pieces of No. 3 rebar which was fastened on top of the top row of straight prestressing strands. With this placement, the centroid of the VWGs was 4-¼ in. nominally from the bottom of the girder and the centroid of prestressing force was 3.3 in. and 3.6 in. from the bottom of the girder for the 36M and 45M girders, respectively. Strain and temperature readings were recorded periodically including before and after times of expected strain changes such as strand release, changes in support locations, and the concrete deck casting. The data from these gages is discussed in Section 3.6.4.

3.4.3 Stirrup Strains

A total of 102 strain gages were attached to the transverse reinforcement in the 45M prestressed concrete girder and 86 strain gages were attached to the transverse reinforcement in the 36M prestressed concrete girder. Texas Measurements FLA-3-11-5LT gages were used to measure the strains in the stirrups due to the applied load. Four gages were applied to the short stirrup leg on the 45M girder and three on the 36M girder in order to capture the distribution of strain on the stirrup legs as cracking occurred.

Certain stirrups also had a duplicate strain gage attached to the longer stirrup leg at the same height as the strain gage closest to the center of the web on the shorter stirrup leg. The duplicate strain gage allowed for strain magnitudes to be compared between stirrups with different anchorage depths. Figure 3-23 shows a cross-sectional view of the gage locations and naming conventions for the 36M and 45M prestressed concrete girders. The 45M girder used the letters A through E to represent gage locations where E was always the single gage attached to the long stirrup leg and the gages on the short

stirrup leg were labeled A through D alphabetically from the bottom to the top of the web. The letters B, M, and T, denoting bottom, middle and top, respectively, were used for gages attached to the short stirrup leg of the 36M girder. The letter S specified that a single gage was attached to the stirrup leg, whether it was the duplicate gage on the long stirrup leg or the only gage attached to the bottom of the short stirrup leg as was the case for the stirrups near the support of the 36M_18F girder spaced at 6 in. As shown in the figure, the bottom gage of the 45M girder was placed at 1 ft 5/8 in. from the bottom of the girder, nominally. The next two gages were spaced at 5 in. each followed by a 10 in. gap to the top gage. For the 36M girder, the bottom gage was located a nominal distance of 1 ft 1-¾ from the bottom of the girder and the middle and top gages were each spaced at 5 in. Figures 3-24 and 3-25 show elevation views of the 45M and 36M prestressed concrete girders, respectively, and the corresponding stirrup number. The stirrups were numbered from 1 to 22 for the 45M girder and from 1 to 40 for the 36M girder, where Stirrup 1 was near the failure end support for the first test of both girders. Using the names mentioned above, the strain gage naming convention was Girder type (i.e., 36M or 45M), Stirrup number (i.e., 1-22 for the 45M and 1-40 for the 36M), Gage location (i.e., A-E for the 45M and B, M, T, or S for the 36M) such that the gage applied to the bottom of the fifth stirrup in the 45M girder would be named 45M_5_A.

3.4.4 Girder Deflections

Girder deflections were captured by linear variable differential transformers (LVDTs) in each of the four girder tests. Half inch LVDT's were attached vertically at both ends of the girders and a 3 in. LVDT was positioned at the location of the displacement controlled actuator (i.e., the 220 kip actuator for the flexure-shear test or 600 kip MTS machine for the web-shear tests). Figures 3-26 and 3-27 show the LVDT locations for the 45M and 36M prestressed concrete girders, respectively. The instruments placed at the girder ends, as shown in the figures, were attached to the abutment face at the centerline of the girder in all tests except for at one end. Figure 3-28

shows the placement of a typical girder end LVDT. This placement allowed for a close approximation of the bearing pad deflection with a single LVDT at each girder end while eliminating errors due to any potential girder twisting during loading. Figure 3-29 shows the atypical LVDT placement used for the 36M_8W end of the 36M girder during the flexure-shear test. Because this end was supported on the back face of the abutment, two LVDTs were attached to both sides of the bottom flange of the girder at the center of bearing. The two LVDTs captured any error in displacement caused by girder twisting allowing for bearing pad deflection to be measured. This configuration was required to get accurate bearing pad deflection measurements due to the increased distance between the center of bearing and the face of the abutment in the flexure-shear test.

Figure 3-30 shows the 3 in. LVDT used to measure girder deflection at the location of the displacement-controlled actuator. This instrument was hot-glued to the girder centerline to avoid errors in measurement due to girder twist and was attached to a stand which rested on the laboratory floor.

3.5 Loading

Two different loading setups were used to test the girder ends of the 36M and 45M prestressed concrete girders; one for the flexure-shear test and another for the web-shear tests. In all tests, the girders were supported by ½ in. thick elastomeric bearing pads which rested on 1 in. thick steel plates that were grouted to the concrete abutment using ULTRACAL 30 Gypsum Cement to ensure a level bearing surface. Similarly, beams attached to the hydraulic actuator piston ends used to distribute the force across the girder were grouted to the girder decks in order to create uniform loading surfaces.

Girders were white washed and had stirrup and gage locations drawn making a grid pattern prior to testing. Figure 3-31 shows the white washing and grid pattern for the 45M_24W girder which was typical of all girders. The white wash was a lime-water mix that was brushed on the girder face. The stirrup grid lines were based on as-built stirrup

locations and the gage marks were based on the nominal gage locations. For the 36M girder, stirrup locations were located prior to deck casting and marks were transferred from the stirrup locations to the girder bottom flange, then from the bottom flange to the web. Unlike the 36M, the 45M girder deck was cast before the stirrups were located so an ultrasonic linear array device was used to non-destructively locate the stirrup locations. Once located and marked, grid lines were drawn on the 45M girder using the same procedure that was used for the 36M girder.

After the first set of tests on the 36M and 45M girders was completed, external stirrups consisting of steel sections and threaded rod were applied to the damaged girder ends to enable achieving the shear capacities during the second girder end tests. The clamps added vertical precompression and external shear reinforcement which ensured the intended girder ends failed. Figure 3-32 shows the two sets of external clamps with nominal spacing equal to the girder depth applied to the 45M_8W girder. A similar configuration was used during the 36M_8W test.

3.5.1 Flexure-Shear Test

A load frame was designed and constructed in the Galambos Structures Laboratory for the flexure-shear test of the 36M_18F girder utilizing two hydraulic actuators. The actuator positioned at midspan of the 36M_18F girder was an MTS Model 244.51 220 kip actuator. The MTS Model 244.41 110-kip actuator was located a distance of 16 ft. 6-½ in. away from the support (40 in. closer to the support than the 220 kip actuator). Figure 3-33 shows an elevation view of the 36M_18F girder. This figure shows the locations of the 110 kip and 220 kip actuators in relation to the center of bearing.

The actuators were controlled with MTS 407 Analog Controllers in a master-slave setup. The 220 kip actuator was displacement controlled and the 110 kip actuator was force controlled and slaved to the 220 kip actuator. The slaving relationship was set to ½

the 220 kip force. The 220 kip actuator displacement rate was set to 0.1 in./min. and was paused at various load points to allow crack marking.

Following the 36M_18F test, the failed girder end was cut off, which was required to reduce the weight for the crane to lift and position the composite girder and deck for the 36M_8W test. Figure 3-34 shows the cut location which removed approximately 16 ft. of the failed girder end.

3.5.2 Web-Shear Tests

Web-shear tests were performed on the 45M_24W, 45M_8W, and 36M_8W girder ends. A universal testing system (i.e., 600 kip MTS Model 311 Material Test frame) was used to apply a single point load to the girders. A load pin was attached to the piston as shown in Figure 3-35, which allowed in plane rotations to occur. In each of the tests, the 600 kip test machine was controlled with an MTS FlexTest IIM Digital Controller and was operated in displacement control during each test. The displacement rates were set to approximately 0.01 in./min. for each test. The loading was paused at various stages throughout testing for the purpose of crack marking. During the tests on the 45M girder ends, an unloading cycle was applied to determine if web-shear cracks would remain visible after the girder was unloaded. To accomplish this, the applied load was reduced to 10 kips shortly after the web-shear cracks appeared. After observations were made, the girder was reloaded and tests continued.

The elevation view of the 45M_24W girder is shown in Figure 3-36. This figure shows that the load point was applied a distance of 12 ft. 4-½ in. from the face of the girder and the span length was 36 ft. 9 in. In order to test the second end of the 45M girder, approximately 9 ft. 6 in. of the failed girder end was cut off as shown in Figure 3-37. This was required to reduce the girder and deck weight below the crane capacity. Figure 3-38 shows the elevation view of the 45M_8W. Similar to the 45M_24W test, the

load point was located 12 ft. 4-½ in. away from the face of the girder. The load locations resulted in an *a/d* ratio for each of the 45M web-shear tests of 2.5.

The loading points for the 36M_8W test are shown in Figure 3-39. This figure shows that the point load was applied 10 ft. from the face of the girder and the nominal span length for the girder was 20 ft. 6 in. This configuration led to an *a/d* ratio of 2.3.

3.6 Results

3.6.1 Girder Concrete Properties

The concrete compressive strength for the girders was measured by Cretex at release. Concrete strengths at 28 days and at time of testing were measured by the University of Minnesota in accordance with ASTM Standard C39 (2012). The results are summarized in Table 3-4. The table shows the average compressive strength of the girders at release was 4.7 ksi. This result was the average of two tests, one being from a cylinder taken from Batch 1 which measured 4.4 ksi and the other taken from Batch 4 measuring 5.0 ksi. At 28 days, a concrete compressive strength of 6.7 ksi was measured by averaging the results of three cylinder tests. This result was conservatively less than the 7.5 ksi designed compressive strength. Compressive strengths were also measured at the time of testing for the 36M_18F, 45M_24W, 45M_8W, and 36M_8W girders, resulting in concrete strengths of 6.3 ksi, 6.8 ksi, 7.0 ksi, and 6.9 ksi, respectively. Similar to the compressive tests at 28 days, each of these measurements were the result of the average strength of three cylinder tests.

Split tension tests were performed at the University of Minnesota at the time of testing for each of the girder ends in accordance with ASTM Standard C496 (2011). The results are summarized in Table 3-5. The values listed were the average strengths of three cylinder tests for each girder end.

Modulus of rupture beams were cast in order to determine the tensile strength of the concrete which was critical in predicting flexure cracking during the 36M_18F test.

The concrete from Batches 3 and 4 were used to cast the 6x6x24 in. beams and were tested at the time of the 36M_18F girder test in accordance with ASTM Standard C78 (2010). The average concrete modulus of rupture stress based on three tests was 635 psi and was used in predicting the cracking moments for both girders. This value was consistent with the 595 psi rupture strength as predicted by the 1989/91 AASHTO STD (AASHTO 1991) assuming a concrete compressive strength of 6300 psi, which was the measured compressive strength of the 36M_18F end at the time of test.

3.6.2 Deck Concrete Properties

A slump test in accordance with ASTM C143 (2012) was performed prior to casting the decks for each of the girders. A 5 in. slump was requested for both batches of concrete. Slump measurements of 7 in. and 5-½ in. were obtained for the 36M and 45M girders, respectively. These values were both higher than requested, but were deemed acceptable.

Table 3-6 shows the measured average concrete compressive strengths for the decks measured at the time of the girder end tests. The measured compressive strengths were the average of results from three cylinder tests performed at the time of each of the tests. All of the measured strengths were higher than the designed 4300 psi compressive strength. The additional compressive strength of the deck increased the likelihood of having a shear failure control over a flexure failure for each of the girder tests.

3.6.3 Reinforcement Properties

The yield strength of the transverse reinforcement of the 36M and 45M girders was essential in determining whether or not yield strains were measured during the girder end tests. Figures 3-40 and 3-41 show stress-strain curves based on the results from tension tests performed in accordance with ASTM Standard A370 (2012) on three steel specimens cut from the transverse reinforcement of the 36M and 45M girders, respectively. Each specimen was instrumented with a single strain gage attached in a

similar manner as explained in Section 2.7.1. These figures show that there was some variation in the yield stress for the 36M tests. The results from the 45M tension tests showed less variability. Table 3-7 summarizes the average yield strains and stresses for the transverse reinforcement of the girders. The average yield strain for the shear reinforcement in the 36M and 45M girders was 2700 μs and 3090 μs, respectively. The average yield stress for the shear reinforcement of the 36M and 45M girders was 70.0 ksi and 67.0 ksi, respectively.

3.6.4 Prestress Force

Two methods were available to estimate the initial tensioning force: strain gages attached to the strand prior to tensioning and the pressure sensor on the Cretex jack. The data collected from the strain gages had an extremely low signal to noise ratio, with noise in the 200 microstrain range, thus making this data unreliable. Therefore, the initial jacking force applied to each strand was based on the pressure gage on the hydraulic jack.

The naming convention used for the prestressing strands is shown in Figure 3-42 assuming a cross-sectional view from the live end of the girders. The rows of prestressing strands were labeled from 1 to 5 starting from the bottom row with the draped strands being 3, 4, and 5. The strand columns were labeled from A to L.

The initial prestress applied to each strand is summarized in Table 3-8. These values were based on the applied jacking force measured by Cretex, the nominal prestressing strand area, and an assumed seating loss of 2.8 ksi which could not be accounted for by the Cretex pressure gage. The seating loss was calculated assuming a live end slip of 3/8 in., a bed length of 3792 in., and a prestressing strand modulus of elasticity of 28,500 ksi. As indicated in the table, the final prestress levels for the strands with a designed prestress of $0.1f_{pu}$ (27 ksi) were not measured. Consequently, the final prestress level for those strands was assumed to be equal to the designed prestress level. The total initial prestress after seating was $0.46f_{pu}$ (124 ksi) for the 45M girder and $0.39f_{pu}$

(104 ksi) for the 36M girder. This was obtained by taking the total prestress force (strand stress after seating times area of the individual prestressing strand) and then dividing that total force by the total area of strand.

The change in strains at release near the center of effort of prestress were measured by the embedded vibrating wire gages. The center of prestress effort location was held constant throughout the girder lifespans as changes in location due to unequal strand prestress losses were assumed negligible. The change in strains measured by the VWGs were used to determine elastic shortening losses in both girders. The accuracy of the strain measurements were determined as follows.

The measured strain in the concrete at the level of the VWG just after release was used to calculate the effective prestress by solving Equation 3.1 for the effective prestressing force:

$$\varepsilon_{vwg} = \frac{P_{eff}}{A_n E_c} + \frac{P_{eff} e y_{vwg}}{I_n E_c} - \frac{M_{sw} y_{vwg}}{I_n E_c} \tag{3.1}$$

where P_{eff} is the effective prestress force after release, A_n is the net area of concrete, I_n is the net concrete moment of inertia, e is the eccentricity to the center of effort of the prestress force, y_{vwg} is the distance from the net section centroid to the depth of the VWG, M_{sw} is the moment due to girder self-weight at the center of the span, E_c is the modulus of elasticity of concrete, and ε_{vwg} is the strain measured by the VWG. The assumed concrete modulus of elasticity was 4050 ksi based on $33 w_c^{1.5} \sqrt{f'_{ci}}$, where the unit weight of concrete was measured as 147.3 lb/ft^3 (i.e., weight of one cylinder measured at time of test) and an average f_{ci}' of 4720 psi (i.e., 36M had a release strength of 5030 psi measured from concrete batched toward the live end and the 45M had a strength of 4400 psi measured from concrete batched toward dead end). The effective prestress force associated with this calculation was found to be larger than the initial prestress force measured by the Cretex hydraulic jack including assumed seating losses prior to transfer,

which was not feasible. Assuming the strains measured by the VWG were reasonable, the error in effective prestress force was assumed to be in the determination of the modulus of elasticity of the concrete.

The concrete moduli of elasticity required to produce the strains measured by the VWG were back-calculated using Equation 3.1 and an equation similar to Equation 3.1 for the strains at the center of effort of prestress. The resulting concrete moduli of elasticity were 3560 and 3220 ksi for the 36 and 45M girders, respectively. The concrete moduli determined through this process were 12 to 20% lower than the predicted elastic modulus based on the concrete compressive strength and unit weight of concrete used to cast the two girders. Using these back calculated moduli of elasticity in Equation 3.1 and recognizing that P_{eff} is equal to the jacking force minus the elastic shorting and relaxation, the elastic shortening losses were determined to be 10.3 and 18.9 ksi for the 36M and 45M girders, respectively.

These prestress losses are termed "measured elastic shortening" values in this study. Table 3-9 summarizes the results including the measured elastic shortening values and the associated back-calculated concrete elastic moduli required to produce those values which assumed that the initial prestress force measured by Cretex was accurate. The results were compared to expected elastic shortening losses using the PCI Committee iterative method based on net sections, assuming the Cretex measured jacking force was accurate with assumed seating and relaxation losses and a concrete elastic modulus of 4050 ksi, which corresponded to the estimated value based on the concrete unit weight and compressive strength. The elastic shortening values predicted by this method were less than those based on the back-calculated moduli (due to the stiffer modulus). In this case however, the strains did not match those measured at the level of the VWGs. The measured values of elastic shortening losses determined from the VWG measurements were deemed sufficiently accurate for the study. Summaries for the elastic shortening calculations are available in Appendix B.2.

The light prestress levels and short span lengths for the girders resulted in small cambers. The measured cambers at release were 3/16 and 5/16 in. measured to the nearest 1/16 in. for the 36M and 45M girders, respectively. Because of the large potential errors in measured cambers associated with the small measurements, the cambers could not be used to accurately relate the prestress levels at transfer.

Time dependent prestress losses were predicted using the time-step method outlined by the PCI committee (Preston 1975) at release, deck casting, and time of test. Creep, shrinkage, and strand relaxation were all predicted based on the prestressing force applied to the strands as measured by Cretex, gross girder section properties, and predicted values for concrete modulus of elasticity at release and at the time of testing as determined by the relationship of the modulus with concrete compressive strength (i.e., $33{w_c}^{1.5}\sqrt{f'_{ci}}$). Tables 3-10 and 3-11 show the predicted time dependent losses during three time steps for the 36M and 45M girders, respectively. These tables show that the steel relaxation losses were predicted to be equal to 0.5% of the initial prestress for the 36M girder and 0.6% for the 45M girder. It was assumed relaxation losses in strands stressed lower than $0.55f_{py}$ bore no practical significance and were considered negligible (Kajfasz 1958). The low level of relaxation loss seemed reasonable given the relatively low level of prestress in the strands. Sample calculations for the estimation of losses due to strand relaxation are included in Appendix B.2.

The total losses predicted by the PCI committee method due to creep and shrinkage for the 36M and 45M girders were 11.2 and 15.8 ksi, respectively, as given in Tables 3-10 and 3-11. These losses were slightly higher than those determined using the strain measurements from the VWGs used in combination with an assumed modulus of elasticity of the strand of 28,500 ksi. These losses are summarized in Tables 3-12 and 3-13 were 9.5 and 14.9 ksi, respectively. For the time dependent losses, the VWGs were assumed to be at the center of effort of the prestress. The difference in strains between the VWG and the center of effort was assumed to be negligible.

A summary of the losses used for girder capacity calculations for the 36M and 45M girders are shown in Table 3-14. Measured losses were used when available (i.e., for elastic shortening and creep and shrinkage). Predicted losses were used when measured losses were not available (i.e. for seating losses and relaxation losses). Considering the prestress force measured by Cretex, the losses summarized in the table, and the self-weight of the girders and decks, the resulting bottom fiber maximum compressive stresses for the 36M_18F and 45M_24W girders at the time of tests were $0.23f_c'$ (1.44 ksi) and $0.30f_c'$ (2.06 ksi), respectively.

3.6.5 Flexure-Shear Test Observations

The flexure-shear test was performed on the 36M_18F girder on November 6, 2013 in the Galambos Structures Laboratory at the University of Minnesota. The load-displacement curve is shown in Figure 3-43. As noted in Section 3.5.1, the 200 kip actuator was operated in displacement control, with the second actuator slaved to the first actuator through load. When the displacement was paused during the test to observe and mark damage, the load sustained by the girder at that displacement level dropped as damage progressed under displacement control. As expected, flexure cracks appeared in the bottom flange of the girder at the stirrup locations prior to shear cracking. Web-shear cracks occurred in both ends of the girder prior to failure; appearing in the failure end of the girder at a lower applied load than the web-shear cracks in the other end of the girder (because of the distance of the two supports relative to the applied loading). The shear force at the critical section in each girder end associated with web-shear crack propagation was approximately equal, as would be expected. Additional photos of the 36M_18F test are included in Appendix C.1.

Figure 3-44 shows the crack pattern associated with the maximum load applied to the 36M_18F girder. The girder reinforcement included in the figure includes prestressing strands, the transverse reinforcement, and confinement hoops. Refer to Section 3.2 for details on the location of the reinforcement. The circles in the figure

designate gage locations on the short stirrup legs, with the solid circles indicating that yield strains were measured.

Table 3-15 summarizes the maximum strains measured in Stirrups 20 through 27 during the 36M_18F test. These stirrups were selected for discussion because they were within and adjacent to the flexure-shear critical region of the girder. These data are also plotted in Figure 3-45 superimposed on the stress-strain curves obtained from rebar tension tests. The plot shows the maximum measured strains in Stirrups 23 through 26 not only exceeded yield strain, but were likely located in the strain hardening region of the stress-strain curve.

In general, smaller strains were measured in the girder region with tight stirrup spacing (Stirrups 20-22) as the larger area of transverse reinforcement crossing the shear cracks in that region required less stress to resist the shear force. Additionally, strain measurements were dependent upon crack proximity to a gage. Stirrups 20 and 22 developed yield at the web-flange interface despite the presence of flexure cracks at the stirrup locations; however, the strain gage on Stirrup 21 did not quite indicate yielding. This was likely due to the combination of less stress being required of the tightly spaced stirrups and the fact that the only gage present on Stirrup 21 was farther away from a shear crack than the gages attached to Stirrups 20 and 22, reducing the maximum strain reading. Flexural cracking in the bottom flange near Stirrups 22 through 26 did not affect the ability of the stirrups to reach yield. Additionally, yield strains were exceeded in gages located nearest to the web/flange interface when cracks intercepted stirrups near that location. The more widely spaced stirrups in the flexure-shear critical region realized the largest strains, with Stirrup 24 achieving the highest measured strain to yield strain ratio of 5.47.

Yielding was not observed in Stirrup 27 as it was located in a region of low shear between the two applied loads as shown in Figure 3-14.

3.6.6 Web-Shear Test Observations

Load-displacement curves for the web shear tests performed on the 45M_24W, 45M_8W, and 36M_8W girders on December 12, 2013, December 20, 2013, and January 6, 2014 are shown in Figures 3-46 through 3-49, respectively. The tests were operated in displacement control, so pauses in the test to observe and mark damage are typically indicated by a decrease in applied load over a constant displacement as damage continued to progress during displacement pauses. Each of the curves indicate the applied load associated with the appearance of web-shear cracks. As expected, the applied load corresponded to equivalent shear forces at web-shear crack initiation for both failure ends of the 45M girder and 36M girder. Additionally, the 45M_24W curve indicates the location of the observed cracking moment. The 36M_8W curve is not complete because the LVDT measuring displacement at the location of the applied load detached from the concrete surface during testing, as indicated in Figure 3-48; however, the displacement curve measured by the universal testing system (i.e., 600 kip MTS Model 311 Material Test frame) is superimposed on the plot to show the approximate girder deflection throughout testing. The displacement from the universal testing system is larger than that of the girder at each load level because it includes the deformation of the bearing pads and the testing frame.

Figures 3-49 to 3-51 show the crack patterns associated with maximum loading for the 45M_24W, 45M_8W, and 36M_8W girder tests respectively. As with Figure 3-44, the circles designate gage locations on the short stirrup legs, with solid circles indicating that strains in excess of the yield strain were measured. Cracking that occurred during the 36M_18F test for the 36M_8W is indicated in the figure by bold lines with the ends of residual cracks indicated by dots. The stirrup gages in the 36M_8W girder end were monitored throughout the 36M_18F test and no yielding was observed despite the propagation of web-shear cracks during the flexure-shear test. No cracking was observed in the region of interest for the 45M_8W girder during the previous test of the opposite

girder end (i.e., 45M_24W). Photos of the failure ends of the 45M_24W, 45M_8W, and 36M_8W girders taken throughout each test are included in Appendices C.2, C.3, and C.4.

Tables 3-15 to 3-18 summarize the maximum stirrup strain measurements for the instrumented stirrups in the failure regions of the 45M_24W, 45M_8W, and 36M_8W tests, respectively. Figures 3-52 to 3-54 show comparisons between the maximum measured stirrup strains and the stress-strain curves obtained from rebar tension tests for the 45M_24W, 45M_8W, and 36M_8W tests, respectively. The data show that the maximum strains measured in many of the stirrups during each test not only exceeded the yield strain, but were located in the strain hardening region of the stress-strain curves. The smallest maximum strain measurements were found in stirrups located in discontinuity or "disturbed" regions of the girders near the concentrated reactions at the supports or the applied point load locations (e.g., 45M_24W Stirrup 5; 45M_8W Stirrups 6-9 and 20-22; 36M_8W Stirrups 28-30 and 39-40). This was likely due to the effect of local compression stresses in those regions. Additionally, the primary shear cracks typically did not cross the stirrups near the load application points nor did they cross the stirrups in close proximity to gage locations near the supports as the shear cracks typically entered the bottom girder flanges in this region.

In the 45M_24W test, strain gages on four stirrups indicated strains in excess of the yield strain, including one stirrup that showed evidence of yielding at the bottom flange-web interface. The stirrup strain magnitudes observed in the 45M_8W test were generally lower than those observed in the other tests. The ratio of $V_{u,testu}/V_n$ for that test was limited by the capacity of the 600 kip MTS Model 311 Material Test Frame, and was the lowest ratio among the four tests. Even in that test, ten of the stirrups had strain gages that indicated strains higher than the yield strain, including five stirrups where that indication was near the bottom flange-web interface. For the 36M_8W test, ten stirrups had strain gages indicating strains in excess of the yield strain, with the majority of these

stirrups showing yielding near the bottom flange-web interface. In summary, these data show that most of the stirrups in the test regions had measured strains that exceeded the transverse reinforcement yield strain. The measured strain magnitudes were dependent on proximity to discontinuity ("disturbed") regions and crack proximity to a gage. This fact is particularly evident in Figure 3-49 which clearly shows that gages were not likely to measure yield strains unless a crack crossed a stirrup near a gage. Where cracks did cross stirrups near gage locations at the web/flange interface, stirrup strains exceeding yield strain were commonly measured in all tests.

In addition to loading the girders to investigate the straight-legged stirrup anchorage detail, the girders were also used to determine if web-shear cracks would remain visible following unloading. Bridge inspections are not likely to occur when there is a heavy load on the bridge, so the likelihood of web-shear cracks remaining detectable following removal of the load that caused the cracking is of importance. During the testing of both ends of the 45M girder, loading was reduced to 10 kips shortly after the web-shear cracks appeared as shown in Figures 3-46 and 3-47. Figures 3-55 to 3-58 show the web-shear cracks under load and immediately following unloading to 10 kips for the 45M_24W and 45M_8W girders, respectively. The web shear cracks in the 45M_24W girder remained visible upon unloading; however, the web shear cracks in the end of the 45M_8W girder closed up and were extremely difficult to locate when the girder was unloaded. In both cases, the stirrups acted elastically as no yielding was yet measured in the stirrups; however, the force provided by the stirrups in the 45M_24W girder end was not sufficient to completely close the shear cracks. The force acting to close shear cracks upon load removal is proportional to the area of transverse reinforcement crossing a crack, thus, a higher force would be expected to be available to close a crack in girders with closely spaced stirrups. For girders with tight stirrup spacing, web-shear cracks that form due to an overload in the field may not be visible upon inspection if the load that

caused crack initiation is removed. Although the cracks remained visible for the wider spaced stirrups, the cracks were difficult to see.

3.6.7 Anchorage Depth

The impact anchorage depth had on the development of yield strains in straight legged reinforcement was investigated in each of the four girder end tests. As mentioned in Sections 3.6.5 and 3.6.6, strains exceeding the transverse reinforcement yield strains were measured in the expected failure regions for the short legged stirrup despite the closer gage proximity to the web/flange interface.

Anchorage depth was also investigated by comparing the measured strains at mid-depth of the web between the gage on the short stirrup leg (45M_17_C, 36M_24_M) and the gage on the long stirrup leg (45M_17_E, 36M_24_S) attached at the same height. Figures 3-59 and 3-60 show the strain curves for the 36M_24_M and 36M_24_S gages during the 36M_18F test and the 45M_17_C and 45M_17_E gages during the 45M_8W test, respectively. The curves represent typical comparisons between the gages applied at the same height to both stirrup legs, showing that differing strain measurements were observed between the two stirrup legs during the tests. No correlation existed between the observation of larger strains during testing and stirrup leg length, thus, the differences were attributed to proximity of the gage to the crack rather than the difference in anchorage depth. Figures 3-61 and 3-62 show shear cracks following the 36M_18F test which were skewed relative to each other and likely crossed the short stirrup leg and long stirrup leg of stirrup 24 at different heights.

3.6.8 Girder Capacities

Girder capacities were recalculated based on measured prestress losses and measured material properties (ignoring strain hardening of the transverse reinforcement). The moment capacity for both girders was determined using strain compatibility as was required by Article 9.17.4.1 in the 1989/91 AASHTO STD (AASHTO 1991) because the

effective prestress after losses in both girders was less than half of the ultimate strength of the prestressing steel. Sample as-built flexural capacity calculations are included in Appendix B.4 of this document. Table 3-19 shows a comparison between the calculated nominal moment capacities and the maximum moment measured in the girders during the shear tests. Comparing the girder flexural capacities to the maximum measured moments gives a capacity to demand ratio of 0.97, 1.63, 1.25, and 1.05 for the 36M_18F, 45M_24W, 45M_8W, and 36M_8W girders, respectively. Both of the 36M girder tests experienced deck crushing after significant shear damage and yielding of the stirrups was observed. The cause of this was an error in the flexural design calculations causing an over prediction of the moment capacity. Because of the additional flexural capacity provided by the strands added to increase the bottom fiber compressive stress in the 45M girder, there was enough reserve capacity to resist a flexural failure during testing.

The cracking moment was predicted for the 36M_18F and 45M_24W girders assuming the rupture strength of the concrete was equal to 635 psi which was measured at the time of the 36M_18F test. Table 3-20 shows that the observed cracking moment to predicted cracking moment ratios for the 36M_18F and 45M_24W girders were 0.82 and 1.02, respectively. A sample calculation for the predicted cracking moment capacity is included in Appendix B.5.

Flexure-shear cracks were observed following flexural cracking of the bottom flange at stirrup locations during the 36M_18F test. Stirrup No. 24 was the first stirrup to be crossed by a flexure-shear crack at an applied shear force of 77.2 kips, which was 88% of the predicted concrete contribution to flexure-shear capacity.

Table 3-21 shows a comparison between the shears associated with the appearance of web-shear cracks and the shears at which they were predicted to occur based on V_{cw} in the 1989/91 AASHTO STD calculated a distance of *h/2* from the face of the support for each girder end. The table shows similar levels of shear force at the

initiation of web-shear cracks in both failure ends of the respective girders. The predicted capacities for the pairs of girder ends were slightly different due to the change in concrete material properties and the moment due to self-weight at the time each respective end was tested (the tests of the second girder ends had shorter span lengths). The web-shear cracks appeared at loads higher than predicted in each of the girder tests with the ratio of observed web-shear cracking to expected web-shear cracking equal to 1.09, 1.20, 1.16, and 1.09 for the 36M_18F, 45M_24W, 45M_8W, and 36M_8W girder ends. Web-shear cracks were observed in both ends of the 36M_18F girder following the propagation of flexure-shear cracks. The shear force corresponding to the first appearance of web-shear cracks in both ends of the girder during the flexure-shear test are included in the table.

The nominal shear capacities of the girders were recalculated with measured material properties, but ignoring strain hardening of the transverse reinforcement. Three different methods were used to determine the capacities: the 1989/91 AASHTO STD, the simplified method in the 2010 AASHTO LRFD Bridge Design Specifications hereafter referred to as 2010 AASHTO LRFD (AASHTO 2010), and Modified Compression Field Theory hereafter referred to as 2000 MCFT (Bentz 2005). For each of the cases, the nominal shear capacity consisted of contributions from the transverse reinforcement, draped prestressing strands, and concrete. Additionally, it was assumed that all stirrups were adequately anchored in the bottom flange such that the stirrups could be fully developed. The 1989/91 AASHTO STD assumes a shear crack angle equal to 45 degrees; whereas the simplified method in the 2010 AASHTO LRFD and 2000 MCFT make use of a variable crack angle. The girder capacities predicted with 2000 MCFT were determined using a spreadsheet developed by Dr. Evan Bentz based on tables for calculating β and θ values from the 2000 Interim Edition of the AASHTO LRFD specifications. As-built girder shear capacity calculations are provided in Appendix B.6 of this report.

The maximum applied shear force is plotted with respect to the predicted shear capacities for the 36M_18F, 45M_24W, 45M_8W, and 36M_8W tests in Figures 3-63 to 3-66, respectively. The figures show the applied shear force exceeded the predicted shear capacities from the three models; however, none of the tests failed in shear. The 45M_24W and 36M_18F tests were terminated prior to a shear failure in order to preserve the second end of the girders for future testing, but after exceeding the nominal shear capacities and observing significant shear damage. The 45M_8W test was terminated due to force capacity limitations prior to a failure and the 36M_8W test was ended due to a flexure failure.

Tables 3-22 to 3-25 summarize calculation parameters, maximum measured shear forces ($V_{u,test}$), and the nominal shear capacities (V_n) predicted by the 1989/91 AASHTO STD, 2010 LRFD, and 2000 MCFT at the predicted failure locations for the 36M_18F, 45M_24W, 45M_8W, and 36M_8W tests, respectively. The critical sections for the girder ends tested in web-shear were calculated a distance *h/2* or d_v away from the face of the support for the 1989/91 AASHTO STD or 2010 AASHTO LRFD as specified in the design codes, respectively. The ratios of applied shear force to the nominal shear capacity predicted by the 1989/91 AASHTO STD for the 36M_18F, 45M_24W, 45M_8W, and 36_8W girders were 1.23, 1.38, 1.19, and 1.35, respectively. One of the reasons for the under prediction of the shear capacities by the models was because strain hardening of the transverse reinforcement was ignored although stirrup strains were observed to reach into the strain hardening range during the tests. The shear loads at which the stirrups were first observed to yield can be determined from a review of the data provided in Appendix D.

Tables 3-22 to 3-25 show a significant decrease in the magnitude of V_c and increase in the magnitude of V_s predicted by the 2010 AASHTO LRFD compared to the 1989/91 AASHTO STD. The implication of this can be seen in Figure 3-63 which shows

the web-shear failure region of the 36M_18F girder predicted by the 2010 AASHTO LRFD extending farther into the span than was predicted by the 1989/91 AASHTO STD.

A sharp increase followed by a decrease in the shear capacity predicted by the 2010 AASHTO LRFD near one of the draped prestressing strand hold down points of the 36M_18F girder is shown in Figure 3-63. This jump, along with others shown in Figures 3-63 to 3-66, occur at transitions between web-shear and flexure-shear controlled regions in the girders. Figure 3-67 shows the V_{ci} and V_{cw} components of the shear capacity plotted with the nominal shear capacity. The jump in predicted shear capacity is caused by a change in the assumed shear crack angle between web-shear and flexure-shear controlled regions of prestressed concrete girders as specified in the simplified procedure in the 2010 AASHTO LRFD. In web-shear controlled regions, the crack angle is dependent upon the effective prestress levels in the concrete which can act to reduce the shear crack angle and in turn, increase the steel component of shear capacity. In flexure-shear controlled regions, a shear crack angle of 45 degrees is always assumed. This assumption resulted an unrealistic change in shear crack angles from 45 degrees to 34 degrees and back again in a 7 in. span for the 36M_18F girder.

Figure 3-68 is a plot of the maximum applied shear force, the shear capacity predicted by the 2010 AASHTO LRFD simplified procedure, and the minimum nominal shear capacity predicted by either a web-shear failure or flexure-shear failure. The figure shows that assuming the minimum capacity predicted by either a web-shear or a flexure-shear failure results in a conservative estimate in shear capacity as predicted with the 2010 AASHTO LRFD and eliminates sharp jumps in capacity due to an assumed change in shear crack angle. Figures 3-64 and 3-65 show a comparison between the 1989/91 AASHTO STD and the 2010 AASHTO LRFD shear capacity predictions in web-shear regions given different stirrup spacings for the 45M section. The figures show that for the 45M_24W girder, the 2010 AASHTO LRFD prediction for shear capacity is more conservative for the end with 24 in. stirrup spacing while the two specifications predict

similar results in the end of the girder with 8 in. stirrup spacing. Similarly, the 2010 AASHTO LRFD predicts a similar shear capacity to that predicted by the 1989/91 AASHTO STD in the 36M_8W girder end with 8 in. stirrup spacing; however, the 2010 AASHTO LRFD prediction for the girder end with 6 in. stirrup spacing is less conservative.

4 Summary and Conclusions

The anchorage of straight legged stirrups in prestressed concrete bridge girders was examined in tests of 13 subassemblages and two prestressed girders. The 13 subassemblage tests were used to examine the influence of key parameters on stirrup anchorage and consisted of 3 ft. 4 in. long bottom flange shaped specimens with one pair of stirrup legs embedded at midspan. The critical situation for embedment of stirrups is where a shear crack crosses the stirrup at the web-flange interface, requiring the stirrup to develop with the least available embedment. These specimens were meant to represent that situation. Specifically, the specimen shapes were the bottom flanges of M- and MN-shaped prestressed concrete girders with nominal stirrup embedment depths of 7 and 9 in., respectively. The reinforcement used was Grade 60, No. 4, epoxy-coated stirrups. Longitudinal steel was kept to a minimum in the test specimens in order to eliminate the effect of longitudinal strand confinement on stirrup anchorage. Two levels of concrete precompression stresses (i.e., near zero—0.015 f_c' and 0.45f_c') were applied to the subassemblages to simulate the effect of prestress on stirrup anchorage. Additionally, the presence of prestressing strand confinement hoops was varied to observe their impact on stirrup confinement. The test specimen measured concrete strengths ranged from 6.6 ksi to 9.5 ksi during the duration of testing.

Strain hardening was observed in all subassemblage specimen tests, while 7 of 13 tests resulted in bar fracture. Bar fracture was achieved in all of the tests with a nominal precompression level of 0.45f_c' as well as in both tests of the MN-shaped subassemblages with near zero precompression and 9.5 ksi concrete compressive strength and one test of an M-shaped specimen with near zero precompression and 9.4 ksi concrete compressive strength. Of the specimens which did not reach bar fracture, two failure modes were observed: pullout cone and concrete splitting. These failures occurred in in M-shaped specimens with near zero precompression levels. The pullout cone failures occurred in two specimens and the splitting failures occurred in four of the specimens. The pull-out

failures occurred in the specimens with lower concrete compressive strengths. No correlation was found between the existence of confinement hoops and stirrup anchorage.

Following the subassemblage tests, two prestressed concrete girders cast with typical No. 4 epoxy-coated U-shaped stirrups with the straight legs embedded into the prestressing steel in the bottom girder flanges were tested monotonically. The girders were 36 in. and 45 in. deep M-shaped girders. The M-shapes were chosen because they had smaller bottom flanges leading to less concrete cover over the stirrups and less embedment depth of the stirrups in the bottom flanges in comparison with the MN shapes. One end of the 36M girder was tested to promote a flexure-shear failure, while the other three girder ends were tested to promote web shear failures. The stirrup spacings in the flexure-shear failure region and web-shear failure region of the 36M girder were 18 and 8 in., respectively. The stirrup spacings in the web-shear failure regions of the 45M girder ends were 24 and 8 in. All of the stirrups in the expected failure regions had one of the legs of each U-shaped stirrup reduced so that the shortest anchorage length into the bottom flange associated with the allowable fabrication tolerances would be achieved. This anchorage length of 6-¾ in. into the bottom flange caused one leg of the stirrup to be approximately 1-¼ in. shorter than the other leg of the U-shaped stirrup. The concrete strengths of the girders measured at the time of test ranged from 6.3 to 7.2 ksi. Unloaded bottom fiber compressive stresses at the time of testing varied between $0.23f_c'$ and $0.30f_c'$ for the 36M and 45M girders, respectively.

None of the girders was taken to ultimate failure in shear, tests were terminated prior to complete failure. Because two tests were performed on each girder (one test on each end), the tests on the first end of each girder were terminated early to preserve the second girder end for testing. Both tests on the 36M girder (one flexure-shear and one web-shear test) approached flexural failures prior to shear failures, although significant shear damage was observed prior to the termination of the tests. The first test on the 45M_24W girder was stopped prior to failure to preserve the other end of the girder for

the next test. The test on the 45M_8W girder with 8 in. stirrup spacing was stopped prior to failure due to testing system capacity limitations.

Although complete shear failures were not experienced during any of the girder tests, significant shear cracking and stirrup yielding were observed prior to the termination of each of the tests. In most of the tests, the stirrup strains in the regions of interest were well into the strain hardening range. Using the measured material properties (without consideration of transverse reinforcement strain hardening) and effective prestress, the girder shear capacities were predicted using three different methods: the 1989/91 AASHTO STD, the simplified method in the 2010 AASHTO LRFD Bridge Design Specifications, and Modified Compression Field Theory. The measured shear capacities all exceeded the predicted capacities, even though the tests were terminated before the ultimate capacities were reached. As an example, the measured results exceeded the 1989/91 AASHTO STD predictions by 19-38%. One of the reasons for the increased capacities realized in the girders relative to the predictions was the achievement of strain hardening in the transverse reinforcement in the tests.

The results of the subassemblage and girder end tests all indicated that the anchorage of straight legged, Grade 60, No. 4, epoxy coated stirrups in M- and MN-shaped prestressed bridge girders with current MnDOT fabrication tolerances cast with a compressive concrete strength of at least 6.3 ksi proved effective in developing yield strains in both web-shear and flexure-shear failure regions as yielding was observed at various web heights, including the web/flange interface, throughout the failure region in each of the four girder end tests including regions of high flexure-shear, where flexural cracks were observed to occur near the stirrup anchorage.

The girder tests did not indicate that stirrup spacing had a noticeable impact on stirrup anchorage; however, it did affect the ability to observe residual cracks following unloading. During the 45M girder tests, the girder was unloaded following the initial

web-shear crack development, prior to stirrup yielding, to investigate whether or not the residual cracks would be visible in an unloaded girder. This information was obtained to inform bridge inspectors of the potential appearance of girders after cracking due to an intermittent overloaded vehicle. The web shear cracks in the 45M girder with 24 in. stirrup spacing were difficult to see upon unloading, but the web shear cracks in the end of the 45M girder with the 8 in. stirrup spacing closed up completely and were extremely difficult to locate when the beam was unloaded. The force acting to close shear cracks upon load removal is related to the area of the transverse reinforcement crossing the crack, thus, for girders with tight stirrup spacing, web-shear cracks that form due to an overload in the field may not be visible upon inspection if the load that caused crack initiation is removed.

The effect of precompression on stirrup anchorage was observed in the subassemblage tests as stirrup anchorage was clearly improved in specimens with increased precompression which acted to counter the splitting tensile stresses caused by bending induced during stirrup pullout. In the 36M flexure-shear test, strain hardening was observed despite the loss of precompression at stirrup locations due to the initiation of flexure cracks. This result was in line with results from the subassemblage tests with near zero precompression which similarly showed stirrup strain hardening; however, the additional confinement and crack width constraint provided by the prestressing strands to the embedded stirrups in the girders was thought to further improve stirrup anchorage over that seen in the subassemblage tests.

The straight-legged anchorage detail was sufficient in developing yield with a nominal stirrup anchorage depth into the bottom flanges of the girders of 6-¾ in. The anchorage depth of the shortened stirrup leg represented a reduction of 1-¼ in. from the nominal design depth due to the application of the worst case fabrication tolerances accepted by MnDOT. Differences in stirrup strain magnitudes between the long and short stirrup legs measured at the same height during the girder tests did not suggest the

shortened stirrup leg performed less favorably than the longer stirrup leg. In some cases, greater strains were measured in the shorter stirrup leg. The difference in strain measurements between the two stirrup legs was likely due to the crack plane not being perpendicular to the axis of the girder causing the stirrup legs to be intercepted by cracks at different locations, as strain measurements were highly dependent upon crack proximity to a strain gage.

The presence of confinement hoops did not show clear benefits to stirrup anchorage or noticeably impact the flexural cracking of the girders. Despite alternating the presence of confinement hoops at stirrup locations in the girders and the absence of confinement hoops in over half of the subassemblage specimens, yield strains were exceeded in each of the tests. This was likely due to the fact that the confinement hoops run parallel to the splitting cracks which typically develop at stirrup locations and act to debond the stirrup legs from the concrete. Greater benefit to stirrup anchorage is likely provided through increased concrete cover over the stirrups and the embedment of stirrups into the prestressing strands which provide confinement and constrain crack widths. As the subassemblage test results indicated, the larger flange size associated with MN-shaped girders provided increased concrete cover and greater nominal anchorage depth which improved the anchorage of straight legged stirrups subjected to high stresses as both MN-shaped specimens with an applied prestress level of $0.015f_c'$ failed by bar fracture; whereas only one of the M-shaped specimens with an applied prestress level of $0.015f_c'$ failed by bar fracture. Thus, girder shapes providing greater concrete cover to stirrups with increased embedment into longitudinal prestressing strands as compared to current MnDOT M-shaped girders can be expected to meet or exceed the results of the girder tests described in this report.

Previous research has shown that straight legged stirrups anchored into the compression region of rectangular shaped girders can limit realized shear capacities (Anderson and Ramirez 1989). In the present study, straight legged stirrups achieved

strains in excess of the yield strains in all of the subassemblage tests and in all four of the girder end tests. The maximum shear forces experienced by the prestressed girders tested in this study exceeded the nominal shear capacities predicted with measured material properties (not considering strain hardening of the transverse reinforcement) using the 1989 Standard Specifications with 1991 Interim Revisions, 2010 AASHTO LRFD Design Specifications, and with Modified Compression Field Theory based on tables from the 2000 AASHTO LRFD Design Specification Interim Revisions. The additional shear capacity realized by the girder ends can be attributed in part to the strain hardening achieved in the transverse reinforcement. The anchorage of the straight-legged stirrups was enhanced by the bottom flange which provided increased concrete cover over the stirrup anchorage and the stirrups were embedded inside longitudinal prestressing strands which helped to constrain crack widths. The effective prestress was also believed to help anchor the stirrups in regions of web-shear cracking. The average ratio of applied shear to shear capacity predicted with the 1989/91 AASHTO STD was equal to 1.29. The ratio was limited by premature test terminations due to unintended flexural failures, to limit extensive damage, or by loading capacity limitations. Higher shear forces likely could have been sustained in each of the tests.

References

AASHTO. 2010. "AASHTO LRFD Bridge Design Specifications." American Association of State Highway and Transportation Officials, Washington DC.

AASHTO. 1991. "Standard Specifications for Highway Bridges with 1991 Interim Revisions, 14th Edition." American Association of State Highway and Transportation Officials, Washington, DC.

ACI Committe 318. 2011. "Building Code Requirements for Reinforced Concrete (ACI 318-11) and Commentary." American Concrete Institute, Detroit, Michigan.

ACI Committee 318. 1983. "Building Code Requirements for Reinforced Concrete (ACI 318-83)." American Concrete Institute, Detroit, Michigan.

ACI Committee 318. 1989. "Building Code Requirements for Reinforced Concrete and Commentary (ACI 318-89)." American Concrete Institute, Detroit, Michigan.

Anderson, Neal S., and Julio A. Ramirez. 1989. "Detailing of Stirrup Reinforcement." *ACI Structural Journal* 507-515.

ASTM Standard A370. 2012. "Standard Test Methods and Definitions for Mechanical Testing of Steel Products." West Conshohocken, PA: ASTM International. doi:10.1520/A0370-12a.

ASTM Standard C143. 2012. "Standard Test Method for Slump of Hydraulic-Cement Concrete." West Conshohocken, PA: ASTM International. doi:10.1520/C0143_C0143M-12.

ASTM Standard C39. 2012. "Standard Test Method for Compressive Strength of Cylindrical Concrete Specimens." West Conshohocken, PA: ASTM International. doi:10.1520/C0039_C0039M-12.

ASTM Standard C496. 2011. "Standard Test Method for Splitting Tensile Strength of Cylindrical Concrete Specimens." West Conshohocken, PA: ASTM International. doi:10.1520/C0496_C0496M-11.

ASTM Standard C78. 2010. "Standard Test Method for Flexural Strength of Concrete (Using Simple Beam with Third-Point Loading)." West Conshohocken, PA: ASTM International. doi:10.1520/C0078/C0078M-10.

Bentz, Evan. 2005. *Modified Compression Field Theory.* Email Correspondance, February 24.

Bentz, Evan, interview by Catherine French. 2005. *Modified Compression Field Theory* (February 24).

Dereli, Ozer, Carol Shield, and Catherine French. 2010. *Discrepancies in Shear Strength of Prestressed Beams with Different Specifications.* Final Report, Minnesota Department of Transportation.

Devalapura, Ravi K., and K. M. Tadros. 1992. "Stress-Strain Modeling of 270 ksi Low-Relaxation Prestressing Strands." *Precast/Prestressed Concrete Institute* 37 (no. 2).

Hawkins, Neil M., Daniel A. Kuchma, Robert F. Mast, M. Lee Marsh, and Karl Heinz Reineck. 2005. *Simplfied Shear Design of Structural Concrete Members.* NCHRP Report, Washington, D.C.: American Association of State Highway and Transportation Officials.

Kajfasz, Stanislaw. 1958. "Some Relaxation Tests on Prestressing Wire." 10 (No. 30): 133-140.

Kuchma, Daniel, Kang Su Kim, Thomas J. Nagle, Shaoyun Sun, and Neil M. Hawkins. 2008. "Shear Tests on High-Strength Prestressed Bulb-Tee Girders: Strengths and Key Observations." *ACI Structural Journal* 358-367.

Lin, T. Y., and Ned H. Burns. 1981. *Design of Prestressed Concrete Structures.* John Wiley & Sons, Inc.

Minor, John, and James O. Jirsa. 1970. *A Study of Bent Bar Anchorages in Concrete.* PhD Thesis, Houston, Texas: Rice University.

Preston, H. Kent. 1975. "Recommendations for Estimating Prestress Losses." *Precast/Prestressed Concrete Institute Journal* No. 4 (20): 44-75.

Prestressed/Precast Concrete Institute. 1997. *Bridge Design Manual.* Chicago.

Regan, P. E., and I. L. Kennedy Reid. 2004. "Shear Strength of RC Beams with Defective Stirrup Anchorages." *Magazine of Concrete Research* 56 (No. 3): 159-166.

Runzell, Brian, Carol Shield, and Catherine French. 2007. *Shear Capacity of Prestressed Concrete Beams.* Minnesota Department of Transportation.

Varney, Jason C., Michael D. Brown, Oguzhan Bayrak, and W. Randall Poston. 2011. "Effect of Stirrup Anchorage on Shear Strength of Reinforced Concrete Beams." *ACI Structural Journal* 469-478.

Wood, S. L. 1991. "Evaluation of the Long-Term Properties of Concrete." *Research and Development Bulletin RD102* (Portland Cement Association).

Tables

Table 2-1: Compressive strength and split tensile strengths

Batch	Concrete Age [days]	Measured Concrete Compressive Strength [ksi]	Measured Concrete Split Tension Strength [psi]
5 to 7.5 ksi Target Strength Cast October 2012	28	8.0 (8.0-8.1)[1]	-
	127	6.6 (5.9-7.6)	786.2
	143	9.4 (9.2-9.7)	-
	147	9.5 (9.2-9.7)	717.5
5 ksi Target Strength Cast April 2013	28	6.4 (5.9-6.9)	576.9
	34	6.6 (6.5-6.8)	-
7.5 ksi Target Strength Cast April 2013	28	8.2 (7.7-8.7)	728.1
	39	8.0 (7.8-8.1)	-

[1]Numbers in parentheses represent the range of compressive strengths observed in the tests of three cylinders.

Table 2-2: Subassemblage test results.

Specimen	Design Concrete Compressive Strength [ksi]	Measured concrete strength on day of test [ksi]	Flange Shape[1]	Confinement Present	Precompression Stress based on Design Concrete Compressive Strength [ksi]	Failure Mode[2]	Stirrup yield plateau [ksi]	Max. Stirrup stress during test [ksi]
6.4M_NC_020A	5.0	6.6	M	No	$0.015f_c'$	Pullout Cone	64.1	81.9
6.4M_NC_020B	5.0	6.6	M	No	$0.015f_c'$	Pullout Cone	63.5	83.0
8.2M_NC_020	5.0	8.0	M	No	$0.015f_c'$	Concrete Splitting	60.7	93.5
8.0M_NC_020A	5.0	6.6[5]	M	No	$0.015f_c'$	Concrete Splitting	62.4	93.7
8.0M_NC_020B	5.0	9.3	M	No	$0.015f_c'$	Concrete Splitting[3]	66.4	93.5
8.0M_WC_020A	5.0	9.4	M	Yes	$0.015f_c'$	Concrete Splitting	65.0	94.2
8.0M_WC_020B	5.0	9.4	M	Yes	$0.015f_c'$	Bar Fracture[4]	64.9	101.8
8.0M_NC_575A	5.0	6.6	M	No	$0.45f_c'$	Bar Fracture	61.9	104.5
8.0M_NC_575B	5.0	6.6	M	No	$0.45f_c'$	Bar Fracture	64.0	105.3
8.0M_WC_575A	5.0	9.4	M	Yes	$0.45f_c'$	Bar Fracture	65.2	106.4
8.0M_WC_575B	5.0	9.5	M	Yes	$0.45f_c'$	Bar Fracture	66.2	106.8
8.0MN_WC_030A	6.0	9.5	MN	Yes	$0.015f_c'$	Bar Fracture	65.1	106.2
8.0MN_WC_030B	6.0	9.5	MN	Yes	$0.015f_c'$	Bar Fracture	64.3	107

[1] Embedment depth corresponding to M- and MN-shaped subassemblages was 7 in. and 9 in., respectively

[2] All stirrups well exceeded yield strains prior to failure

[3] Coupler slipped off north stirrup after yielding was measured

[4] Significant bond deterioration at the concrete face prior to fracture

[5] Average of three compressive strength tests ranging from 5.9 to 7.6 ksi.

Table 3-1: Nominal distance between prestressing strand centroids and girder bottoms for the full-length girders.

45M Girder			
	No.	Centerline [in.]	Ends [in.]
Straight Strands	20	3.0	3.0
Draped Strands	6	7.0	40.0
Total Strands	26	3.92	11.54
36M Girder			
Straight Strands	12	3.0	3.0
Draped Strands	6	5.0	29.0
Total Strands	18	3.67	11.67

Table 3-2: MnDOT standard reinforcing details for decks built on prestressed concrete girders (from MnDOT LRFD Bridge Manual, 2010)

REINFORCEMENT FOR DECK ON PRESTRESSED CONCRETE BEAMS

(Negative Moment @ 10 inches from CL I-Beam & 8.7 inches from CL Rectangular Beam)

Maximum Beam Spacing①	Transverse Reinforcement				Deck Thickness ②	Longitudinal Reinforcement Bottom③	Longitudinal Reinforcement Top③
	Bottom		Top				
	w/ Wearing Course	w/o Wearing Course	Deck on I-Beam	Deck on Rect. Beam			
5'-0"	13 @ 5"	13 @ 6.5"	13 @ 10"	13 @ 9.5"	9''	13 @ 7"	13 @ 1'-6"
5'-6"	13 @ 5"	13 @ 6"	13 @ 9"	13 @ 8.5"	9''	13 @ 7"	13 @ 1'-6"
6'-0"	16 @ 7"	13 @ 6"	13 @ 8.5"	13 @ 7.5"	9''	16 @ 10"	13 @ 1'-6"
6'-6"	16 @ 7"	13 @ 6"	13 @ 7.5"	13 @ 7"	9''	16 @ 10"	13 @ 1'-6"
7'-0"	16 @ 7"	13 @ 6"	13 @ 6.5"	13 @ 6"	9''	16 @ 10"	13 @ 1'-6"
7'-6"	16 @ 7"	13 @ 6"	13 @ 6"	13 @ 5.5"	9''	16 @ 10"	13 @ 1'-6"
8'-0"	16 @ 7"	13 @ 6"	13 @ 5.5"	13 @ 5"	9''	16 @ 10"	13 @ 1'-6"
8'-6"	16 @ 7"	13 @ 6"	13 @ 5"	13 @ 5"	9''	16 @ 10"	13 @ 1'-6"
9'-0"	16 @ 7"	13 @ 6"	13 @ 5"	16 @ 7"	9''	16 @ 10"	13 @ 1'-6"

Table 3-3: Designed nominal moment capacity and expected moment.

Test	Nominal Moment M_n [ft·kip]	Expected Moment[1] M_u [ft·kip]	$0.9 \cdot M_n/M_u$
36M_18F	3037	3339	0.82
45M_24W	4912	2823	1.56
45M_8W	4921	4061	1.10
36M_8W	2621	2431	0.98

[1] Based on applied load to cause shear failure assuming 30% increase in shear capacity

Table 3-4: Measured girder concrete compressive strengths.

Event	Concrete Age [days]	Average f_c' [ksi]
Release	2	4.7
28 days	28	6.7
36M_18F Test	98	6.3
45M_24W Test	114	6.8
45M_8W Test	122	7.0
36M_8W Test	139	6.9

Table 3-5: Measured girder split tension strengths at time of tests.

Event	Concrete Age [days]	Average Tensile Strength [psi]
36M_18F	98	614
45M_24W	114	599
45M_8W	122	549
36M_8W	139	606

Table 3-6: Measured girder deck compressive strengths at time of tests.

Event	Concrete Age [days]	Average Compressive Strength [psi]
36M_18F	49	5.13
45M_24W	44	4.78
45M_8W	52	4.89
36M_8W	90	5.86

Table 3-7: Measured yield strength and yield strain of primary transverse reinforcement for both girders.

Specimen	Transverse Reinforcement Yield Strength [ksi]	Corresponding Yield Strain [μs]
36M	70.0	2700
45M	67.0	3090

Table 3-8: Strand stresses after seating according to Cretex gage data.

Strand Name	Applied Stress [ksi]
1A	167
1B[1]	167
1C	169
1D[1]	169
1E	169
1H	169
1I[1]	170
1J	170
1K[1]	170
1L	170
2A[1]	170
2B	27[2]
2C[1]	171
2D	27[2]
2E	27[2]
2H	27[2]
2I	27[2]
2J[1]	171
2K	27[2]
2L[1]	169
3F	117
3G	117
4F	117
4G	114
5F	121
5G	114

[1] Strands were debonded from the 36M girder
[2] Estimated prestress

Table 3-9: Measured and expected values of elastic shortening and associated elastic moduli.

Girder	Measured Elastic Shortening [ksi]	Required[1] Modulus of Elasticity at Release [ksi]	Expected Elastic Shortening [ksi]	Predicted Modulus of Elasticity at Release $w_c^{1.5} \cdot 33 \cdot \sqrt{f_c'}$ [ksi]
45M	18.9	3220	15.6	4050
36M	10.3	3560	9.3	4050

[1]Required modulus to produce measured elastic shortening

Table 3-10: PCI predicted time dependent prestress losses for 36M girder.

Prestress Loss:	Tensioning to Release [ksi]	Release to Composite Deck Cast [ksi]	Deck cast to Girder Test [ksi]	Total Loss at Test [ksi]	% of Initial Prestress
Relaxation	0.28	0.19	.02	0.49	0.5
Creep	0	4.73	1.00	5.73	5.6
Shrinkage	0	4.29	1.14	5.43	5.3
Total Losses	0.28	9.21	2.16	11.65	11.3

Table 3-11: PCI predicted time dependent prestress losses for 45M girder.

Prestress Loss:	Tensioning to Release [ksi]	Release to Composite Deck Cast [ksi]	Deck cast to Girder Test [ksi]	Total Loss at Test [ksi]	% of Initial Prestress
Relaxation	0.46	0.25	0.02	0.73	0.6
Creep	0	9.28	1.10	10.38	8.4
Shrinkage	0	4.72	0.69	5.41	4.4
Total Losses	0.46	14.25	1.81	16.52	13.4

Table 3-12: VWG creep and shrinkage measurements for 36M girder.

Prestress Loss:	Tensioning to Release [ksi]	Release to Composite Deck Cast [ksi]	Deck cast to Girder Test [ksi]	Total Loss at Test [ksi]	% of Initial Prestress
Creep & Shrinkage	-	8.0	1.5	9.5	9.2

Table 3-13: VWG creep and shrinkage measurements for 45M girder.

Prestress Loss:	Tensioning to Release [ksi]	Release to Composite Deck Cast [ksi]	Deck cast to Girder Test [ksi]	Total Loss at Test [ksi]	% of Initial Prestress
Creep & Shrinkage	-	12.5	2.4	14.9	12.1

Table 3-14: Summary of prestress losses and remaining prestress used for calculating girder capacities.

	36M Girder		45M Girder		
Type of Loss	Total Loss [ksi]	Remaining Prestress [ksi]	Total Loss [ksi]	Remaining Prestress [ksi]	Measured or Predicted
-	-	106.0	-	126.4	Measured
Seating Loss	2.8	103.2	2.8	123.6	Predicted
Elastic Shortening	10.3	92.9	18.9	104.7	Measured
Relaxation	0.5	92.4	0.7	104.0	Predicted
Creep & Shrinkage	9.5	82.9	14.9	89.1	Measured
Assumed Losses	**23.1**	**82.9**	**37.3**	**89.1**	-

Table 3-15: Maximum stirrup strain to yield ratio for 36M_18F test in failure region.

Stirrup Number	Strain [μs]	Measured Strain/Yield Strain
20	2848	1.05
21	2497	0.92
22	2778	1.03
23	14503	5.37
24	14759	5.47
25	9639	3.57
26	10382	3.85
27	397	0.15

Table 3-16: Maximum stirrup strain to yield ratio for 45M_24W test in failure region.

Stirrup Number	Strain [μs]	Measured Strain/Yield Strain
1	16988	5.50
2	8692	2.82
3	10205	3.30
4	11648	3.77
5	1212	0.39

Table 3-17: Maximum stirrup strain to yield ratio for 45M_8W test in failure region.

Stirrup Number	Strain [μs]	Measured Strain/Yield Strain
6	243	0.08
7	707	0.23
8	1135	0.37
9	1948	0.63
10	3586	1.16
11	2875	0.93
12	9361	3.03
13	5177	1.68
14	8743	2.83
15	9193	2.98
16	4215	1.36
17	12769	4.13
18	11303	3.66
19	9113	2.95
20	3835	1.24
21	350	0.11

Table 3-18: Maximum stirrup strain to yield ratio for 36M_8W test in failure region.

Stirrup Number	Strain [μs]	Measured Strain/Yield Strain
28	60	0.02
29	1428	0.53
30	3125	1.16
31	7253	2.69
32	8961	3.31
33	10167	3.77
34	13545	5.02
35	11058	4.10
36	10290	3.81
37	14578	5.40
38	9077	3.36
39	4263	1.58
40	788	0.29

Table 3-19: Predicted moment capacity compared to maximum moment measured during testing.

Test	Maximum Measured Moment[1] (M_u) [ft·kip]	Moment Capacity (M_n) [ft·kip]	M_n/M_u
36M_18F	3213	3112	0.97[2]
45M_24W	3015	4921	1.63
45M_8W	3957	4946	1.25
36M_8W	2725	2853	1.05[1]

[1] All tests were terminated before ultimate failure was observed.
[2] Deck crushing observed at point of load application at failure

Table 3-20: Comparison of observed cracking moment and predicted cracking moment.

Test	Observed Cracking Moment ($M_{cr,test}$) [ft·kip]	Predicted Cracking Moment ($M_{cr,predicted}$) [ft·kip]	$M_{cr,test}/M_{cr,predicted}$
36M_18F	1018	1248	0.82
45M_24W	2136	2101	1.02

Table 3-21: Comparison of observed web-shear cracking and predicted web-shear cracking.

Girder End	Observed Web-Shear ($V_{cw,test}$) [kip]	Predicted Web-Shear ($V_{cw,predicted}$) [kip]	$V_{cw,test}/V_{cw,predicted}$
36M_18F[1]	111.9	102.4	1.09
45M_24W	166.3	139.0	1.20
45M_8W	161.9	139.5	1.16
36M_8W[1]	113.7[2]	104.0	1.09

[1] Web-shear cracks occurred following flexure-shear cracking during the 36M_18F test

Table 3-22: Comparison of design methods in predicting ultimate shear capacity for 36M_18F.

Design Method	Predicted Failure Location from Center of Bearing [in.]	Assumed Crack Angle [in.]	Observed Crack Angle [deg.]	V_c[1] [kip]	V_s [kip]	V_n [kip]	$V_{u,test}$ [kip]	$V_{u,test}/V_n$
1989/91 AASHTO STD	206.0	45	47	77	64	141	174	1.23
2010 AASHTO LRFD		45		67	57	124		1.40
2000 MCFT		37		49[2]	70	119		1.46

[1] V_{ci} controls failure at evaluated location rather than V_{cw}
[2] Value equals $V_c + V_p$

Table 3-23: Comparison of design methods in predicting ultimate shear capacity for 45M_24W.

Design Method	Predicted Failure Location from Center of Bearing [in.]	Assumed Crack Angle [in.]	Observed Crack Angle [deg.]	V_c [kip]	V_s [kip]	V_n [kip]	$V_{u,test}$ [kip]	$V_{u,test}/V_n$
1989/91 AASHTO STD	34.5	45	28	139	49	188	259	1.38
2010 AASHTO LRFD	47.5	31		96	74	170	258	1.52
2000 MCFT	148.5	25		81[1]	102	183	251	1.37

[1] Value equals $V_c + V_p$

Table 3-24: Comparison of design methods in predicting ultimate shear capacity for 45M_8W

Design Method	Predicted Failure Location from Center of Bearing [in.]	Assumed Crack Angle [in.]	Observed Crack Angle [deg.]	V_c [kip]	V_s [kip]	V_n [kip]	$V_{u,test}$ [kip]	$V_{u,test}/V_n$
1989/91 AASHTO STD	34.5	45	26	140	148	288	343	1.19
2010 AASHTO LRFD	47.5	32		96	218	314	341	1.09
2000 MCFT	148.5	35		65[1]	197	262	335	1.28

[1] Value equals $V_c + V_p$

Table 3-25: Comparison of design methods in predicting ultimate shear capacity for 36M_8W

Design Method	Predicted Failure Location from Center of Bearing [in.]	Assumed Crack Angle [in.]	Observed Crack Angle [deg.]	V_c [kip]	V_s [kip]	V_n [kip]	$V_{u,test}$ [kip]	$V_{u,test}/V_n$
1989/91 AASHTO STD	30.0	45	35	104	126	230	311	1.35
2010 AASHTO LRFD	40.2	34		69	170	239	308	1.29
2000 MCFT	120.0	37		47[1]	144	191	304	1.59

[1] Value equals $V_c + V_p$

Figures

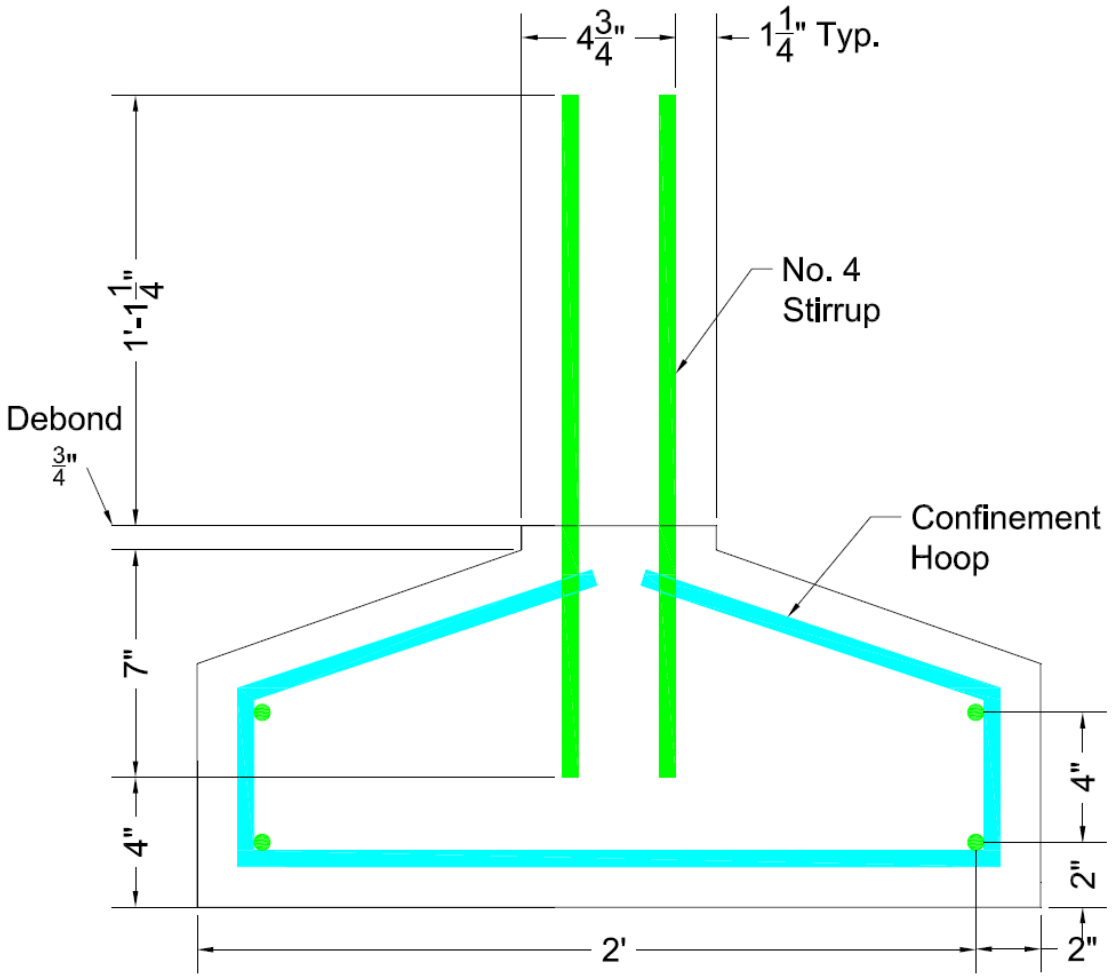

Figure 2-1: Cross-sectional view of typical M-shaped subassemblage specimen.

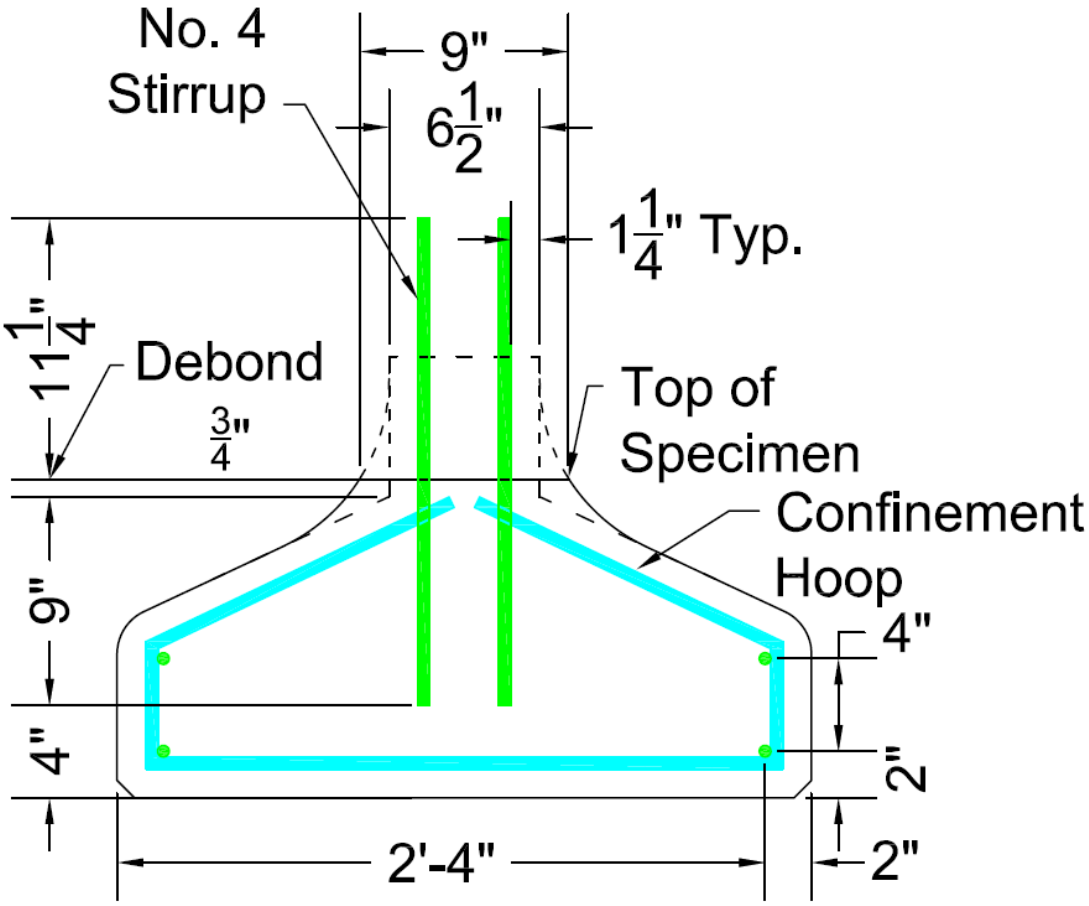

Figure 2-2: Cross-sectional view of typical MN-shaped subassemblage specimen.

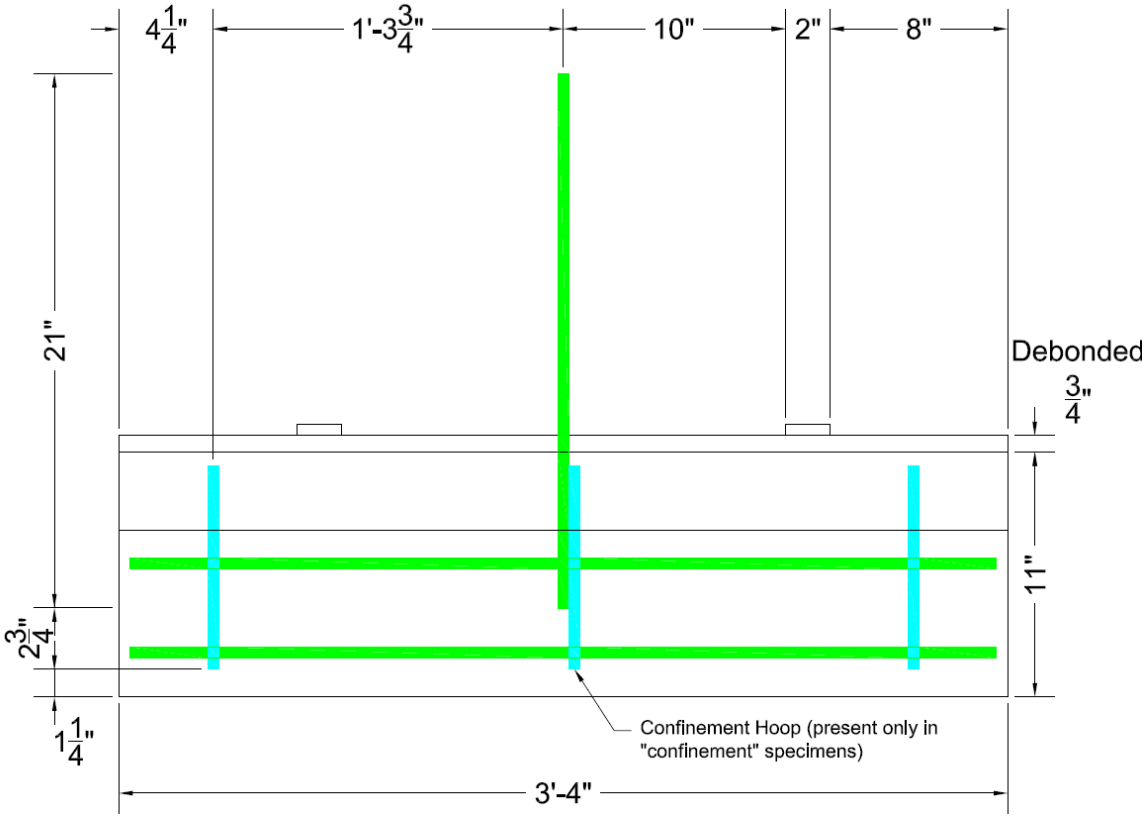

Figure 2-3: Side view of M-shaped subassemblage specimen showing typical placement of confinement hoops.

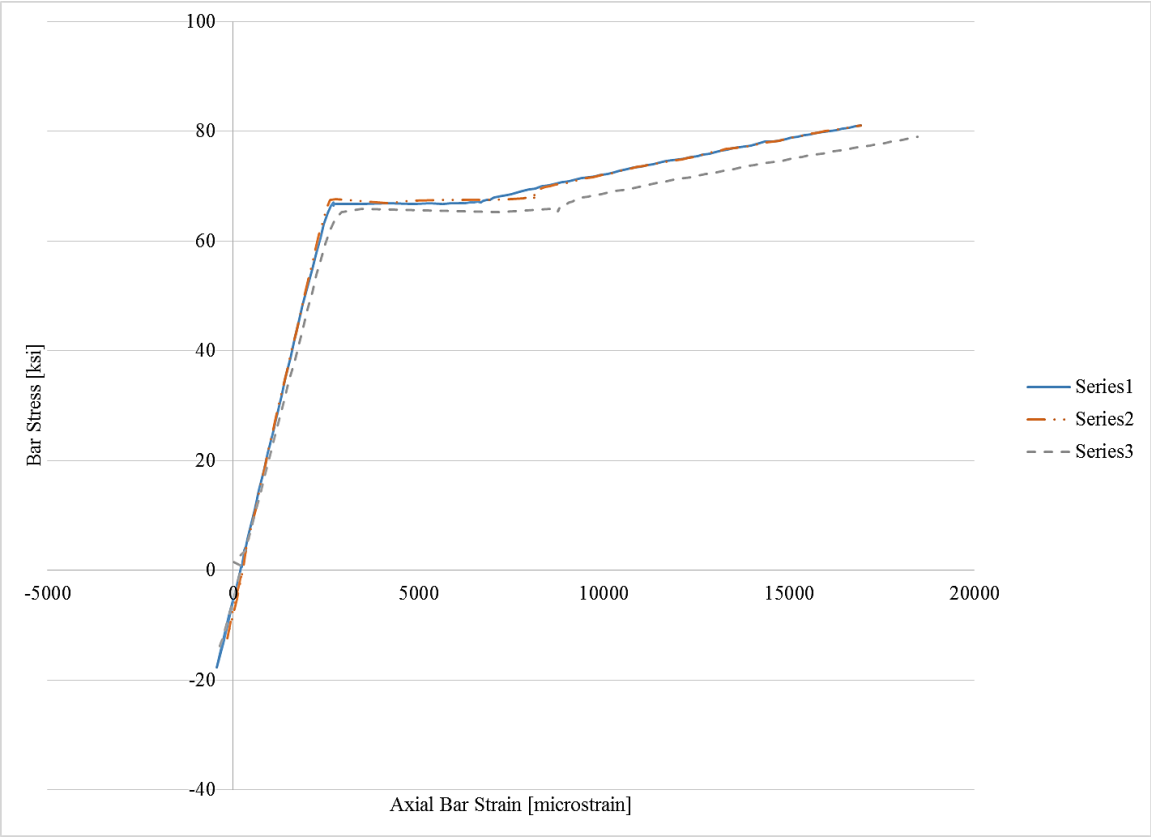

Figure 2-4: Subassemblage rebar direct tension test results.

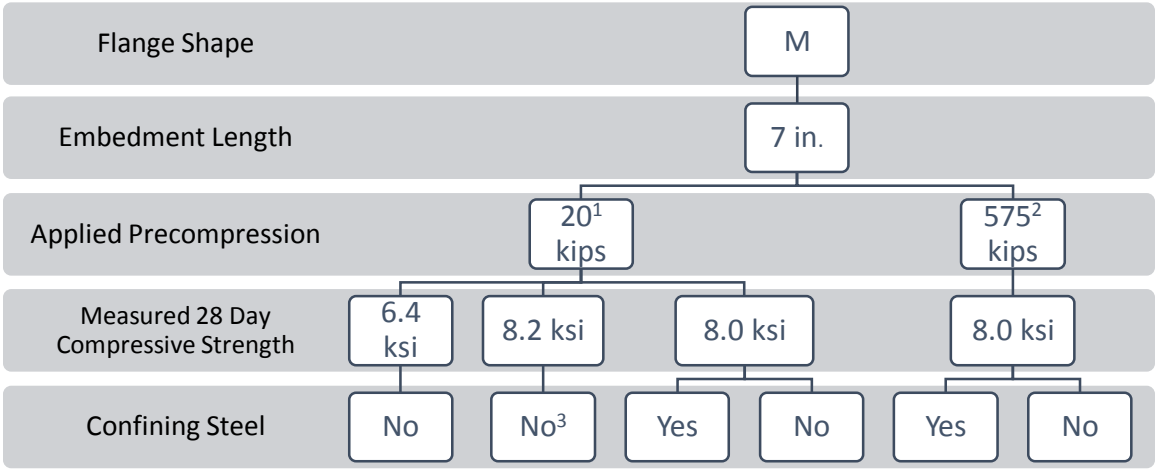

[1]corresponds to 0.015 f_c', based on 28-day design compressive strength of 5 ksi

[2] corresponds to 0.45f_c', based on nominal 28-day compressive strength

[3] Duplicate test was not run.

Figure 2-5: M-shaped subassemblage test specimen parameters.

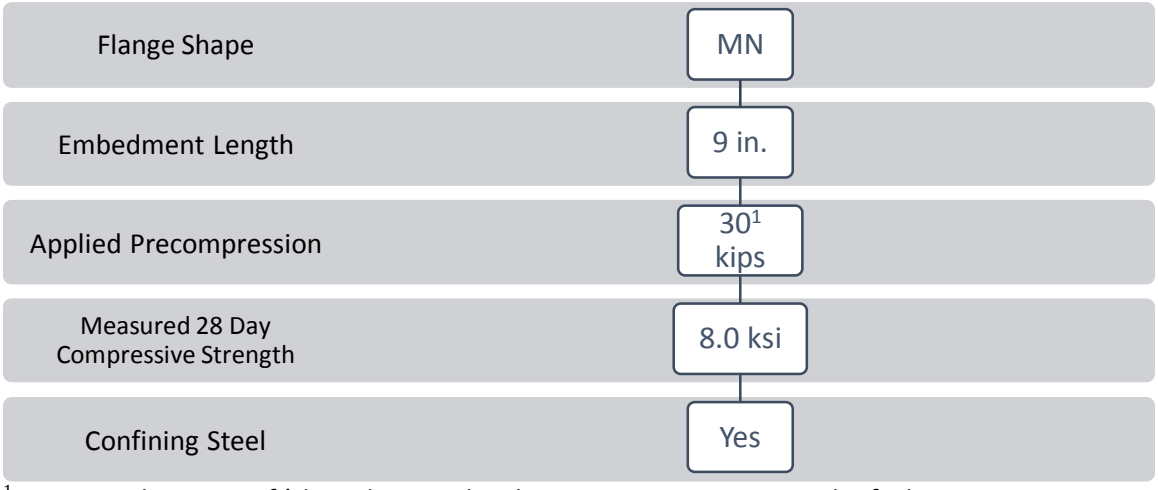

[1]corresponds to 0.015f_c', based on 28-day design compressive strength of 6 ksi

Figure 2-6: MN-shaped subassemblage test specimen parameters.

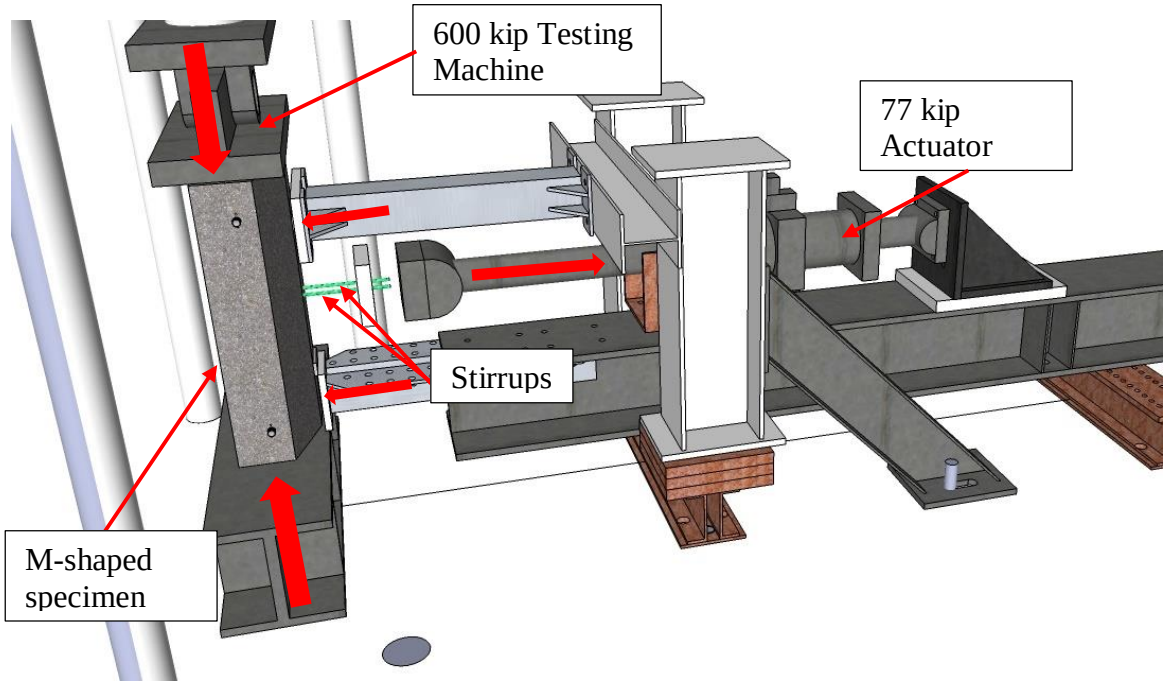

Figure 2-7: Overview of testing apparatus shown here for an M-shaped subassemblage specimen

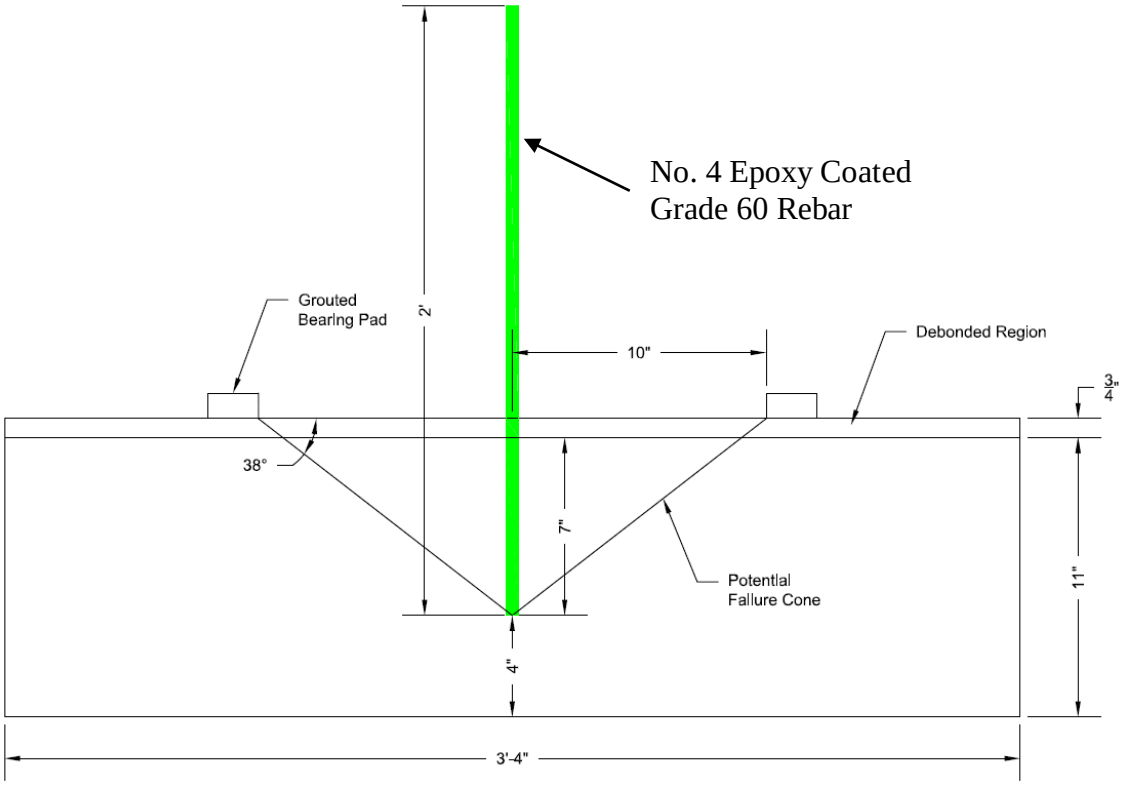

Figure 2-8: Side view of typical M-shaped subassemblage specimen including grouted bearing pads and potential failure cone.

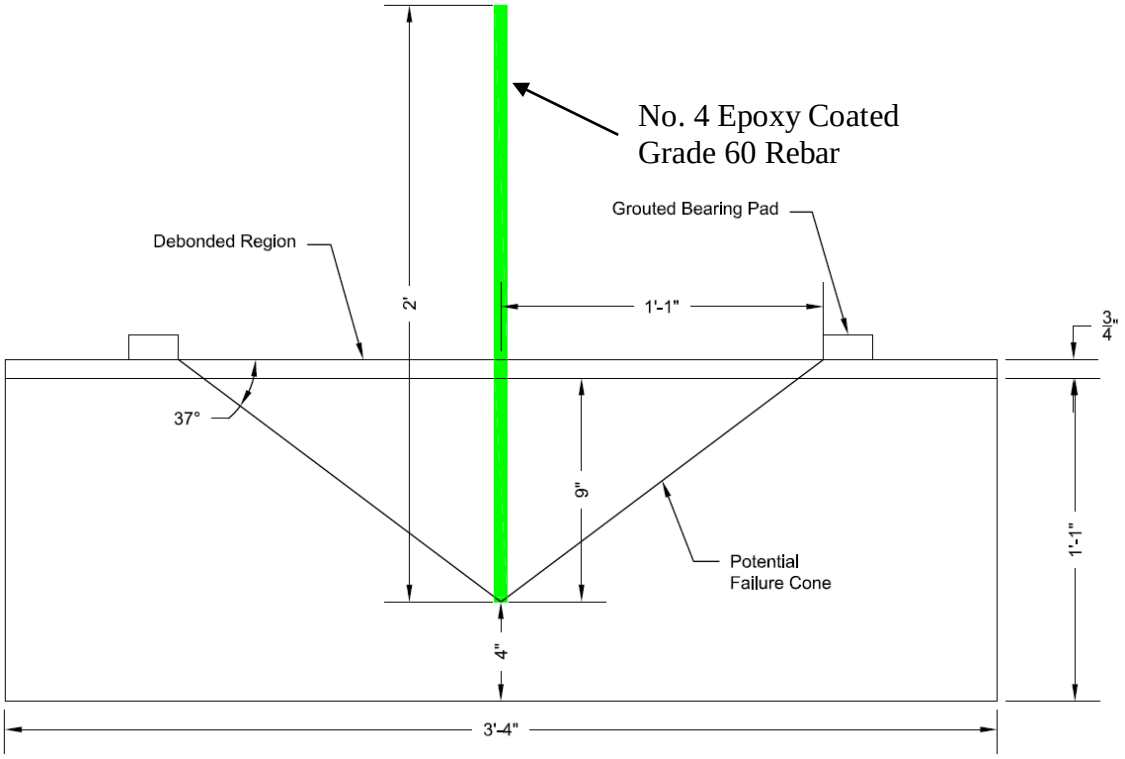

Figure 2-9: Side view of typical MN-shaped subassemblage specimen including grouted bearing pads and potential failure cone.

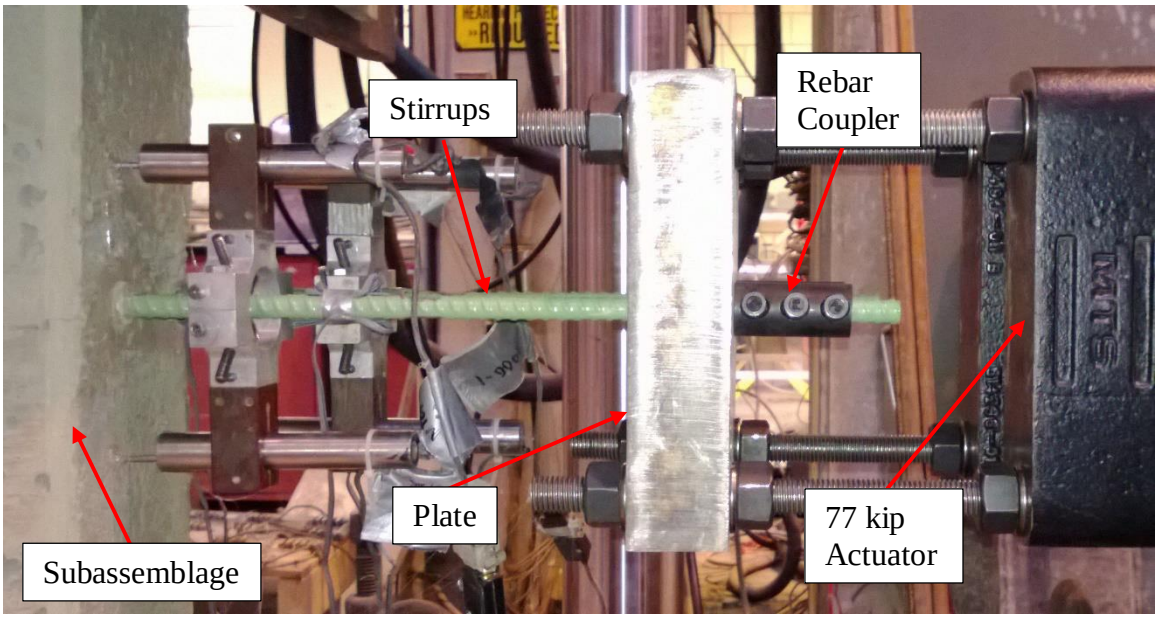

Figure 2-10: Subassemblage tension assembly (mirror image of photograph so orientation consistent with Fig. 2-7).

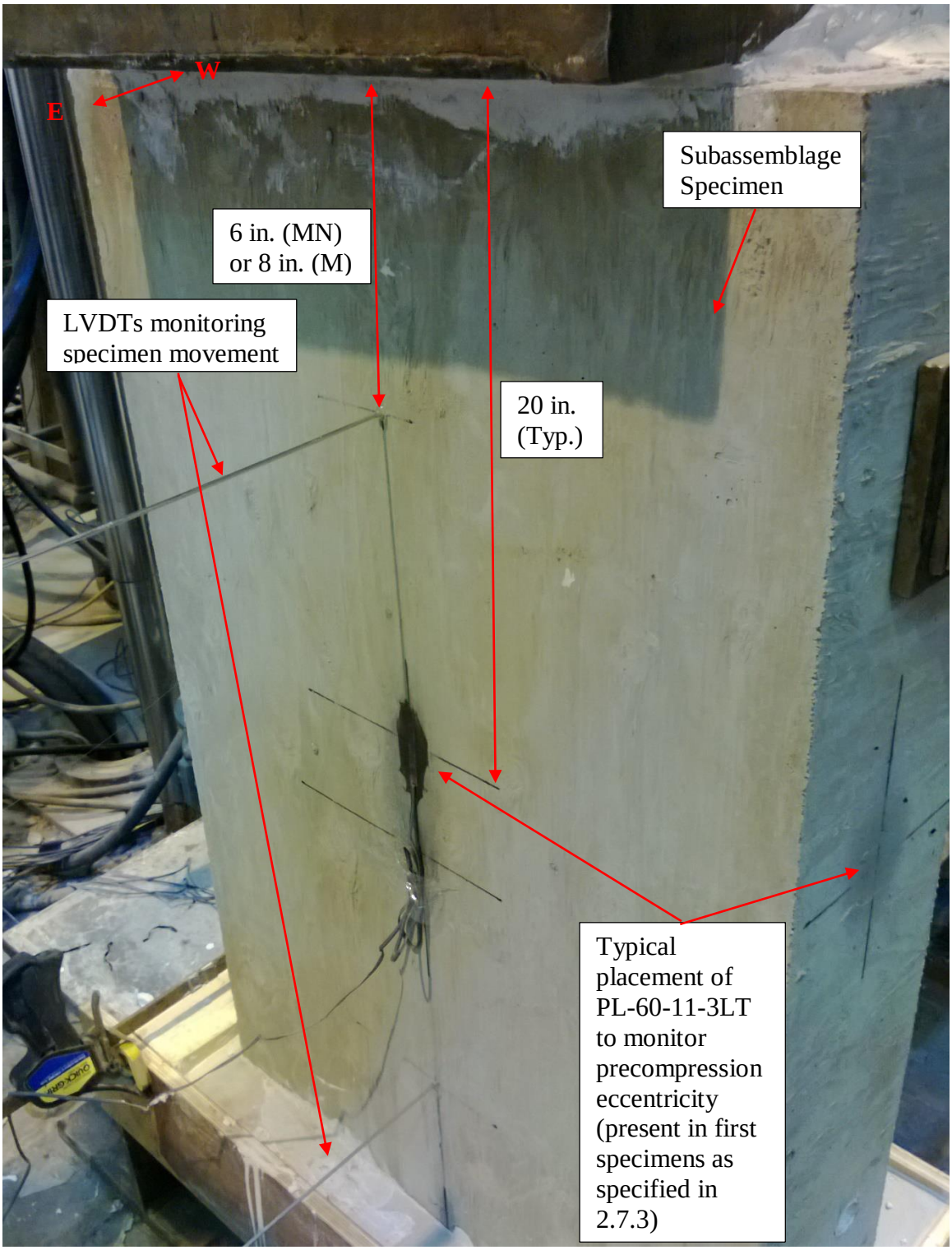

Figure 2-11: Rear view of instrumentation used to monitor typical subassemblage specimen.

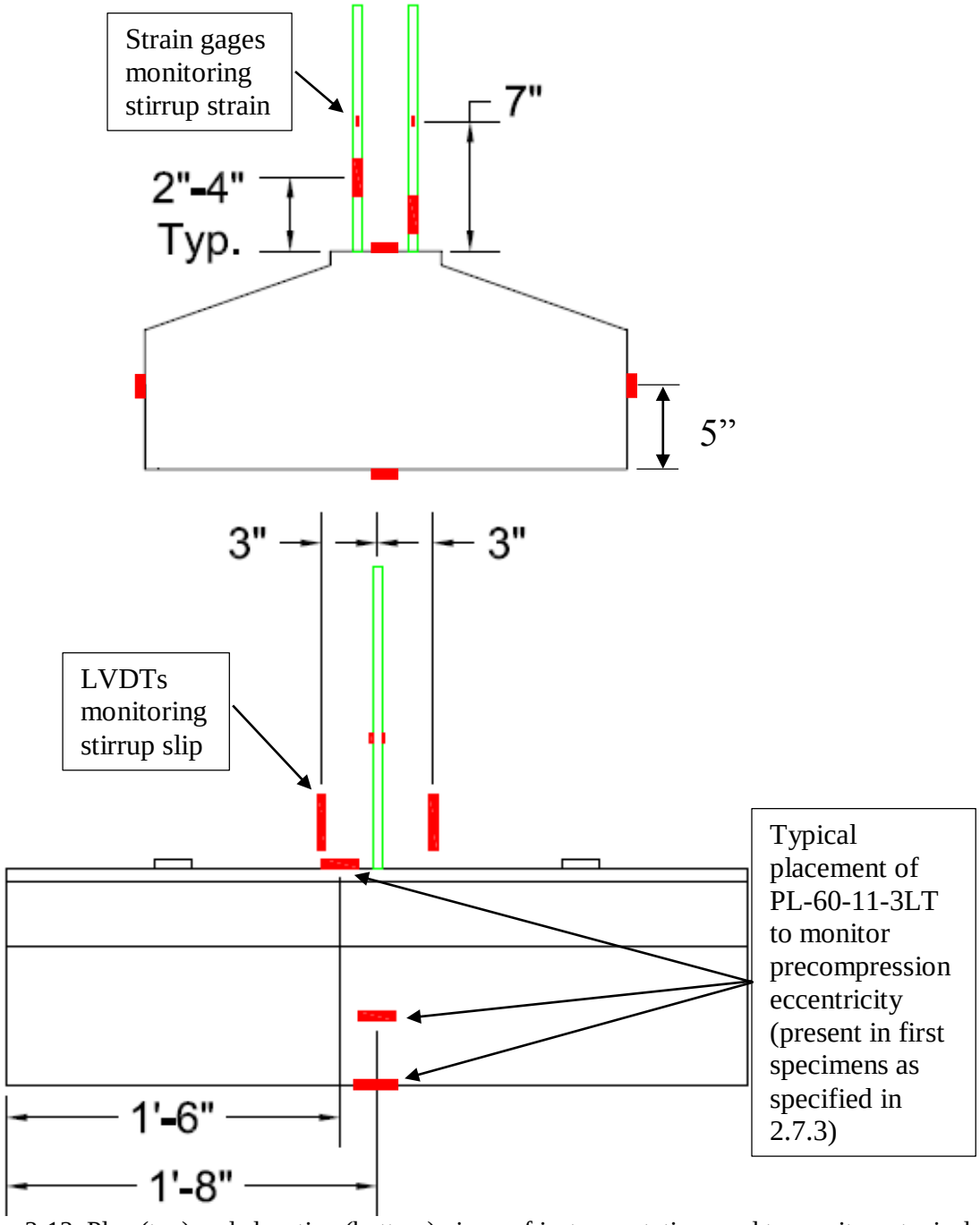

Figure 2-12: Plan (top) and elevation (bottom) views of instrumentation used to monitor a typical subassemblage specimen.

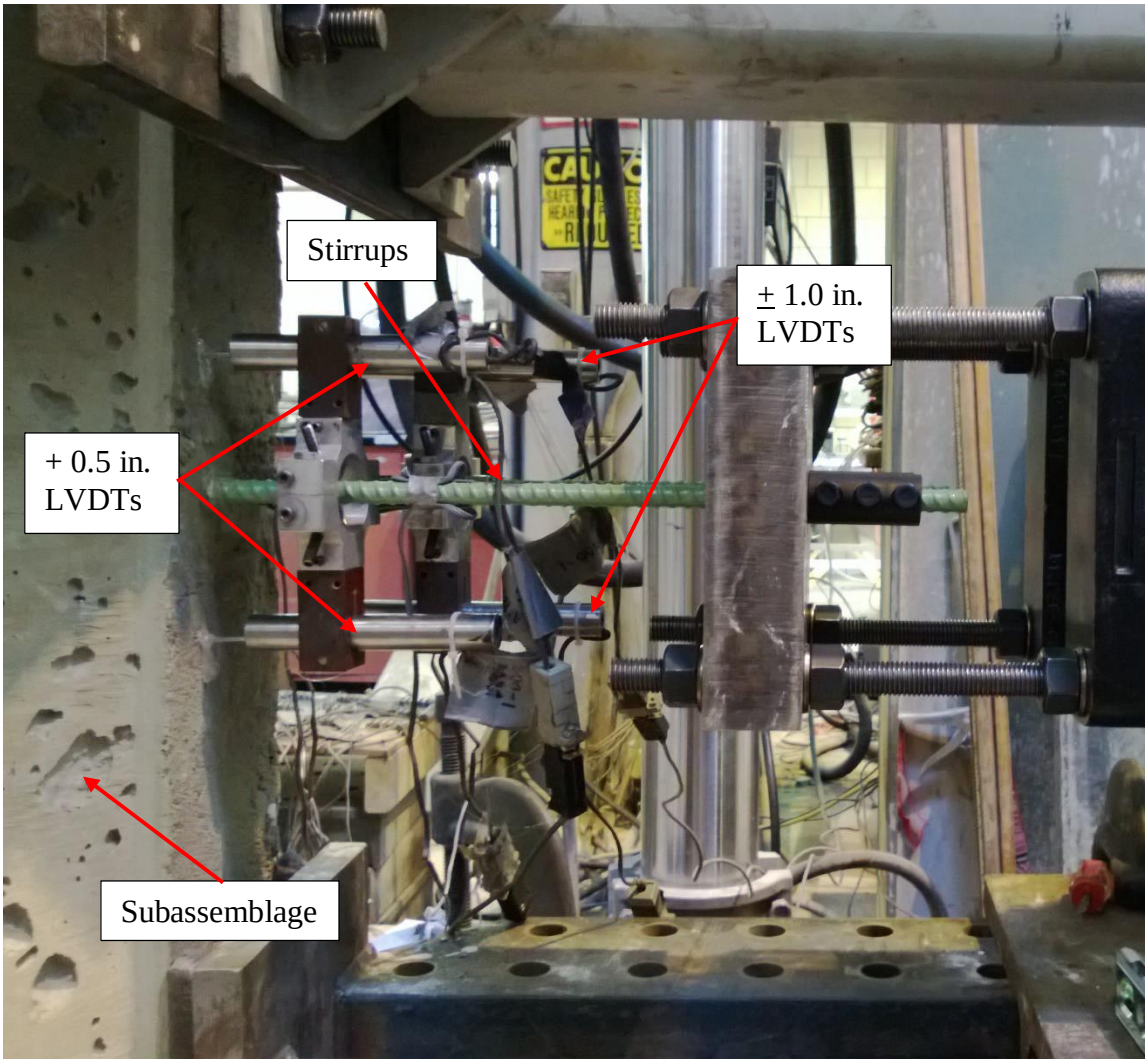

Figure 2-13: Pairs of LVDT's attached to each stirrup leg to measure slip.

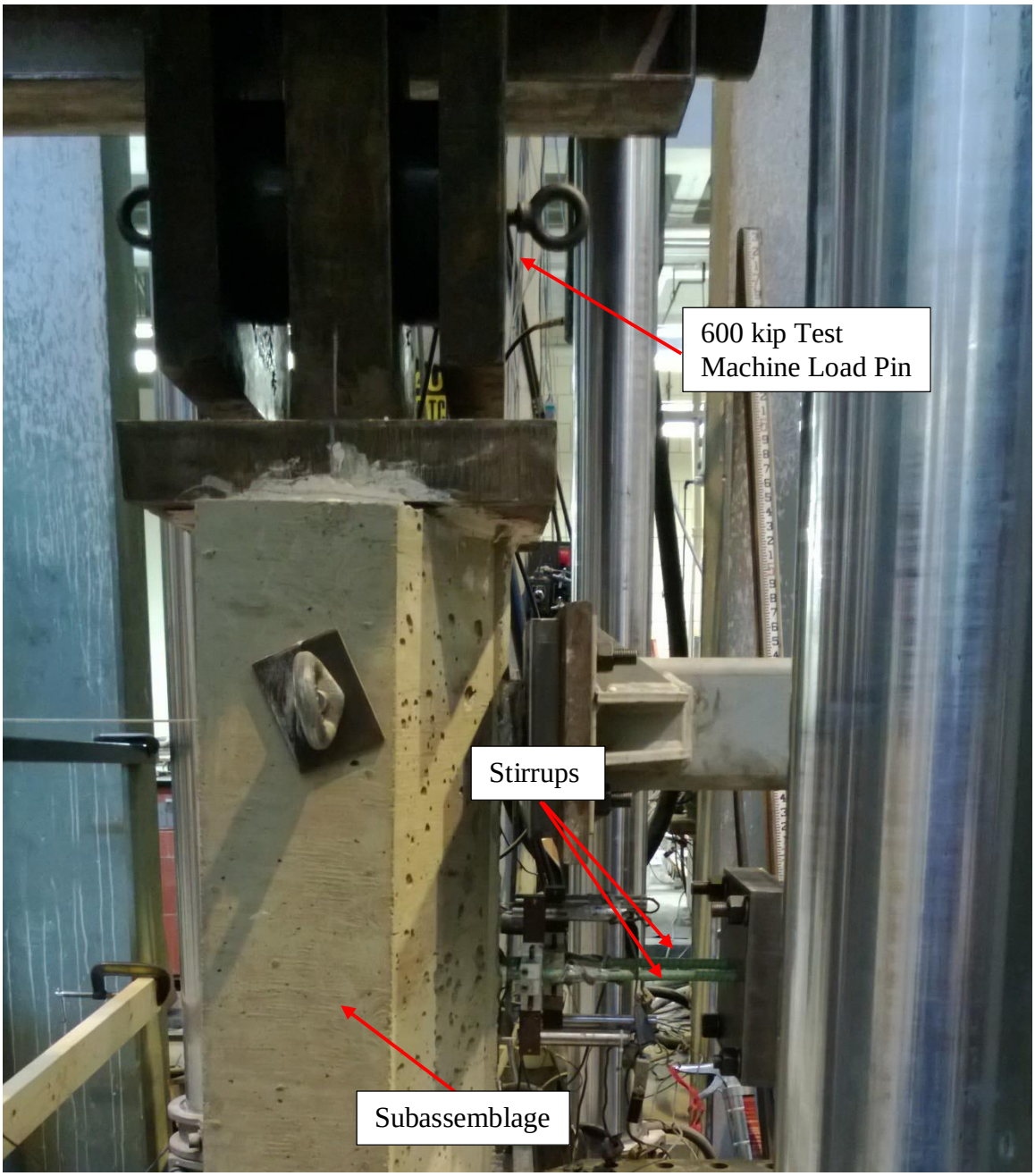

Figure 2-14: Load pin applied nominal precompressive force to subassemblage specimens.

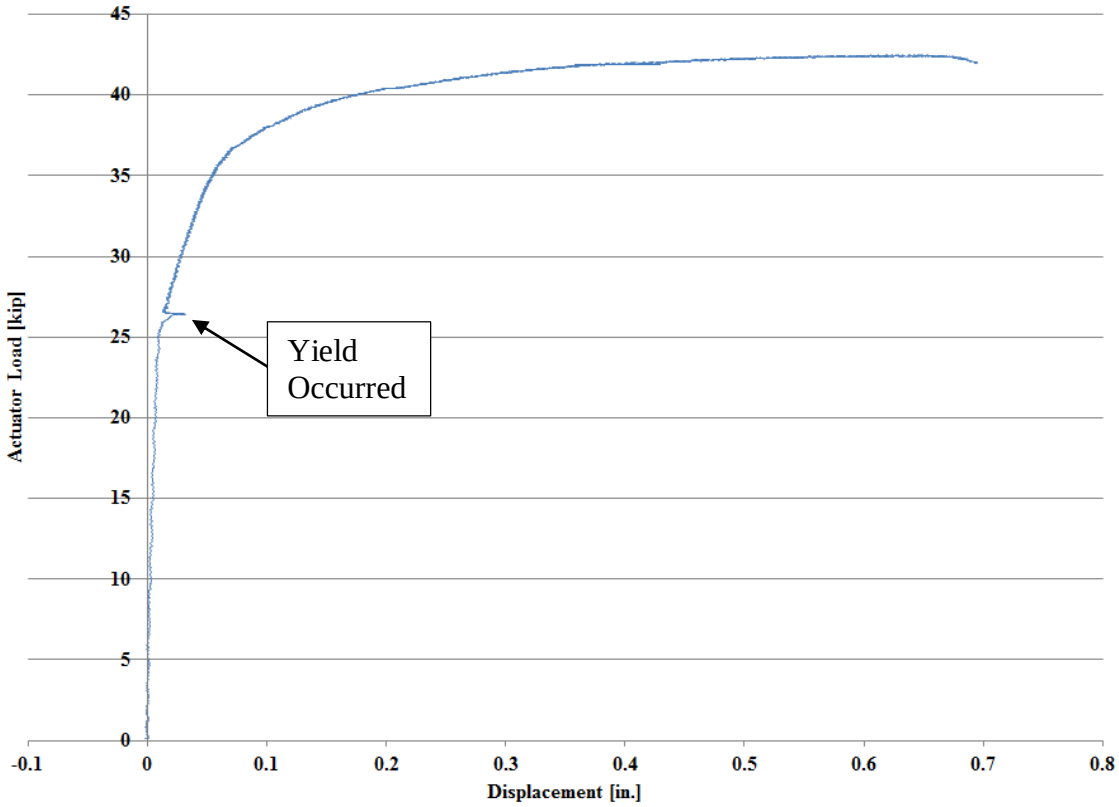

Figure 2-15: Measured slip for the south bar during the 8.0MN_WC_30A test.

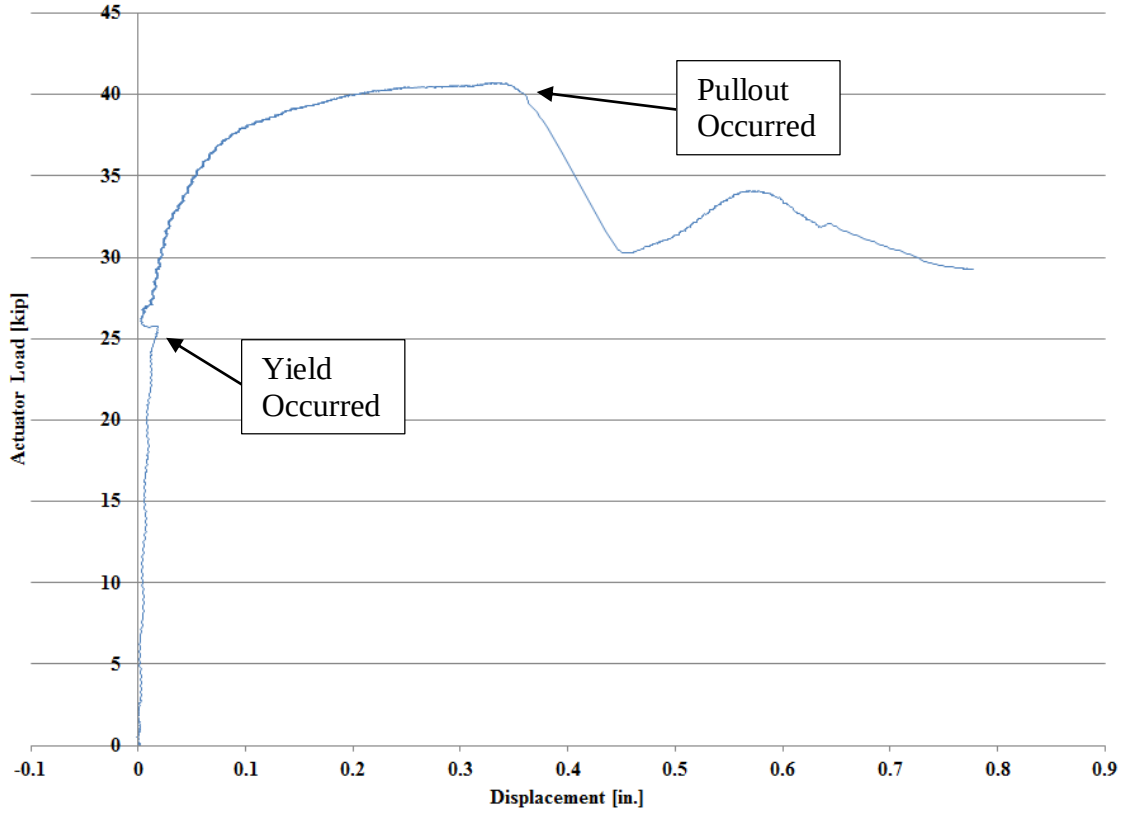

Figure 2-16: Measured slip for the north bar during the 8.0M_NC_20A test.

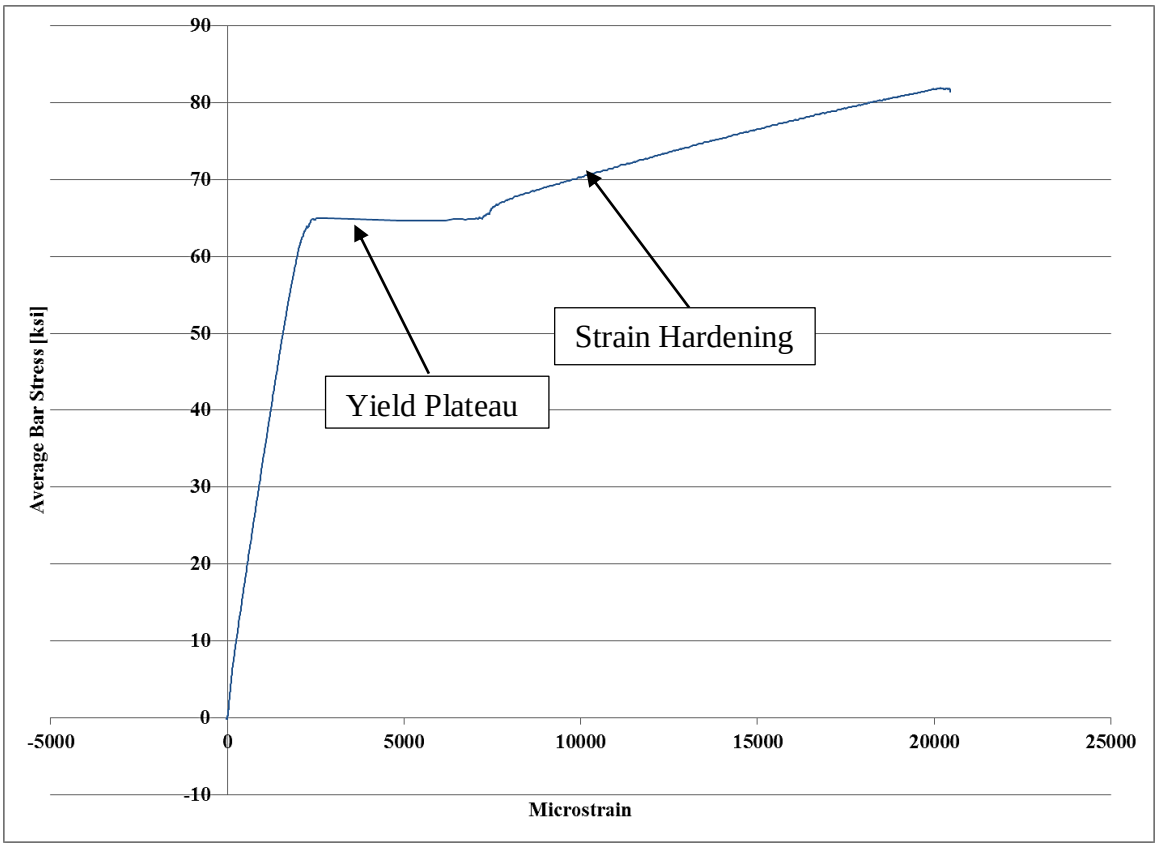

Figure 2-17: Average bar stress vs axial bar strain in the north bar for the 6.4M_NC_20A subassemblage test.

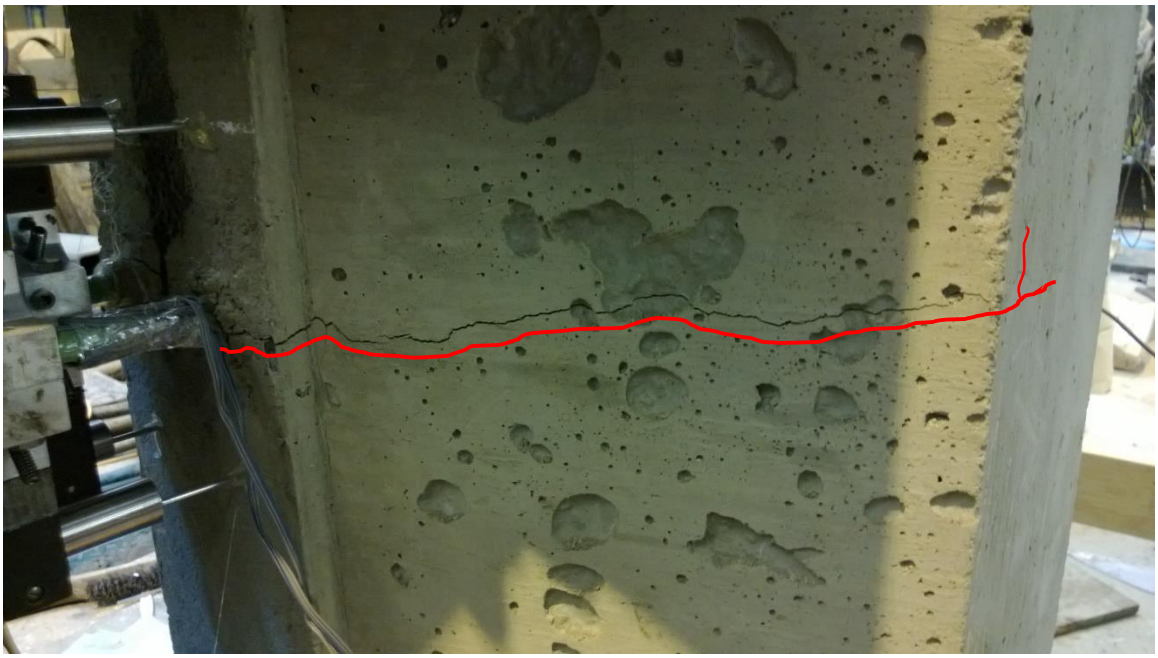

Figure 2-18: 8.0M_WC_20A splitting cracks at failure on the angled face of the flange representative of typical concrete splitting failure with minimum applied compressive force.

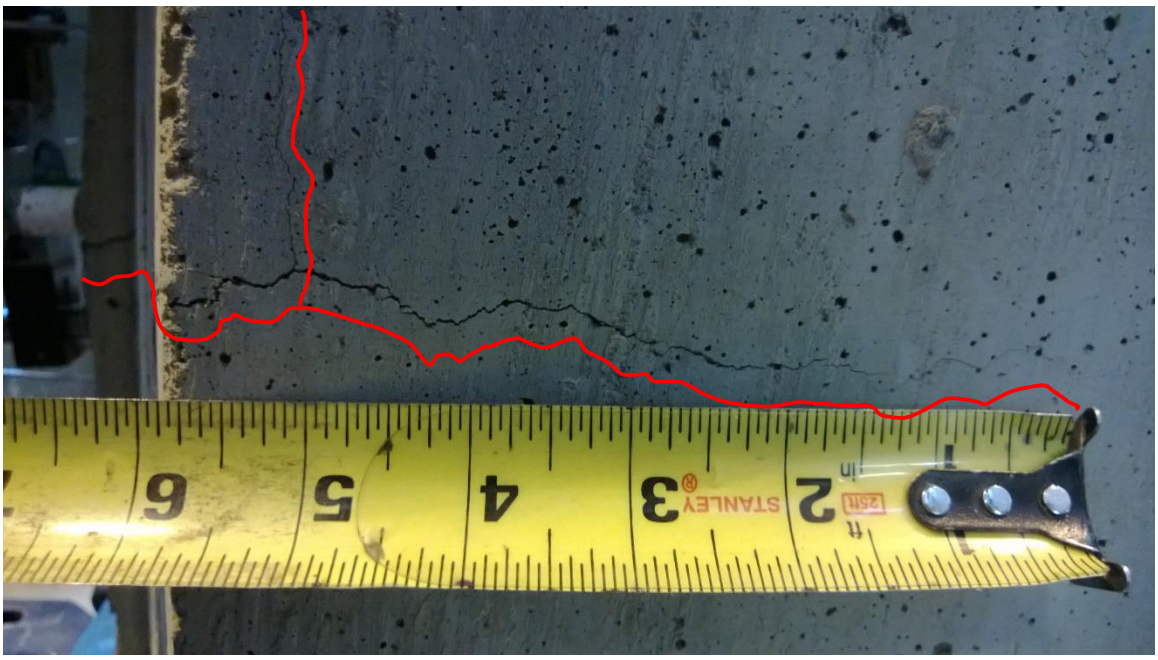

Figure 2-19: 8.0M_WC_20A splitting cracks at failure on side of the flange representative of typical concrete splitting during subassemblage tests with minimum applied compressive force.

Figure 2-20: Splitting cracks following test of 8.0MN_WC_30A test which formed prior to bar fracture.

Figure 2-21: 6.4M_NC_20A cone breakout failure representative of both 6.4M specimen failures.

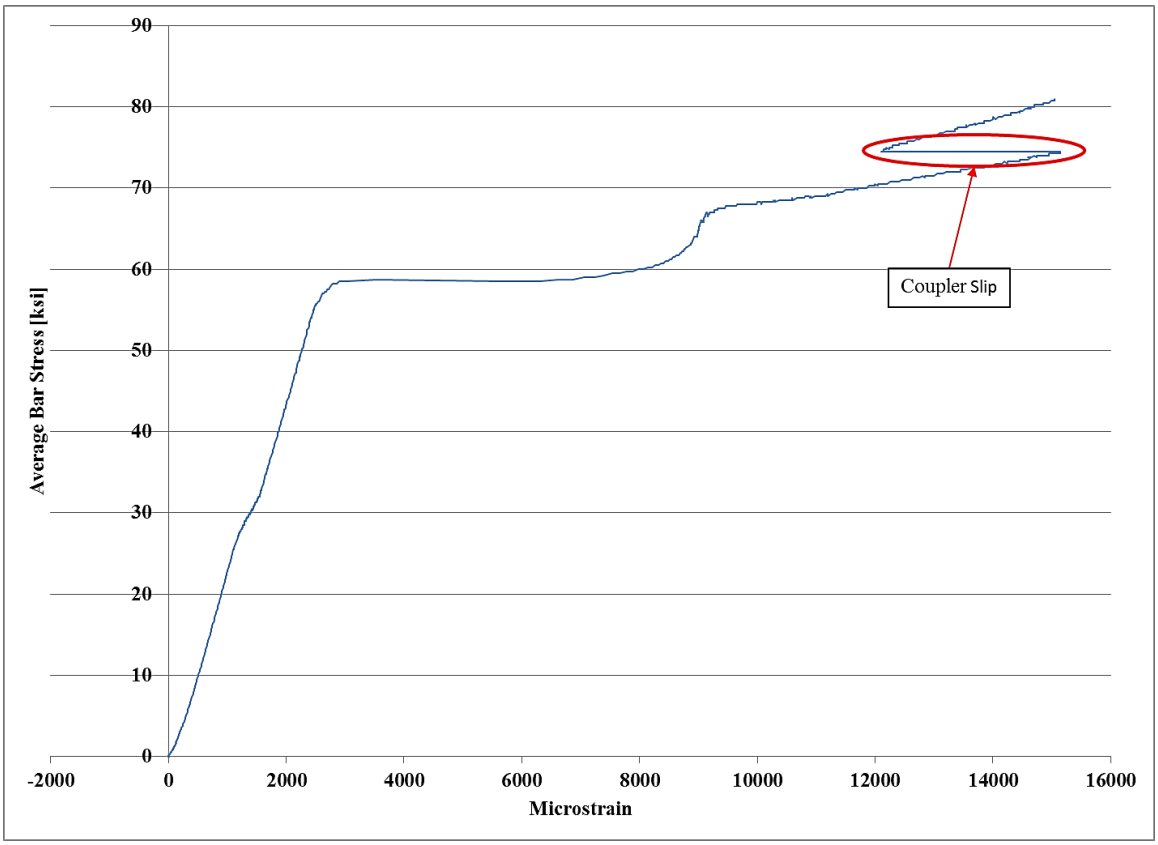

Figure 2-22: Stress-strain curve for 8.0M_NC_20A specimen showing coupler slip.

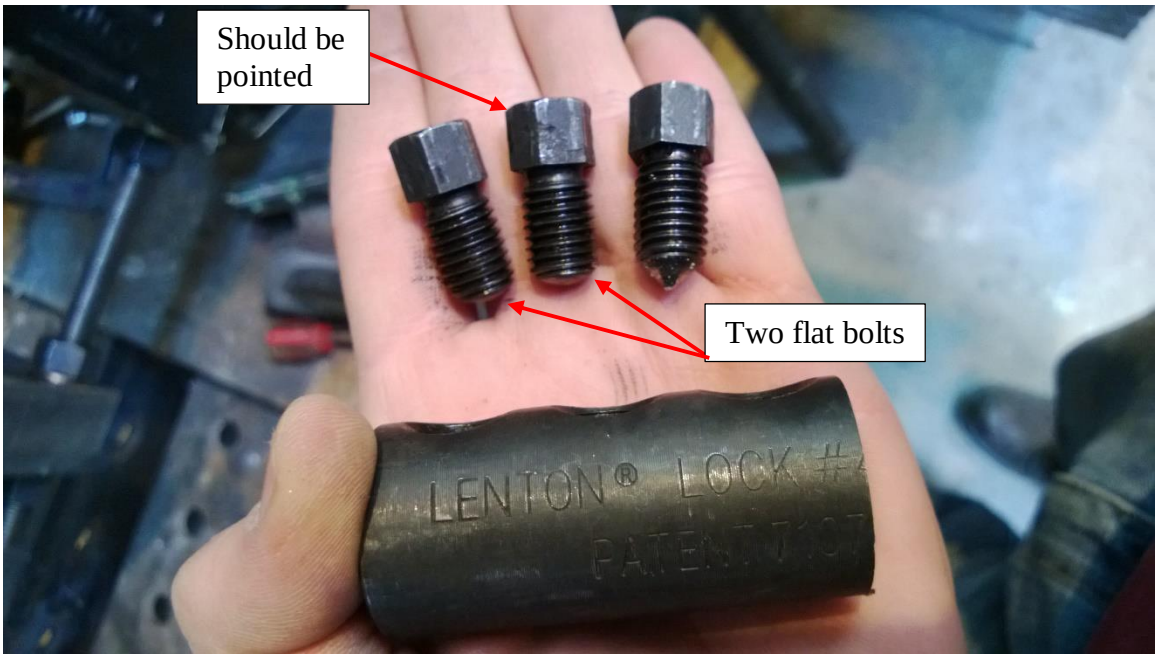

Figure 2-23: Cause of coupler slip during 8.0M_NC_20A subassemblage test.

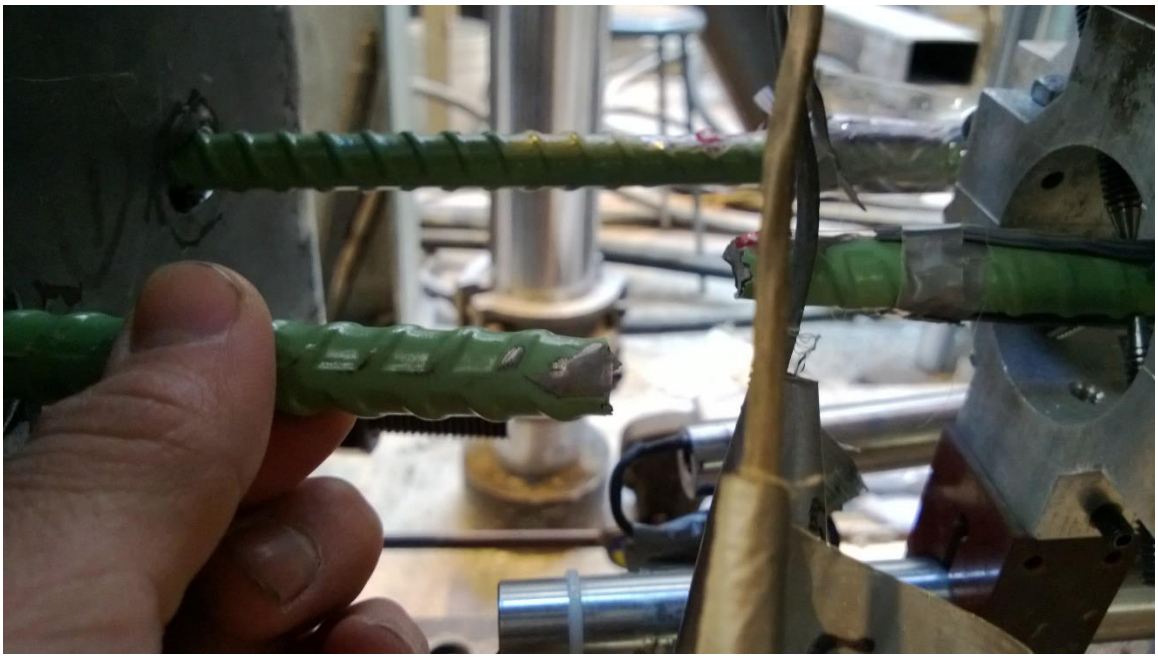
Figure 2-24: Typical stirrup fracture failure during the 8.0M_WC_575B test.

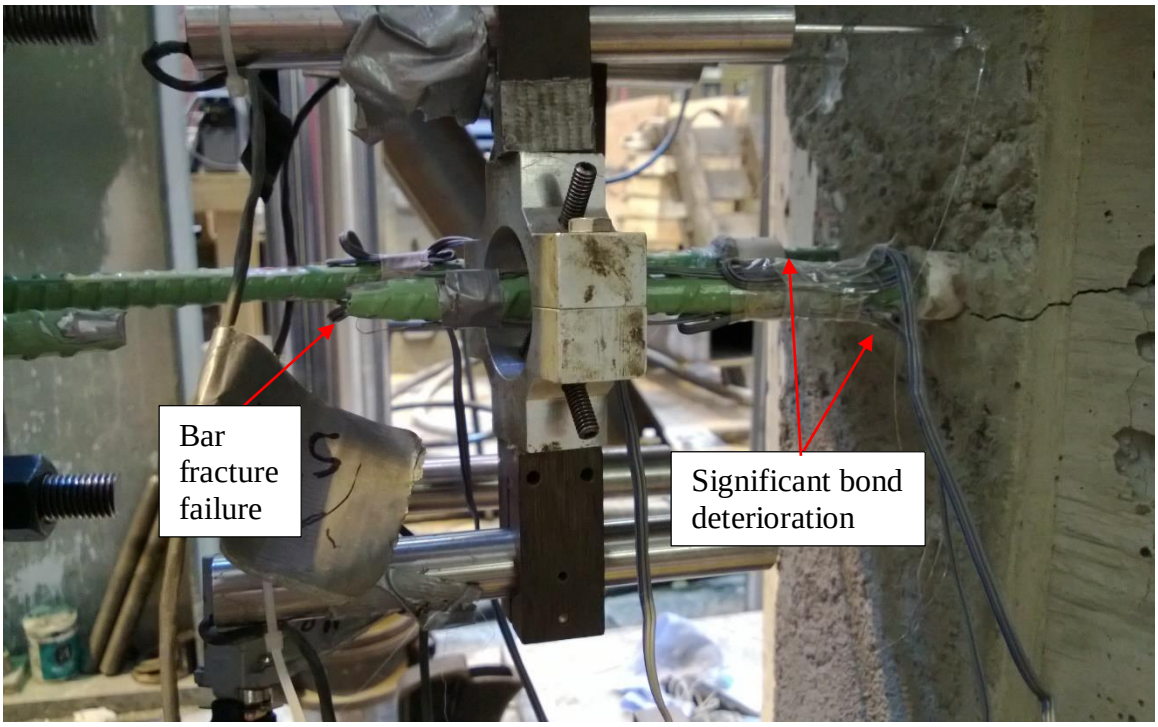

Figure 2-25: Significant bond deterioration prior to bar fracture in 8.0M_WC_020B test.

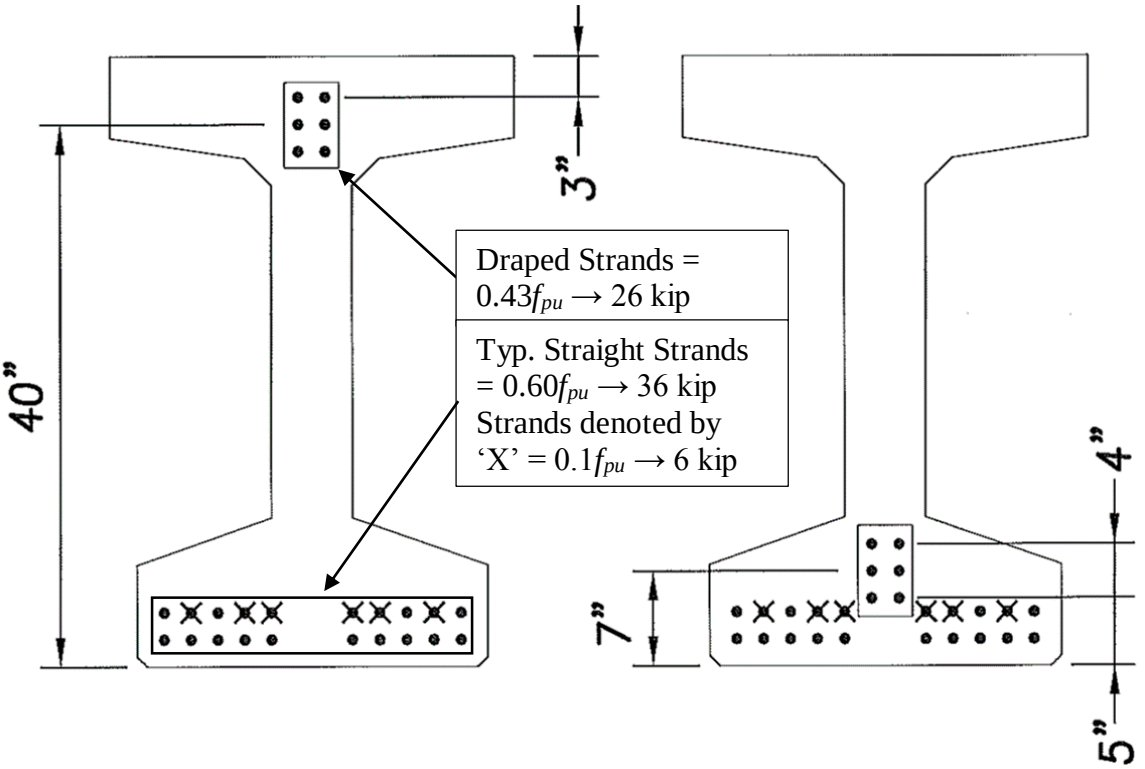

Figure 3-1: Cross-sectional view of prestressing strand layout and stress levels for 45M girder.

Figure 3-2: Plastic sheaths and duct tape used to debond prestressing strands from the concrete in the 36M girder.

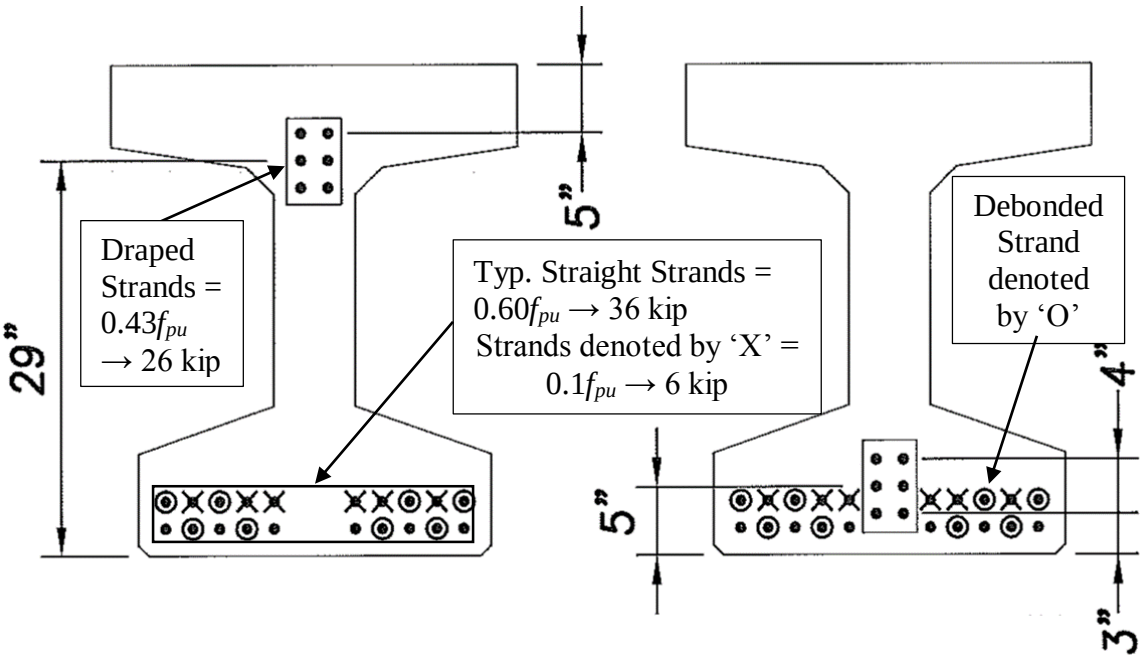

Figure 3-3: Cross-sectional view of prestressing strand layout and stress levels for 36M girder.

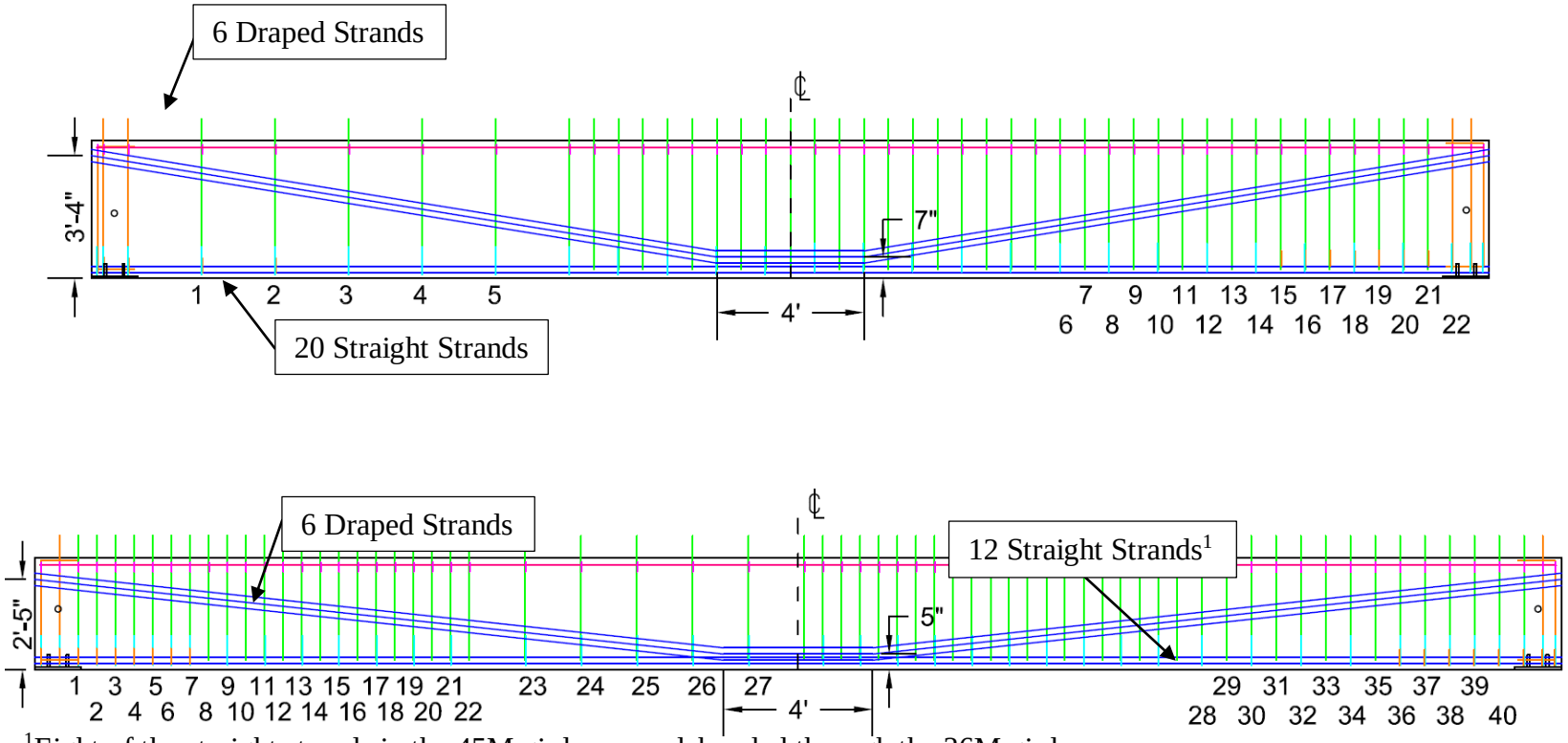

[1]Eight of the straight strands in the 45M girder were debonded through the 36M girder.

Figure 3-4: Elevation view of prestressing strand layout for 45M (top) and 36M (bottom) girders.

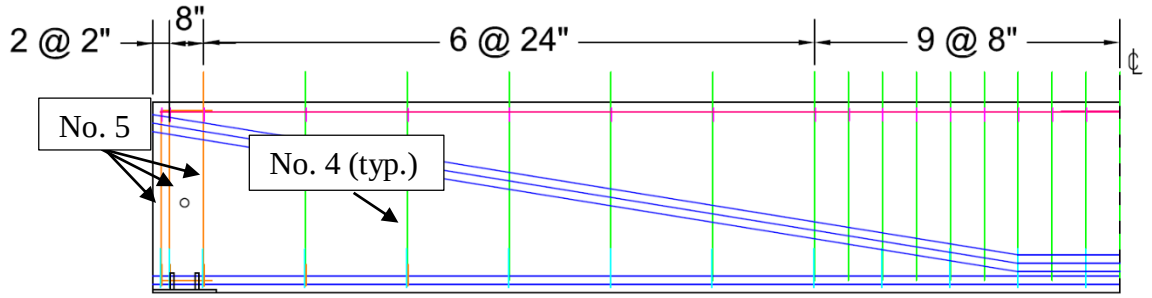

Figure 3-5: Transverse reinforcement layout for the 45M_24W girder end.

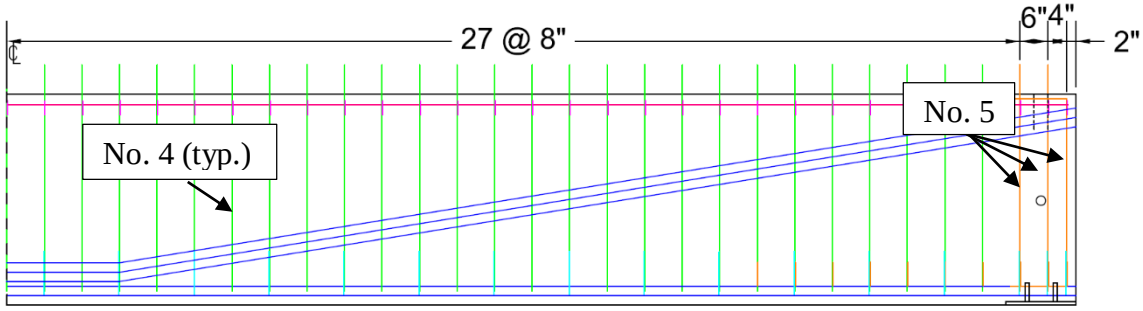

Figure 3-6: Transverse reinforcement layout for the 45M_8W girder end.

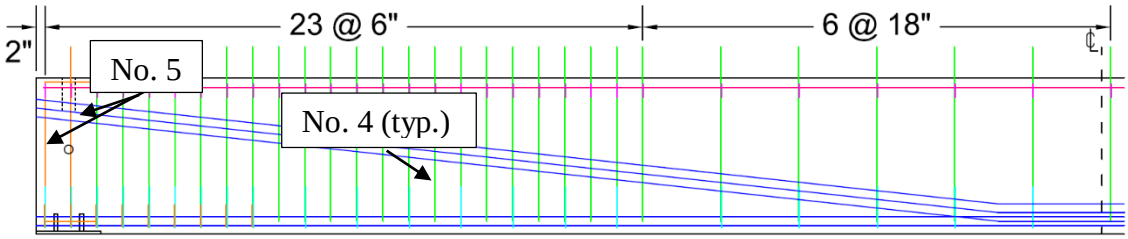

Figure 3-7: Transverse reinforcement layout for the 36M_18F girder end.

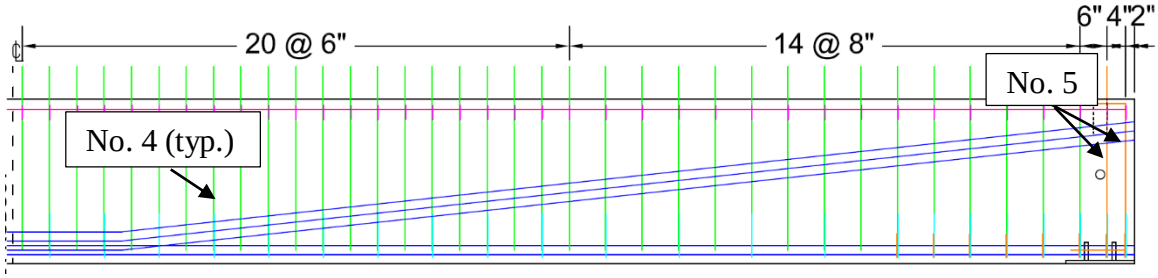

Figure 3-8: Transverse reinforcement for the 36M_8W girder end.

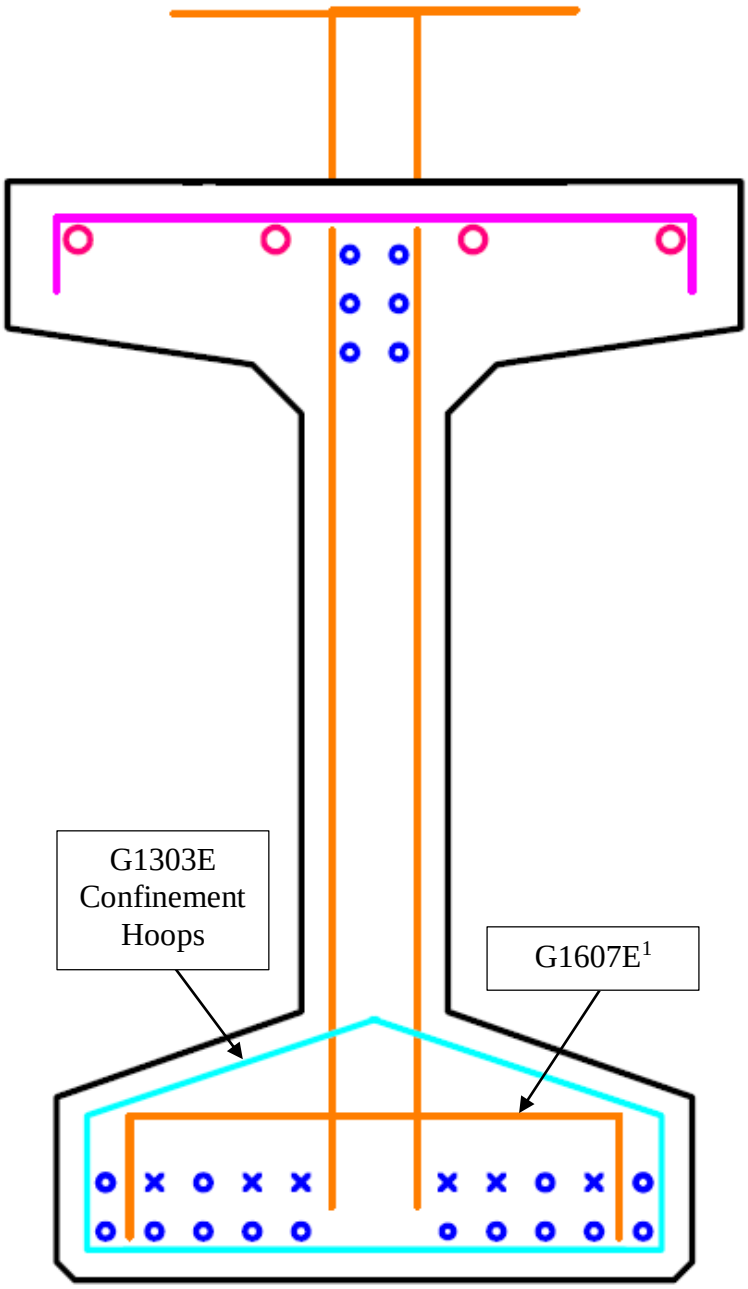

[1] Only present at girder ends (i.e., within 1.5*h* from ends) to prevent bursting

Figure 3-9: Cross-sectional view of 45M girder showing prestressing strand confinement hoops for a typical M-shaped girder.

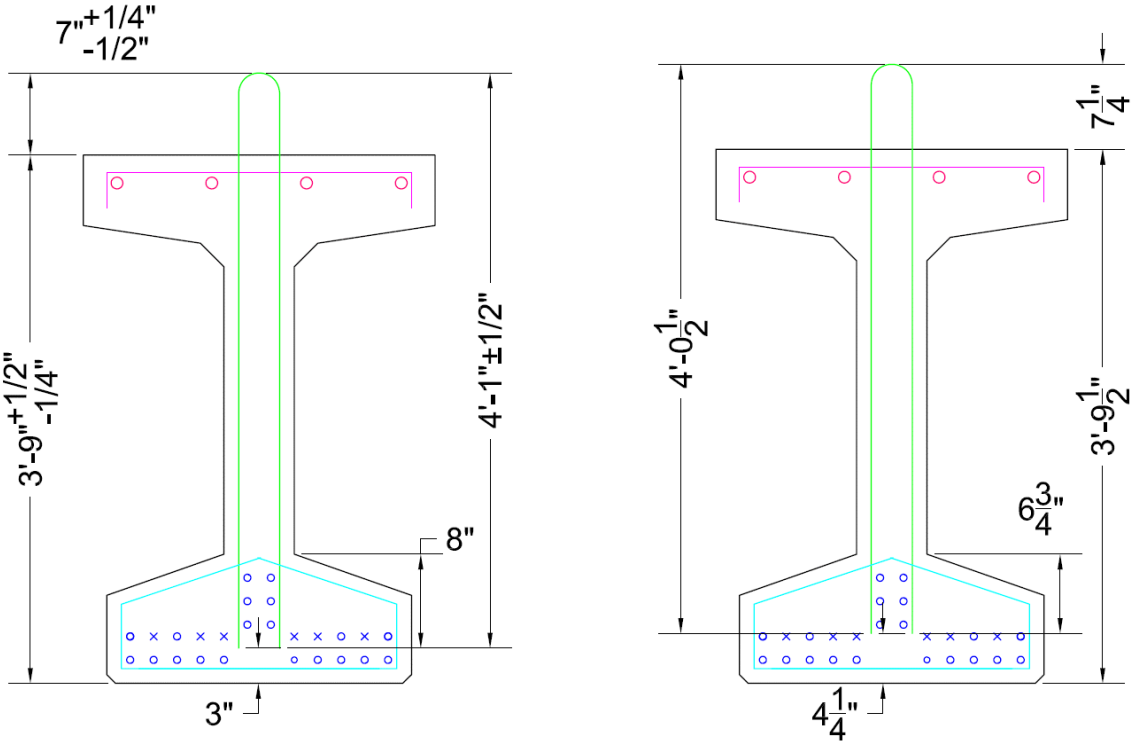

Figure 3-10: 45M girder fabrication tolerances (left) affecting stirrup leg anchorage depth and worst case anchorage depth scenario (right).

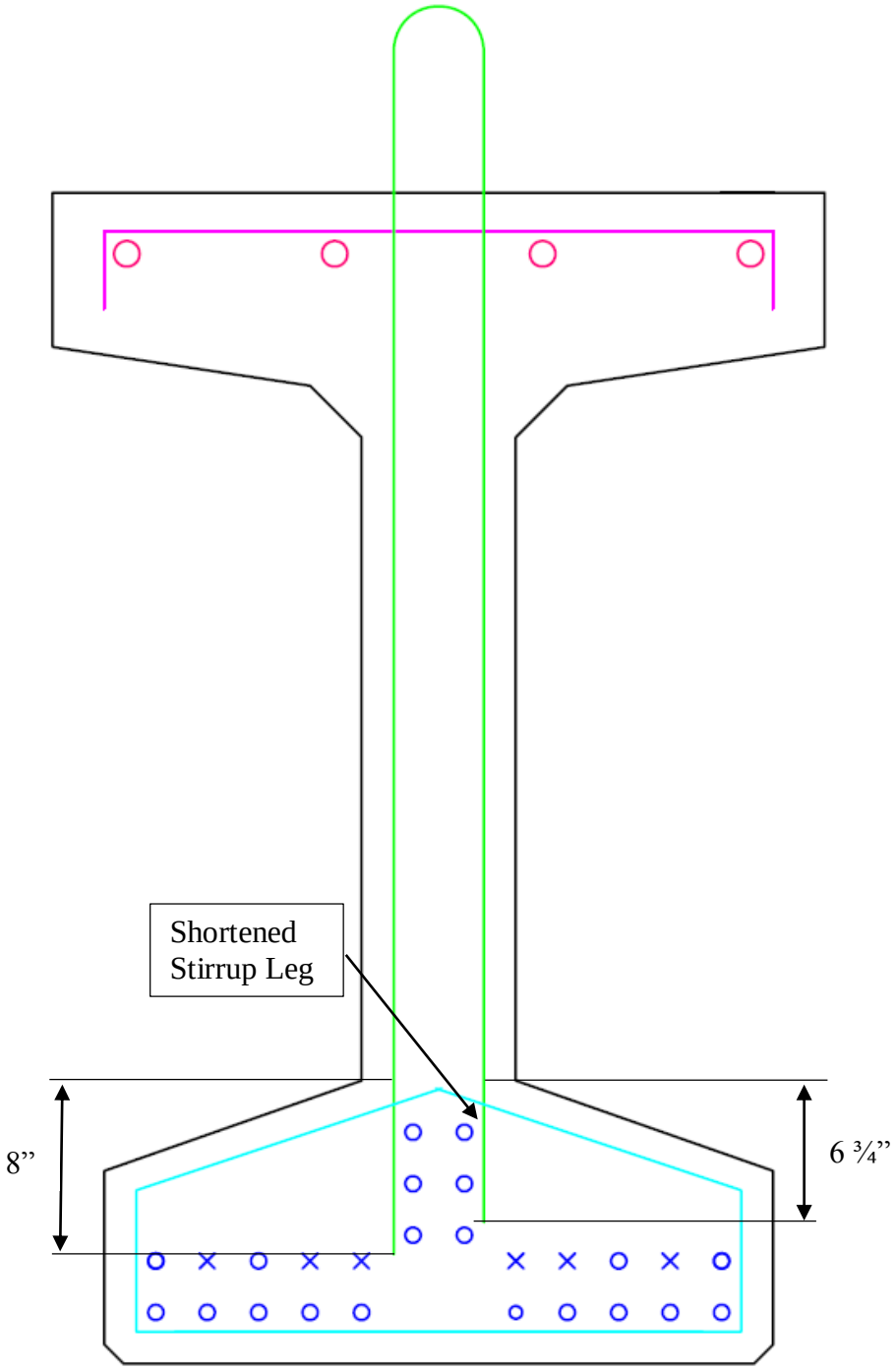

Figure 3-11: Stirrup leg anchorage depths for the 45M girder representing the typical anchorage depths for an M-shaped girder.

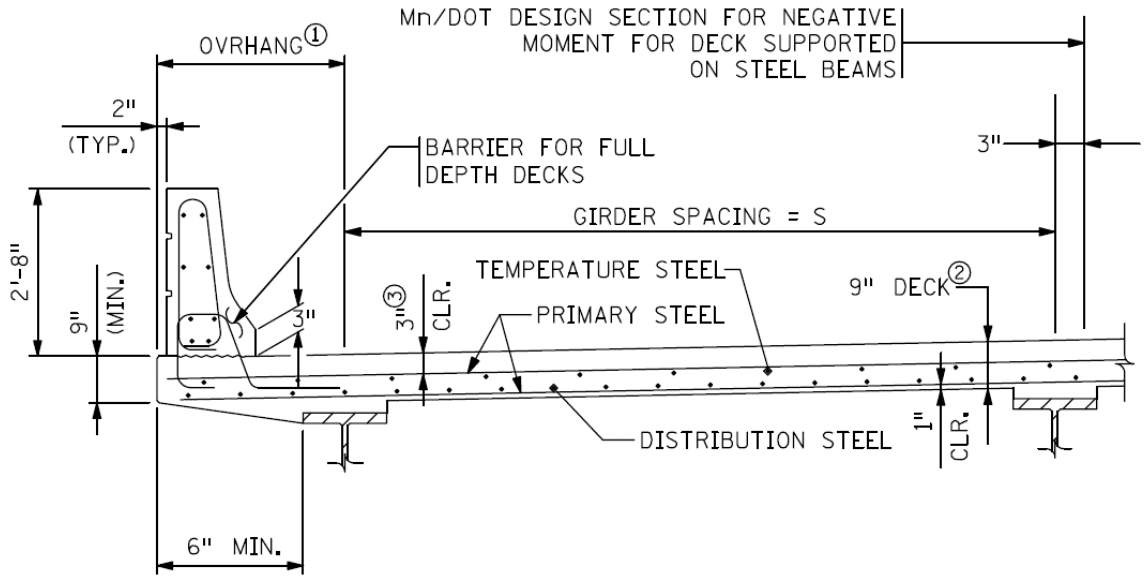

Figure 3-12: Layout of steel in a typical MnDOT concrete deck (from MnDOT LRFD Bridge Manual, 2010)

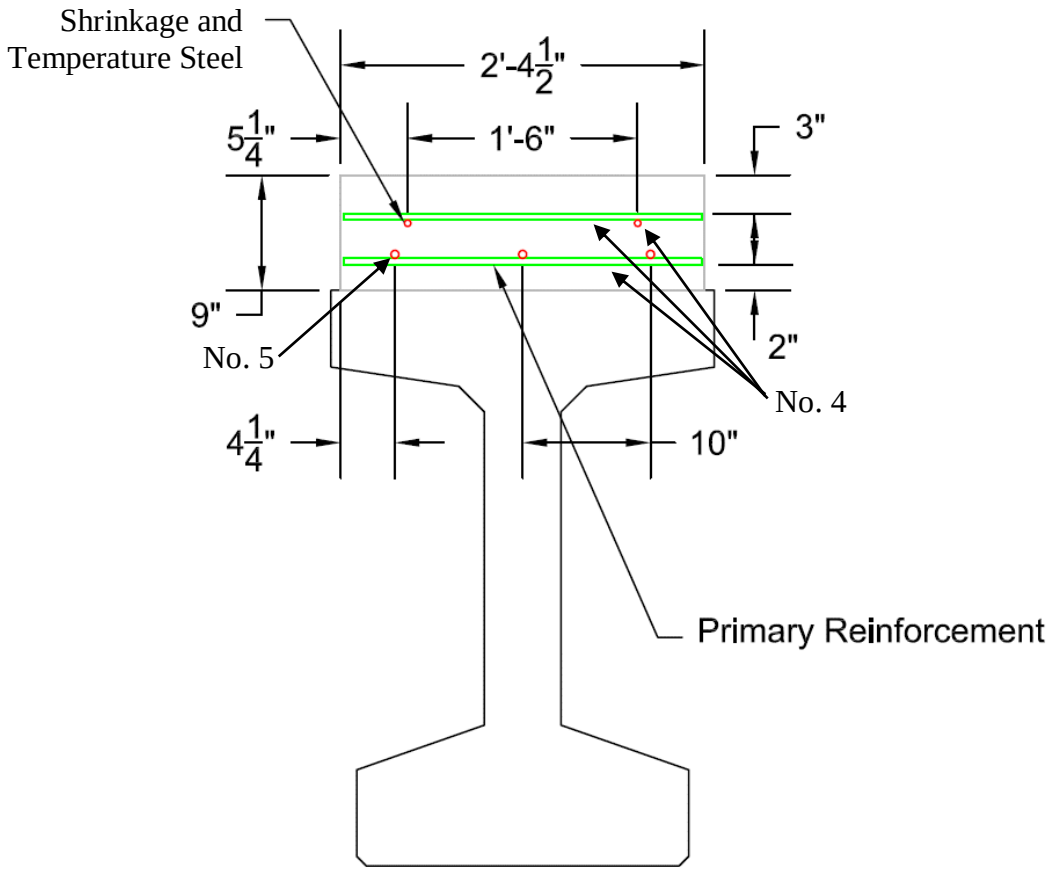

Figure 3-13: Cross-sectional view of deck dimensions and reinforcement layout

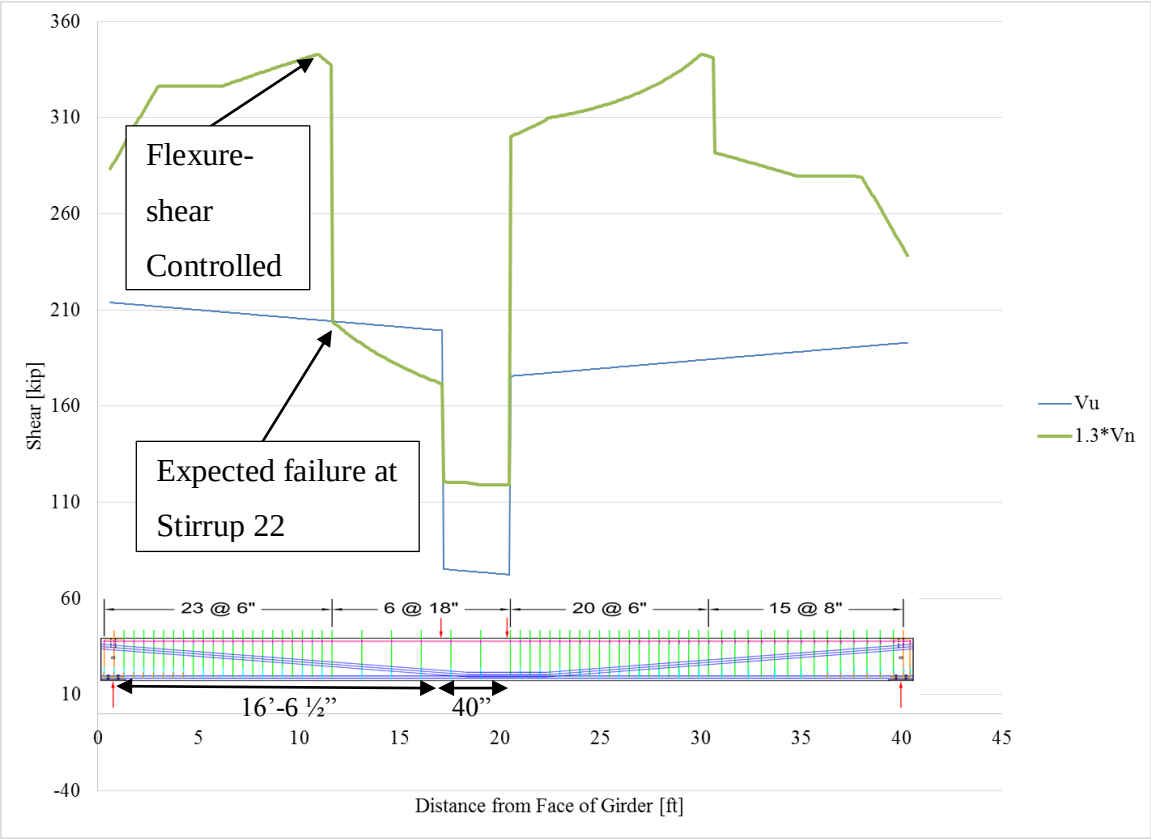

Figure 3-14: Increased nominal shear capacity ($1.3V_n$) and applied shear (V_u) required to reach capacity at Stirrup #22 of 36M_18F, which corresponded to a total applied load of 248 kip.

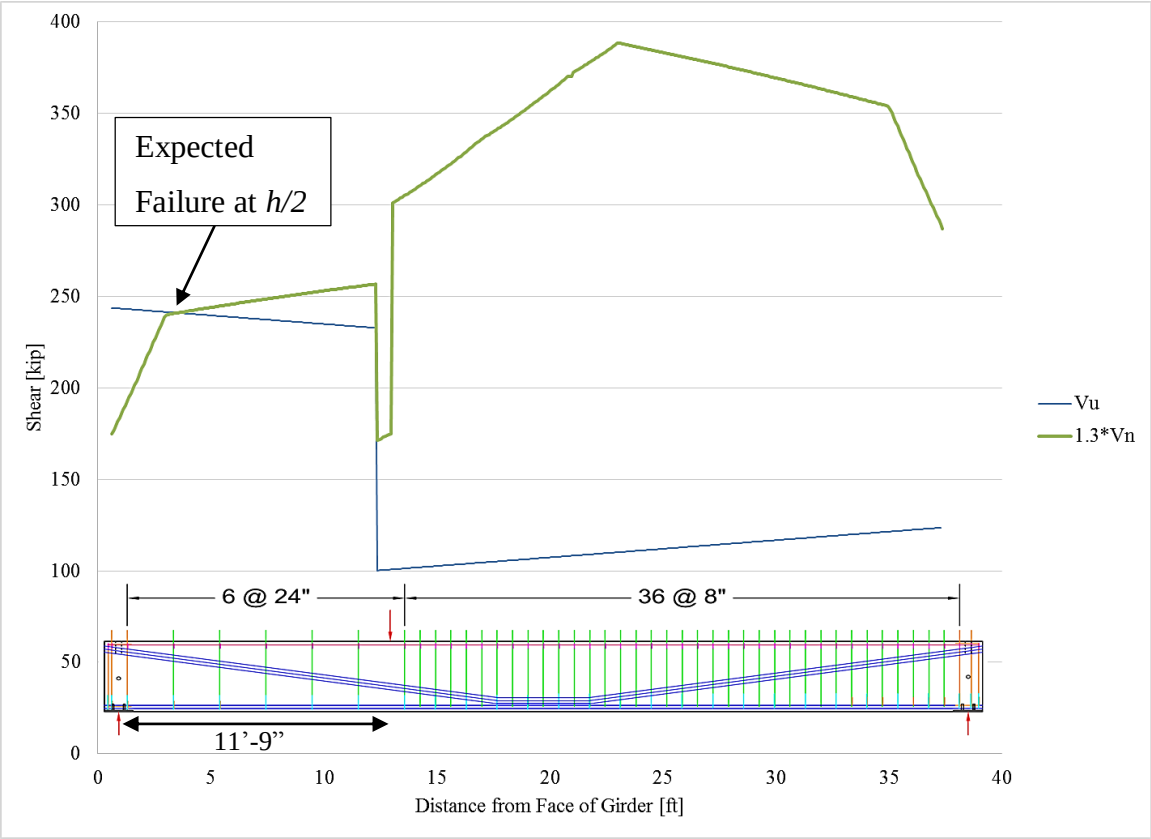

Figure 3-15: Increased nominal shear capacity ($1.3V_n$) and applied shear (V_u) required to reach capacity at critical section of 45M_24W, which corresponded to applied load of 336 kip.

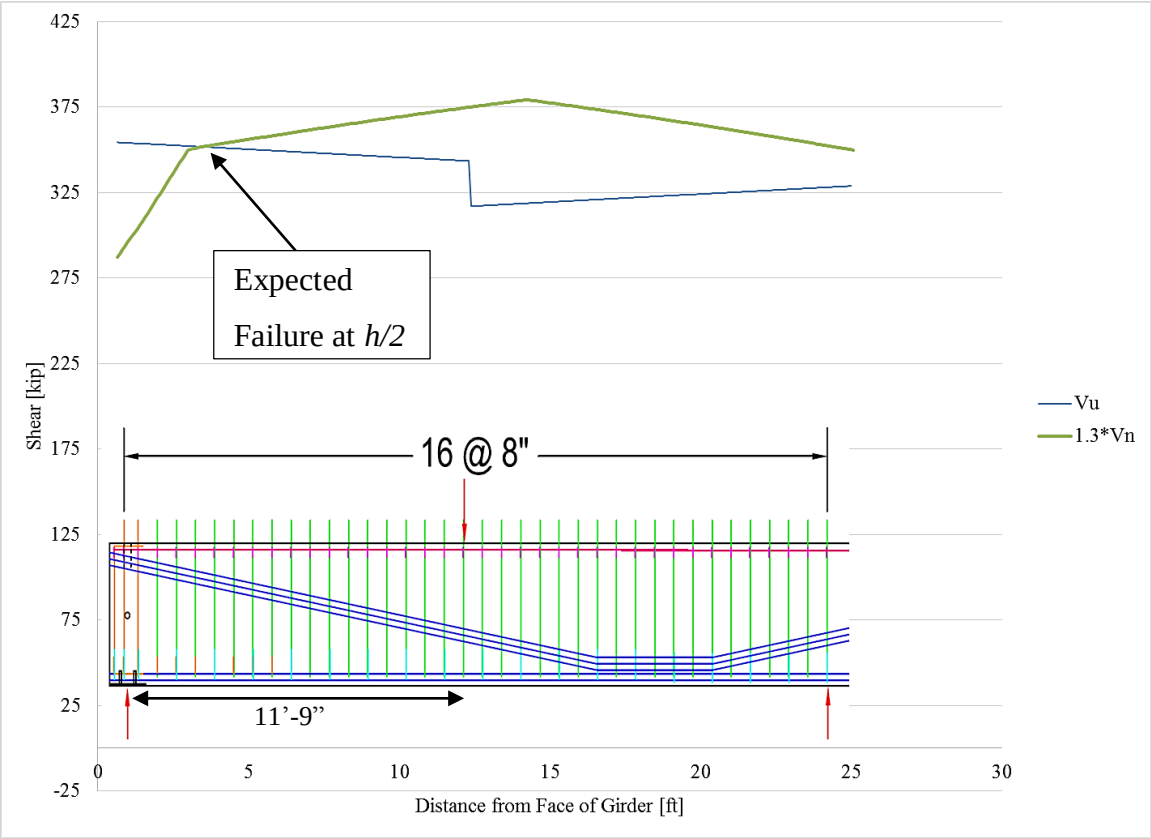

Figure 3-16: Increased nominal shear capacity ($1.3V_n$) and applied shear (V_u) required to reach that capacity at critical section of 45M_8W, which corresponded to applied load of 660 kip.

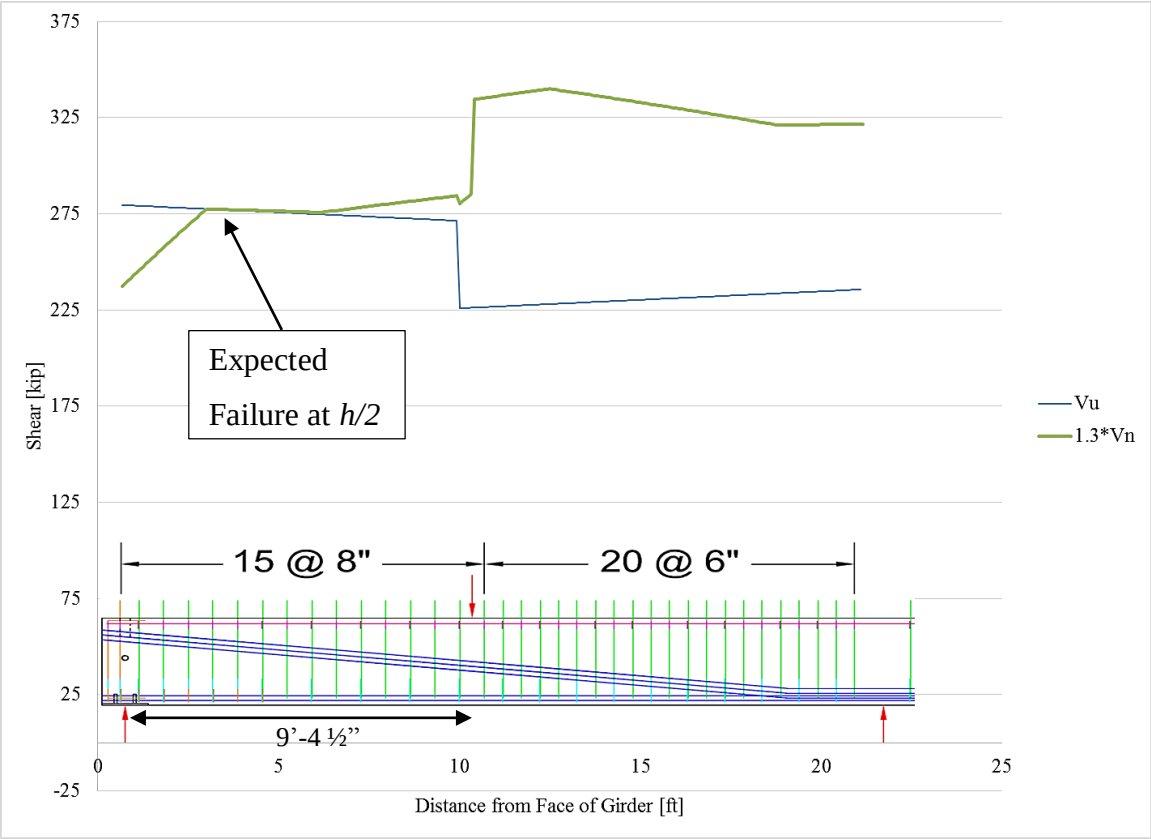

Figure 3-17: Increased nominal shear capacity ($1.3V_n$) and applied shear (V_u) required to reach that capacity at critical section of 36M_8W, which corresponded to applied load of 497 kip.

Figure 3-18: Remaining volume in 36M_18F girder end which was filled by a fifth batch of concrete.

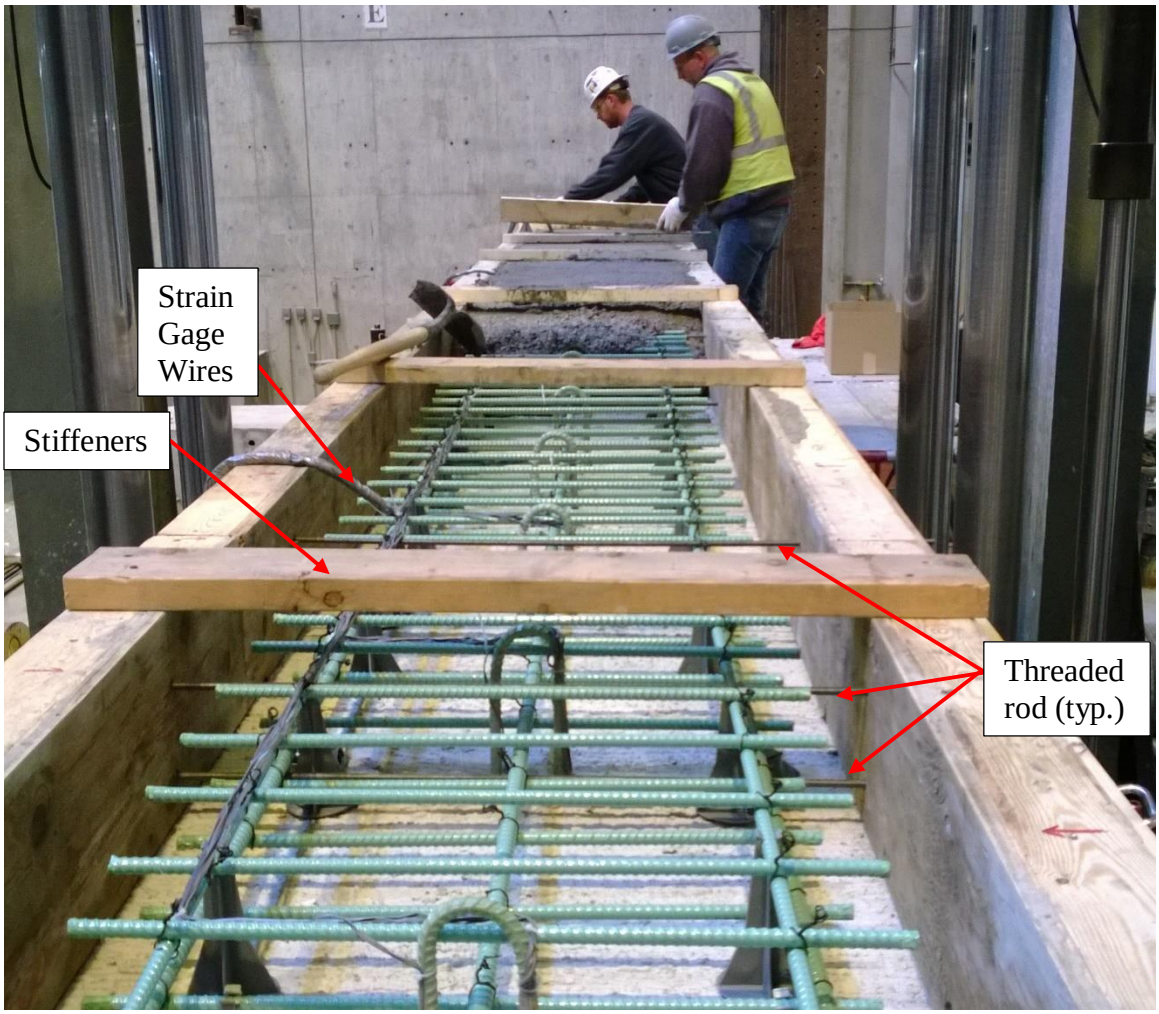

Figure 3-19: Deck casting for 45M girder.

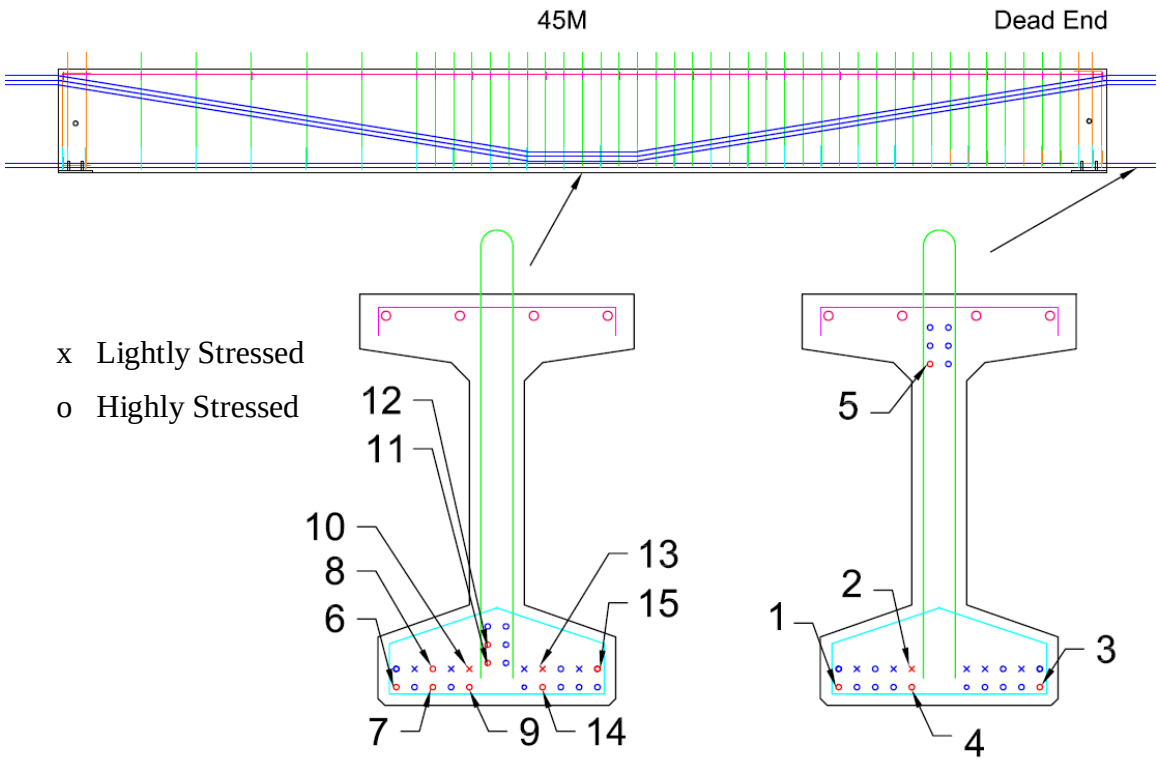

Figure 3-20: Prestressing strand strain gage locations and naming convention for the 45M girder. The cross-sectional view is looking down the girder from the dead end.

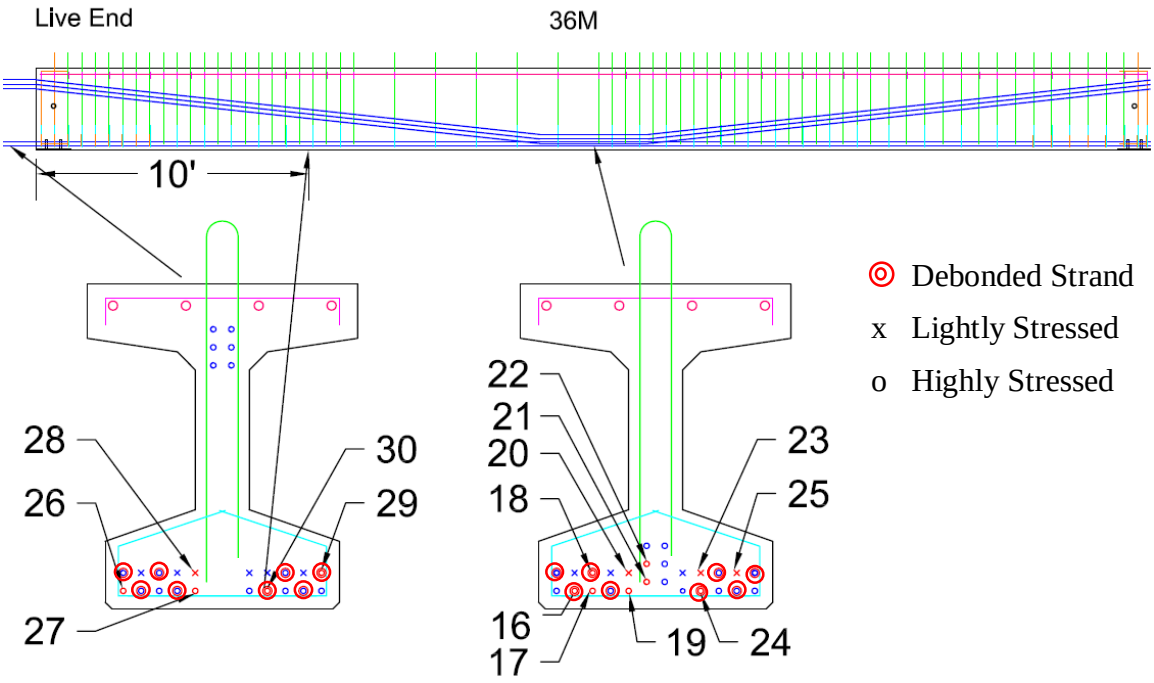

Figure 3-21: Prestressing strand strain gage locations and naming conventions for the 36M girder. The cross-sectional view is looking down the girder towards the live end.

Figure 3-22: Vibrating wire gage placement shown for the 36M girder.

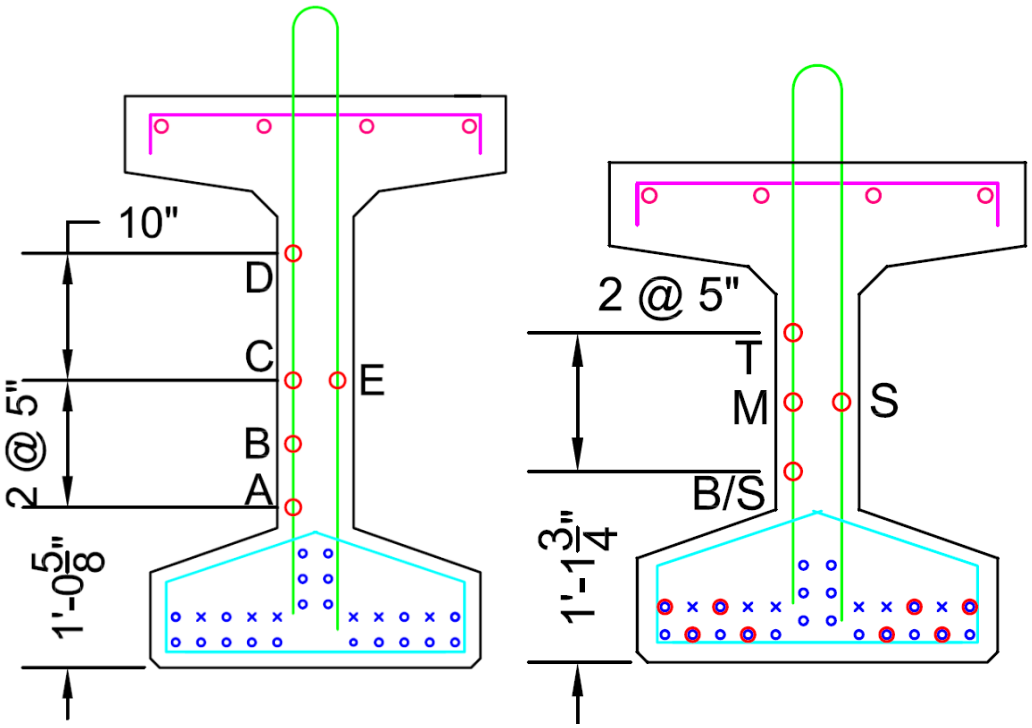

Figure 3-23: Cross-sectional view of strain gage locations for 45M (left) and 36M (right) prestressed concrete girders.

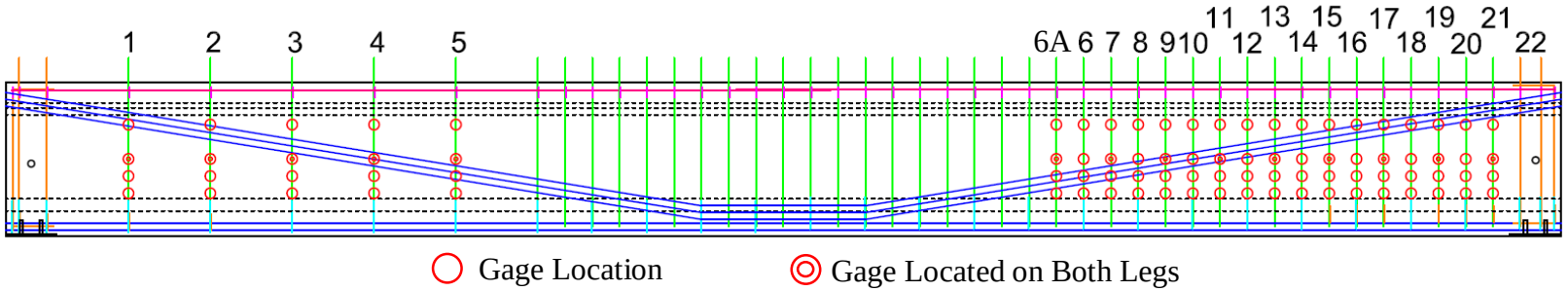

Figure 3-24: Elevation view of strain gage locations for the 45M prestressed concrete girder.

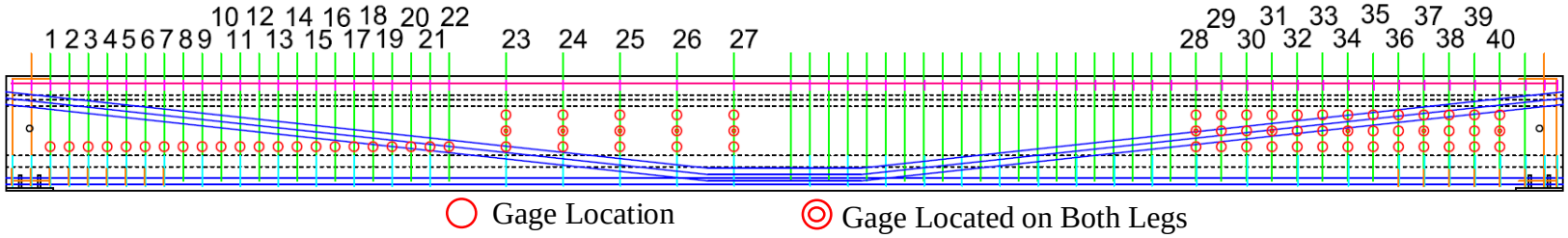

Figure 3-25: Elevation view of strain gage locations for the 36M prestressed concrete girder.

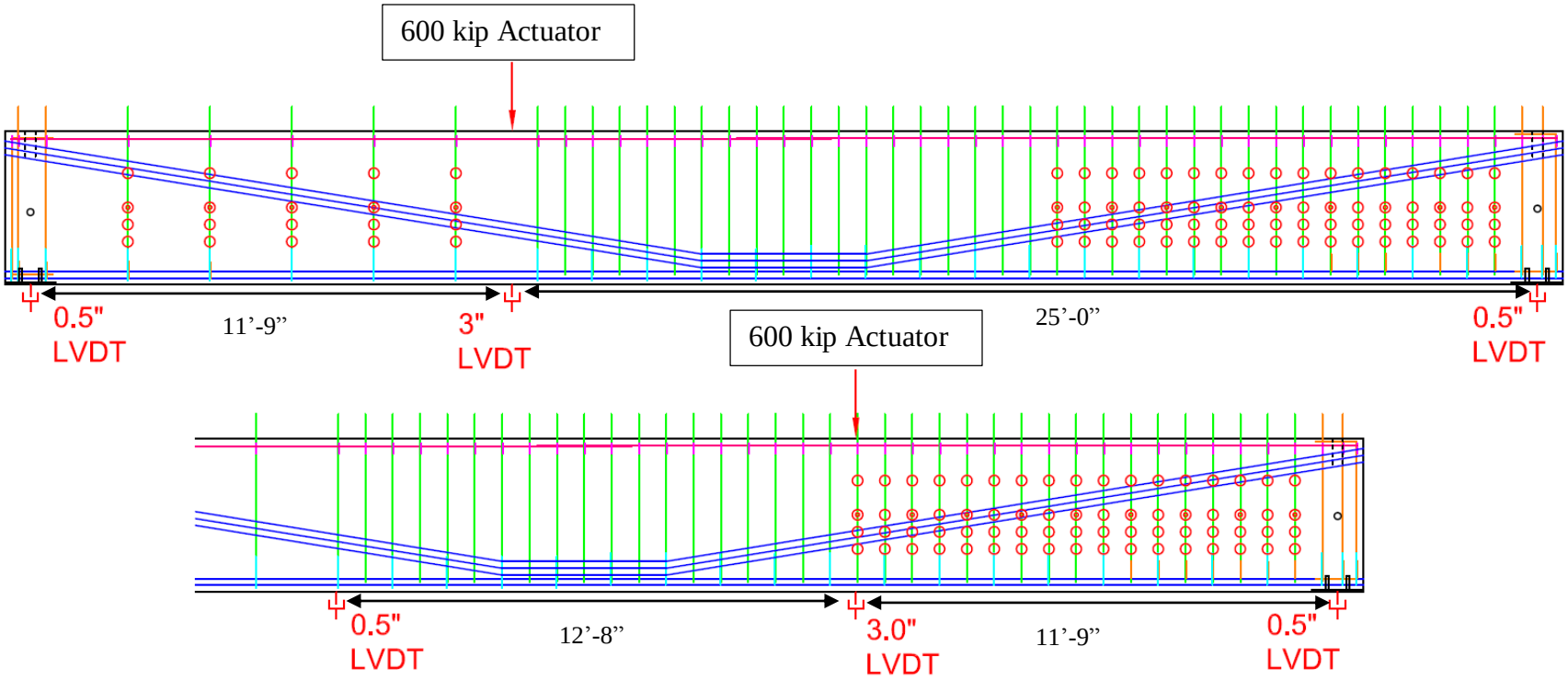

Figure 3-26: LVDT locations for the first (top) and second (bottom) tests on the 45M prestressed concrete girder.

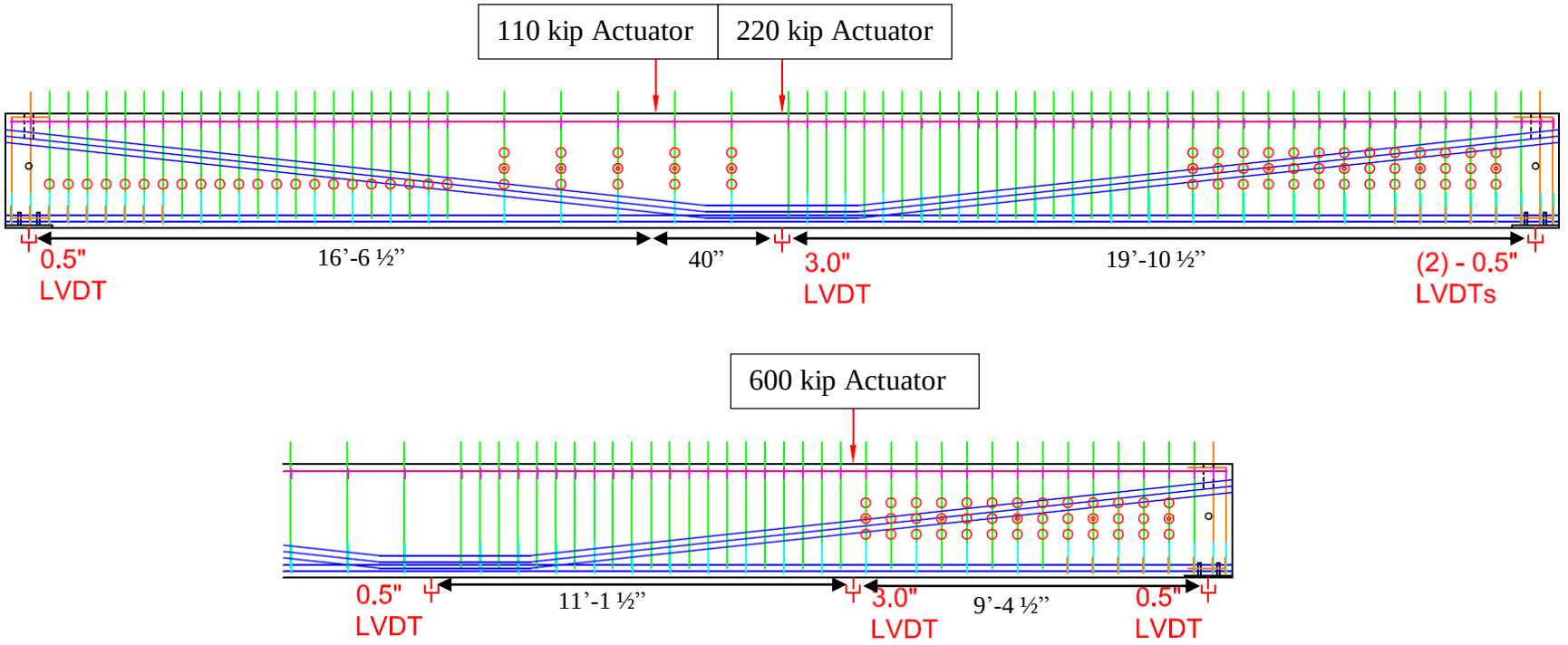

Figure 3-27: LVDT locations for the first (top) and second (bottom) tests on the 36M prestressed concrete girder.

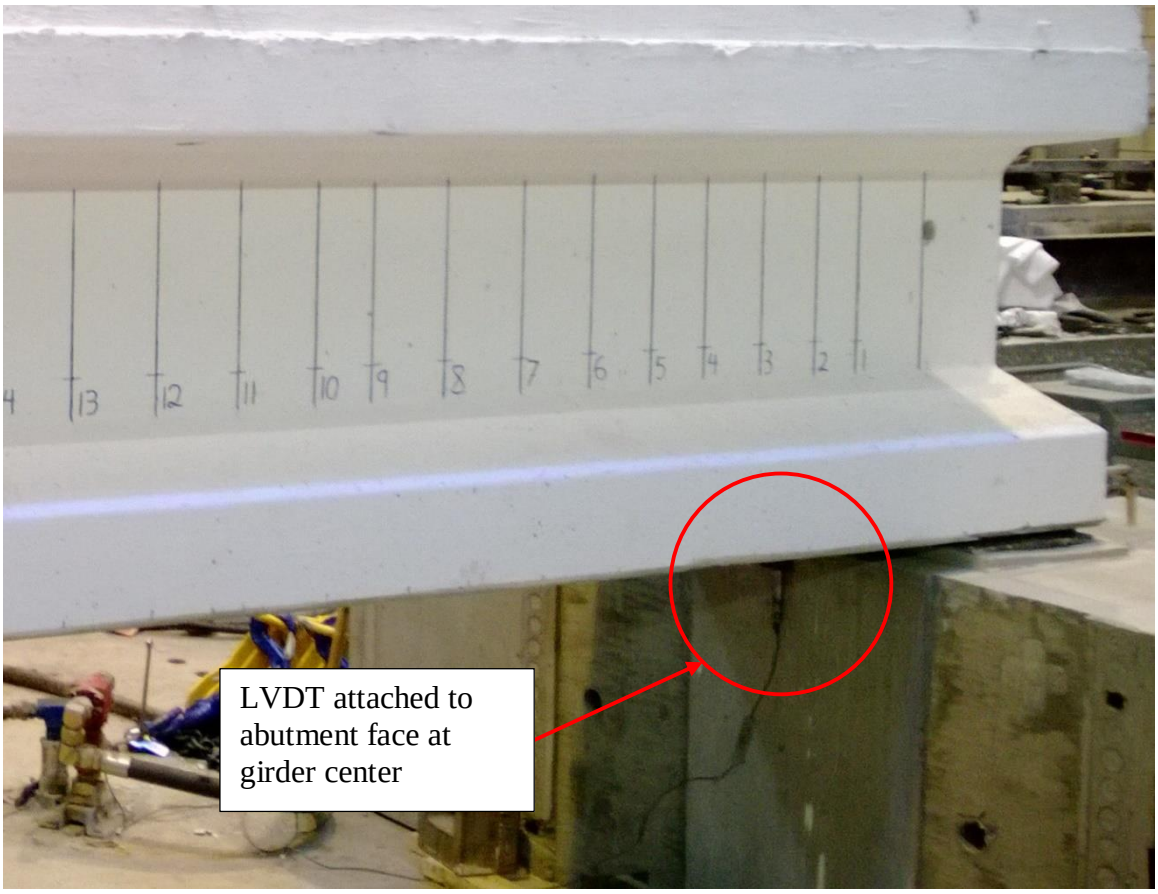

Figure 3-28: LVDT placement for the 36M_18F test representing typical LVDT placement at girder ends.

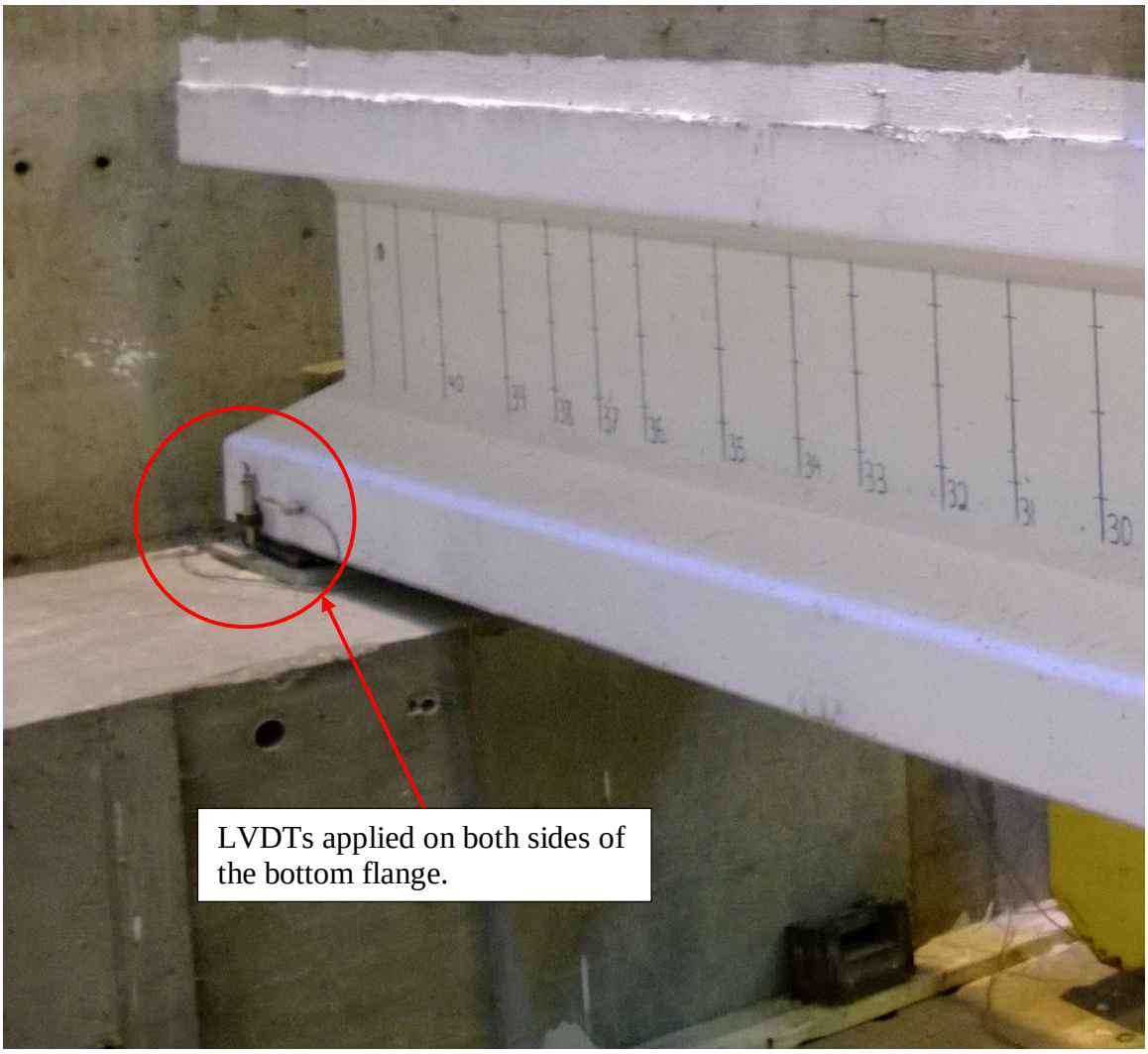

Figure 3-29: LVDT placement at the 36M_8W end during the 36M_18F test.

Figure 3-30: LVDT attached at the centerline of the 36M prestressed girder at the displacement controlled actuator location representing the typical placement for the 3 in. LVDT.

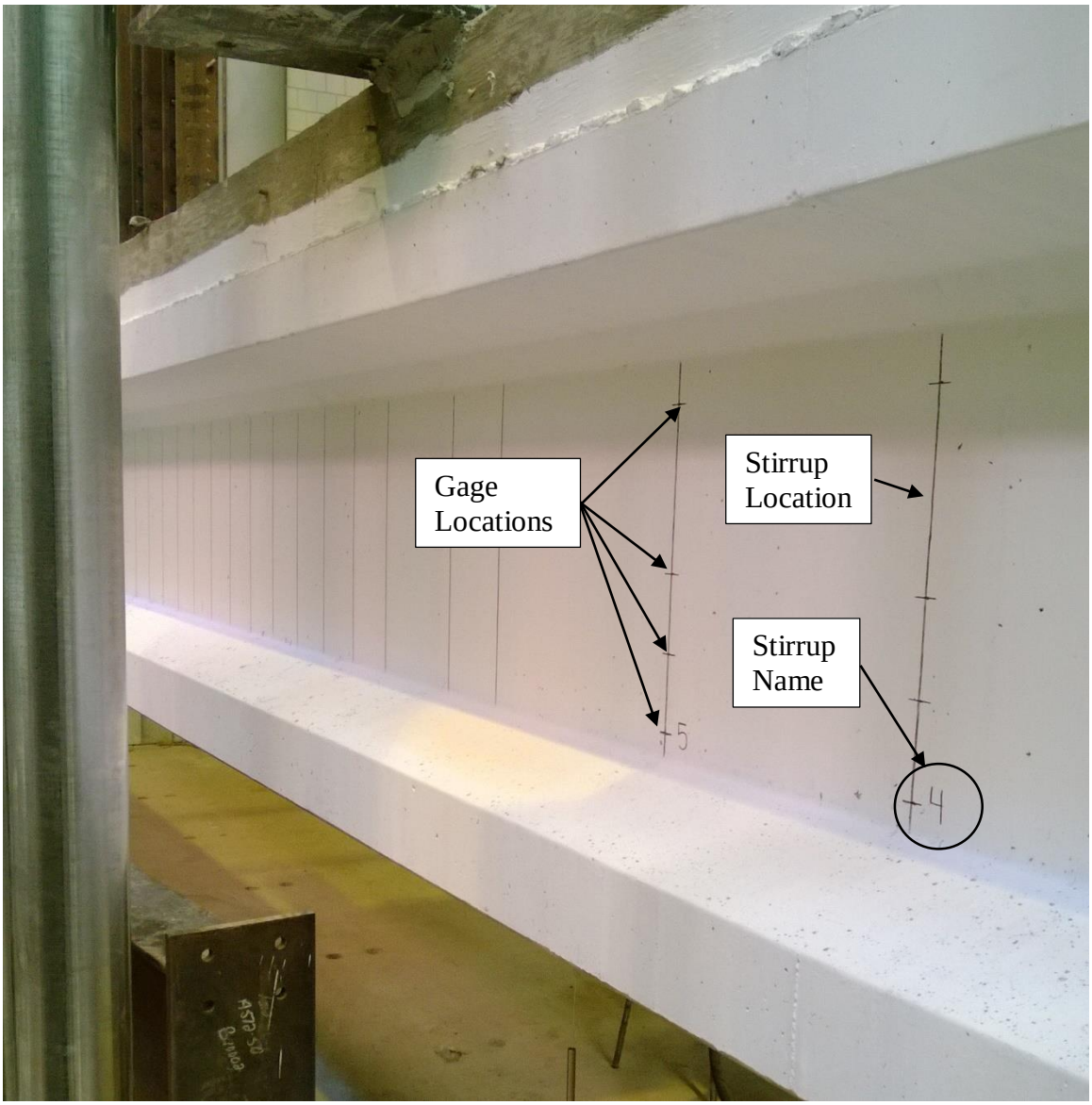

Figure 3-31: Grid pattern used to denote stirrup and gage locations for 45M_24W. Typical of all girders.

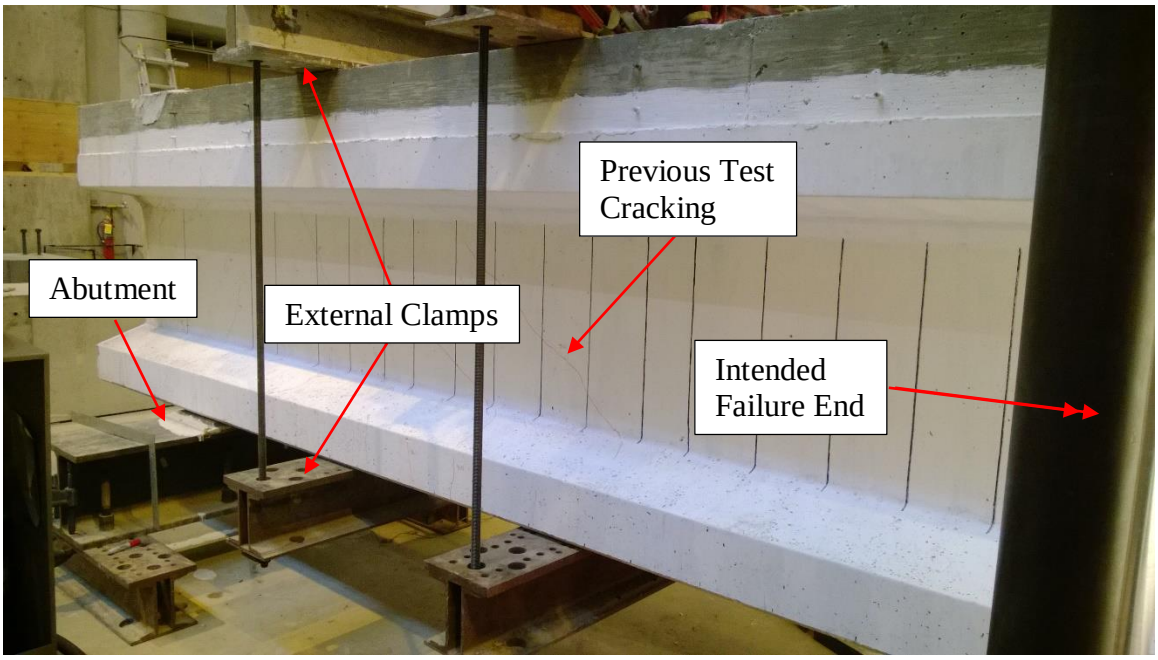

Figure 3-32: Steel clamps provided additional external shear reinforcement during the second end tests for the 36M and 45M (shown here) girders.

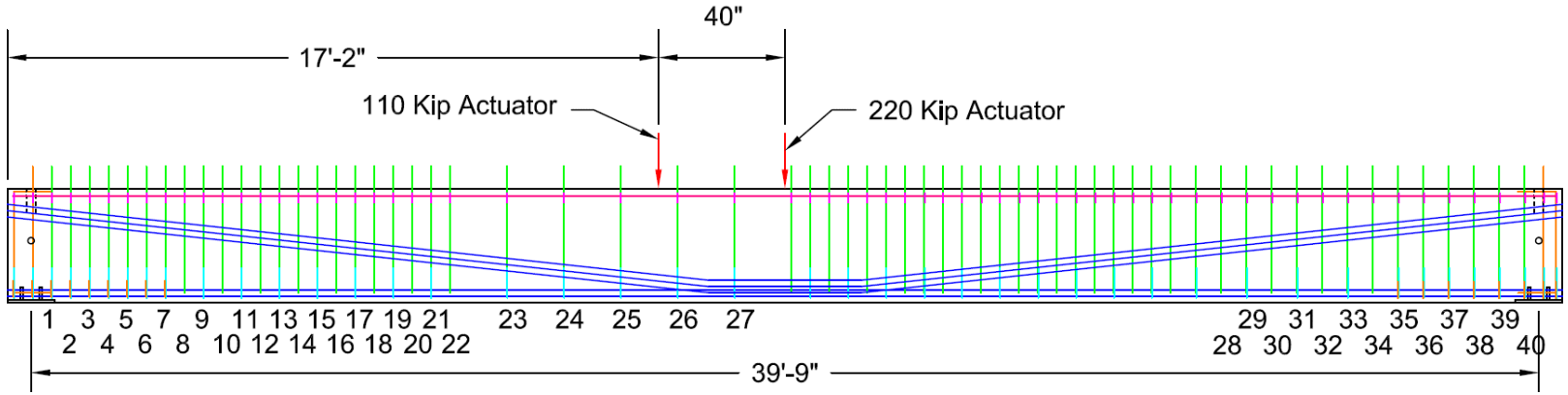

Figure 3-33: Elevation view of 36M_18F including load point locations.

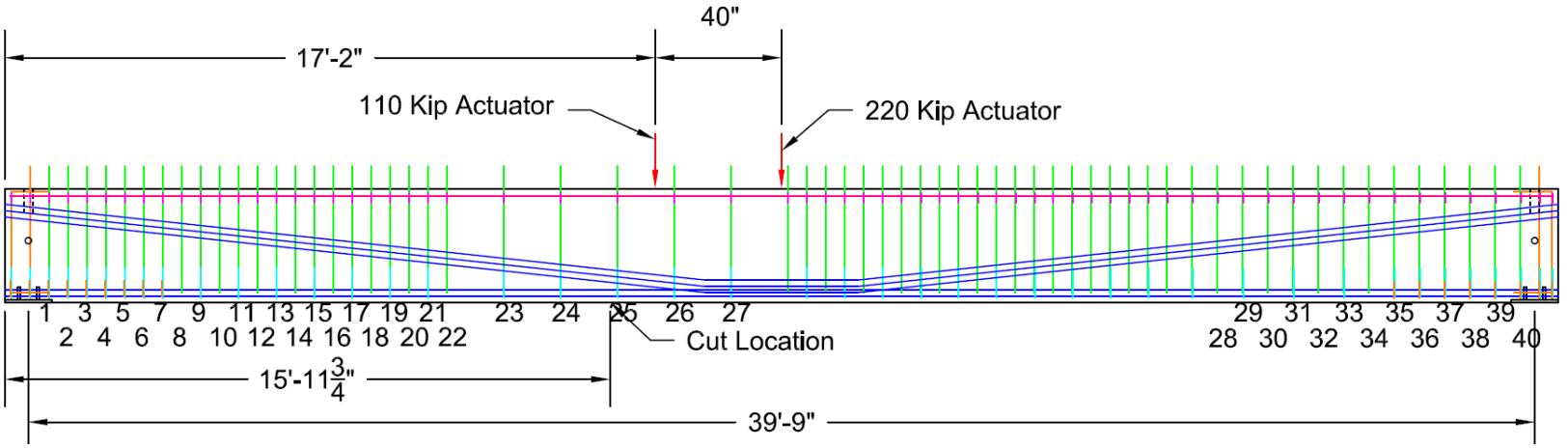

Figure 3-34: Elevation view of cut location after 36M_18F test.

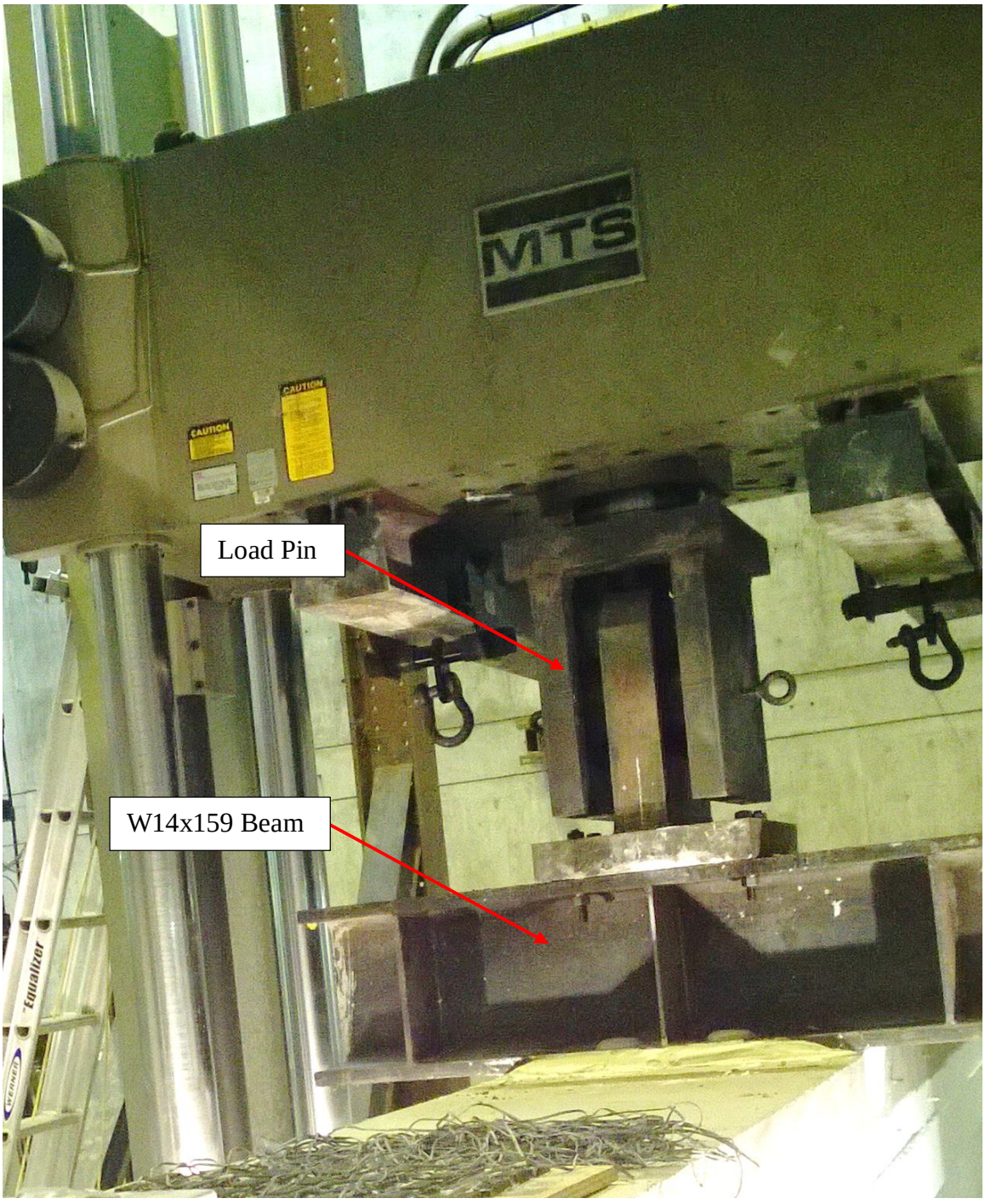

Figure 3-35: 600 kip MTS Model 311 Material Test frame

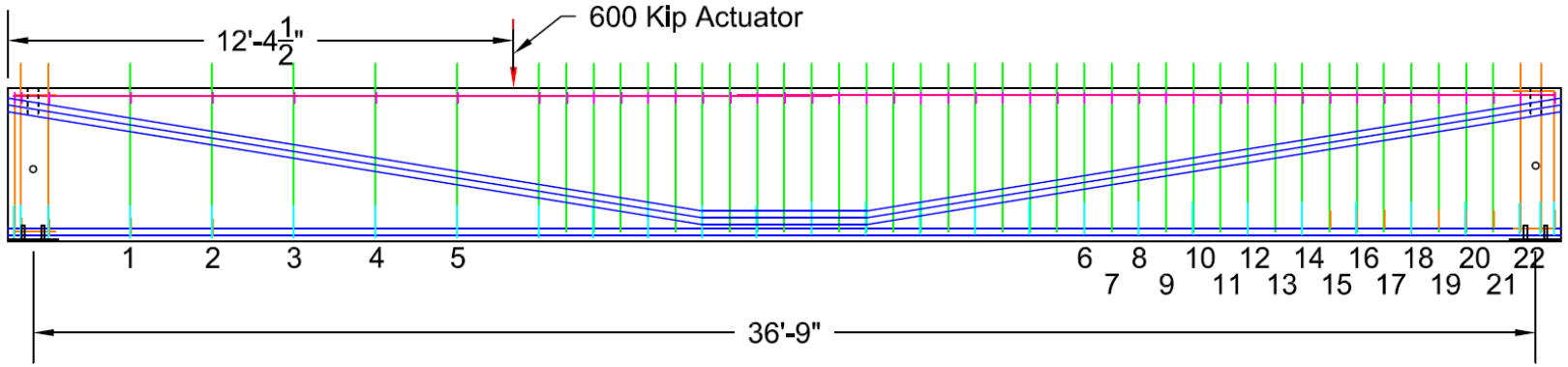

Figure 3-36: Elevation view of 45M_24W girder including load point and nominal span length.

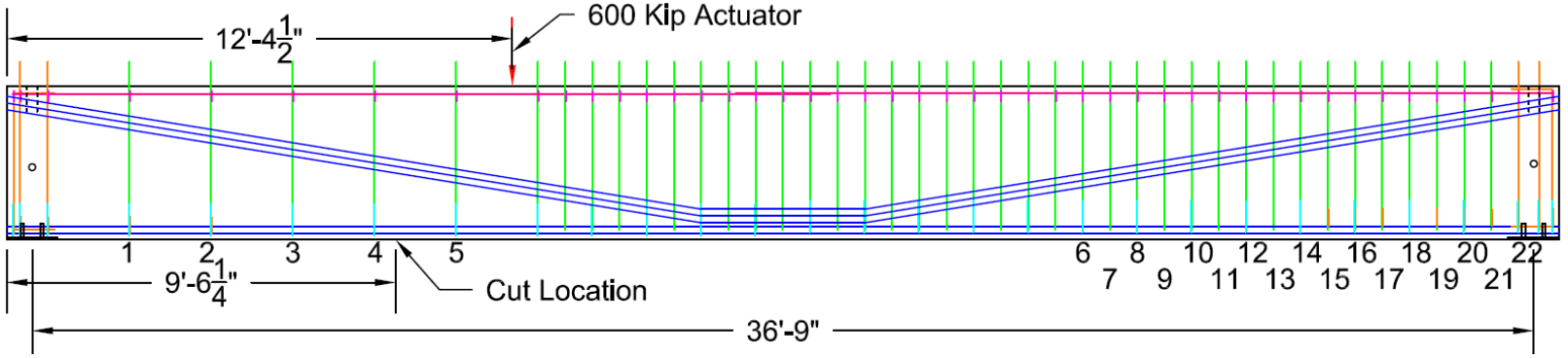

Figure 3-37: Elevation view of cut location after 45M_24W test.

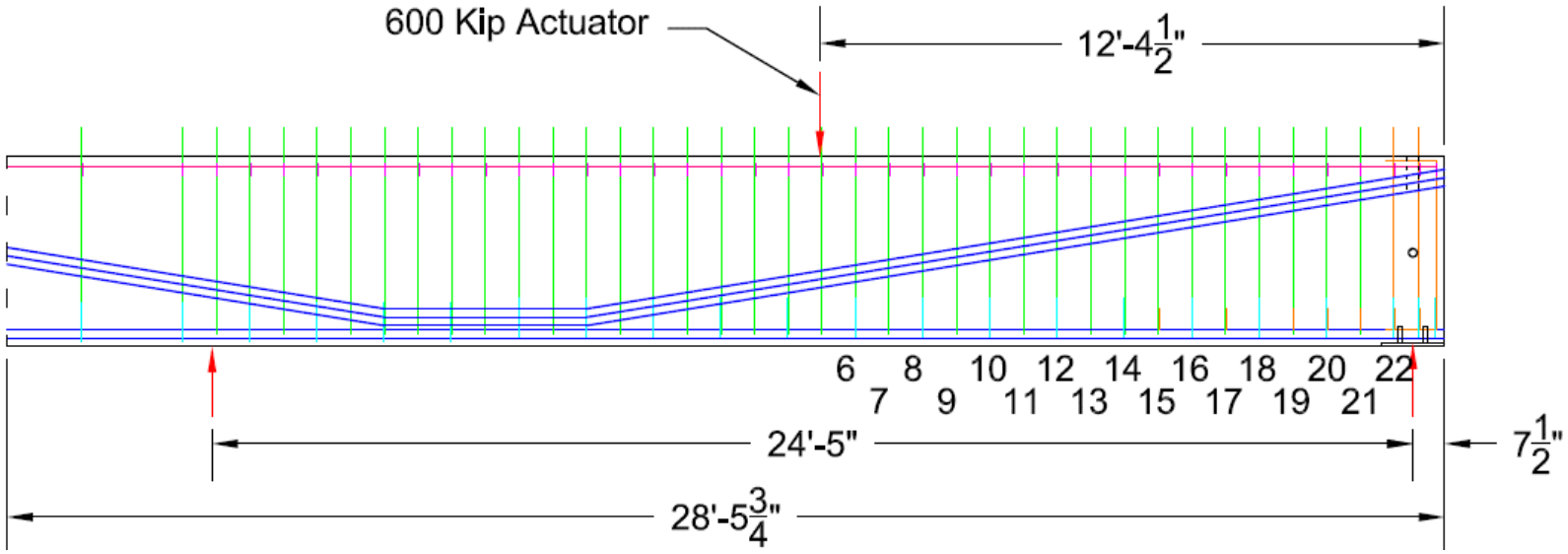

Figure 3-38: Elevation view of 45M_8W girder including load point location and nominal span length.

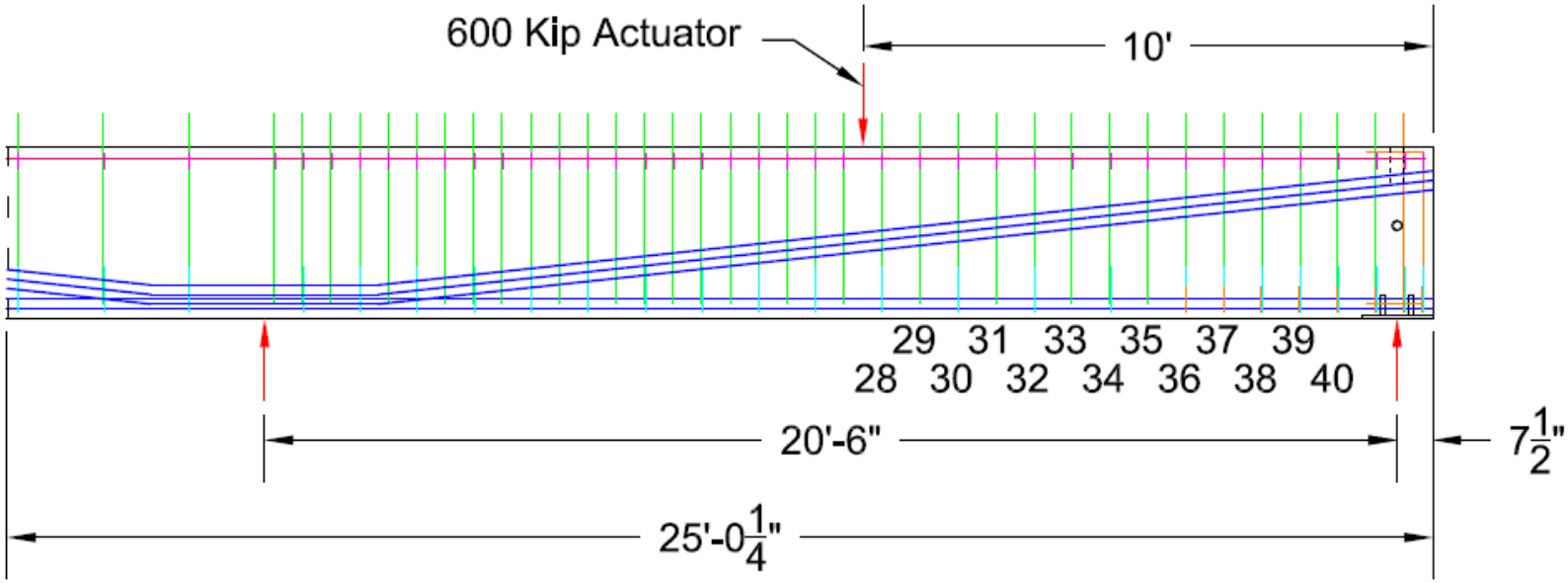

Figure 3-39: Elevation view of 36M_8W girder including load point location and nominal span length.

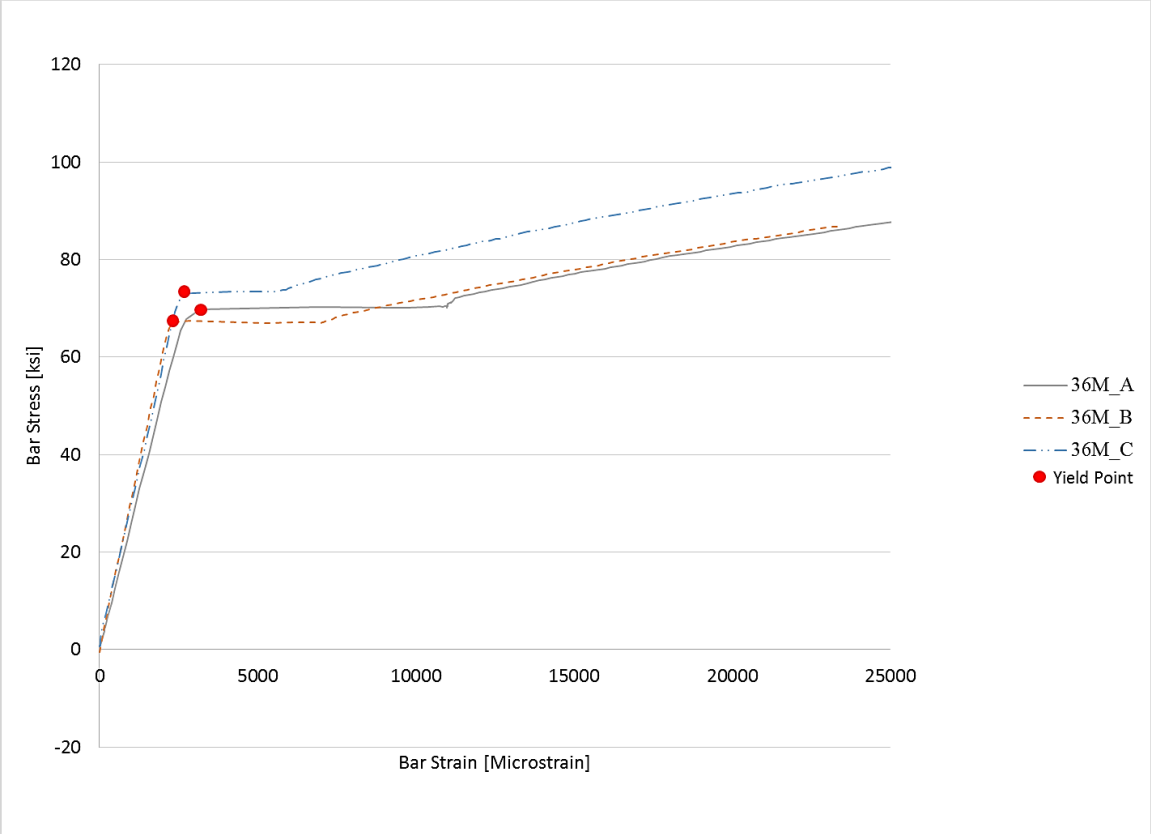

Figure 3-40: Stress-strain curves from 36M transverse reinforcement tension tests.

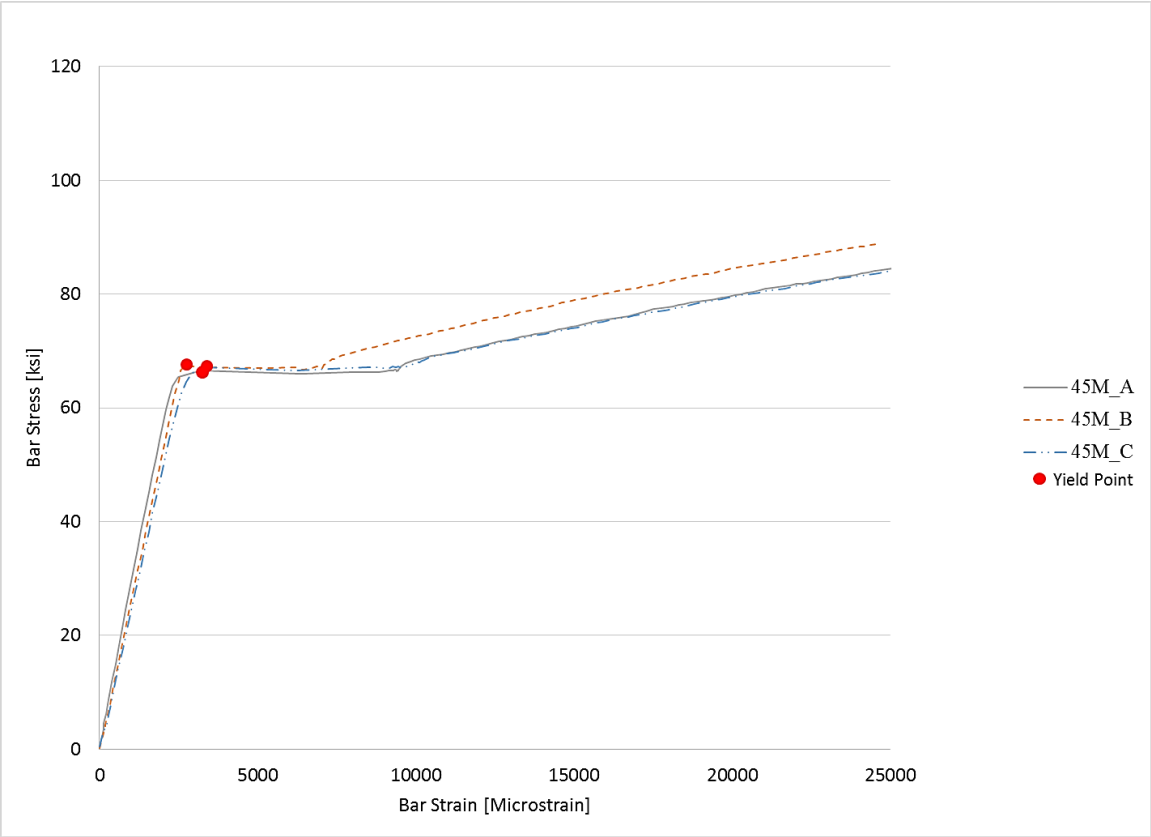

Figure 3-41: Stress-strain curves from 45M transverse reinforcement tension tests.

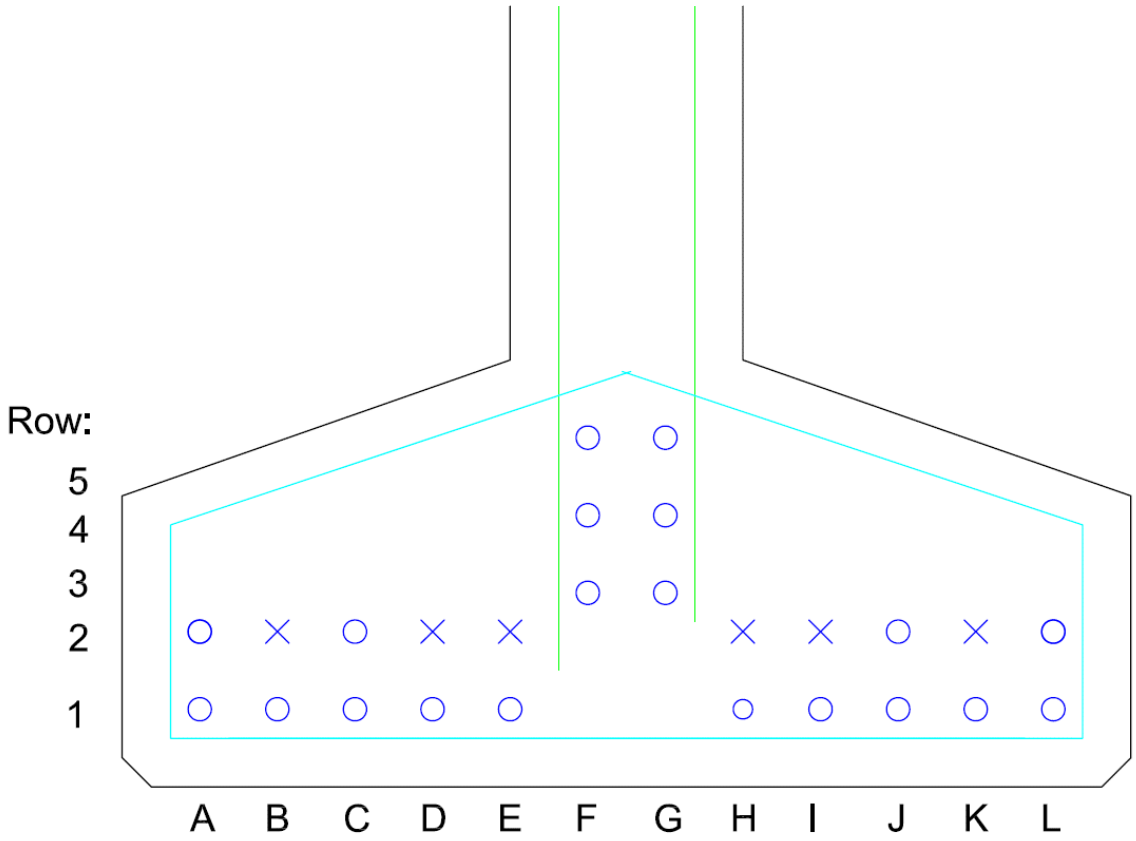

Figure 3-42: Live end view of naming scheme to denote jacking stresses measured by Cretex.

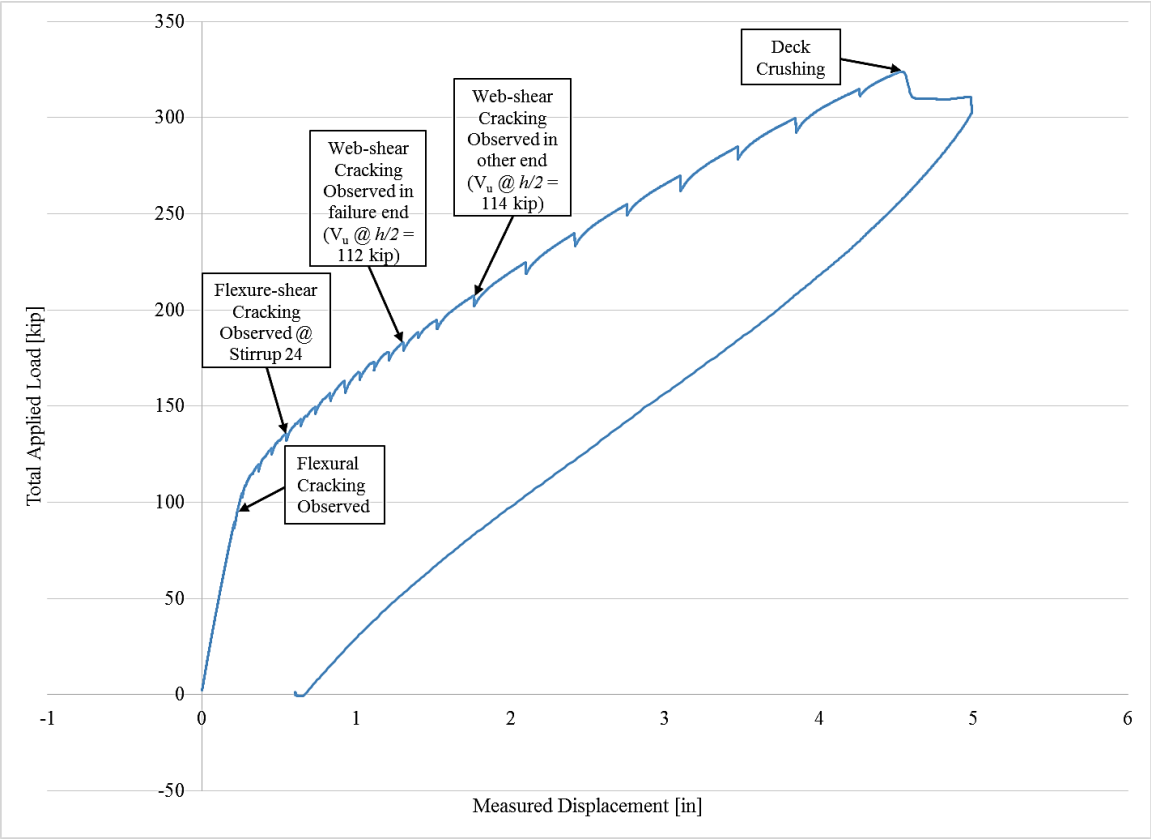

Figure 3-43: Load-displacement curve for 36M_18F test.

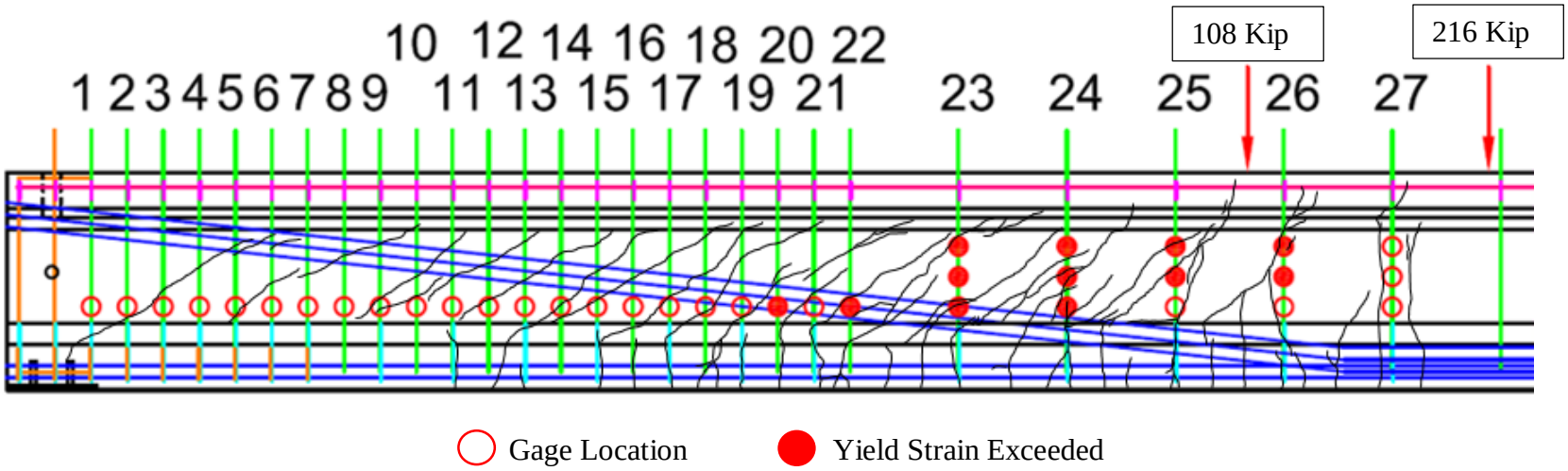

Figure 3-44: Crack pattern associated with $V_{u,test}/V_n$ = 1.23 due to maximum loading for the 36M_18F test.

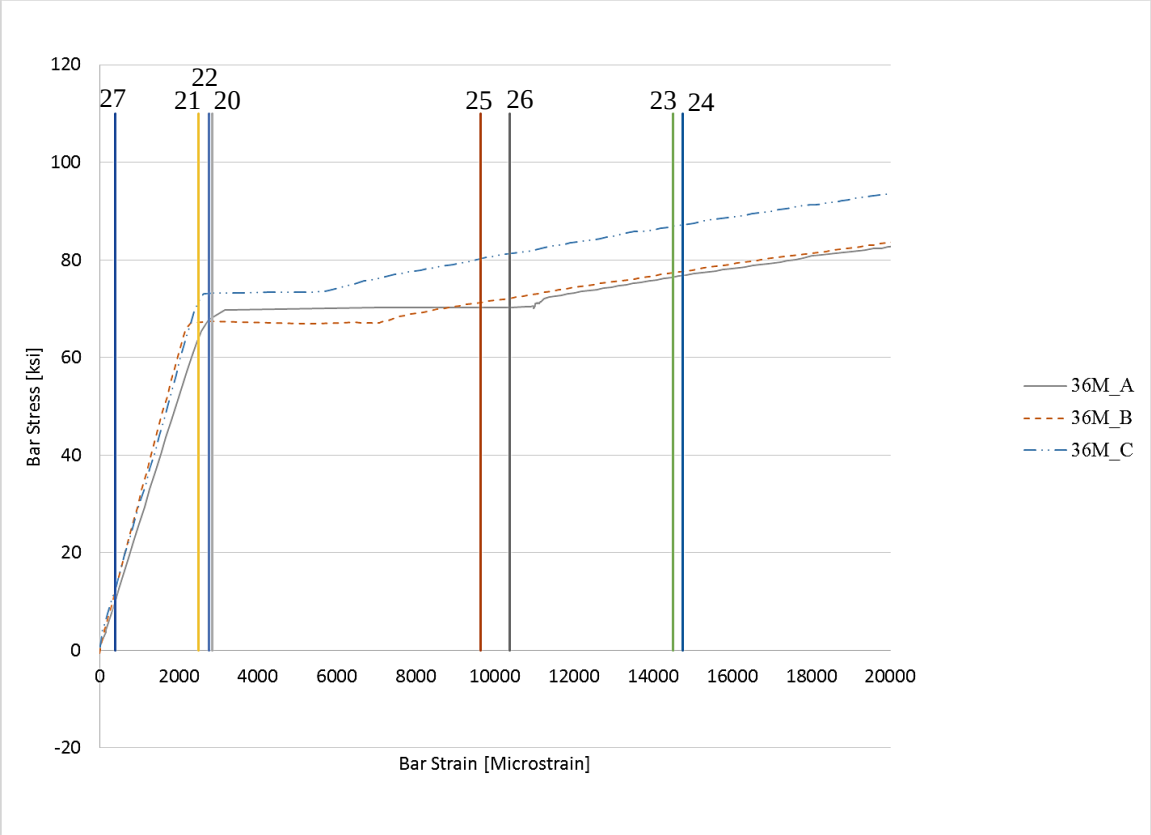

Figure 3-45: Maximum strain measured at Stirrups 20 through 27 throughout the 36M_18F test overlaid on reinforcement stress-strain curves.

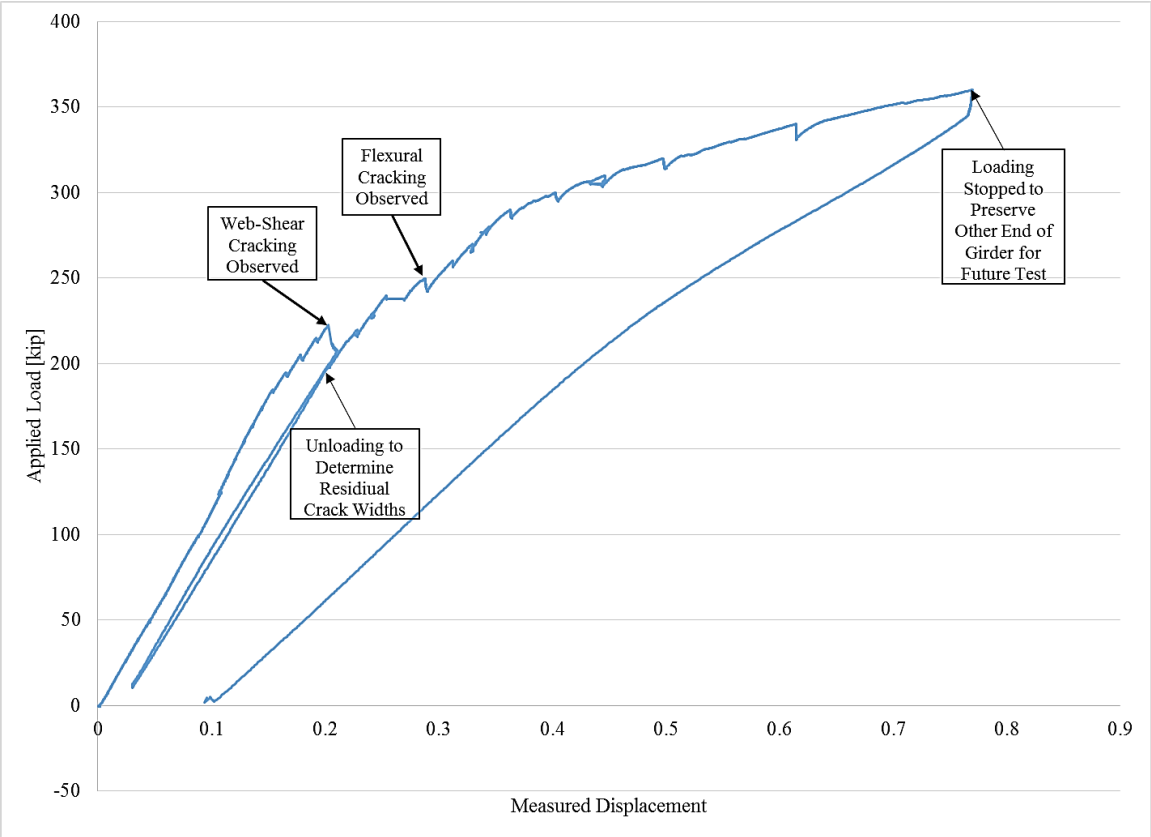

Figure 3-46: Load-displacement curve for 45M_24W test.

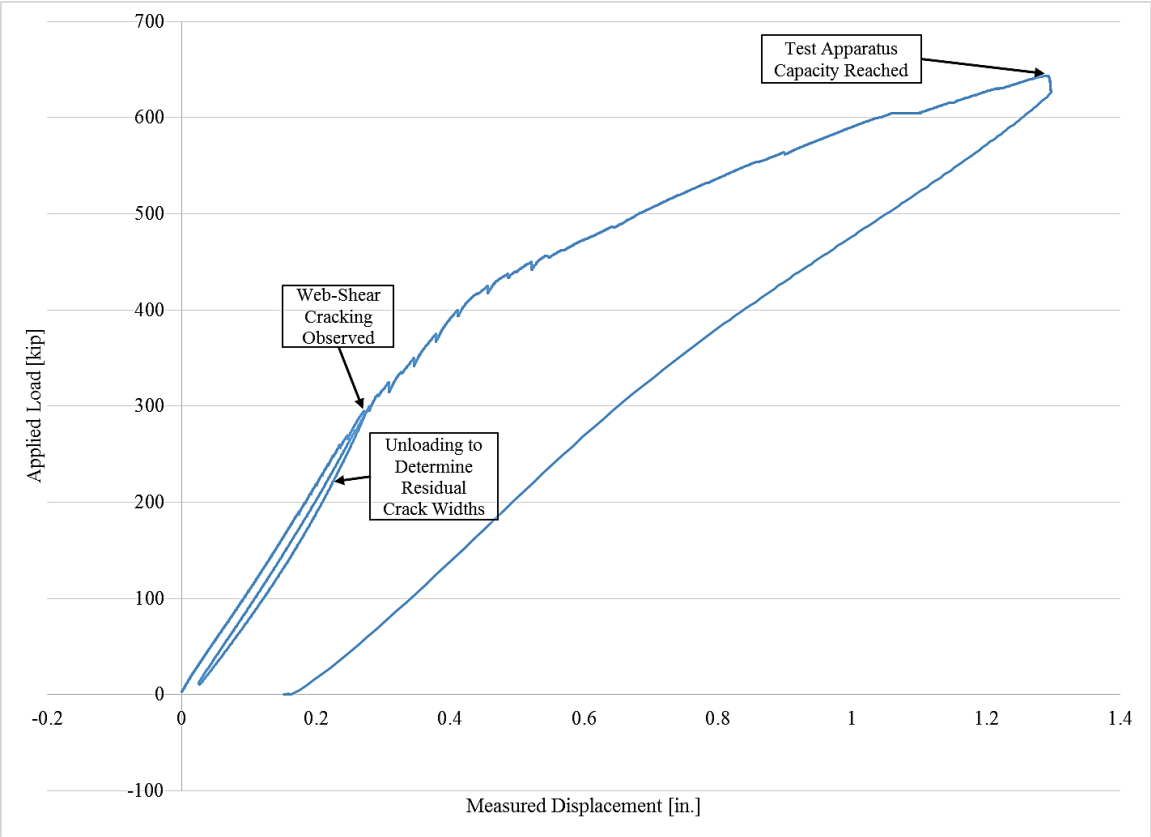

Figure 3-47: Load-displacement curve for 45M_8W test.

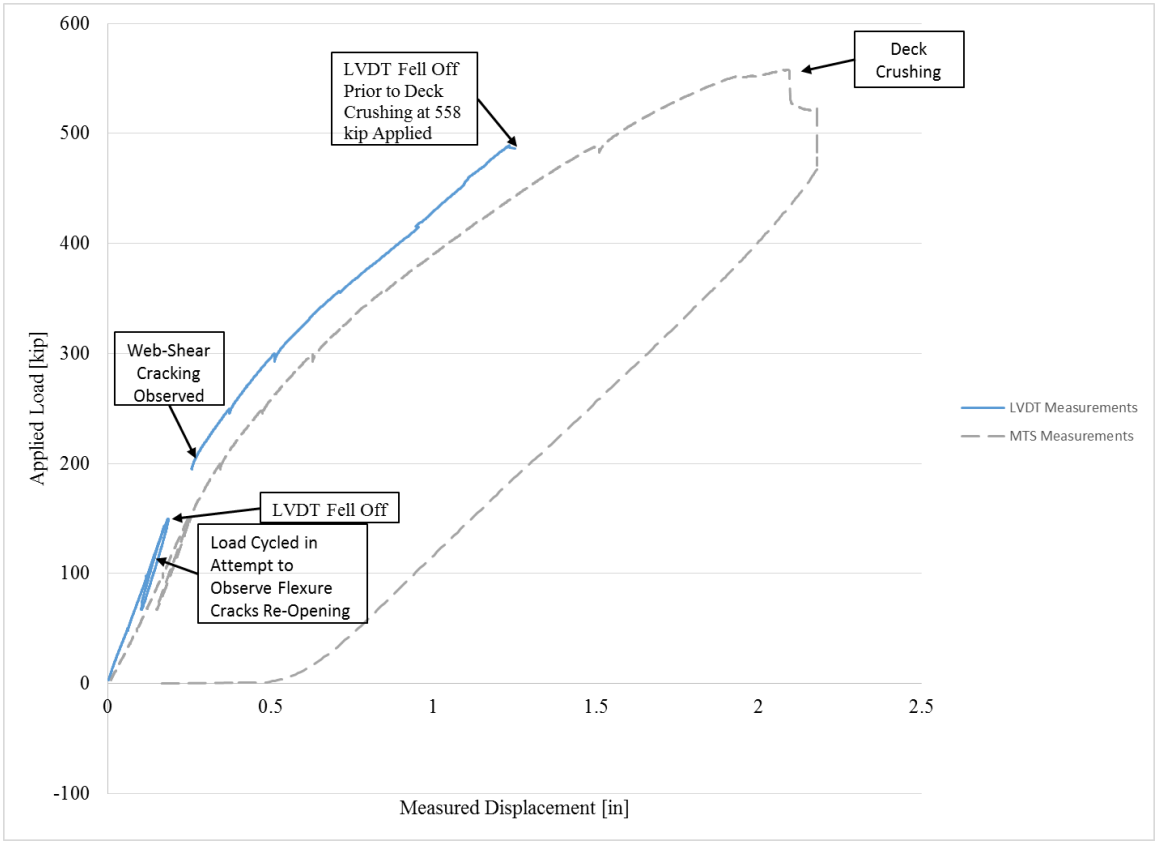

Figure 3-48: Load-displacement curve for 36M_8W test.

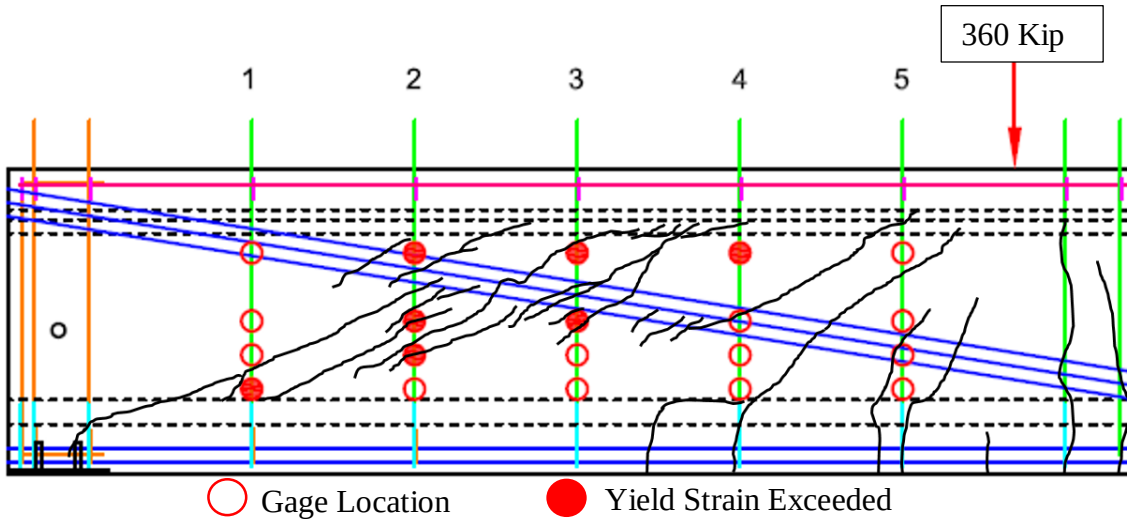

Figure 3-49: Crack pattern associated with $V_{u,test}/V_n$ = 1.38 due to maximum loading for the 45M_24W test.

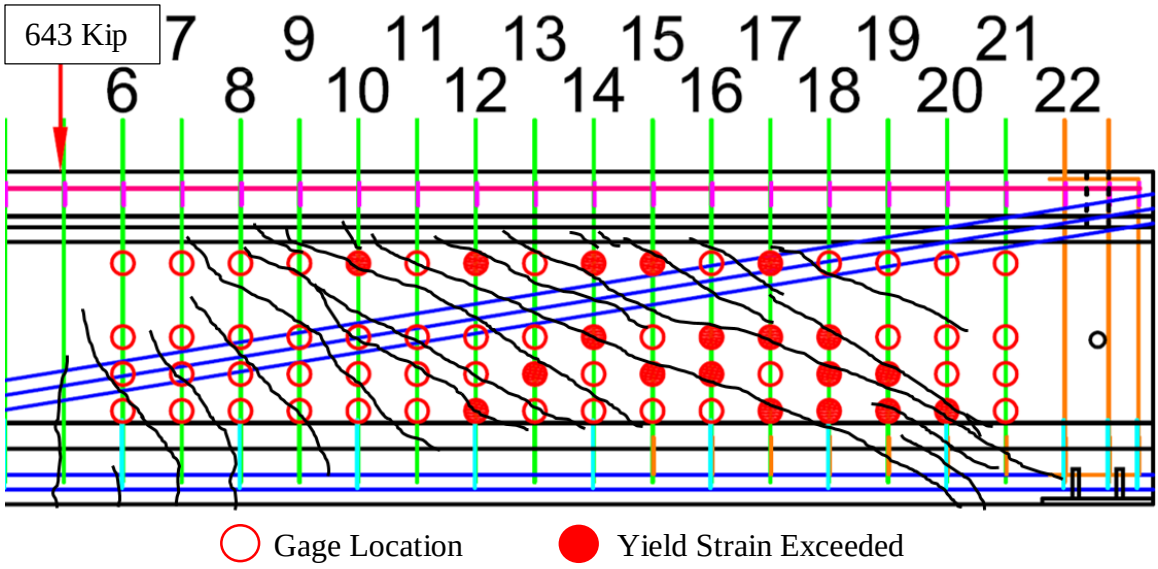

Figure 3-50: Crack pattern associated with $V_{u,test}/V_n$ = 1.19 due to maximum loading for the 45M_8W test.

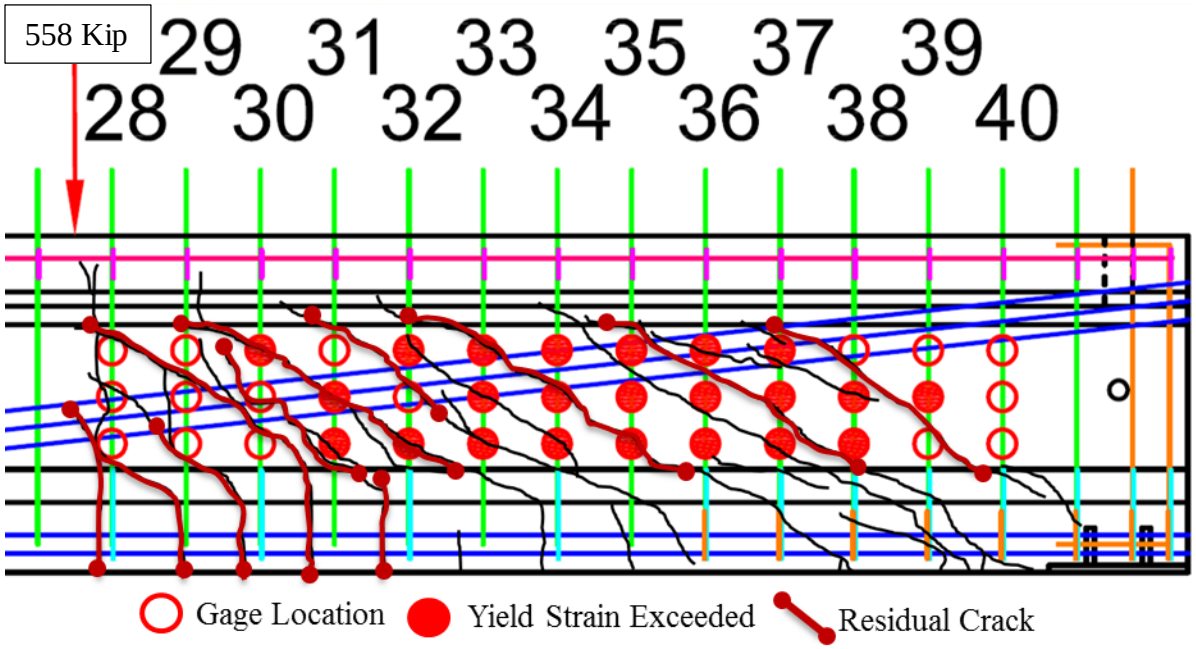

Figure 3-51: Crack pattern associated with $V_{u,test}/V_n$ = 1.35 due to maximum loading for the 36M_8W test.

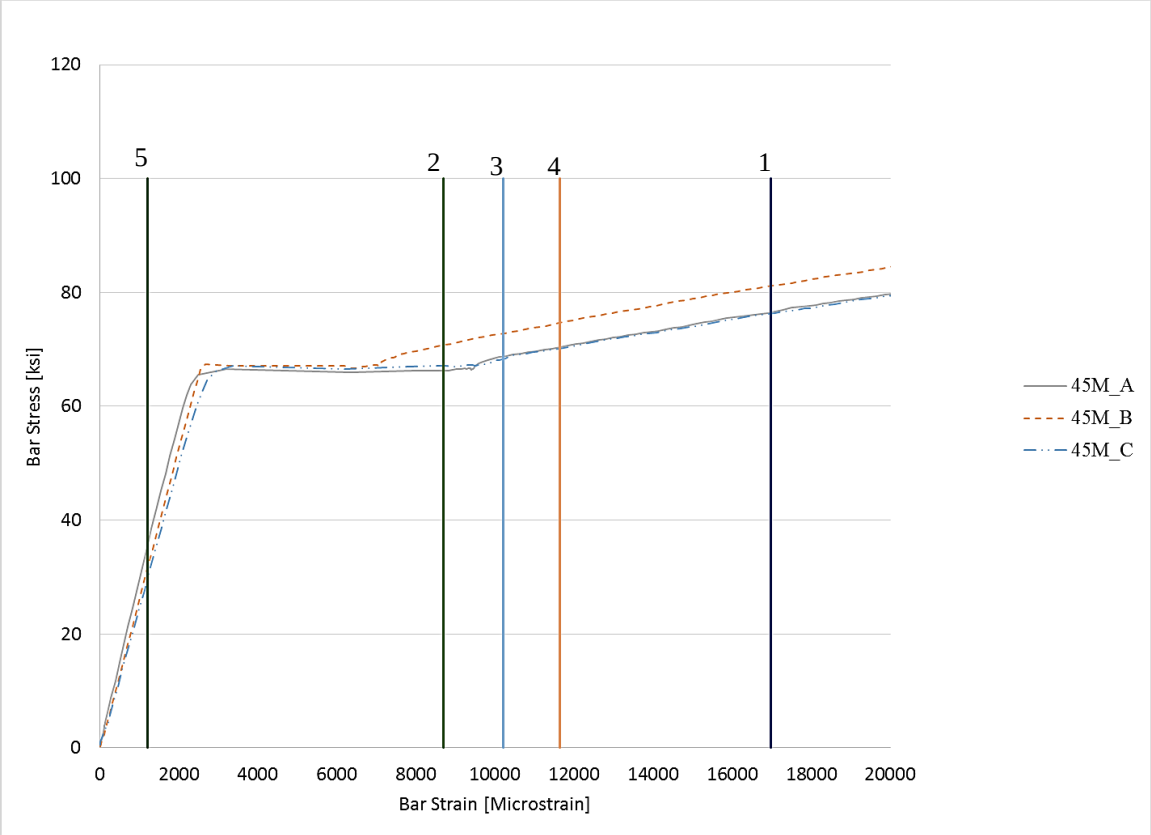

Figure 3-52: Maximum strains measured in Stirrups 1 through 5 throughout the 45M_24W test overlaid on reinforcement stress-strain curve.

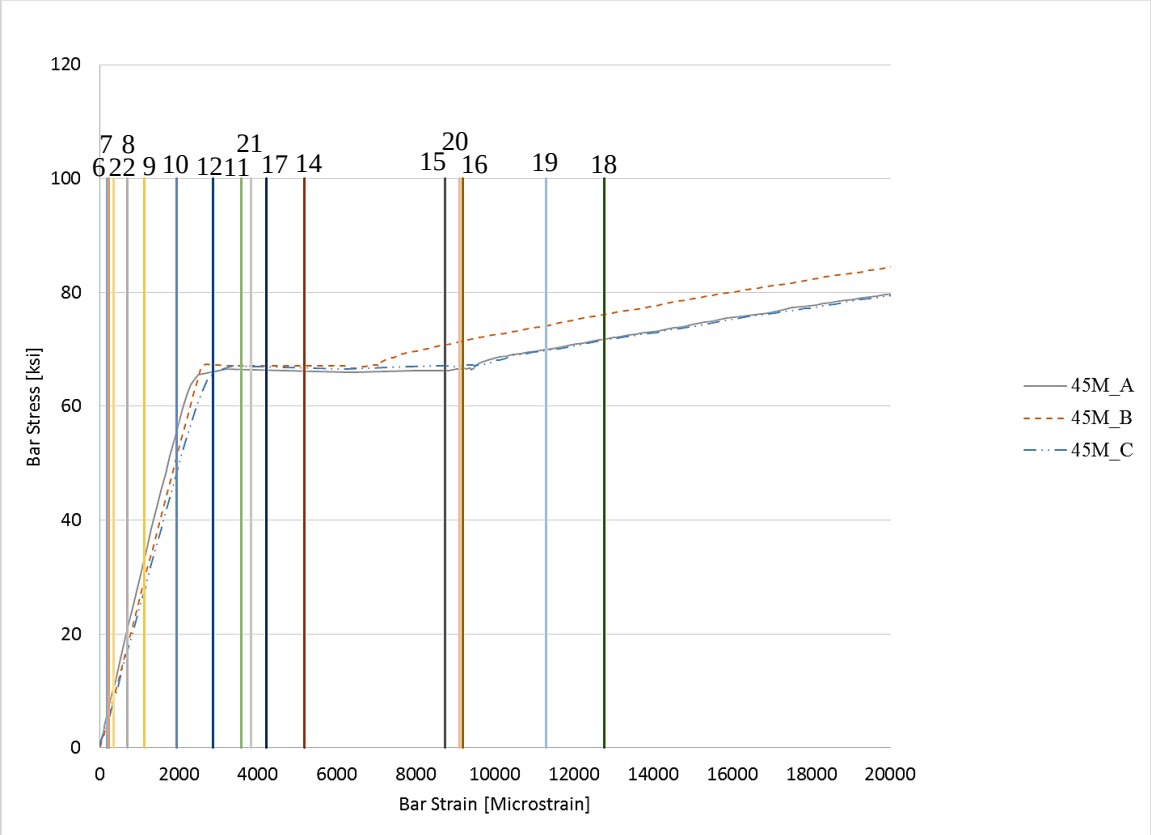

Figure 3-53: Maximum strain measured across stirrups 7 through 20 throughout the 45M_8W test overlaid on reinforcement stress-strain curve.

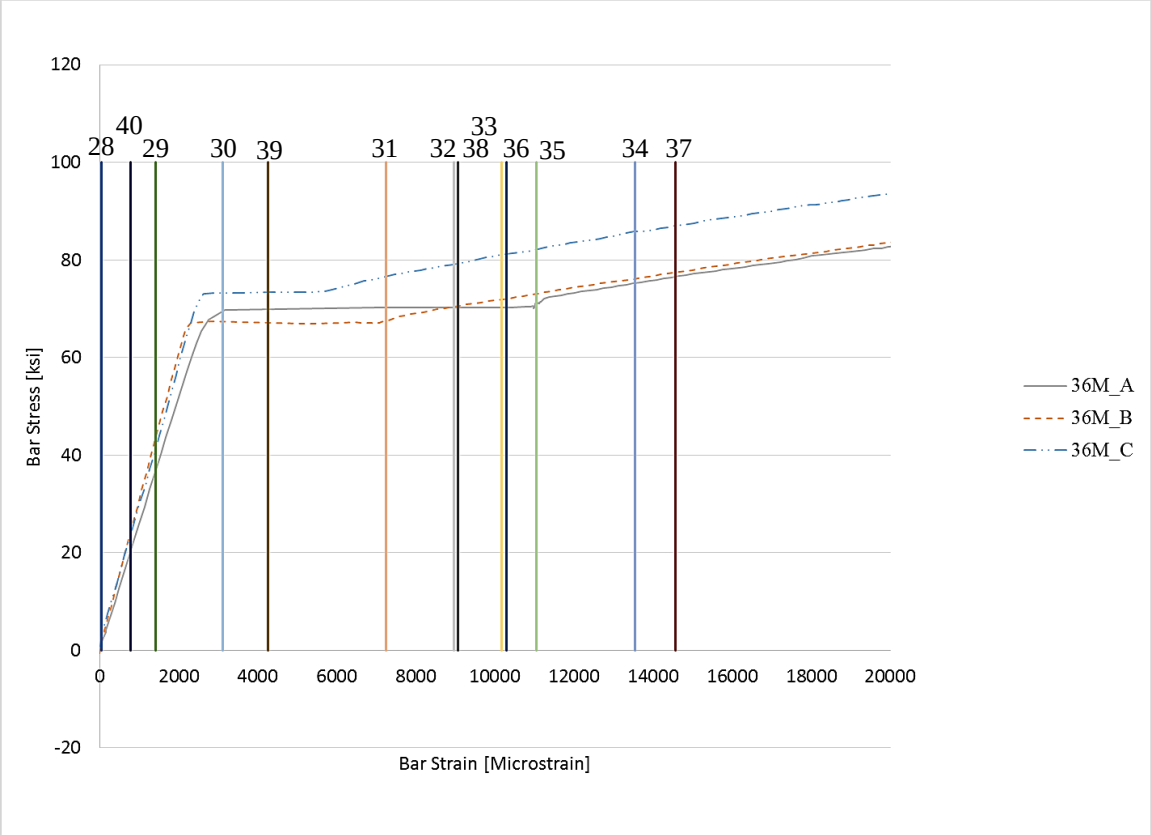

Figure 3-54: Maximum strain measured in Stirrups 28 through 40 throughout the 36M_8W test overlaid on reinforcement stress-strain curve.

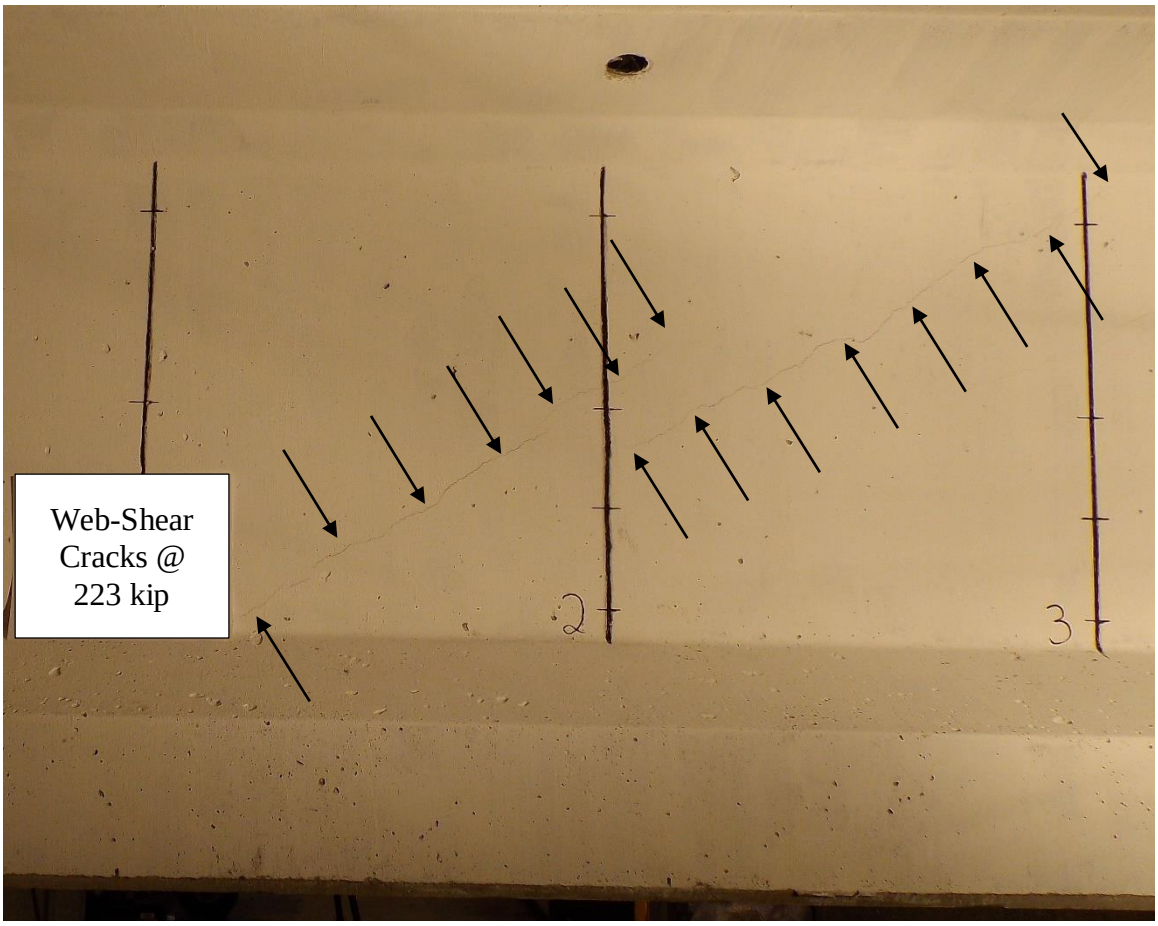

Figure 3-55: Initial web-shear cracks in 45M_24W with 223 kips applied.

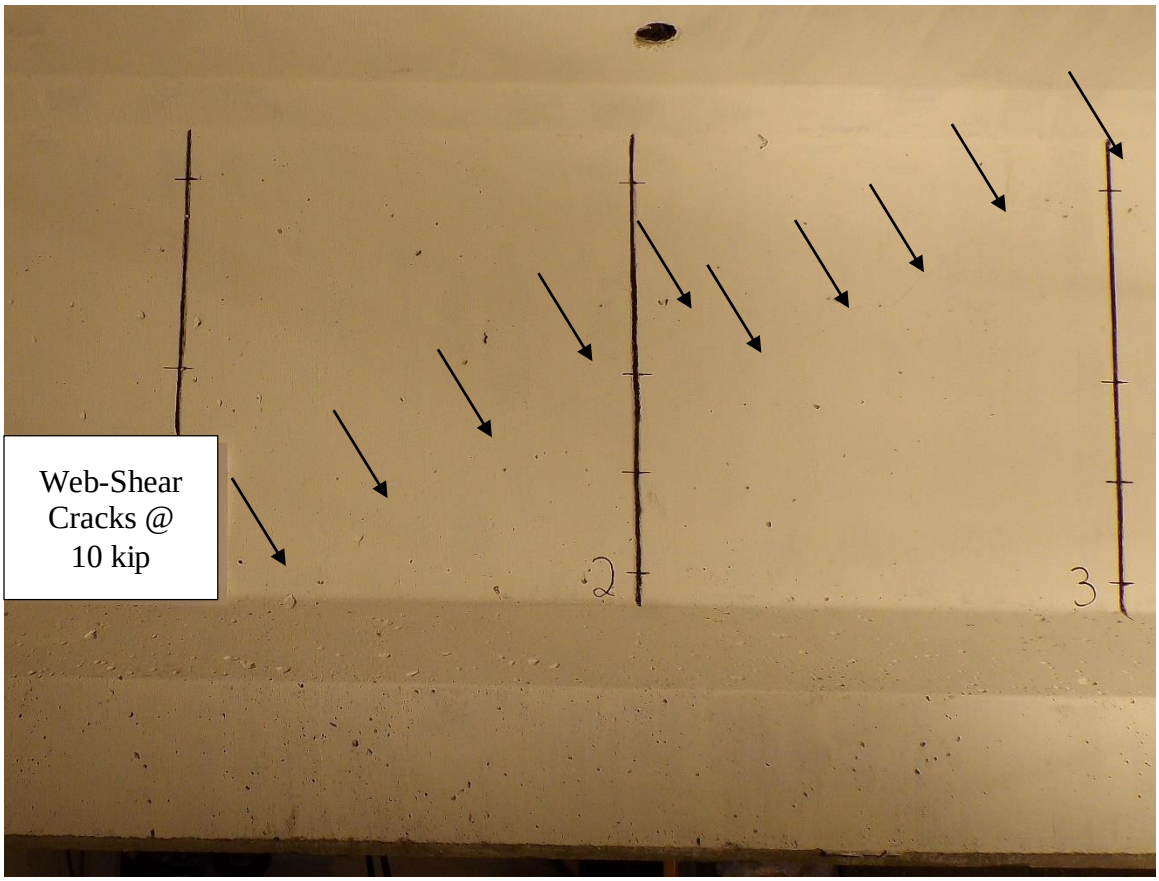

Figure 3-56: Initial web-shear cracks in 45M_24W unloaded to 10 kips applied.

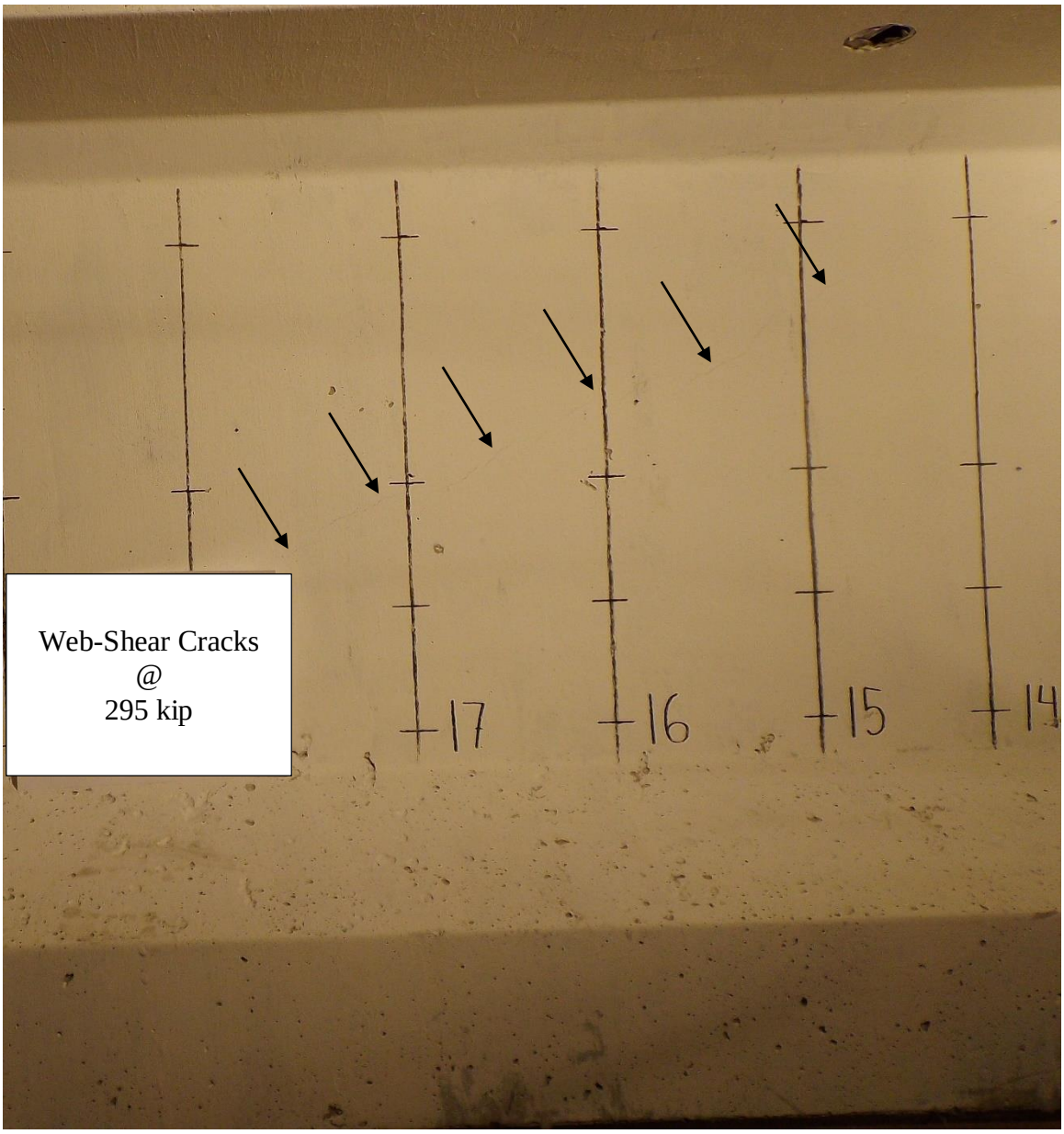

Figure 3-57: Initial web-shear cracks in 45M_8W with 295 kips applied.

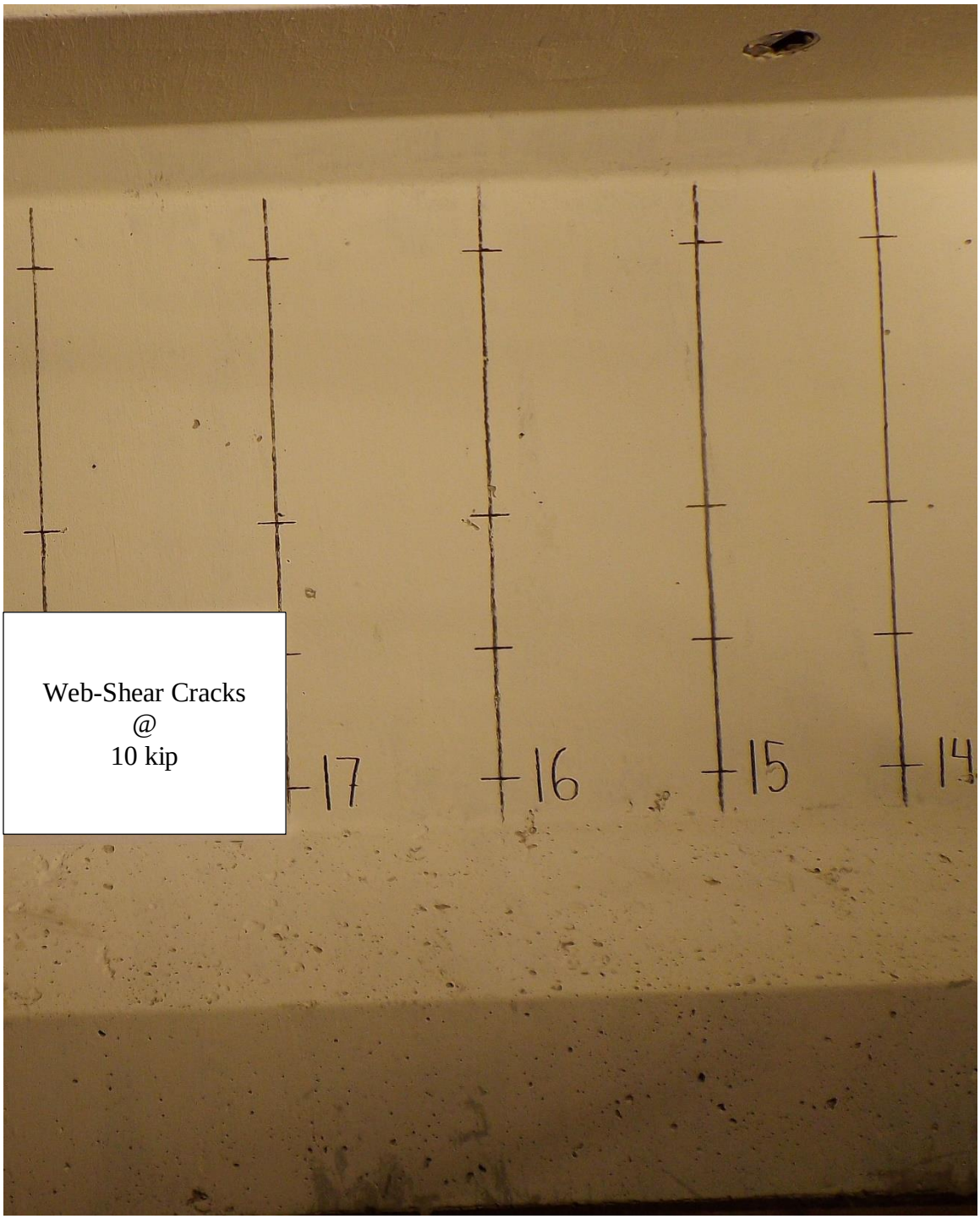

Figure 3-58: Initial web-shear cracks in 45M_8W unloaded to 10 kips applied.

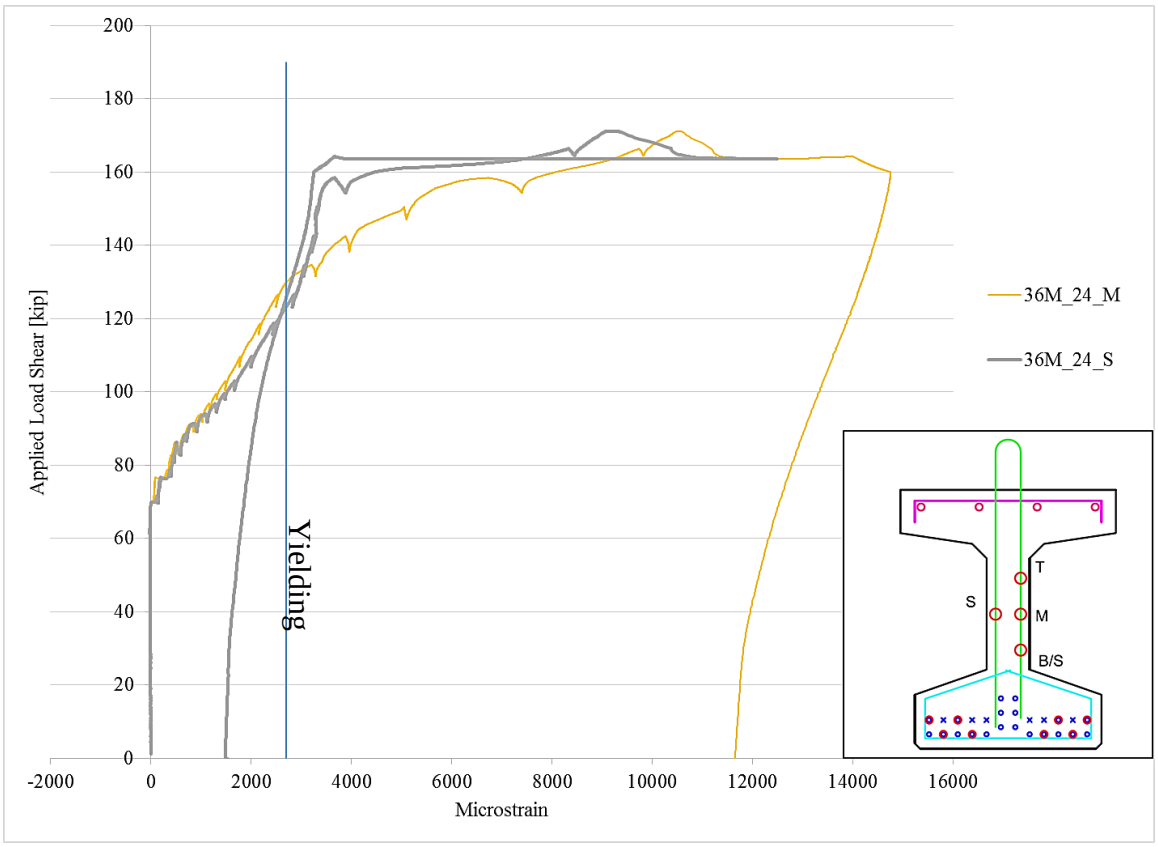

Figure 3-59: Comparison of strain measurements between similarly placed gages on the short and long stirrup legs for the 36M_18F test at Stirrup 24

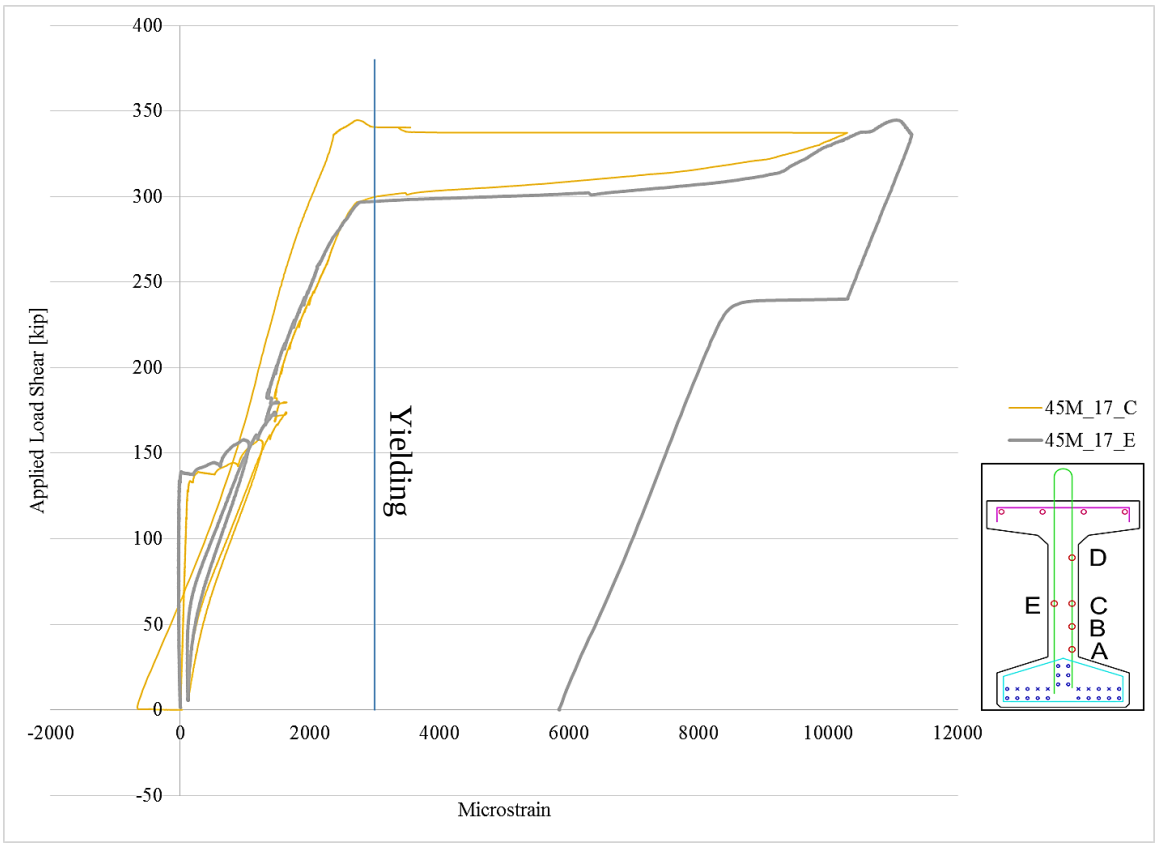

Figure 3-60: Comparison of strain measurements between similarly placed gages on the short and long stirrup legs for the 45M_8W test at Stirrup 17.

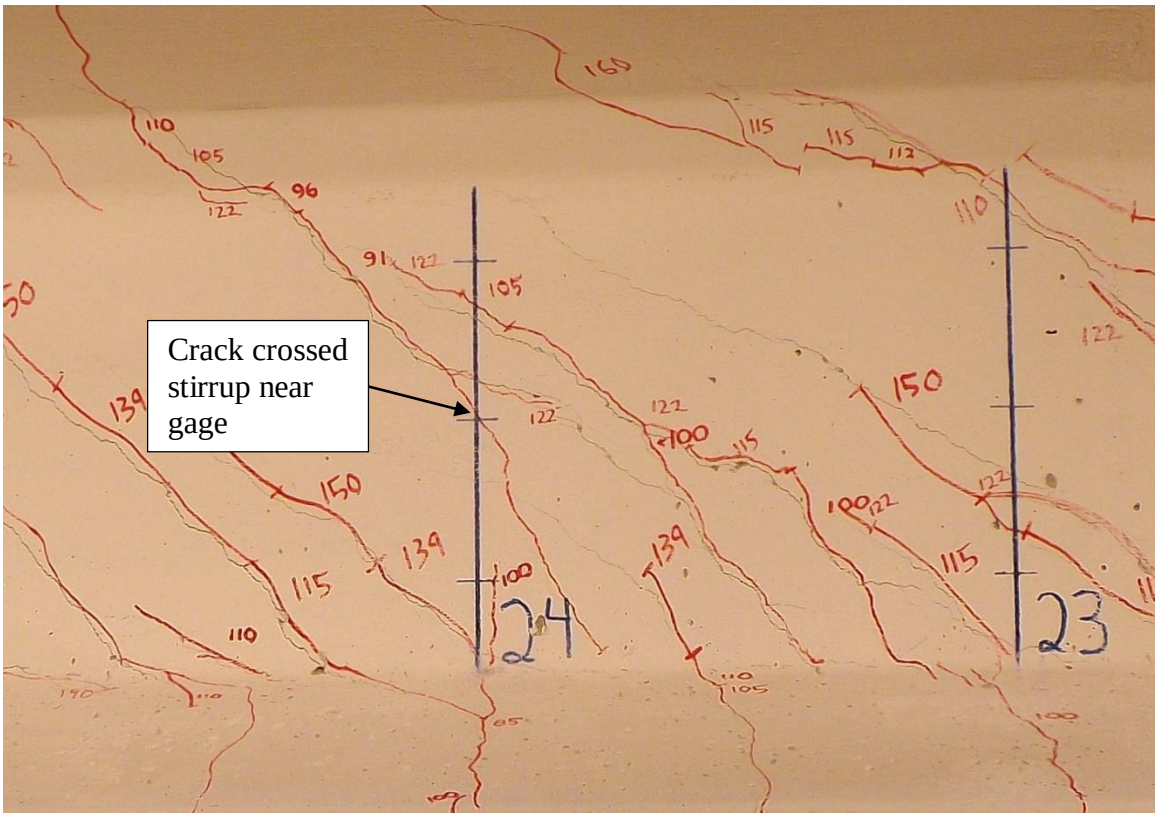

Figure 3-61: Shear crack crossing short leg of stirrup 24 following 36M_18F test (offset relative to opposite side of web).

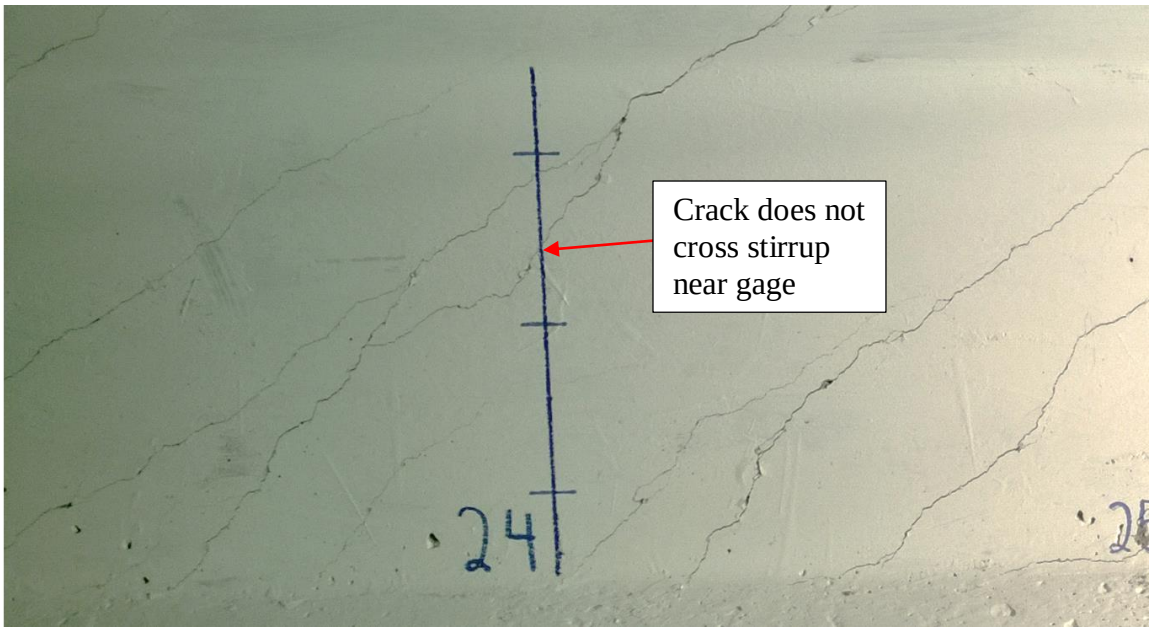

Figure 3-62: Shear crack crossing long leg of stirrup 24 following 36M_18F test (offset relative to opposite side of web).

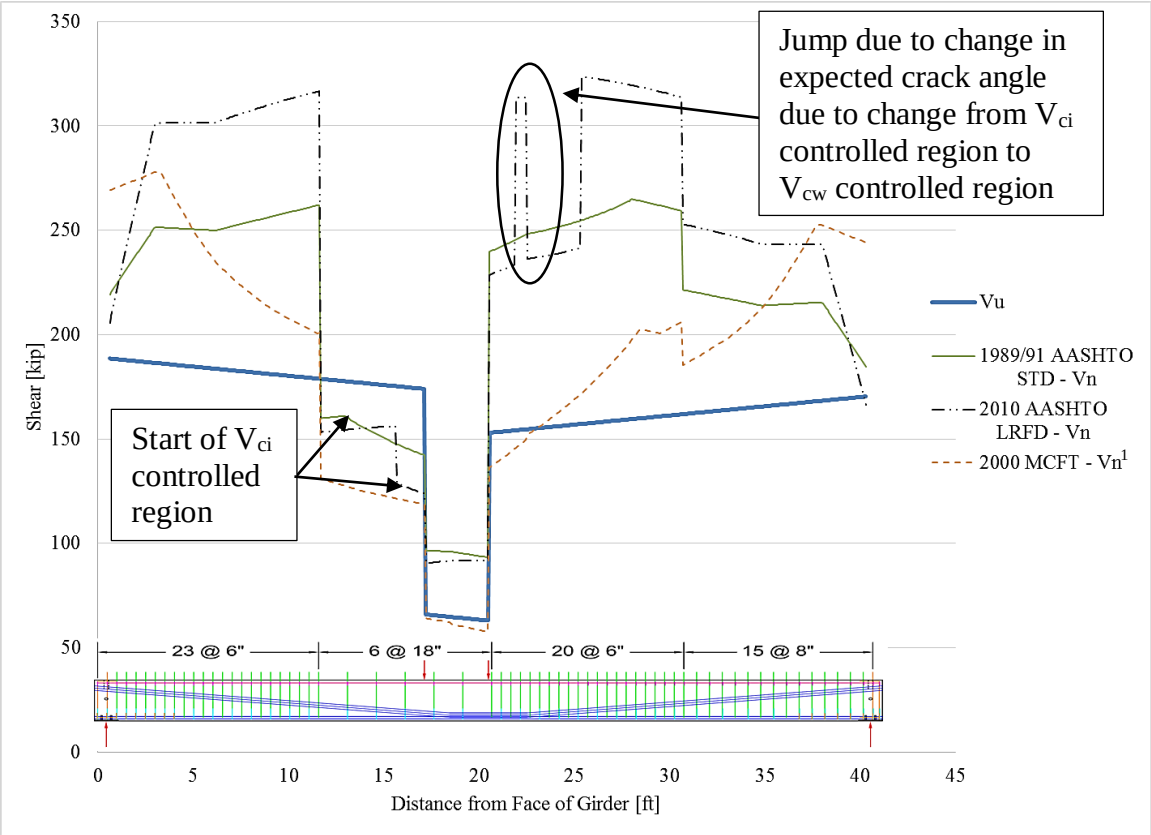

Figure 3-63: Applied shear force and predicted shear capacity for 36M_18F girder due to an applied load at midspan of 216 kip (total load of 324 kip).

[1] Stirrup contribution limited to $720 \cdot b_w \cdot s$ [*lbs*] corresponding to minimum stirrup spacing of 6.5 in.

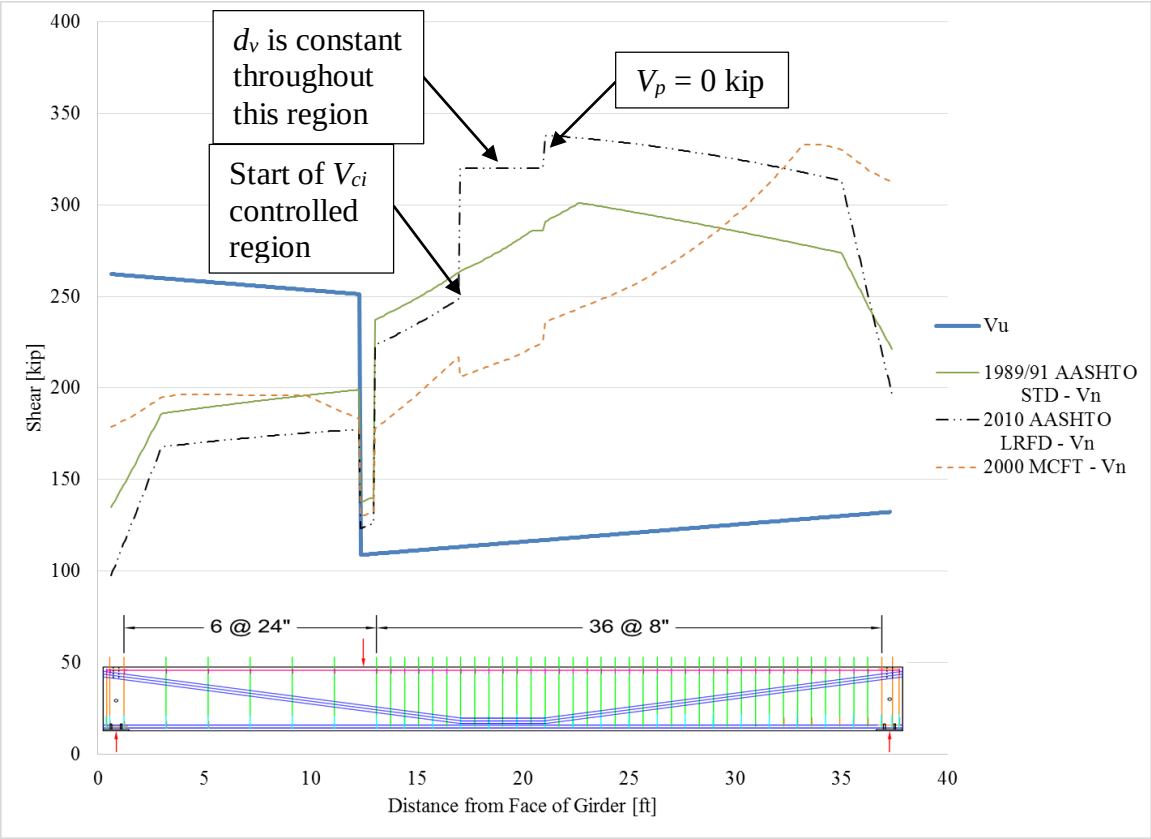

Figure 3-64: Applied shear force and predicted shear capacity for 45M_24W due to applied load of 360 kip.

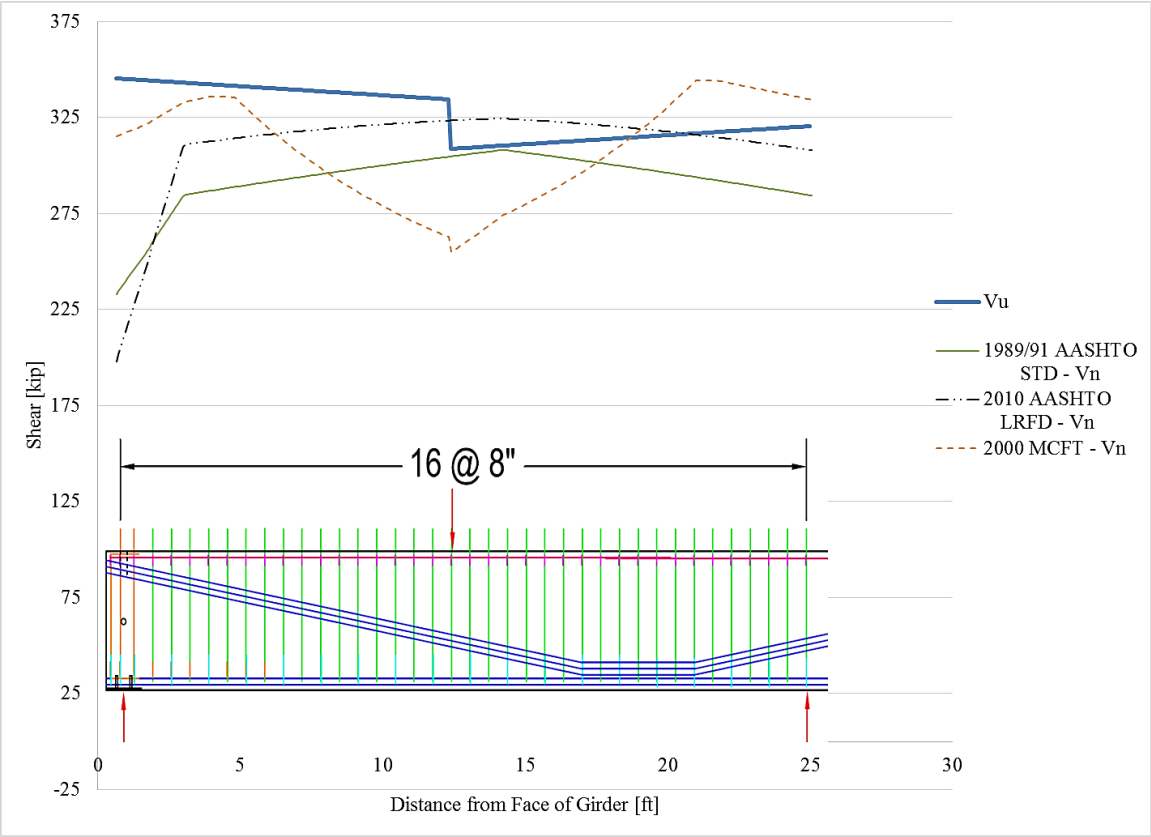

Figure 3-65: Applied shear and predicted shear capacity for 45M_8W due to applied load of 643 kip.

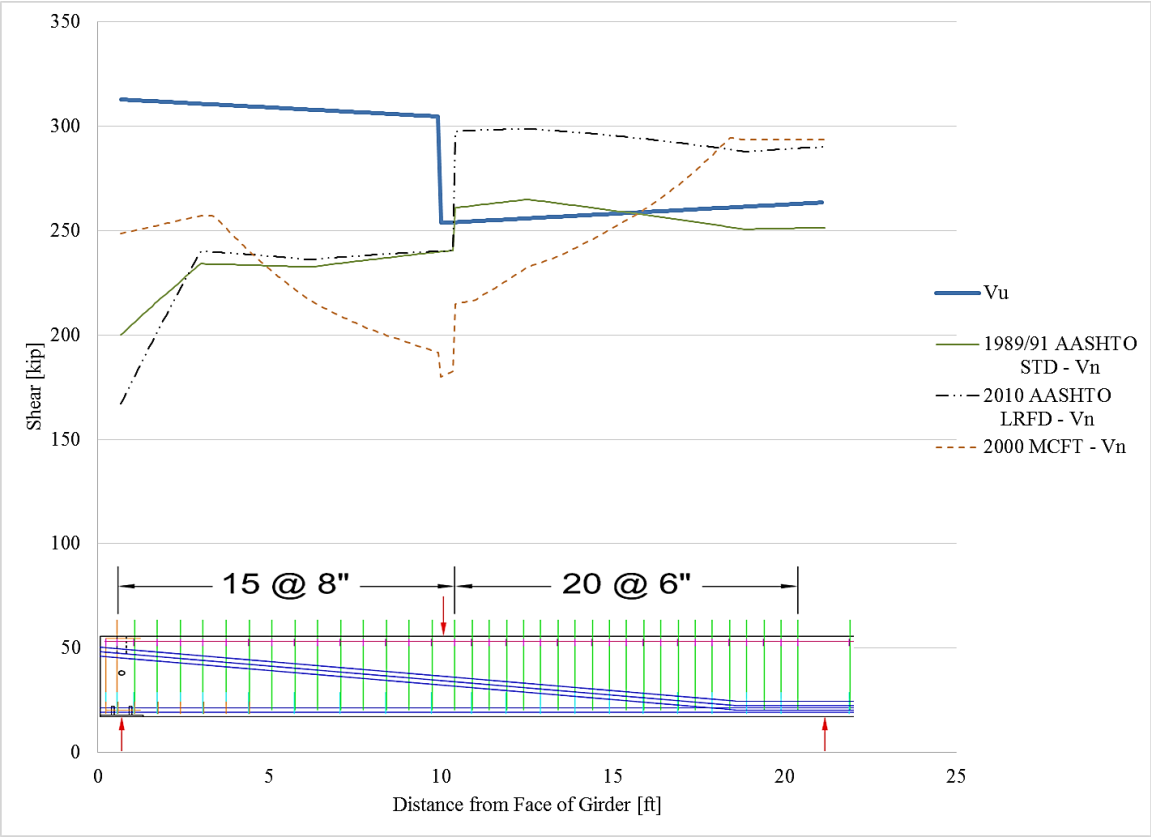

Figure 3-66: Applied shear and predicted shear capacity for 36M_8W due to applied load of 558 kip.

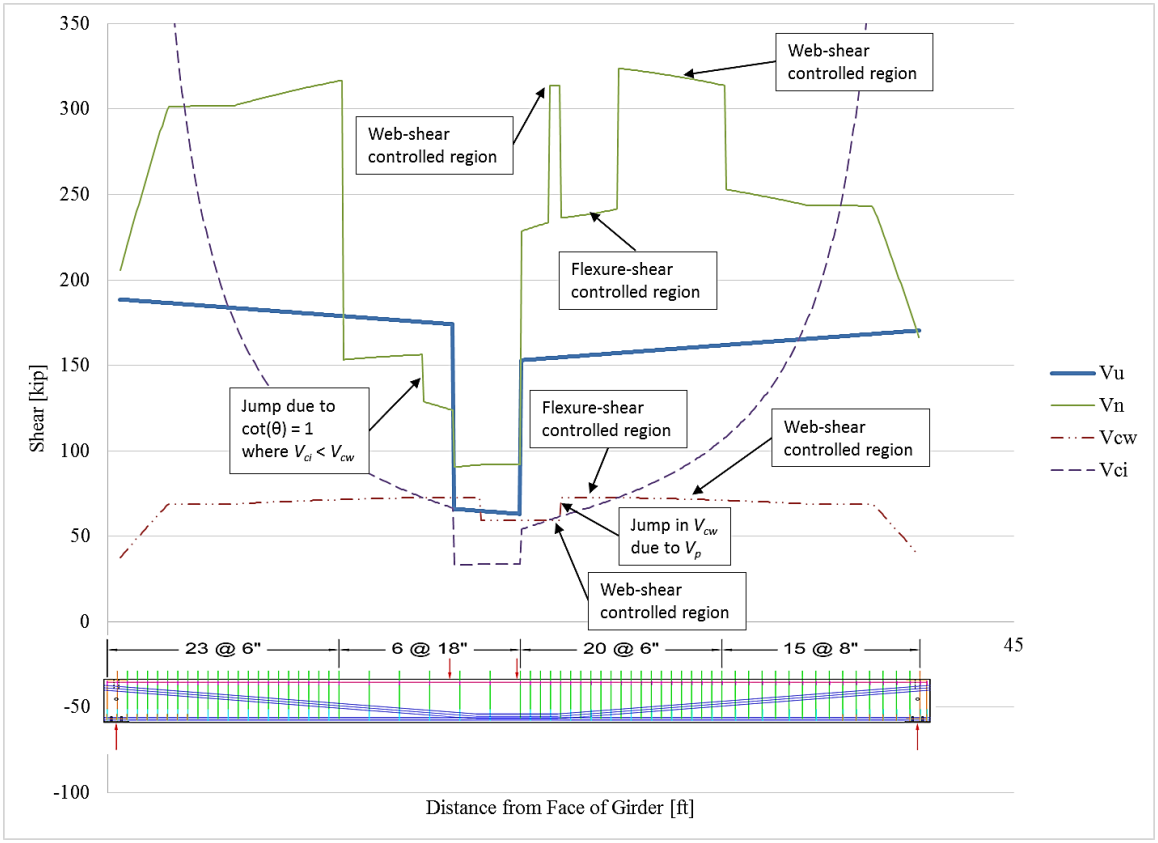

Figure 3-67: Shear due to applied load at midspan of 216 kips (total load of 324 kip) and 2010 AASHTO LRFD shear capacities in flexure-shear and web-shear controlled regions of 36M_18F.

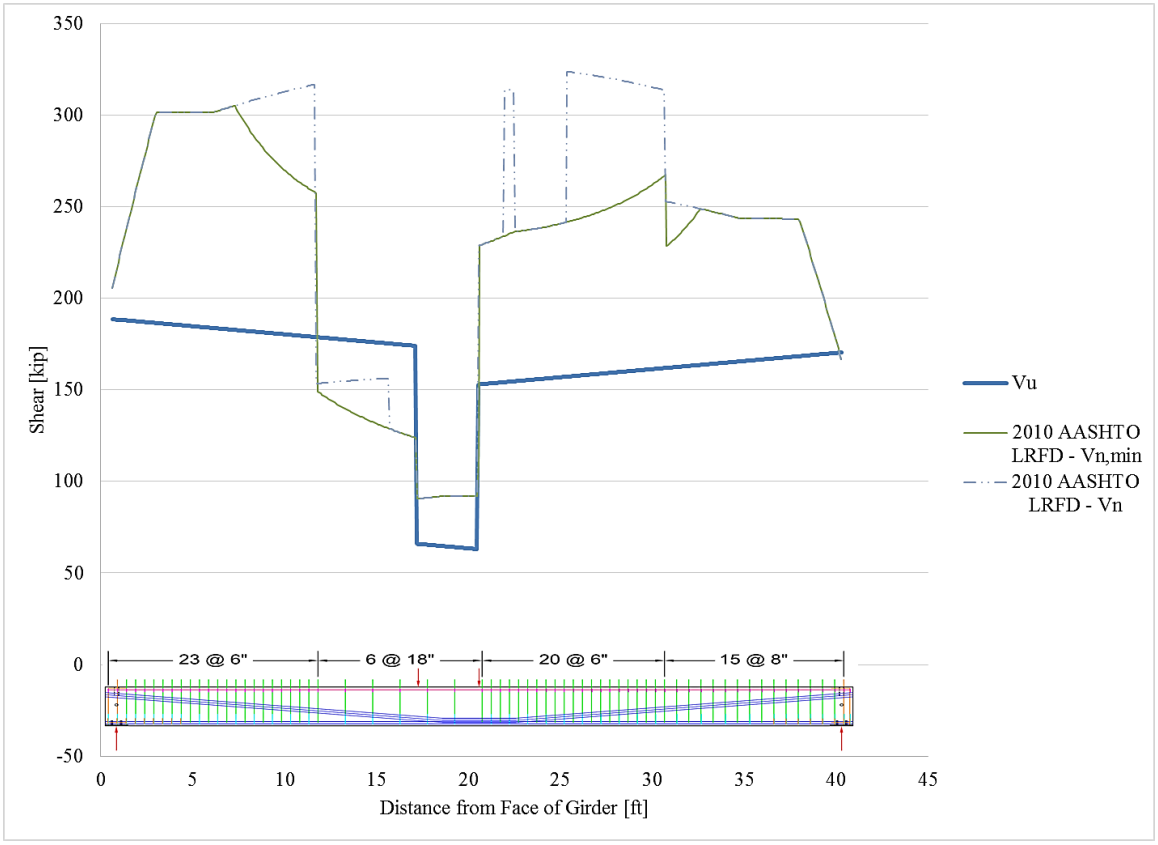

Figure 3-68: Shear due to applied load at midspan of 216 kips (total load of 324 kip) and 2010 AASHTO LRFD shear capacities for 36M_18F.

Appendices

Appendix A Girder Transverse Reinforcement Details

The steel reinforcing details and names used to describe the reinforcement of the prestressed concrete bridge girders described in this report correspond to the details and naming conventions currently used by MnDOT in their prestressed concrete bridge girders. Figures A-1 and A-2 show the out-to-out dimensions of the bars and the names associated with the shape. The bar size is indicated by the first two digits following the "G" in each of the names. The "E" at the end of the names indicates that the bars are epoxy coated. The layouts of the transverse reinforcement in the girder ends are indicated by Figures A-3 to A-6 for the 36M_18F, 45M_24W, 45M_8W, and 36M_8W girder ends, respectively.

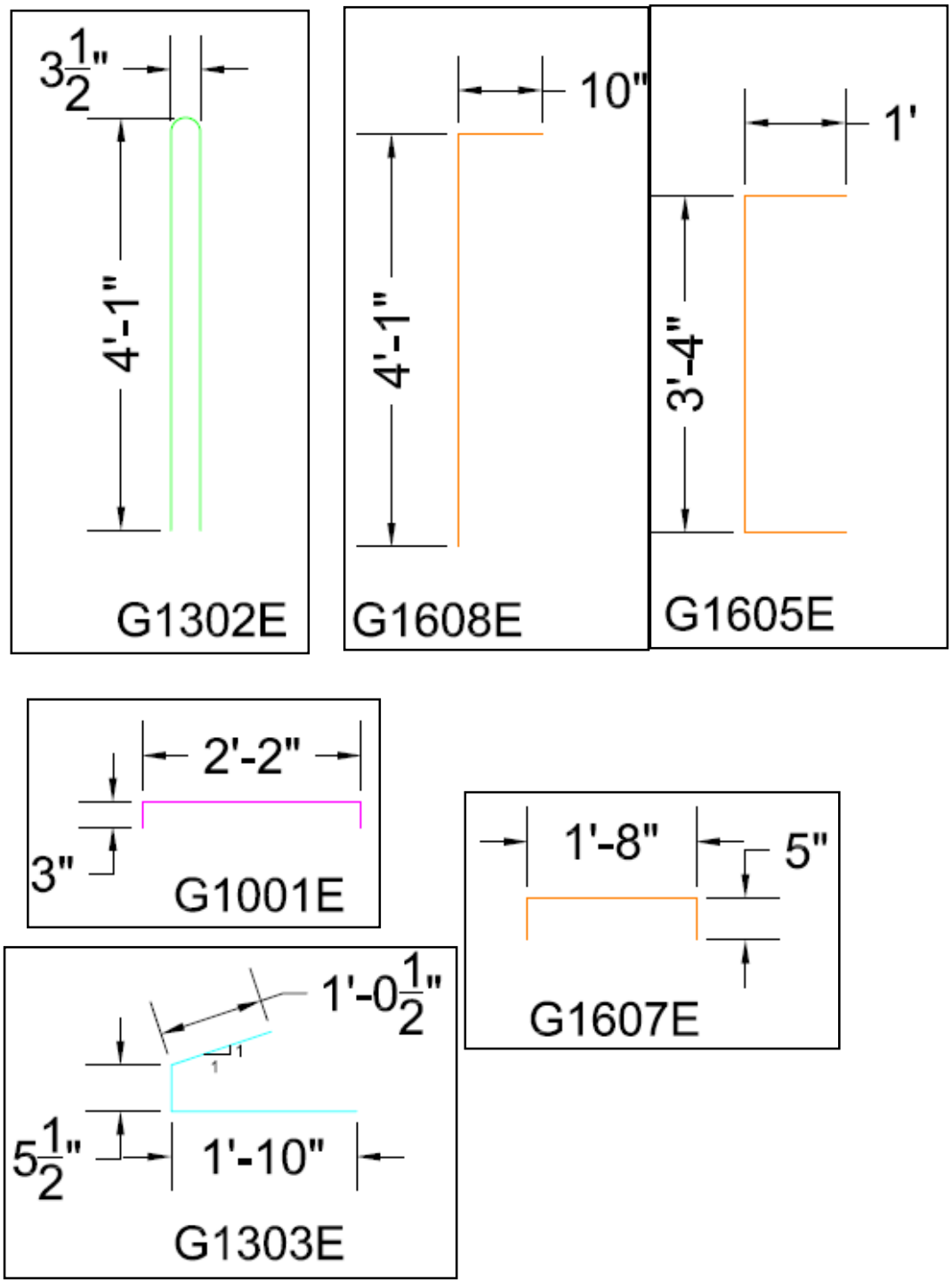

Figure A-1: 45M girder transverse reinforcement

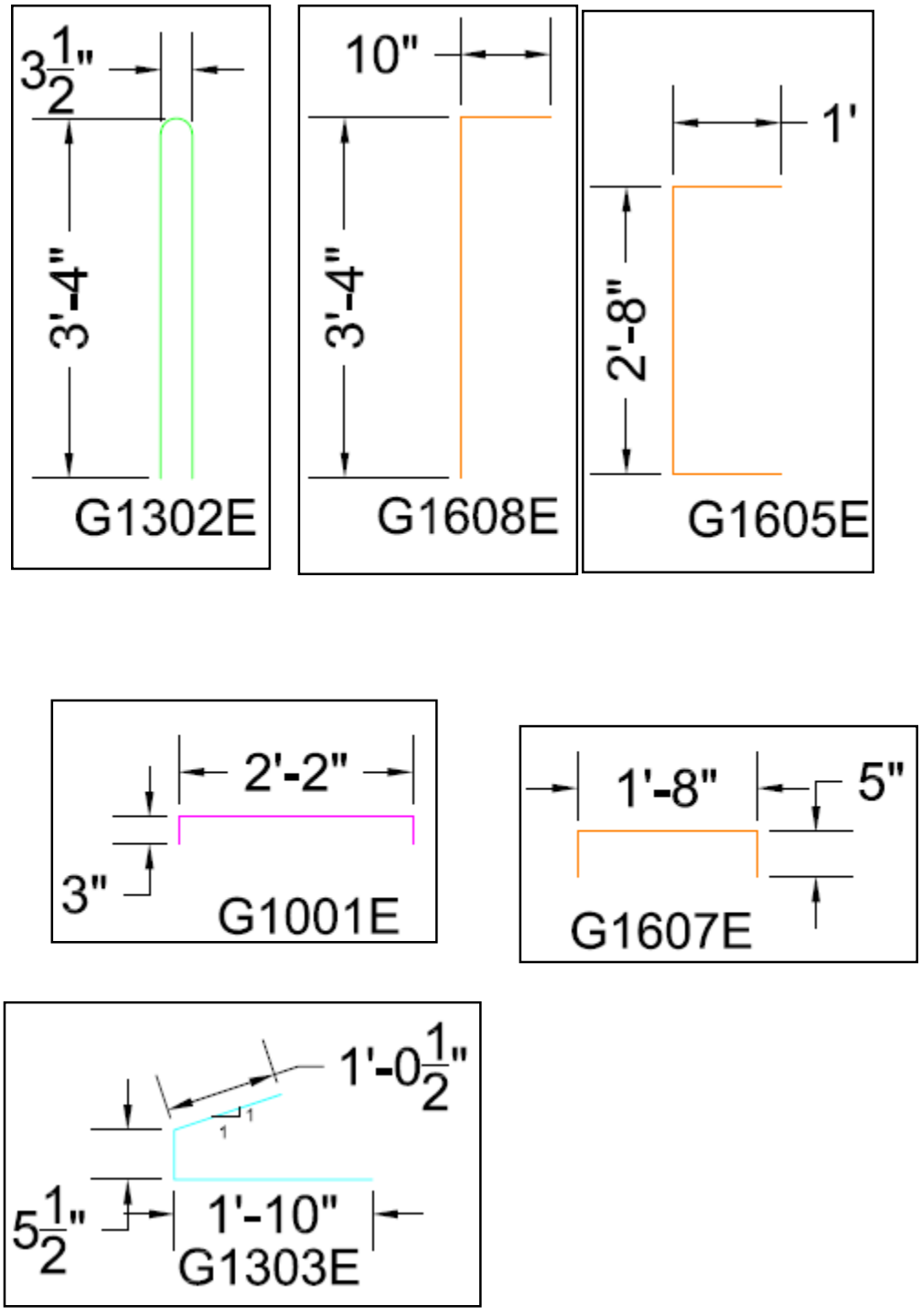

Figure A-2: 36M transverse reinforcement

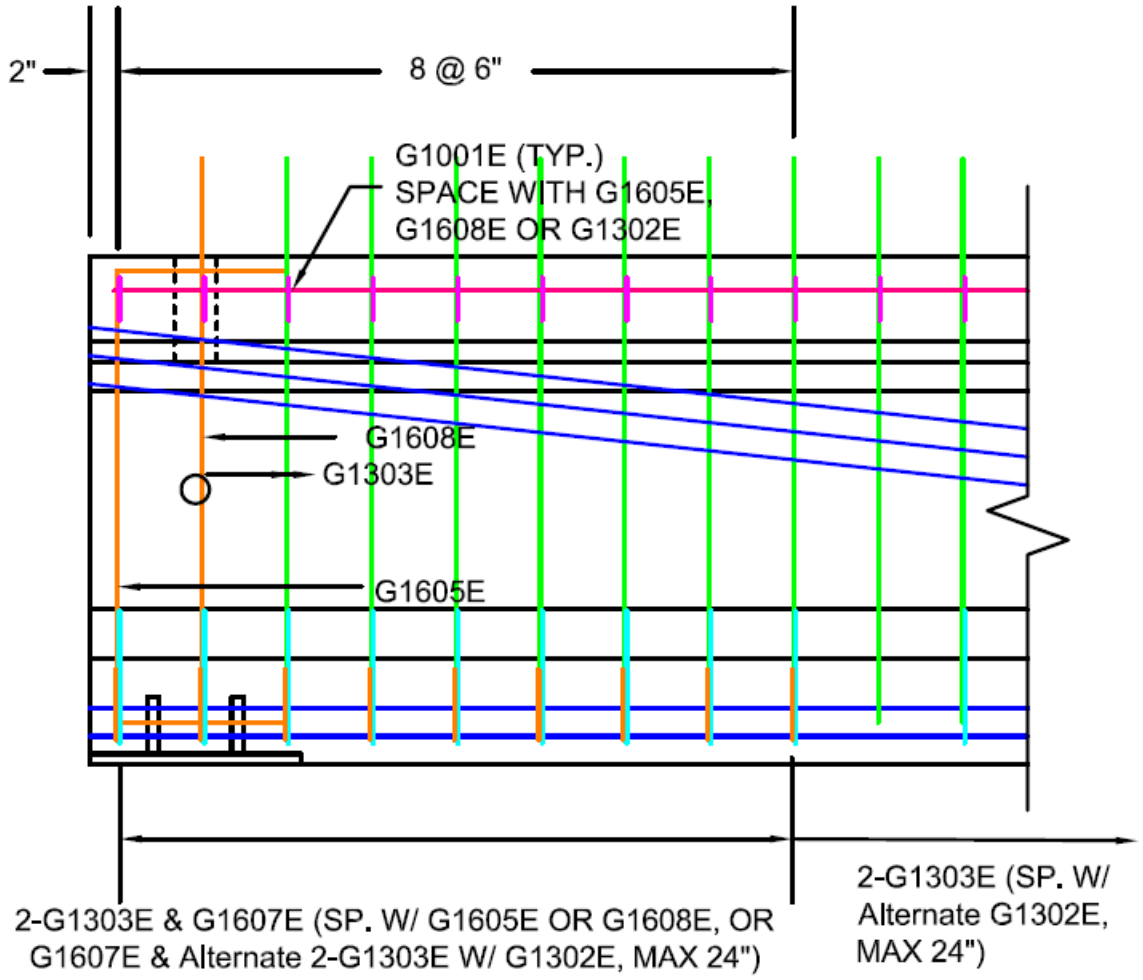

Figure A-3: Transverse reinforcement layout for 36M_18F end.

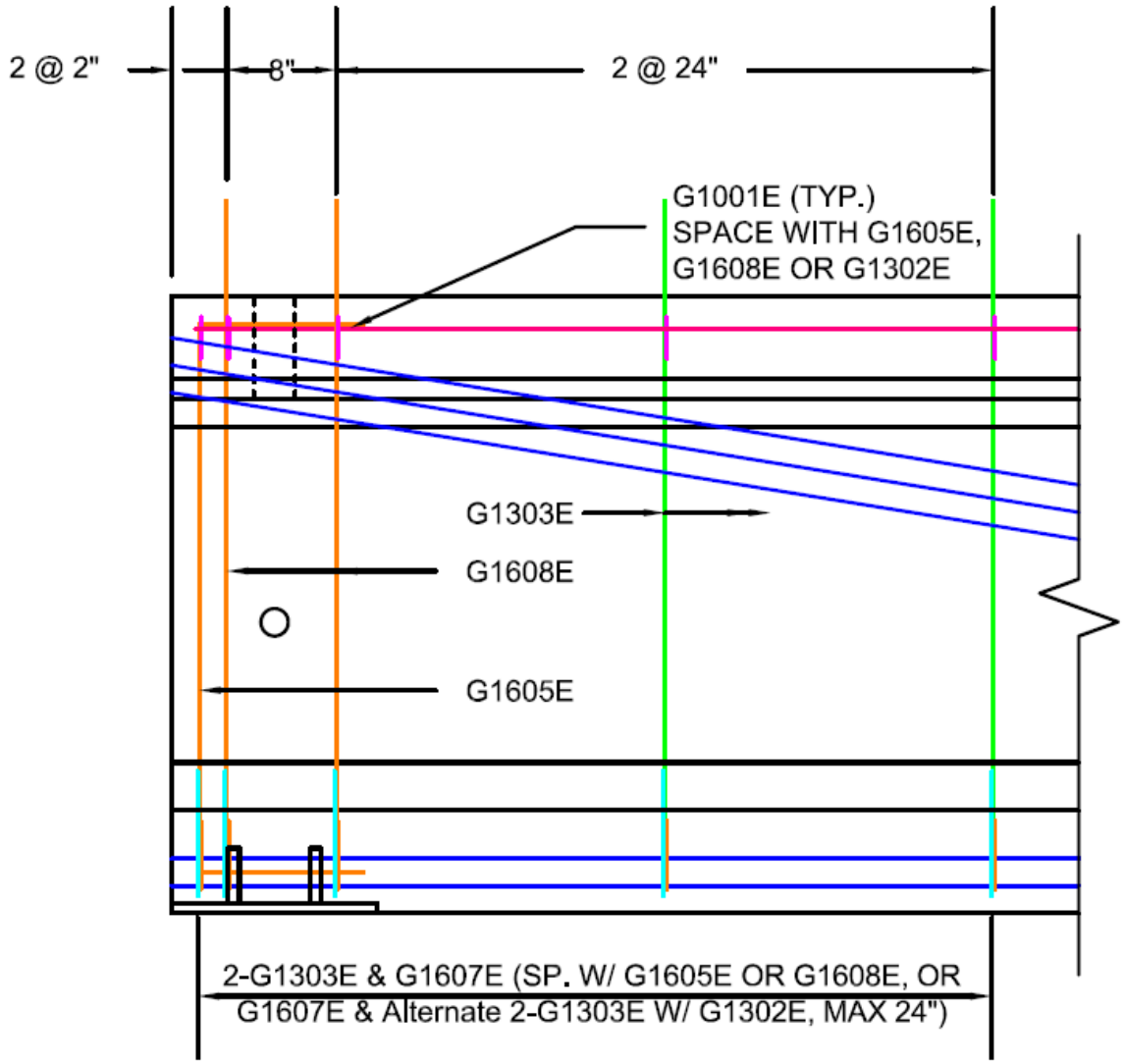

Figure A-4: Transverse reinforcement layout for 45M_24W end.

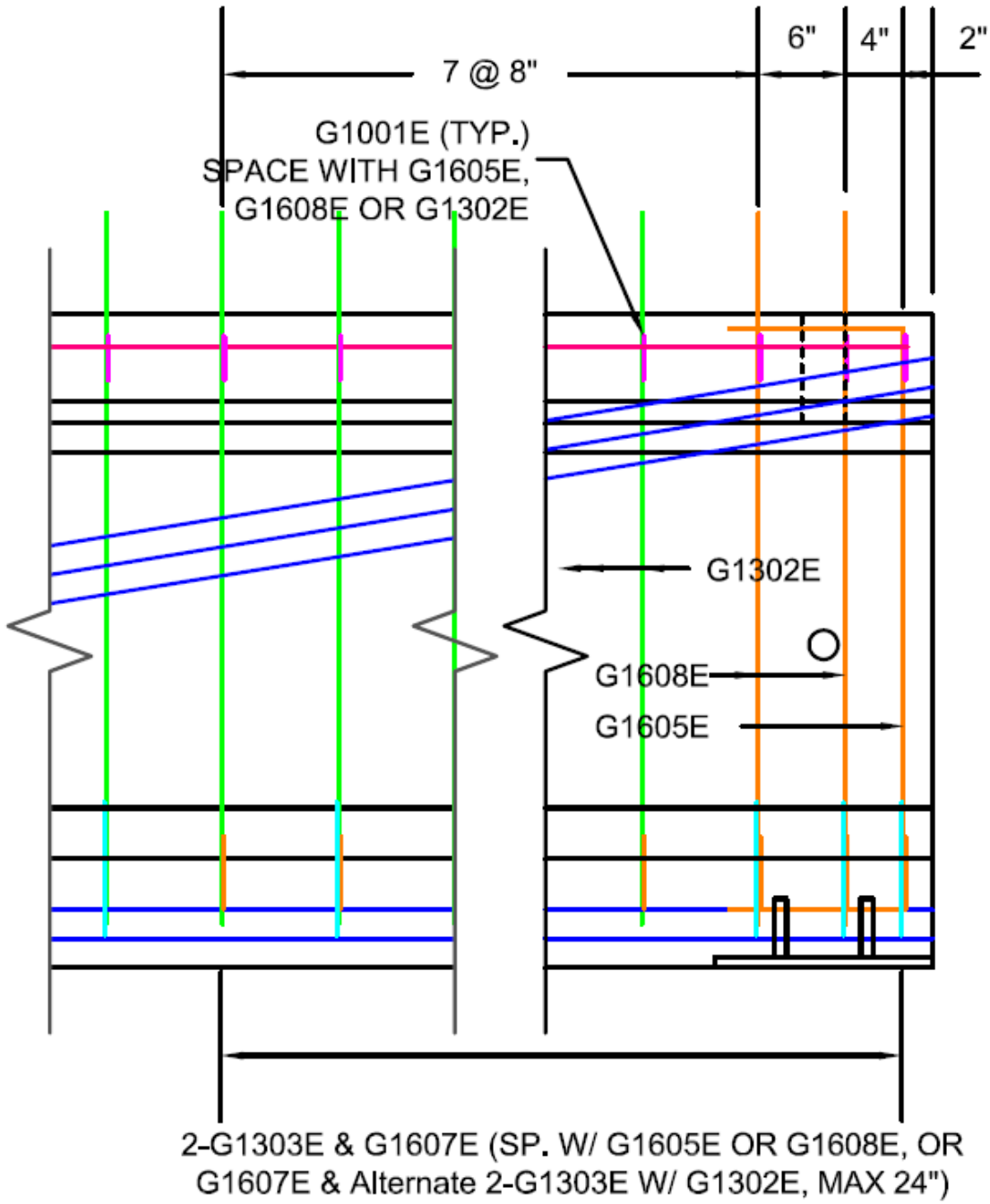

Figure A-5: Transverse reinforcement layout for 45M_8W end.

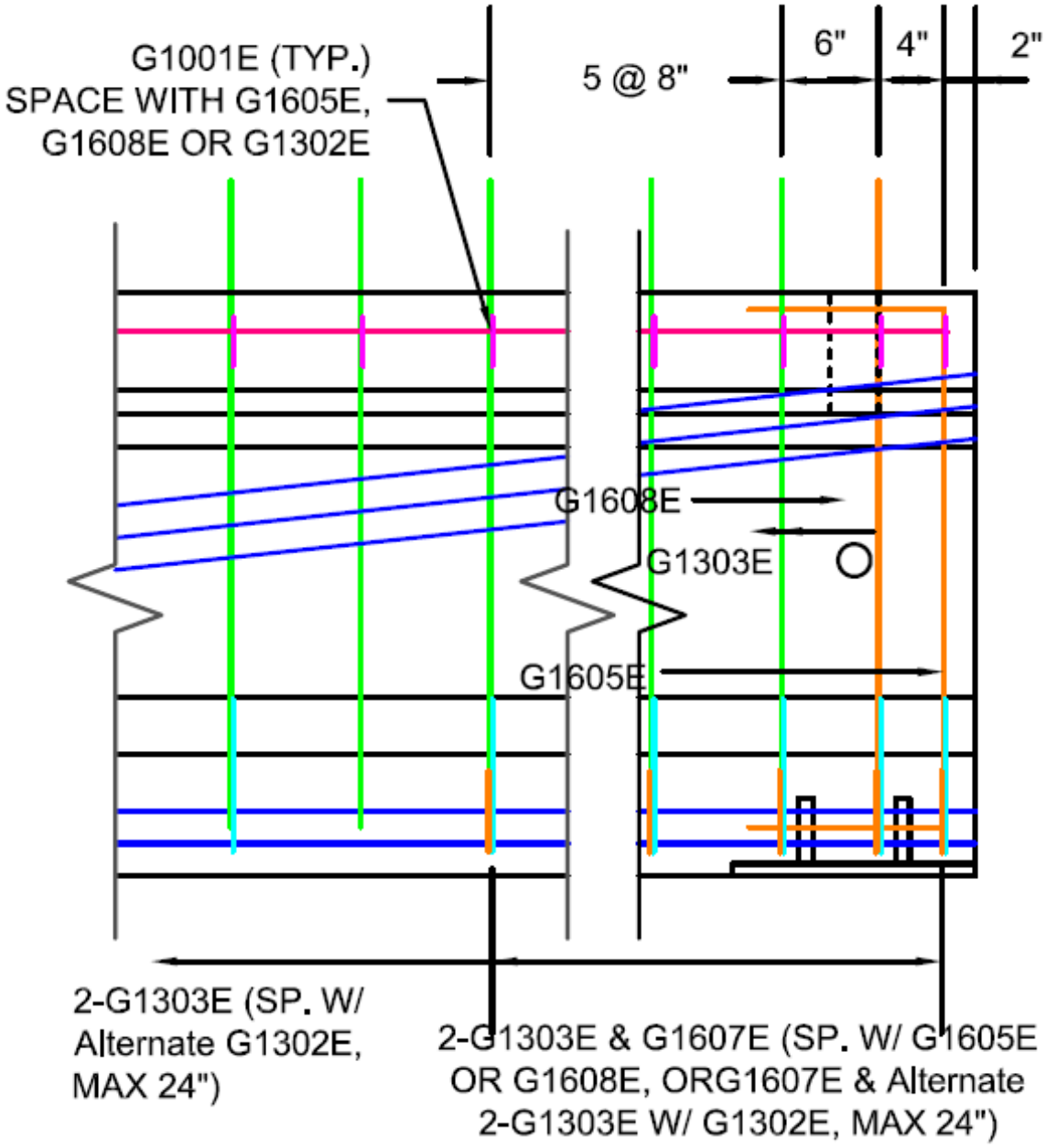

Figure A-6: Transverse reinforcement layout for 36M_8W end.

Appendix B As-Built Girder Capacity Sample Calculations

This appendix outlines the calculations used to determine the as-built girder capacities including flexural capacity, cracking moment, and shear capacity. The relaxation losses were predicted using the time-step method outlined by the PCI committee (Preston 1975).The calculated flexural and shear capacities are based on the 1989/91 AASHTO Standard Design Specification with 1991 Interim (AASHTO 1991). Additionally, detailed shear calculations based on the 2010 AASHTO LRFD Bridge Design Specifications (AASHTO 2010) are included.

B.1 Girder Properties and Geometry

Table Appendix B-1 summarizes the measured girder properties and the girder geometry used in the as-built girder calculations.

Table B-1: As-built girder properties and geometries used for girder calculations.

Property	Symbol [Units]	36M_18F	45M_24W	45M_8W	36M_8W
Girder Concrete Compressive Strength	f_c' [ksi]	6.3	6.8	7.0	6.9
Deck Concrete Compressive Strength	f_{dc}' [ksi]	5.13	4.78	4.89	5.86
Composite Slab Depth[1]	t_d [in.]	9.0	9.0	9.0	9.0
Stirrup Yield Strength	f_y [ksi]	70.0	67.0	67.0	70.0
Stirrup Leg Area	A_v [in.^{2}]	0.20	0.20	0.20	0.20
Stirrup Spacing	s [in.]	18	24	8	8
Measured Elastic Shortening Loss	ES [ksi]	10.3	18.9	18.9	10.3
Measured Creep & Shrinkage Loss	$C\&S$ [ksi]	9.5	14.9	14.9	9.5
Strand Loss After Seating	[ksi]	See Table 3-8			
Span Length	L_s [in.]	477	441	293	246
Web Width	b_w [in.]	6	6	6	6
Jacking Force	P_j [kip]	425	732	732	425
Girder Centroid (from girder bottom)	y_{gb} [in.]	18.0	22.3	22.3	18.0
Girder Net Centroid (from girder bottom)	y_{ngb} [in.]	18.2	22.6	22.6	18.2
Composite Girder Centroid (from girder bottom)	y_{Tcb} [in.]	24.5	29.3	29.3	24.5
Center of Prestress Effort (from girder bottom)	y_{COP} [in.]	3.3	3.6	3.6	3.3
VWG Location (from girder bottom)	y_{VWG} [in.]	4.25			
Girder Area	A_g [in.^{2}]	570	624	624	570
Girder Net Area	A_n [in.^{2}]	562	616	616	562
Strand Grade	[ksi]	270			
Strand Type		Low-Relaxation			
Strand Diameter	[in.]	0.6			
Strand Area	A_{ps} [in.^{2}]	0.22			
Draped Strand Area	A_{psd} [in^2]	1.34	1.34	1.34	1.34
Straight Strand Area	A_{pss} [in^2]	2.67	4.45	4.45	2.67
Draped Strand Centroid at Hold Down	$y_{d,hp}$ [in.]	5	7	7	5
Straight Strand Centroid	y_s [in.]	3	3	3	3
Gross Moment of Inertia	I_g [in.^{4}]	93,400	167,000	167,000	93,400
Net Moment of Inertia	I_n [in.^{4}]	91,800	164,000	164,000	91,800
Transformed Moment of Inertia	I_{Tc} [in.^{4}]	178,000	286,000	286,000	178,000

[1]Composite slab depth including 8 in. deck and 1 in. stool.

B.2 Elastic Shortening Calculations

Elastic shortening losses were estimated using the change in strain at release near the center of effort of prestress as measured by the embedded vibrating wire gage (VWG). The center of prestress effort was defined as the resultant prestress force location based on strand prestress following seating. The center of prestress effort location was held constant throughout the girder lifespans as changes in location due to unequal strand prestress losses were assumed negligible. Summaries of the elastic shortening losses calculated for the 36M and 45M girders as explained in Section 3.6.4 are shown below.

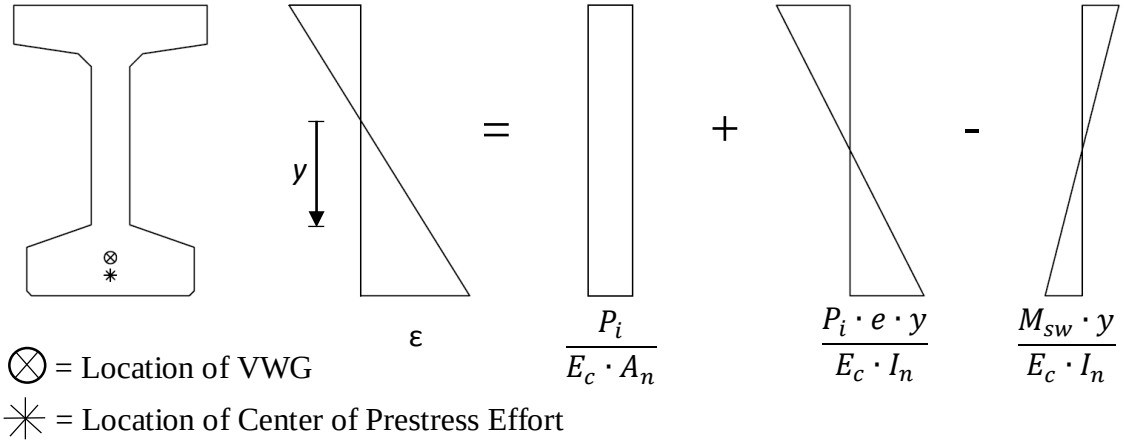

Figure B-1: Strain distribution in typical girder section due to initial prestress force.

Components of the strain due to effective prestress after release are shown in Figure B.1 and the total strain can be calculated across the girder cross section by

$$\varepsilon = \frac{P_i}{E_c \cdot A_n} + \frac{P_i \cdot e \cdot y}{E_c \cdot I_n} - \frac{M_{sw} \cdot y}{E_c \cdot I_n} \quad \text{(B.1)}$$

where P_i is the effective prestress force following release, e is the eccentricity of the center of prestress effort measured from the neutral axis of the net girder section, y is the eccentricity of the VWG location measured from the neutral axis of the net girder section, M_{sw} is the moment at midspan due to the self-weight of the girder, E_c is the concrete

modulus of elasticity, A_n is the net cross-sectional area of the girder, and I_n is the moment of inertia of the net girder section. Equation B.1 was iterated in order to solve for the effective prestress force required to produce strains of 349 and 651 μs, as measured by the VWG at release, for the 36M and 45M girders, respectively. Sample calculations for the required effective prestress are as follows.

$$349\ \mu s = \frac{414\ kip}{4050\ ksi \cdot 562\ in^2} + \frac{414\ kip \cdot 14.9\ in \cdot 13.9\ in}{4050\ ksi \cdot 91800\ in^4} - \frac{1695\ kip \cdot in \cdot 13.9\ in}{4050\ ksi \cdot 91800\ in^4} \quad \text{(B.2)}$$

$$651\ \mu s = \frac{748\ kip}{4050\ ksi \cdot 616\ in^2} + \frac{748\ kip \cdot 19.0\ in \cdot 18.3\ in}{4050\ ksi \cdot 164200\ in^4} - \frac{1455\ kip \cdot in \cdot 18.3\ in}{4050\ ksi \cdot 164200\ in^4} \quad \text{(B.3)}$$

where Equations B.2 and B.3 represent the calculations for the 36M and 45M girders, respectively. The assumed concrete modulus of elasticity was 4050 ksi based on $33{w_c}^{1.5}\sqrt{f'_{ci}}$, where the unit weight of concrete was measured as 147.3 lb/ft^3 (i.e., weight of one cylinder measured at time of test) and an average f_{ci}' of 4720 psi (i.e., 36M had a release strength of 5030 psi measured from concrete batched toward the live end and the 45M had a strength of 4400 psi measured from concrete batched toward dead end). By setting the *y* terms in Equations B.2 and B.3 equal to the eccentricity of the center of prestress efforts, the strains at the centers of prestress effort were determined as 360 and 663 μs for the 36M and 45M girders, respectively. These strains, multiplied by the modulus of elasticity of prestressing steel, resulted in predicted elastic shortening losses of and 10.3 and 18.9 ksi for the 36M and 45M girders, respectively. The resulting effective prestress forces previously calculated were, however, higher than the jacking

force measured by Cretex in both calculations, which was not feasible. This indicated an error in the calculation.

Assuming the strains measured by the VWG were reasonable, the error in effective prestress force was assumed to be in the determination of the modulus of elasticity of the concrete. To determine the required concrete moduli of elasticity of the girders at release, the effective prestress force was set equal to the difference of the initial jacking force after seating losses measured by Cretex and the elastic shortening losses predicted in the previous step. The required concrete moduli of elasticity to produce strains of 349 and 651 μs at the location of the VWG were 3560 and 3220 ksi for the 36M and 45M girders, respectively, as shown below.

$$349\ \mu s = \frac{371\ kip}{3560\ ksi \cdot 562\ in^2} + \frac{371\ kip \cdot 14.9\ in \cdot 13.9\ in}{3560\ ksi \cdot 91800\ in^4} - \frac{1695\ kip \cdot in \cdot 13.9\ in}{3560\ ksi \cdot 91800\ in^4} \quad \text{(B.4)}$$

$$651\ \mu s = \frac{603\ kip}{3220\ ksi \cdot 616\ in^2} + \frac{603\ kip \cdot 19.0\ in \cdot 18.3\ in}{3220\ ksi \cdot 164200\ in^4} - \frac{1455\ kip \cdot in \cdot 18.3\ in}{3220\ ksi \cdot 164200\ in^4} \quad \text{(B.5)}$$

The resulting concrete moduli were 12 to 20% lower than the predicted elastic moduli based on the concrete compressive strength and unit weight of concrete. Once again, by setting the *y* terms in Equations B.4 and B.5 equal to the eccentricity of the center of prestress efforts, the strains at the centers of prestress effort were determined as 360 and 663 μs for the 36M and 45M girders, respectively. As calculated previously, these strains, multiplied by the modulus of elasticity of prestressing steel, resulted in predicted elastic shortening losses of and 10.3 and 18.9 ksi for the 36M and 45M girders, respectively. These measured values of elastic shortening losses determined from the VWG strain measurements were deemed sufficiently accurate for the study.

B.3 Relaxation Loss Calculations

Prestress losses were predicted using the time-step method outlined by the PCI committee (Preston 1975); however, the need to stress different strands to different prestress levels in the 36M and 45M girders complicated the prediction of the prestressing strand relaxation losses. Strands with greater levels of prestress were expected to relax at a higher rate than strands with lighter prestress. Kajfasz (1958) stated that relaxation losses in strands prestressed less than $0.55f_{py}$ bear no practical significance and can be neglected.

Strand relaxation losses for the girders were calculated in two parts. First, the relaxation for strands stressed higher than $0.55f_{py}$ was calculated using the time-step method

$$RET = f_{st} \cdot \left\{ \frac{[\log 24 \cdot t - \log 24 \cdot t_1]}{45} \right\} \cdot \left[\frac{f_{st}}{f_{py}} - 0.55 \right] \quad \text{(B.6)}$$

where f_{st} is the stress in prestressing steel at time t_1 (psi), t is the time at the end of time interval (days), t_1 is the time at beginning of time interval (days), and f_{py} is yield stress of prestressing steel (psi). Second, the effective loss due to strand relaxation on the total prestress was determined by subtracting the weighted relaxation losses undergone by strands stressed higher than $0.55f_{py.}$

A sample calculation for the relaxation losses occurring in the 36M girder between the time of stressing to the time of release is shown below, given that the strand yield stress was 243,000 psi and an average prestress of 168,900 psi for the straight strands designed to be stressed to $0.6f_{pu}$.

$$RET = 168.9\ ksi \cdot \left\{ \frac{\left[\log 24 \cdot 1.5\ d - \log 24 \cdot \frac{1}{24}\ d\right]}{45} \right\} \cdot \left[\frac{168.9\ ksi}{243\ ksi} - 0.55 \right] = 0.847\ ksi \quad \text{(B.7)}$$

Because the relaxation loss of 0.847 ksi only affected the strands stressed higher than $0.55f_{py}$, a weighted relaxation loss was used to determine the effective prestress loss due to relaxation. This was accomplished by dividing the predicted relaxation loss by the total number of prestressing strands and multiplying it by the number of strands stressed over $0.55f_{py}$ as shown below.

$$RET_{effective} = RET \cdot \frac{N_{>55\%}}{N} \tag{B.8}$$

$$RET_{effective} = 0.847\ ksi \cdot \frac{6}{18} = \mathbf{0.283\ ksi} \tag{B.9}$$

The effective relaxation losses were calculated in a similar manner for the remaining time steps. The sum of the predicted effective relaxation loss from each time step was equal to the total prestress relaxation loss experienced by the girders.

Table B-2: Relaxation losses at time of test for as-built girders.

Variable	36M_18F	45M_24W	45M_8W	36M_8W
RET [ksi]	1.5	1.3	1.3	1.5
$RET_{effective}$ [ksi]	0.5	0.7	0.7	0.5

B.4 Flexural Capacity

The flexural capacity of the beams were calculated using the 1989/91 AASHTO Standard Design Specification with 1991 Interim (AASHTO 1991). The code provided formulas for determining the force in the prestressing steel at ultimate are only valid if the effective prestress after losses is larger than $0.5f_{pu}$. Because the effective prestress was less than the specified limit for both girders, the strain compatibility approach presented in the PCI Bridge Design Manual (Prestressed/Precast Concrete Institute 1997) was used to calculate flexural capacity. A detailed moment capacity calculation is provided for the 36M_18F girder followed by tabulated results for the capacity calculations of the remaining girders, each evaluated at the location of maximum applied moment.

An iterative approach was used to determine the flexural capacity by assuming the depth of the neutral axis, c_{sc}. The strain in each layer of prestressing steel for each nominal level of effective prestress, $\varepsilon_{sc,}$ was determined as

$$\varepsilon_{sc} = 0.003 \cdot \left(\frac{d_{sc}}{c_{sc}} - 1\right) + \frac{f_{pe}}{E_{ps}} \tag{B.10}$$

where d_{sc} is the distance from the top of the deck to the centroid of the strand, f_{pe} is the effective stress in the prestress steel after losses, and E_{ps} is the modulus of elasticity of the prestressing strand. The stress in the strand was then determined using formulas developed by Devalapura and Tadros (1992) for low-relaxation prestressing strand

$$f_{sc} = \varepsilon_{sc} \cdot \left\{887 + \frac{27613}{[1 + (112.4 \cdot \varepsilon_{sc})^{7.36}]^{\frac{1}{7.36}}}\right\} \tag{B.11}$$

Once the strand stress was determined, the total prestressing force was calculated by multiplying the strand stress by the strand area. The resulting tension force, F_s, was compared to the compression force in the concrete, F_c, associated with an equivalent

rectangular stress block. The depth of the stress block, a_{sc}, was equal to the product of a modification factor based on the concrete strength of the composite deck, $\beta_{1,}$ and the assumed neutral axis depth. If the compression and tension were not equal, a new location of the neutral axis was assumed and the process was repeated. The nominal moment capacity of the girder, M_n, was calculated by summing the moments of the steel tension force and concrete compressive force about the top of the girder, such that the moment arm for the concrete compression was equal to half the stress block depth.

The as-built girder flexural capacity calculations are as follows:

The following calculations are used to determine the as-built girder flexural strength based on the 1989 LRFD Standard Specification with 1991 Interim Revisions.

Length of girder	L_g =	492	in
First bearing pad center		7.5	in
Second bearing pad center		484.5	in
Span length	L =	477	in
Concrete compressive strength	f'_c =	6.3	ksi
Width of the girder web	b_w =	6	in
Height of deck	h_d =	9	in
Height of girder	h_g =	36	in
Jacking force	P_j =	424.9	kip
Width of the deck	b_d =	28.5	in
Girder centroid from the bottom	y_{gb} =	17.97	in
Girder centroid from the bottom for the net section	y_{ngb} =	18.16	in
Area of the girder	A_g =	570	in^2
	A_n =	562.1	in^2
Self weight of the girder	w_g =	0.051	kip/in
Self weight of the deck (assuming 150 lb/ft^3 for the self weight of concrete)	w_d =	0.022	kip/in
Strand area		0.2227	in^2
Strand diameter	d_s =	0.6	in
Area of draped prestressing steel	A_{psd} =	1.34	in^2
Area of straight prestressing steel	A_{pss} =	2.67	in^2
Area of prestressing steel	A_{ps} =	4.01	in^2
Centroid of draped strands at girder end	$y_{d,end}$ =	29.0	in
Centroid of draped strands at hold down point	$y_{d,hp}$ =	5.0	in
Centroid of the area of the straight strands	y_s =	3.00	in
Distance to hold down point	L_{hp} =	222	in
Angle of draped strands	α =	0.00	deg.
Eccentricity of the resultant of the prestress force at the location of interest "x"	e =	14.87	in
Moment of inertia for the girder	I_g =	93351.373	in^4
Net moment of inertia for the girder	I_n =	91767.365	in^4
Transformed moment of inertia for the composite girder	I_{Tc} =	178419	in^4

Centroid of the transformed composite section	y_{Tcb} =	24.48	in
Transverse reinforcement yield stress	f_y =	70.2	ksi
Transverse reinforcement spacing	s =	18	in

Prestress losses:

Seating loss	SL =	2.82	ksi
Elastic shortening losses	ES =	10.3	ksi
Relaxation prior to release		0.3	ksi
Relaxation following release		0.12	ksi
Relaxation of prestressing steel	CR_s =	0.420	ksi
Shrinkage + creep of concrete	SH & CR_c =	9.5	ksi

f_{cir} is the stress at the center of gravity of the strands due to prestress force and the dead load of the beam at release calculated at the location of maximum moment.

f_{cds} is the stress at the center of gravity of the strands due to the dead load on the beam except that applied at the time of release.

Eccentricity of the strand force at the location of maximum moment due to dead load (L/2)	e_{hp} =	14.87	in
The prestressing force after release includes the elastic shortening losses	P_i =	371.10	kip
Maximum moment due to self weight of girder at release (full length)	M_{maxi} =	1547.0	kip-in

$$f_{cir} = \frac{P_i}{A_n} + \frac{P_i \cdot e^2}{I_n} - \frac{M_{max,i} \cdot e}{I_n}$$

= 0.65 ksi + 0.88 ksi - 0.25 ksi f_{cir} = 1.30 ksi

The maximum moment due to all dead load applied except that at the time of release	$M_{max,d-i}$ =	632.6	kip-in
	f_{cds} =	0.102	ksi

$$f_{cds} = \frac{M_{max,d-i} \cdot e}{I_n}$$

Total prestress losses	$TL = ES + SH + CR_c + CR_s + SL$	TL =	23.0	ksi
The effective prestress force after accounting for losses		P_e=	332.5	kip

Flexural Capacity:

Concrete compressive strength of deck	f'_{dc} =	5.13	ksi
Depth of neutral axis	c =	10.145204	in.
Modifaction factor	β_1 =	0.79	
Depth of stress block	a =	8.05	in.

Consider each row of strands seperately (row 1 is the bottom row, row 5 is the top row of draped strands)

y_1	2.0 in.	d_1	43.0 in.	$f_{pe,1}$ =	147.7 ksi
y_2	4.0 in.	d_2	41.0 in.	$f_{pe,2}$ =	7.1 ksi
y_3	3.0 in.	d_3	42.0 in.	$f_{pe,3}$ =	96.8 ksi
y_4	5.0 in.	d_4	40.0 in.	$f_{pe,4}$ =	95.5 ksi
y_5	7.0 in.	d_5	38.0 in.	$f_{pe,5}$ =	97.7 ksi

$$\varepsilon_i = 0.003 \cdot \left(\frac{d_i}{c} - 1\right) + \frac{f_{pe,i}}{E_{ps}}$$

ε_1 =	0.015
ε_2 =	0.009
ε_3 =	0.013
ε_4 =	0.012
ε_5 =	0.012

Using the formula developed by Devalapura and Tadros (1992) that defines the stress-strain relationship of 270 ksi low-relaxation strands to determine the stress in the strands.

$$f_{sc,i} = \min\left(\varepsilon_i \cdot \left(887 + \frac{27613}{[1 + (112.4 \cdot \varepsilon_i)^{7.36}]^{\frac{1}{7.36}}}, 270\ ksi\right)\right)$$

f_{sc1} =	258.1 ksi
f_{sc2} =	237.3 ksi
f_{sc3} =	254.8 ksi
f_{sc4} =	253.3 ksi
f_{sc5} =	251.8 ksi

Determine effective concrete compressive area $A_{beff} = b_d \cdot \frac{f'_{dc}}{f'_c} \cdot a$ A_{beff} = 186.8 in^2

The total force in the steel is: $F_s = \sum f_{sc,i} \cdot A_{ps}$ F_s = 1000.4 kip

The compressive force in the concrete is: $F_c = 0.85 \cdot f'_c \cdot A_{beff}$ F_c = 1000.4 kip

Equilibrium: 0.0 kip

Determine flexural capacity: $M_n = \sum f_{sc,i} \cdot A_{ps} \cdot d_i - F_c \cdot \frac{a}{2}$ M_n = 3112 ft·kip

The following calculations are used to determine the as-built girder flexural strength based on the 1989 LRFD Standard Specification with 1991 Interim Revisions.

Length of girder	L_g =	456	in
First bearing pad center		7.5	in
Second bearing pad center		448.5	in
Span length	L =	441	in
Concrete compressive strength	f'_c =	6.8	ksi
Width of the girder web	b_w =	6	in
Height of deck	h_d =	9	in
Height of girder	h_g =	45	in
Jacking force	P_j =	732.15	kip
Width of the deck	b_d =	28.5	in
Girder centroid from the bottom	y_{gb} =	22.34	in
Girder centroid from the bottom for the net section	y_{ngb} =	22.58	in
Area of the girder	A_g =	624	in^2
	A_n =	616.1	in^2
Self weight of the girder	w_g =	0.056	kip/in
Self weight of the deck (assuming 150 lb/ft^3 for the self weight of concrete)	w_d =	0.022	kip/in
Strand area		0.2227	in^2
Strand diameter	d_s =	0.6	in
Area of draped prestressing steel	A_{psd} =	1.34	in^2
Area of straight prestressing steel	A_{pss} =	4.45	in^2
Area of prestressing steel	A_{ps} =	5.79	in^2
Centroid of draped strands at girder end	$y_{d,end}$ =	40.0	in
Centroid of draped strands at hold down point	$y_{d,hp}$ =	7.0	in
Centroid of the area of the straight strands	y_s =	3.00	in
Distance to hold down point	L_{hp} =	204	in
Angle of draped strands	α =	9.27	deg.
Eccentricity of the resultant of the prestress force at the location of interest "x"	e =	17.02	in
Moment of inertia for the girder	I_g =	167050	in^4
Net moment of inertia for the girder	I_n =	164212	in^4
Transformed moment of inertia for the composite girder (excluding effect of steel)	I_{Tc} =	285967	in^4

Centroid of the transformed composite section	y_{Tcb} =	29.32	in
Transverse reinforcement yield stress	f_y =	67.0	ksi
Transverse reinforcement spacing	s =	24	in

Prestress losses:

Seating loss	SL =	2.82	ksi
Elastic shortening losses	ES =	18.9	ksi
Relaxation prior to release		0.5	ksi
Relaxation following release		0.168	ksi
Relaxation	CR_s =	0.668	ksi
Shrinkage + creep of concrete	SH & CR_c =	14.9	ksi

f_{cir} is the stress at the center of gravity of the strands due to prestress force and the dead load of the beam at release calculated at the location of maximum moment.

f_{cds} is the stress at the center of gravity of the strands due to the dead load on the beam except that applied at the time of release.

Eccentricity of the strand force at the location of maximum moment due to dead load (L/2)	e_{bp} =	18.97	in
The prestressing force after release includes the elastic shortening losses	P_i =	603.49	kip
Maximum moment due to self weight of girder at release (full length)	M_{maxi} =	1454.8	kip-in

$$f_{cir} = \frac{P_i}{A_n} + \frac{P_i \cdot e^2}{I_n} - \frac{M_{max,i} \cdot e}{I_n}$$

= 0.97 ksi + 1.3 ksi - 0.17 ksi f_{cir} = 2.13 ksi

The maximum moment due to all dead load applied except that at the time of release	$M_{max,d-i}$ =	540.7	kip-in

$$f_{cds} = \frac{M_{max,d-i} \cdot e}{I_n}$$

f_{cds} = 0.062 ksi

Total prestress losses $TL = ES + SH + CR_c + CR_s + SL$	TL =	37.3	ksi
The effective prestress force after accounting for losses	P_e =	516.2	kip

Flexural Capacity:

Concrete compressive strength of deck	f'_{dc} =	4.78	ksi
Depth of neutral axis	c =	13.5	in.
Modifaction factor	β_1 =	0.81	
Depth of stress block	a =	11.0	in.

Consider each row of strands seperately (row 1 is the bottom row, row 5 is the top row of draped strands)

y_1	2.0 in.	d_1	52.0 in.		$f_{pe,1}$ =	133.9 ksi
y_2	4.0 in.	d_2	50.0 in.	$f_{pe,0.6fpu}$ = 135.28	$f_{pe,2}$ =	-6.9 ksi
y_3	14.0 in.	d_3	40.0 in.		$f_{pe,3}$ =	82.8 ksi
y_4	16.0 in.	d_4	38.0 in.		$f_{pe,4}$ =	81.5 ksi
y_5	18.0 in.	d_5	36.0 in.		$f_{pe,5}$ =	83.7 ksi

$$\varepsilon_i = 0.003 \cdot \left(\frac{d_i}{c} - 1\right) + \frac{f_{pe,i}}{E_{ps}}$$

$\varepsilon_{0.6fpu}$ = 0.013

ε_1 =	0.013
ε_2 =	0.008
ε_3 =	0.009
ε_4 =	0.008
ε_5 =	0.008

Using the formula developed by Devalapura and Tadros (1992) that defines the stress-strain relationship of 270 ksi low-relaxation strands to determine the stress in the strands.

$$f_{sc,i} = \min\left(\varepsilon_i \cdot \left(887 + \frac{27613}{[1 + (112.4 \cdot \varepsilon_i)^{7.36}]^{\frac{1}{7.36}}}, 270\ ksi\right)\right.$$

$f_{sc,0.6fpu}$ = 254.9 ksi

f_{sc1} =	255.7 ksi
f_{sc2} =	214.4 ksi
f_{sc3} =	230.0 ksi
f_{sc4} =	222.4 ksi
f_{sc5} =	215.7 ksi

Determine effective concrete compressive area $A_{beff} = b_d \cdot \frac{f'_{dc}}{f'_c} \cdot a$ — A_{beff} = 238.9 in^2

The total force in the steel is: $F_s = \sum f_{sc,i} \cdot A_{ps}$ — F_s = 1380.6 kip

The compressive force in the concrete is: $F_c = 0.85 \cdot f'_c \cdot A_{beff}$ — F_c = 1380.6 kip

Equilibrium: 0.0 kip

Determine flexural capacity: $M_n = \sum f_{sc,i} \cdot A_{ps} \cdot d_i - F_c \cdot \frac{a}{2}$ — M_n = 4921 ft·kip

University of Minnesota
45M_8W Calculations

The following calculations are used to determine the as-built girder flexural strength based on the 1989 LRFD Standard Specification with 1991 Interim Revisions.

Length of girder	L_g =	341.75	in
First bearing pad center		7.75	in
Second bearing pad center		300.75	in
Span length	L =	293	in
Concrete compressive strength	f'_c =	7	ksi
Width of the girder web	b_w =	6	in
Height of deck	h_d =	9	in
Height of girder	h_g =	45	in
Jacking force	P_j =	732.15	kip
Width of the deck	b_d =	28.5	in
Girder centroid from the bottom	y_{gb} =	22.34	in
Girder centroid from the bottom for the net section	y_{ngb} =	22.58	in
Area of the girder	A_g =	624	in^2
	A_n =	616.1	in^2
Self weight of the girder	w_g =	0.056	kip/in
Self weight of the deck (assuming 150 lb/ft^3 for the self weight of concrete)	w_d =	0.022	kip/in
Strand area		0.2227	in^2
Strand diameter	d_s =	0.6	in
Area of draped prestressing steel	A_{psd} =	1.34	in^2
Area of straight prestressing steel	A_{pss} =	4.45	in^2
Area of prestressing steel	A_{ps} =	5.79	in^2
Centroid of draped strands at girder end	$y_{d,end}$ =	40.0	in
Centroid of draped strands at hold down point	$y_{d,hp}$ =	7.0	in
Centroid of the area of the straight strands	y_s =	3.00	in
Distance to hold down point	L_{hp} =	204	in
Angle of draped strands	α =	9.27	deg.
Eccentricity of the resultant of the prestress force at the location of interest "x"	e =	17.02	in
Moment of inertia for the girder	I_g =	167050	in^4
Net moment of inertia for the girder	I_n =	164212	in^4
Transformed moment of inertia for the composite girder	I_{Tc} =	285967	in^4

Centroid of the transformed composite section	y_{Tcb} =	29.32	in
Transverse reinforcement yield stress	f_y =	67.0	ksi
Transverse reinforcement spacing	s =	8	in

Prestress losses:

Seating loss	SL =	2.82	ksi
Elastic shortening losses	ES =	18.9	ksi
Relaxation prior to release		0.5	ksi
Relaxation following release		0.168	ksi
Relaxation of prestressing steel	CR_s =	0.668	ksi
Shrinkage + creep of concrete	SH & CR_c=	14.9	ksi

f_{cir} is the stress at the center of gravity of the strands due to prestress force and the dead load of the beam at release calculated at the location of maximum moment.

f_{cds} is the stress at the center of gravity of the strands due to the dead load on the beam except that applied at the time of release.

Eccentricity of the strand force at the location of maximum moment due to dead load (L/2)	e_{bp} =	18.97	in
The prestressing force after release includes the elastic shortening losses	P_i =	603.49	kip
Maximum moment due to self weight of girder at release (full length)	M_{maxi} =	817.1	kip-in

$$f_{cir} = \frac{P_i}{A_n} + \frac{P_i \cdot e^2}{I_n} - \frac{M_{max,i} \cdot e}{I_n}$$

= 0.97 ksi + 1.3 ksi - 0.09 ksi f_{cir} = 2.21 ksi

The maximum moment due to all dead load applied except that at the time of release	$M_{max,d-i}$ =	225.1	kip-in

$$f_{cds} = \frac{M_{max,d-i} \cdot e}{I_n}$$

f_{cds} = 0.026 ksi

Total prestress losses $TL = ES + SH + CR_c + CR_s$+SL TL = 37.3 ksi

The effective prestress force after accounting for losses P_e= 516.2 kip

Flexural Capacity:

Concrete compressive strength of deck	f'_{dc} =	4.89	ksi
Depth of neutral axis	c =	13.4	in.
Modifaction factor	β_1 =	0.81	

Depth of stress block $a =$ 10.8 in.

Consider each row of strands seperately (row 1 is the bottom row, row 5 is the top row of draped strands)

y_1	2.0 in.	d_1	52.0 in.			$f_{ps,1} =$	133.9 ksi
y_2	4.0 in.	d_2	50.0 in.	$f_{ps,2.5} =$	135.28	$f_{ps,2} =$	-6.9 ksi
y_3	14.0 in.	d_3	40.0 in.			$f_{ps,3} =$	82.8 ksi
y_4	16.0 in.	d_4	38.0 in.			$f_{ps,4} =$	81.5 ksi
y_5	18.0 in.	d_5	36.0 in.			$f_{ps,5} =$	83.7 ksi

$$\varepsilon_i = 0.003 \cdot \left(\frac{d_i}{c} - 1\right) + \frac{f_{pe,i}}{E_{ps}}$$

$\varepsilon_{2.5} =$ 0.013

$\varepsilon_1 =$ 0.013
$\varepsilon_2 =$ 0.008
$\varepsilon_3 =$ 0.009
$\varepsilon_4 =$ 0.008
$\varepsilon_5 =$ 0.008

Using the formula developed by Devalapura and Tadros (1992) that defines the stress-strain relationship of 270 ksi low-relaxation strands to determine the stress in the strands.

$$f_{sc,i} = \min\left(\varepsilon_i \cdot \left(887 + \frac{27613}{[1 + (112.4 \cdot \varepsilon_i)^{7.36}]^{\frac{1}{7.36}}}, 270\ ksi\right)\right)$$

$f_{sc2} =$ 255.1 ksi

$f_{sc1} =$ 255.9 ksi
$f_{sc2} =$ 216.2 ksi
$f_{sc3} =$ 231.1 ksi
$f_{sc4} =$ 223.6 ksi
$f_{sc5} =$ 217.0 ksi

Determine effective concrete compressive area $A_{beff} = b_d \cdot \frac{f'_{dc}}{f'_c} \cdot a$ $A_{beff} =$ 232.8 in^2

The total force in the steel is: $F_s = \sum f_{sc,i} \cdot A_{ps}$ $F_s =$ 1385.1 kip

The compressive force in the concrete is: $F_c = 0.85 \cdot f'_c \cdot A_{beff}$ $F_c =$ 1385.1 kip

Equilibrium: 0.0 kip

Determine flexural capacity: $M_n = \sum f_{sc,i} \cdot A_{ps} \cdot d_i - F_c \cdot \frac{a}{2}$ $M_n =$ 4946 ft-kip

The following calculations are used to determine the as-built girder flexural strength based on the 1989 LRFD Standard Specification with 1991 Interim Revisions.

Length of girder	L_g =	300.25	in
First bearing pad center		8	in
Second bearing pad center		254	in
Span length	L =	246	in
Concrete compressive strength	f'_c =	6.9	ksi
Width of the girder web	b_w =	6	in
Height of deck	h_d =	9	in
Height of girder	h_g =	36	in
Jacking force	P_j =	424.9	kip
Width of the deck	b_d =	28.5	in
Girder centroid from the bottom	y_{gb} =	17.97	in
Girder centroid from the bottom for the net section	y_{ngb} =	18.16	in
Area of the girder	A_g =	570	in^2
	A_n =	562.1	in^2
Self weight of the girder	w_g =	0.051	kip/in
Self weight of the deck (assuming 150 lb/ft^3 for the self weight of concrete)	w_d =	0.022	kip/in
Strand area		0.2227	in^2
Strand diameter	d_s =	0.6	in
Area of draped prestressing steel	A_{psd} =	1.34	in^2
Area of straight prestressing steel	A_{pss} =	2.67	in^2
Area of prestressing steel	A_{ps} =	4.01	in^2
Centroid of draped strands at girder end	y_{dend} =	29.0	in
Centroid of draped strands at hold down point	y_{dhp} =	5.0	in
Centroid of the area of the straight strands	y_s =	3.00	in
Distance to hold down point	L_{hp} =	222	in
Angle of draped strands	α =	6.19	deg.
Eccentricity of the resultant of the prestress force at the location of interest "x"	e =	10.73	in
Moment of inertia for the girder	I_g =	93351.373	in^4
Net moment of inertia for the girder	I_n =	91767.365	in^4
Transformed moment of inertia for the composite girder	I_{Tc} =	178419	in^4

Centroid of the transformed composite section	y_{cb} =	24.48	in
Transverse reinforcement yield stress	f_y =	70	ksi
Transverse reinforcement spacing	s =	8	in

Prestress losses:

Seating loss	SL =	2.82	ksi
Elastic shortening losses	ES =	10.3	ksi
Relaxaion prior to release		0.3	ksi
Relaxation following release		0.12	ksi
Relaxation of prestressing steel	CR_s =	0.420	ksi
Shrinkage & creep of concrete	SH & CR_c =	9.5	ksi

f_{cir} is the stress at the center of gravity of the strands due to prestress force and the dead load of the beam at release calculated at the location of maximum moment.

f_{cds} is the stress at the center of gravity of the strands due to the dead load on the beam except that applied at the time of release.

Eccentricity of the strand force at the location of maximum moment due to dead load (L/2)	e_{hp} =	14.87	in
The prestressing force after release includes the elastic shortening losses	P_i =	371.10	kip
Maximum moment due to self weight of girder at release (full length)	M_{maxi} =	576.2	kip·in

$$f_{cir} = \frac{P_i}{A_n} + \frac{P_i \cdot e^2}{I_n} - \frac{M_{max,i} \cdot e}{I_n}$$

= 0.65 ksi + 0.88 ksi - 0.09 ksi f_{cir} = 1.46 ksi

The maximum moment due to all dead load applied except that at the time of release	$M_{max,d-i}$ =	150.3	kip·in
	f_{cds} =	0.024	ksi

$$f_{cds} = \frac{M_{max,d-i} \cdot e}{I_n}$$

Total prestress losses $TL = ES + SH + CR_c + CR_s + SL$	TL =	23.0	ksi
The effective prestress force after accounting for losses	P_e =	332.5	kip

Flexural Capacity:

Concrete compressive strength of deck	f'_{dc} =	5.86	ksi
Depth of neutral axis	c =	9.2819403	in.
Modifaction factor	β_1 =	0.76	

Made by: Brian Mathys
Date: 5/19/2014

University of Minnesota
36M_8W Calculations

Depth of stress block — a = 7.03 in.

Consider each row of strands seperately (row 1 is the bottom row, row 5 is the top row of draped strands)

y_1	2.0 in.	d_1	43.0 in.	$f_{ps,1}$ =	147.7 ksi
y_2	4.0 in.	d_2	41.0 in.	$f_{ps,2}$ =	7.1 ksi
y_3	14.0 in.	d_3	31.0 in.	$f_{ps,3}$ =	96.8 ksi
y_4	16.0 in.	d_4	29.0 in.	$f_{ps,4}$ =	95.5 ksi
y_5	18.0 in.	d_5	27.0 in.	$f_{ps,5}$ =	97.7 ksi

$$\varepsilon_i = 0.003 \cdot \left(\frac{d_i}{c} - 1\right) + \frac{f_{pe,i}}{E_{ps}}$$

ε_1 =	0.016
ε_2 =	0.011
ε_3 =	0.010
ε_4 =	0.010
ε_5 =	0.009

Using the formula developed by Devalapura and Tadros (1992) that defines the stress-strain relationship of 270 ksi low-relaxation strands to determine the stress in the strands.

$$f_{sc,i} = \min\left(\varepsilon_i \cdot \left(887 + \frac{27613}{[1 + (112.4 \cdot \varepsilon_i)^{7.86}]^{\frac{1}{7.86}}}, 270\ ksi\right)\right)$$

f_{sc1} =	259.5 ksi
f_{sc2} =	246.5 ksi
f_{sc3} =	246.0 ksi
f_{sc4} =	240.7 ksi
f_{sc5} =	234.8 ksi

Determine effective concrete compressive area — $A_{beff} = b_d \cdot \frac{f'_{dc}}{f'_c} \cdot a$ — A_{beff} = 170.1 in^2

The total force in the steel is: $F_s = \sum f_{sc,i} \cdot A_{ps}$ — F_s = 997.5 kip

The compressive force in the concrete is: $F_c = 0.85 \cdot f'_c \cdot A_{beff}$ — F_c = 997.5 kip

Equilibrium: 0.0 kip

Determine flexural capacity: $M_n = \sum f_{sc,i} \cdot A_{ps} \cdot d_i - F_c \cdot \frac{a}{2}$ — M_n = 2853 ft·kip

B.5 Cracking Moment

The cracking moment was predicted by determining the moment required to cause the maximum tensile stress in the concrete to reach the rupture stress as defined in Section 3.6.1. A sample calculation is shown below for the 36M_18F girder. The girder

and deck mild reinforcement were ignored in calculating the transformed moment of inertia of the composite girder section in order to simplify the cracking moment calculations.

Made by: Brian Mathys
Date: 4/2/2014

University of Minnesota
36M_18F Calculations

Carried Loads:

Number of point loads		2	.
Applied point load maginitude at midspan	P =	76.4	kip
Applied point load location measured from the face of the girder	a =	246	in

for x < the first center of bearing: $V_u = -w \cdot x$

for x < the second center of bearing: $V_u = R_a - w \cdot x$

for x > the second center of bearing: $V_u = R_a + R_b - w \cdot x$

R_a =	60.5	kip
V_u =	-54.1	kip
V_s =	64.5	kip
V_n =	129.2	kip

Cracking Moment:

The cracking moment is calculated by taking into account the following stresses and cross sectional properties:

$$\sigma_c \geq -\frac{P_e}{A_g} - \frac{P_e \cdot e_g \cdot y_{gb}}{I_g} + \frac{M_g \cdot y_{gb}}{I_g} + \frac{M_d \cdot y_{gb}}{I_g} + \frac{M_L \cdot y_{Tcb}}{I_{Tc}}$$

σ_c = 0.6364 ksi

The cracking stress of concrete was determined using rupture test results

σ_{cr} = 0.635 ksi

Cracked

where P_e is the prestressing force following losses summarized in Table 3-14, A_g is the gross cross-sectional area of the non-composite girder, e_g is the eccentricity of the prestress force for the gross non-composite girder, y_{gb} is the distance between centroid and the bottom of the gross non-composite girder, I_g is the moment of inertia of the gross non-composite girder, M_g is the moment due to girder self-weight, M_d is the moment due to self-weight of composite deck, M_L is the moment due to applied load, y_{Tcb} is the distance between centroid and the bottom of the transformed composite girder, I_{Tc} is the moment of inertia of the transformed composite girder. The results from this sample calculation for the as-built girders is summarized in Table 3-20.

B.6 Shear Capacity Calculations

The shear strength provided by web reinforcement is given in the 1989/91 AASHTO STD as

$$V_s = \frac{A_v \cdot f_{sy} \cdot d}{s} \tag{B.12}$$

where A_v is the area of web reinforcement, f_{sy} is the yield strength of transverse reinforcement, d is the distance from extreme compression fiber to the centroid of the prestressing force, and s is the stirrup spacing.

The concrete contribution to shear was taken as the lesser of the concrete resistance to web-shear or flexure-shear. The resistance to flexure-shear, V_{ci}, and web-shear, V_{cw}, was provided by the 1989/91 AASHTO STD Equation (9-27) and (9-29), respectively.

$$V_{ci} = 0.6 \cdot \sqrt{f_c'} \cdot b_w \cdot d + V_d + \frac{V_i \cdot M_{cr}}{M_{max}} \tag{B.13}$$

$$V_{cw} = \left(3.5 \cdot \sqrt{f_c'} + 0.3 \cdot f_{pc}\right) \cdot b_w \cdot d + V_p \tag{B.14}$$

where f_c is the measured concrete compressive strength (psi), b_w is the web width (in.), V_d is the shear force at section due to unfactored dead load (lb.), V_i is the factored shear force at the section due to externally applied loads occurring simultaneously with M_{max} (lb.), M_{cr} is the cracking moment (in.·lb.), M_{max} is the maximum factored moment at section due to externally applied loads (in.·lb.), f_{pc} is the compressive stress in concrete (after losses) at the centroid of cross section (psi), and V_p is the vertical component of effective prestress force at the section of interest (lb.).

Sample calculations for shear capacity are shown below for the 36M_18F, 45M_24W, 45M_8W, and 36M_8W girders evaluated at their respective critical sections.

The following calculations are used to determine the concrete contribution to shear strength based on the 1989 LRFD Standard Specification with 1991 Interim Revisions.

Length of girder	L_g =	492	in
First bearing pad center		7.5	in
Second bearing pad center		484.5	in
Span length	L =	477	in
Concrete compressive strength	f'_c =	6.3	ksi
Width of the girder web	b_w =	6	in
Height of deck	h_d =	9	in
Height of girder	h_g =	36	in
Jacking force	P_j =	424.9	kip
Width of the deck	b_d =	28.5	in
Girder centroid from the bottom	y_{gb} =	17.97	in
Girder centroid from the bottom for the net section	y_{ngb} =	18.16	in
Area of the girder	A_g =	570	in^2
	A_n =	562.1	in^2
Self weight of the girder	w_g =	0.051	kip/in
Self weight of the deck (assuming 150 lb/ft^3 for the self weight of concrete)	w_d =	0.022	kip/in
Strand area		0.2227	in^2
Strand diameter	d_s =	0.6	in
Area of draped prestressing steel	A_{psd} =	1.34	in^2
Area of straight prestressing steel	A_{pss} =	2.67	in^2
Area of prestressing steel	A_{ps} =	4.01	in^2
Centroid of draped strands at girder end	$y_{d,end}$ =	29.0	in
Centroid of draped strands at hold down point	$y_{d,hp}$ =	5.0	in
Centroid of the area of the straight strands	y_s =	3.00	in
Distance to hold down point	L_{hp} =	222	in
Angle of draped strands	α =	0.00	deg.
Eccentricity of the resultant of the prestress force at the location of interest "x"	e =	14.87	in
Moment of inertia for the girder	I_g =	93351.373	in^4
Net moment of inertia for the girder	I_n =	91767.365	in^4
Transformed moment of inertia for the composite girder	I_{Tc} =	178419	in^4

Centroid of the transformed composite section	y_{Tcb} =	24.48	in
Transverse reinforcement yield stress	f_y =	70.2	ksi
Transverse reinforcement spacing	s =	18	in

Prestress losses:

Seating loss	SL =	2.82	ksi
Elastic shortening losses	ES =	10.3	ksi
Relaxation prior to release		0.3	ksi
Relaxation following release		0.12	ksi
Relaxation of prestressing steel	CR_s =	0.420	ksi
Shrinkage + creep of concrete	SH & CR_c =	9.5	ksi

f_{cir} is the stress at the center of gravity of the strands due to prestress force and the dead load of the beam at release calculated at the location of maximum moment.

f_{cds} is the stress at the center of gravity of the strands due to the dead load on the beam except that applied at the time of release.

Eccentricity of the strand force at the location of maximum moment due to dead load (L/2) e_{hp} = 14.87 in

The prestressing force after release includes the elastic shortening losses P_i = 371.10 kip

Maximum moment due to self weight of girder at release (full length) M_{maxi} = 1547.0 kip·in

$$f_{cir} = \frac{P_i}{A_n} + \frac{P_i \cdot e^2}{I_n} - \frac{M_{max,i} \cdot e}{I_n}$$

= 0.65 ksi + 0.88 ksi - 0.25 ksi f_{cir} = 1.30 ksi

The maximum moment due to all dead load applied except that at the time of release $M_{max,d-i}$ = 632.6 kip·in

$$f_{cds} = \frac{M_{max,d-i} \cdot e}{I_n}$$ f_{cds} = 0.102 ksi

Total prestress losses $TL = ES + SH + CR_c + CR_s + SL$ TL = 23.0 ksi

The effective prestress force after accounting for losses P_e = 332.5 kip

Shear Calculation:

The first portion of shear capacity which will be calculated is the V_{cw} portion, which accurately predicts the formation of web shear cracks in prestressed girders.

Web shear capacity $$V_{cw} = \left(3.5 \cdot \sqrt{f_c'} + 0.3 \cdot f_{pc}\right) \cdot b_w \cdot d_p + V_p$$

Determine the stress at the centroid of the composite section due to the prestress force and dead load

$$f_{pc} = \frac{L_t \cdot P_e}{A_g} - \frac{L_t \cdot P_e \cdot e \cdot (y_{Tcb} - y_{gb})}{I_g} + \frac{M_g \cdot (y_{Tcb} - y_{gb})}{I_g} + \frac{M_d \cdot (y_{Tcb} - y_{gb})}{I_g}$$

Location of interest measured from face of girder	x =	246 in
The moment due to the self weight of the girder at location x	M_g =	1452.7 kip·in
The moment due to the self weight of the slab at location x	M_d =	632.6 kip·in
The moment due to live load at location x	M_L =	36477.0 kip·in
Development percentage where the total length is equal to 60 bar diameters	L_t =	1.00 .
	f_{pc} =	0.384 ksi
Depth of prestressing strand area	d =	41.33 in
Shear component due to the vertical component of the draped strand's effective prestress force	V_p =	0.0 kip
Vcw = (277.8 + 115.25) * 247.99 + 0	V_{cw} =	97.47 kip

Flexure shear capacity

$$V_{ci} = \max\left(0.6 \cdot \sqrt{f_c} \cdot b_w \cdot d_p + (V_g + V_d) + \frac{1.6 \cdot V_L \cdot M_{cre}}{1.6 \cdot M_L}, 1.7 \cdot \sqrt{f_c} \cdot b_w \cdot d_p\right)$$

V_{ci} = 64.7 kip

$$M_{cre} = \frac{I_{Tc}}{y_{Tcb}} \cdot \left(6 \cdot \sqrt{f_c} + f_{cpe} - \frac{M_g \cdot y_{gb}}{I_g}\right)$$

M_{cre} = 12622 kip·in

$$f_{cpe} = \frac{P_e}{A_g} + \frac{P_e \cdot e \cdot y_{gb}}{I_g}$$

f_{cpe} = 1.54 ksi

V_{cg} = 0.0 kip

Shear capacity is minimum of web-shear and flexure-shear capacities	V_c =	64.7 kip

Carried Loads:

Number of point loads		2 .
Applied point load maginitude at midspan	P =	216 kip
Applied point load location measured from the face of the girder	a =	246 in

for x < the first center of bearing: $V_u = -w \cdot x$

for x < the second center of bearing: $V_u = R_a - w \cdot x$ — R_a = 171.1 kip

for x > the second center of bearing: $V_u = R_a + R_b - w \cdot x$ — V_u = -152.9 kip

V_s = 64.5 kip

V_n = 129.2 kip

The following calculations are used to determine the concrete contribution to shear strength based on the 1989 LRFD Standard Specification with 1991 Interim Revisions.

Length of girder	L_g =	456	in
First bearing pad center		7.5	in
Second bearing pad center		448.5	in
Span length	L =	441	in
Concrete compressive strength	f'_c =	6.8	ksi
Width of the girder web	b_w =	6	in
Height of deck	h_d =	9	in
Height of girder	h_g =	45	in
Jacking force	P_j =	732.15	kip
Width of the deck	b_d =	28.5	in
Girder centroid from the bottom	y_{gb} =	22.34	in
Girder centroid from the bottom for the net section	y_{ngb} =	22.58	in
Area of the girder	A_g =	624	in^2
	A_n =	616.1	in^2
Self weight of the girder	w_g =	0.056	kip/in
Self weight of the deck (assuming 150 lb/ft^3 for the self weight of concrete)	w_d =	0.022	kip/in
Strand area		0.2227	in^2
Strand diameter	d_s =	0.6	in
Area of draped prestressing steel	A_{psd} =	1.34	in^2
Area of straight prestressing steel	A_{pss} =	4.45	in^2
Area of prestressing steel	A_{ps} =	5.79	in^2
Centroid of draped strands at girder end	$y_{d,end}$ =	40.0	in
Centroid of draped strands at hold down point	$y_{d,hp}$ =	7.0	in
Centroid of the area of the straight strands	y_s =	3.00	in
Distance to hold down point	L_{hp} =	204	in
Angle of draped strands	α =	9.27	deg.
Eccentricity of the resultant of the prestress force at the location of interest "x"	e =	17.02	in
Moment of inertia for the girder	I_g =	167050	in^4
Net moment of inertia for the girder	I_n =	164212	in^4
Transformed moment of inertia for the composite girder (excluding effect of steel)	I_{Tc} =	285967	in^4

Centroid of the transformed composite section	y_{Tcb} =	29.32	in
Transverse reinforcement yield stress	f_y =	67.0	ksi
Transverse reinforcement spacing	s =	24	in

Prestress losses:

Seating loss	SL =	2.82	ksi
Elastic shortening losses	ES =	18.9	ksi
Relaxation prior to release		0.5	ksi
Relaxation following release		0.168	ksi
Relaxation	CR_s =	0.668	ksi
Shrinkage + creep of concrete	SH & CR_c =	14.9	ksi

f_{cir} is the stress at the center of gravity of the strands due to prestress force and the dead load of the beam at release calculated at the location of maximum moment.

f_{cds} is the stress at the center of gravity of the strands due to the dead load on the beam except that applied at the time of release.

Eccentricity of the strand force at the location of maximum moment due to dead load (L/2)	e_{hp} =	18.97	in
The prestressing force after release includes the elastic shortening losses	P_i =	603.49	kip
Maximum moment due to self weight of girder at release (full length)	M_{maxi} =	1454.8	kip·in

$$f_{cir} = \frac{P_i}{A_n} + \frac{P_i \cdot e^2}{I_n} - \frac{M_{max,i} \cdot e}{I_n}$$

= 0.97 ksi + 1.3 ksi - 0.17 ksi f_{cir} = 2.13 ksi

The maximum moment due to all dead load applied except that at the time of release	$M_{max,d-i}$ =	540.7	kip·in

$$f_{cds} = \frac{M_{max,d-i} \cdot e}{I_n}$$

f_{cds} = 0.062 ksi

Total prestress losses $TL = ES + SH + CR_c + CR_s + SL$ TL = 37.3 ksi

The effective prestress force after accounting for losses P_e = 516.2 kip

Shear Calculation:

The first portion of shear capacity which will be calculated is the V_{cw} portion, which accurately predicts the formation of web shear cracks in prestressed girders.

Web shear capacity $$V_{cw} = \left(3.5 \cdot \sqrt{f_c'} + 0.3 \cdot f_{pc}\right) \cdot b_w \cdot d_p + V_p$$

Determine the stress at the centroid of the composite section due to the prestress force and dead load

$$f_{pc} = \frac{L_t \cdot P_e}{A_g} - \frac{L_t \cdot P_e \cdot e \cdot (y_{Tcb} - y_{gb})}{I_g} + \frac{M_g \cdot (y_{Tcb} - y_{gb})}{I_g} + \frac{M_d \cdot (y_{Tcb} - y_{gb})}{I_g}$$

Location of interest measured from face of girder	x =	148.5	in
The moment due to the self weight of the girder at location x	M_g =	1182.2	kip·in
The moment due to the self weight of the slab at location x	M_d =	470.3	kip·in
The moment due to live load at location x	M_L =	34530.6	kip·in
Development percentage where the total length is equal to 60 bar diameters	L_t =	1.00	.
	f_{pc} =	0.529	ksi
Depth of prestressing strand area	d =	48.00	in
Shear component due to the vertical component of the draped strand's effective prestress force	V_p =	18.1	kip
Vcw = (288.62 + 158.8) * 288.02 + 18102.23	V_{cw} =	146.97	kip

Flexure shear capacity

$$V_{ci} = \max\left(0.6 \cdot \sqrt{f_c} \cdot b_w \cdot d_p + (V_g + V_d) + \frac{1.6 \cdot V_L \cdot M_{cre}}{1.6 \cdot M_L}, 1.7 \cdot \sqrt{f_c} \cdot b_w \cdot d_p\right)$$ V_{ci} = 88.3 kip

$$M_{cre} = \frac{I_{Tc}}{y_{Tcb}} \cdot \left(6 \cdot \sqrt{f_c} + f_{cpe} - \frac{M_g \cdot y_{gb}}{I_g}\right)$$ M_{cre} = 22811 kip·in

$$f_{cpe} = \frac{P_e}{A_g} + \frac{P_e \cdot e \cdot y_{gb}}{I_g}$$ f_{cpe} = 2.00 ksi

V_{cg} = 6.2 kip

Shear capacity is minimum of web-shear and flexure-shear capacities	V_c =	88.3	kip

Carried Loads:

Number of point loads		1	.
Applied point load maginitude	P =	360	kip
Applied point load location measured from the face of the girder	a =	148.5	in

for x < the first center of bearing: $V_u = -w \cdot x$

for x < the second center of bearing: $V_u = R_a - w \cdot x$ R_a = 244.9 kip

for x > the second center of bearing: $V_u = R_a + R_b - w \cdot x$ V_u = -108.9 kip

V_s = 53.6 kip

V_n = 141.9 kip

The following calculations are used to determine the concrete contribution to shear strength based on the 1989 LRFD Standard Specification with 1991 Interim Revisions.

Length of girder	L_g =	341.75	in
First bearing pad center		7.75	in
Second bearing pad center		300.75	in
Span length	L =	293	in
Concrete compressive strength	f'_c =	7	ksi
Width of the girder web	b_w =	6	in
Height of deck	h_d =	9	in
Height of girder	h_g =	45	in
Jacking force	P_j =	732.15	kip
Width of the deck	b_d =	28.5	in
Girder centroid from the bottom	y_{gb} =	22.34	in
Girder centroid from the bottom for the net section	y_{ngb} =	22.58	in
Area of the girder	A_g =	624	in^2
	A_n =	616.1	in^2
Self weight of the girder	w_g =	0.056	kip/in
Self weight of the deck (assuming 150 lb/ft^3 for the self weight of concrete)	w_d =	0.022	kip/in
Strand area		0.2227	in^2
Strand diameter	d_s =	0.6	in
Area of draped prestressing steel	A_{psd} =	1.34	in^2
Area of straight prestressing steel	A_{pss} =	4.45	in^2
Area of prestressing steel	A_{ps} =	5.79	in^2
Centroid of draped strands at girder end	$y_{d,end}$ =	40.0	in
Centroid of draped strands at hold down point	$y_{d,hp}$ =	7.0	in
Centroid of the area of the straight strands	y_s =	3.00	in
Distance to hold down point	L_{hp} =	204	in
Angle of draped strands	α =	9.27	deg.
Eccentricity of the resultant of the prestress force at the location of interest "x"	e =	17.02	in
Moment of inertia for the girder	I_g =	167050	in^4
Net moment of inertia for the girder	I_n =	164212	in^4
Transformed moment of inertia for the composite girder	I_{Tc} =	285967	in^4

Centroid of the transformed composite section	y_{Tcb} =	29.32	in
Transverse reinforcement yield stress	f_y =	67.0	ksi
Transverse reinforcement spacing	s =	8	in

Prestress losses:

Seating loss	SL =	2.82	ksi
Elastic shortening losses	ES =	18.9	ksi
Relaxation prior to release		0.5	ksi
Relaxation following release		0.168	ksi
Relaxation of prestressing steel	CR_s =	0.668	ksi
Shrinkage + creep of concrete	SH & CR_c=	14.9	ksi

f_{cir} is the stress at the center of gravity of the strands due to prestress force and the dead load of the beam at release calculated at the location of maximum moment.

f_{cds} is the stress at the center of gravity of the strands due to the dead load on the beam except that applied at the time of release.

Eccentricity of the strand force at the location of maximum moment due to dead load (L/2)	e_{hp} =	18.97	in
The prestressing force after release includes the elastic shortening losses	P_i =	603.49	kip
Maximum moment due to self weight of girder at release (full length)	M_{maxi} =	817.1	kip-in

$$f_{cir} = \frac{P_i}{A_n} + \frac{P_i \cdot e^2}{I_n} - \frac{M_{max,i} \cdot e}{I_n}$$

= 0.97 ksi + 1.3 ksi - 0.09 ksi f_{cir} = 2.21 ksi

The maximum moment due to all dead load applied except that at the time of release	$M_{max,d-i}$ =	225.1	kip-in
	f_{cds} =	0.026	ksi

$$f_{cds} = \frac{M_{max,d-i} \cdot e}{I_n}$$

Total prestress losses	$TL = ES + SH + CR_c + CR_s$+SL	TL =	37.3	ksi
The effective prestress force after accounting for losses		P_e=	516.2	kip

Shear Calculation:

The first portion of shear capacity which will be calculated is the V_{cw} portion, which accurately predicts the formation of web shear cracks in prestressed girders.

Web shear capacity $$V_{cw} = \left(3.5 \cdot \sqrt{f_c'} + 0.3 \cdot f_{pc}\right) \cdot b_w \cdot d_p + V_p$$

Determine the stress at the centroid of the composite section due to the prestress force and dead load

$$f_{pc} = \frac{L_t \cdot P_e}{A_g} - \frac{L_t \cdot P_e \cdot e \cdot (y_{Tcb} - y_{gb})}{I_g} + \frac{M_g \cdot (y_{Tcb} - y_{gb})}{I_g} + \frac{M_d \cdot (y_{Tcb} - y_{gb})}{I_g}$$

Location of interest measured from face of girder	x =	148.5 in
The moment due to the self weight of the girder at location x	M_g =	576.2 kip·in
The moment due to the self weight of the slab at location x	M_d =	229.2 kip·in
The moment due to live load at location x	M_L =	47027.2 kip·in
Development percentage where the total length is equal to 60 bar diameters	L_t =	1.00 .
	f_{pc} =	0.494 ksi
Depth of prestressing strand area	d =	48.00 in
Shear component due to the vertical component of the draped strand's effective prestress force	V_p =	18.1 kip
Vcw = (292.83 + 148.18) * 288.02 + 18102.23	V_{cw} =	145.12 kip

Flexure shear capacity

$$V_{ci} = \max\left(0.6 \cdot \sqrt{f_c} \cdot b_w \cdot d_p + (V_g + V_d) + \frac{1.6 \cdot V_L \cdot M_{cre}}{1.6 \cdot M_L}, 1.7 \cdot \sqrt{f_c} \cdot b_w \cdot d_p\right)$$ V_{ci} = 170.7 kip

$$M_{cre} = \frac{I_{Tc}}{y_{Tcb}} \cdot \left(6 \cdot \sqrt{f_c} + f_{cpe} - \frac{M_g \cdot y_{gb}}{I_g}\right)$$ M_{cre} = 23671 kip·in

$$f_{cpe} = \frac{P_e}{A_g} + \frac{P_e \cdot e \cdot y_{gb}}{I_g}$$ f_{cpe} = 2.00 ksi

V_{cg} = 1.8 kip

Shear capacity is minimum of web-shear and flexure-shear capacities	V_c =	145.1 kip

Carried Loads:

Number of point loads		1 .
Applied point load maginitude	P =	643 kip
Applied point load location measured from the face of the girder	a =	148.5 in

for x < the first center of bearing: $V_u = -w \cdot x$

for x < the second center of bearing: $V_u = R_a - w \cdot x$ R_a = 334.1 kip

for x > the second center of bearing: $V_u = R_a + R_b - w \cdot x$ V_u = -308.6 kip

V_s = 160.8 kip

V_n = 305.9 kip

The following calculations are used to determine the concrete contribution to shear strength based on the 1989 LRFD Standard Specification with 1991 Interim Revisions.

Length of girder	L_g =	300.25	in
First bearing pad center		8	in
Second bearing pad center		254	in
Span length	L =	246	in
Concrete compressive strength	f'_c =	6.9	ksi
Width of the girder web	b_w =	6	in
Height of deck	h_d =	9	in
Height of girder	h_g =	36	in
Jacking force	P_j =	424.9	kip
Width of the deck	b_d =	28.5	in
Girder centroid from the bottom	y_{gb} =	17.97	in
Girder centroid from the bottom for the net section	y_{ngb} =	18.16	in
Area of the girder	A_g =	570	in^2
	A_n =	562.1	in^2
Self weight of the girder	w_g =	0.051	kip/in
Self weight of the deck (assuming 150 lb/ft^3 for the self weight of concrete)	w_d =	0.022	kip/in
Strand area		0.2227	in^2
Strand diameter	d_s =	0.6	in
Area of draped prestressing steel	A_{psd} =	1.34	in^2
Area of straight prestressing steel	A_{pss}=	2.67	in^2
Area of prestressing steel	A_{ps} =	4.01	in^2
Centroid of draped strands at girder end	$y_{d,end}$ =	29.0	in
Centroid of draped strands at hold down point	$y_{d,hp}$ =	5.0	in
Centroid of the area of the straight strands	y_s =	3.00	in
Distance to hold down point	L_{hp} =	222	in
Angle of draped strands	α =	6.19	deg.
Eccentricity of the resultant of the prestress force at the location of interest "x"	e =	10.73	in
Moment of inertia for the girder	I_g =	93351.373	in^4
Net moment of inertia for the girder	I_n =	91767.365	in^4
Transformed moment of inertia for the composite girder	I_{Tc} =	178419	in^4

Centroid of the transformed composite section	y_{cb} =	24.48	in
Transverse reinforcement yield stress	f_y =	70	ksi
Transverse reinforcement spacing	s =	8	in

Prestress losses:

Seating loss	SL =	2.82	ksi
Elastic shortening losses	ES =	10.3	ksi
Relaxaion prior to release		0.3	ksi
Relaxation following release		0.12	ksi
Relaxation of prestressing steel	CR_s =	0.420	ksi
Shrinkage & creep of concrete	SH & CR_c =	9.5	ksi

f_{cir} is the stress at the center of gravity of the strands due to prestress force and the dead load of the beam at release calculated at the location of maximum moment.

f_{cds} is the stress at the center of gravity of the strands due to the dead load on the beam except that applied at the time of release.

Eccentricity of the strand force at the location of maximum moment due to dead load (L/2) e_{hp} = 14.87 in

The prestressing force after release includes the elastic shortening losses P_i = 371.10 kip

Maximum moment due to self weight of girder at release (full length) M_{maxi} = 576.2 kip·in

$$f_{cir} = \frac{P_i}{A_n} + \frac{P_i \cdot e^2}{I_n} - \frac{M_{max,i} \cdot e}{I_n}$$

= 0.65 ksi + 0.88 ksi - 0.09 ksi f_{cir} = 1.46 ksi

The maximum moment due to all dead load applied except that at the time of release $M_{max,d-i}$ = 150.3 kip·in

$$f_{cds} = \frac{M_{max,d-i} \cdot e}{I_n}$$

f_{cds} = 0.024 ksi

Total prestress losses $TL = ES + SH + CR_c + CR_s + SL$ TL = 23.0 ksi

The effective prestress force after accounting for losses P_e = 332.5 kip

Shear Calculation:

The first portion of shear capacity which will be calculated is the V_{cw} portion, which accurately predicts the formation of web shear cracks in prestressed girders.

Web shear capacity $$V_{cw} = \left(3.5 \cdot \sqrt{f_c'} + 0.3 \cdot f_{pc}\right) \cdot b_w \cdot d_p + V_p$$

Determine the stress at the centroid of the composite section due to the prestress force and dead load

$$f_{pc} = \frac{L_t \cdot P_e}{A_g} - \frac{L_t \cdot P_e \cdot e \cdot (y_{Tcb} - y_{gb})}{I_g} + \frac{M_g \cdot (y_{Tcb} - y_{gb})}{I_g} + \frac{M_d \cdot (y_{Tcb} - y_{gb})}{I_g}$$

Location of interest measured from face of girder	x =	120 in
The moment due to the self weight of the girder at location x	M_g =	357.9 kip·in
The moment due to the self weight of the slab at location x	M_d =	155.9 kip·in
The moment due to live load at location x	M_L =	34042.5 kip·in
Development percentage where the total length is equal to 60 bar diameters	L_t =	1.00 .
	f_{pc} =	0.371 ksi
Depth of prestressing strand area	d =	37.66 in
Shear component due to the vertical component of the draped strand's effective prestress force	V_p =	13.5 kip
Vcw = (290.73 + 111.16) * 225.94 + 13460.46	V_{cw} =	104.26 kip

Flexure shear capacity

$$V_{ci} = \max\left(0.6 \cdot \sqrt{f_c} \cdot b_w \cdot d_p + (V_g + V_d) + \frac{1.6 \cdot V_L \cdot M_{cre}}{1.6 \cdot M_L}, 1.7 \cdot \sqrt{f_c} \cdot b_w \cdot d_p\right)$$

V_{ci} = 104.9 kip

$$M_{cre} = \frac{I_{Tc}}{y_{Tcb}} \cdot \left(6 \cdot \sqrt{f_c} + f_{cpe} - \frac{M_g \cdot y_{gb}}{I_g}\right)$$

M_{cre} = 12390 kip·in

$$f_{cpe} = \frac{P_e}{A_g} + \frac{P_e \cdot e \cdot y_{gb}}{I_g}$$

f_{cpe} = 1.27 ksi

V_{cg} = 2.2 kip

Shear capacity is minimum of web-shear and flexure-shear capacities — V_c = 104.3 kip

Carried Loads:

Number of point loads		1 .
Applied point load maginitude	P =	558 kip
Applied point load location measured from the face of the girder	a =	120 in

for x < the first center of bearing: $V_u = -w \cdot x$

for x < the second center of bearing: $V_u = R_a - w \cdot x$ — R_a = 304.0 kip

for x > the second center of bearing: $V_u = R_a + R_b - w \cdot x$ — V_u = -253.6 kip

V_s = 131.8 kip

V_n = 236.1 kip

The shear strength provided by web reinforcement is given in the 2010 AASHTO LRFD as

$$V_s = \frac{A_v \cdot f_{sy} \cdot d_v \cdot cot\theta}{s} \tag{B.15}$$

where A_v is the area of web reinforcement, f_{sy} is the yield strength of transverse reinforcement, d_v is the distance from centroid of the rectangular compression block to the centroid of the prestressing force, $cot\theta$ is $\left(1 + 3 \cdot \frac{f_{pc}}{\sqrt{f_c'}}\right)$ in the web-shear controlled region and unity in the flexure-shear controlled region, and s is the stirrup spacing.

The concrete contribution to shear was taken as the lesser of the concrete resistance to web-shear or flexure-shear. The resistance to flexure-shear, V_{ci}, and web-shear, V_{cw}, was provided by the 2010 AASHTO LRFD as

$$V_{ci} = 0.02 \cdot \sqrt{f_c'} \cdot b_w \cdot d_v + V_d + \frac{V_i \cdot M_{cr}}{M_{max}} \tag{B.16}$$

$$V_{cw} = \left(0.06 \cdot \sqrt{f_c'} + 0.3 \cdot f_{pc}\right) \cdot b_w \cdot d_v + V_p \tag{B.17}$$

where f_c is the measured concrete compressive strength (ksi), b_w is the web width (in.), V_d is the shear force at section due to unfactored dead load (kip.), V_i is the factored shear force at the section due to externally applied loads occurring simultaneously with M_{max} (kip), M_{cr} is the cracking moment (in.·kip.), M_{max} is the maximum factored moment at section due to externally applied loads (in.·kip), f_{pc} is the compressive stress in concrete (after losses) at the centroid of cross section (ksi), and V_p is the vertical component of effective prestress force at the section of interest (kip).

Sample calculations for shear capacity are shown below for the 36M_18F, 45M_24W, 45M_8W, and 36M_8W girders evaluated at their respective critical sections.

The following calculations are used to determine the nominal shear capacity based on the AASHTO 2010 LRFD manual for a prestressed, I-shaped girder. The General Procedure outlined in section 5.8.3.4.3 was used.

Length of girder	L_g =	492	in
First bearing pad center		7.5	in
Second bearing pad center		484.5	in
Span length	L =	477	in
Concrete compressive strength	f'_c =	6.3	ksi
Width of the girder web	b_w =	6	in
Height of deck	h_d =	9	in
Height of girder	h_g =	36	in
Jacking force	P_j =	424.9	kip
Width of the deck	b_d =	28.5	in
Girder centroid from the bottom	y_{gb} =	17.97	in
Girder centroid from the bottom for the net section	y_{ngb} =	18.16	in
Area of the girder	A_g =	570	in^2
	A_n =	562.1	in^2
Self weight of the girder	w_g =	0.051	kip/in
Self weight of the deck (assuming 150 lb/ft^3 for the self weight of concrete)	w_d =	0.022	kip/in
Strand area		0.2227	in^2
Strand diameter	d_s =	0.6	in
Area of draped prestressing steel	A_{psd} =	1.34	in^2
Area of straight prestressing steel	A_{pss} =	2.67	in^2
Area of prestressing steel	A_{ps} =	4.01	in^2
Centroid of draped strands at girder end	$y_{d,end}$ =	29.0	in
Centroid of draped strands at hold down point	$y_{d,hp}$ =	5.0	in
Centroid of the area of the straight strands	y_s =	3.00	in
Distance to hold down point	L_{hp} =	222	in
Angle of draped strands	α =	0.00	deg.
Eccentricity of the resultant of the prestress force at the location of interest "x"	e =	14.87	in
Moment of inertia for the girder	I_g =	93351.373	in^4
Net moment of inertia for the girder	I_n =	91767.365	in^4
Transformed moment of inertia for the composite girder	I_{Tc} =	178419	in^4
Centroid of the transformed composite section	y_{Tcb} =	24.48	in

Transverse reinforcement yield stress	f_y =	70.2 ksi
Transverse reinforcement spacing	s =	6 in

Prestress losses:

Seating loss	SL =	2.82 ksi
Elastic shortening losses	ES =	10.3 ksi
Relaxation prior to release		0.3 ksi
Relaxation following release		0.12 ksi
Relaxation of prestressing steel	CR_s =	0.420 ksi
Shrinkage	SH =	4.75 ksi
Creep of concrete	CR_c =	4.75 ksi

f_{cir} is the stress at the center of gravity of the strands due to prestress force and the dead load of the beam at release calculated at the location of maximum moment.

f_{cds} is the stress at the center of gravity of the strands due to the dead load on the beam except that applied at the time of release.

Eccentricity of the strand force at the location of maximum moment due to dead load (L/2)	e_{hp} =	14.87 in
The prestressing force after release includes the elastic shortening losses	P_i =	371.10 kip
Maximum moment due to self weight of girder at release (full length)	M_{maxi} =	1547.0 kip·in

$$f_{cir} = \frac{P_i}{A_n} + \frac{P_i \cdot e^2}{I_n} - \frac{M_{max,i} \cdot e}{I_n}$$

= 0.65 ksi + 0.88 ksi - 0.25 ksi	f_{cir} =	1.30 ksi
The maximum moment due to all dead load applied except that at the time of release	$M_{max,d-i}$ =	632.6 kip·in

$$f_{cds} = \frac{M_{max,d-i} \cdot e}{I_n}$$

		f_{cds} =	0.102 ksi
Total prestress losses	$TL = ES + SH + CR_c + CR_s + SL$	TL =	23.0 ksi
The effective prestress force after accounting for losses		P_e =	332.5 kip

Shear Calculation:

The first portion of shear capacity which will be calculated is the V_{cw} portion, which accurately predicts the formation of web shear cracks in prestressed girders.

Web shear capacity $$V_{cw} = \left(0.06 \cdot \sqrt{f_c'} + 0.3 \cdot f_{pc}\right) \cdot b_w \cdot d_v + V_p$$

Determine the stress at the centroid of the composite section due to the prestress force and dead load

$$f_{pc} = \frac{L_t \cdot P_e}{} - \frac{L_t \cdot P_e \cdot e \cdot (y_{Tcb} - y_{gb})}{} + \frac{M_g \cdot (y_{Tcb} - y_{gb})}{} + \frac{M_d \cdot (y_{Tcb} - y_{gb})}{}$$

$f_{pc} = \frac{A_g}{I_g} \quad ' \quad \frac{I_g}{I_g} \quad ' \quad \frac{I_g}{I_g}$

Location of interest measured from face of girder	x =	246.0	in
The moment due to the self weight of the girder at location x	M_g =	1452.7	kip·in
The moment due to the self weight of the slab at location x	M_d =	632.6	kip·in
The moment due to live load at location x	M_L =	36477.0	kip·in
Development percentage where the total length is equal to 60 bar diameters	L_t =	1.00	.
	f_{pc} =	0.384	ksi
Depth of prestressing strand area	d =	41.33	in
Shear component due to the vertical component of the draped strand's effective prestress force	V_p =	0.0	kip
	V_{cw} =	59.45	kip
	d_v =	37.27	in

Flexure shear capacity

$$V_{ci} = \max\left(0.02 \cdot \sqrt{f_c} \cdot b_w \cdot d_v + (V_g + V_d) + \frac{1.6 \cdot V_L \cdot M_{cre}}{1.6 \cdot M_L}, 0.06 \cdot \sqrt{f_c} \cdot b_w \cdot d_v\right)$$ V_{ci} = 54.0 kip

$$M_{cre} = \frac{I_{Tc}}{y_{Tcb}} \cdot \left(0.20 \cdot \sqrt{f_c} + f_{cpe} - \frac{M_g \cdot y_{gb}}{I_g}\right)$$ M_{cre} = 12810 kip·in

$$f_{cpe} = \frac{P_e}{A_g} + \frac{P_e \cdot e \cdot y_{gb}}{I_g}$$ f_{cpe} = 1.54 ksi

V_{cg} = 0.0 kip

Shear capacity is minimum of web-shear and flexure-shear capacities V_c = 54.0 kip

Carried Loads:

Number of point loads		2	.
Applied point load maginitude at midspan	P =	216	kip
Applied point load location measured from the face of the girder	a =	246	in

for x < the first center of bearing: $V_u = -w \cdot x$

for x < the second center of bearing: $V_u = R_a - w \cdot x$ R_a = 171.1 kip

for x > the second center of bearing: $V_u = R_a + R_b - w \cdot x$ V_u = -152.9 kip

Shear capacity due to transverse reinforcement

cot(θ) used in calculating V_s $\cot\theta = 1 + 3 \cdot \frac{f_{pc}}{\sqrt{f_c'}}$ cot(θ) = 1.00

$V = \frac{A_v \cdot f_y \cdot d_v \cdot \cot\theta}{}$ θ = 32.0

$v_s =$ s

$V_i =$ 174.4 kip

$V_n < 0.25 \cdot f_c' \cdot b_w \cdot d_v + V_p =$ 352.22 kip

$V_n =$ 228.5 kip

The following calculations are used to determine the nominal shear capacity based on the AASHTO 2010 LRFD manual for a prestressed, I-shaped girder. The General Procedure outlined in section 5.8.3.4.3 was used.

Length of girder	L_g =	456	in
First bearing pad center		7.5	in
Second bearing pad center		448.5	in
Span length	L =	441	in
Concrete compressive strength	f'_c =	6.8	ksi
Width of the girder web	b_w =	6	in
Height of deck	h_d =	9	in
Height of girder	h_g =	45	in
Jacking force	P_j =	732.15	kip
Width of the deck	b_d =	28.5	in
Girder centroid from the bottom	y_{gb} =	22.34	in
Girder centroid from the bottom for the net section	y_{ngb} =	22.58	in
Area of the girder	A_g =	624	in^2
	A_n =	616.1	in^2
Self weight of the girder	w_g =	0.056	kip/in
Self weight of the deck (assuming 150 lb/ft^3 for the self weight of concrete)	w_d =	0.022	kip/in
Strand area		0.2227	in^2
Strand diameter	d_s =	0.6	in
Area of draped prestressing steel	A_{psd} =	1.34	in^2
Area of straight prestressing steel	A_{pss} =	4.45	in^2
Area of prestressing steel	A_{ps} =	5.79	in^2
Centroid of draped strands at girder end	$y_{d,end}$ =	40.0	in
Centroid of draped strands at hold down point	$y_{d,hp}$ =	7.0	in
Centroid of the area of the straight strands	y_s =	3.00	in
Distance to hold down point	L_{hp} =	204	in
Angle of draped strands	α =	9.27	deg.
Eccentricity of the resultant of the prestress force at the location of interest "x"	e =	17.02	in
Moment of inertia for the girder	I_g =	167050	in^4
Net moment of inertia for the girder	I_n =	164212	in^4
Transformed moment of inertia for the composite girder (excluding effect of steel)	I_{Tc} =	285967	in^4
Centroid of the transformed composite section	y_{Tcb} =	29.32	in

Transverse reinforcement yield stress	f_y =	67.0 ksi
Transverse reinforcement spacing	s =	24 in

Prestress losses:

Seating loss	SL =	2.82 ksi
Elastic shortening losses	ES =	18.9 ksi
Relaxation prior to release		0.5 ksi
Relaxation following release		0.168 ksi
Relaxation	CR_s =	0.668 ksi
Shrinkage	SH =	7.45 ksi
Creep of concrete	CR_c =	7.45 ksi

f_{cir} is the stress at the center of gravity of the strands due to prestress force and the dead load of the beam at release calculated at the location of maximum moment.

f_{cds} is the stress at the center of gravity of the strands due to the dead load on the beam except that applied at the time of release.

Eccentricity of the strand force at the location of maximum moment due to dead load (L/2)	e_{bp} =	18.97 in
The prestressing force after release includes the elastic shortening losses	P_i =	603.49 kip
Maximum moment due to self weight of girder at release (full length)	M_{maxi} =	1454.8 kip·in

$$f_{cir} = \frac{P_i}{A_n} + \frac{P_i \cdot e^2}{I_n} - \frac{M_{max,i} \cdot e}{I_n}$$

= 0.97 ksi + 1.3 ksi - 0.17 ksi f_{cir} = 2.13 ksi

The maximum moment due to all dead load applied except that at the time of release	$M_{max,d-i}$ =	540.7 kip·in

$$f_{cds} = \frac{M_{max,d-i} \cdot e}{I_n}$$ f_{cds} = 0.062 ksi

Total prestress losses $TL = ES + SH + CR_c + CR_s + SL$ TL = 37.3 ksi

The effective prestress force after accounting for losses P_e = 516.2 kip

Shear Calculation:

The first portion of shear capacity which will be calculated is the V_{cw} portion - (5.8.3.4.3-3)

Web shear capacity $$V_{cw} = \left(0.06 \cdot \sqrt{f_c'} + 0.3 \cdot f_{pc}\right) \cdot b_w \cdot d_v + V_p$$

Determine the stress at the centroid of the composite section due to the prestress force and dead load

$$f_{..} = \frac{L_t \cdot P_e}{} - \frac{L_t \cdot P_e \cdot e \cdot (y_{Tcb} - y_{gb})}{} + \frac{M_g \cdot (y_{Tcb} - y_{gb})}{} + \frac{M_d \cdot (y_{Tcb} - y_{gb})}{}$$

$f_{pc} = \frac{A_g}{I_g} \quad ' \quad \frac{I_g}{I_g} \quad ' \quad \frac{I_g}{I_g}$

Location of interest measured from face of girder	x =	148.49	in
The moment due to the self weight of the girder at location x	M_g =	1182.2	kip·in
The moment due to the self weight of the slab at location x	M_d =	470.3	kip·in
The moment due to live load at location x	M_L =	34528.2	kip·in
Development percentage where the total length is equal to 60 bar diameters	L_t =	1.00	.
	f_{pc} =	0.529	ksi
Depth of prestressing strand area	d =	48.00	in
Shear component due to the vertical component of the draped strand's effective prestress force	V_p =	18.1	kip
	V_{cw} =	99.82	kip
$d_v = d - \frac{a}{2}$	d_v =	43.20	in

Flexure shear capacity

$$V_{ci} = \max\left(0.02 \cdot \sqrt{f_c} \cdot b_w \cdot d_v + (V_g + V_d) + \frac{1.6 \cdot V_L \cdot M_{cre}}{1.6 \cdot M_L}, 0.06 \cdot \sqrt{f_c} \cdot b_w \cdot d_v\right)$$ V_{ci} = 170.2 kip

$$M_{cre} = \frac{I_{Tc}}{y_{Tcb}} \cdot \left(0.20 \cdot \sqrt{f_c} + f_{cpe} - \frac{M_g \cdot y_{gb}}{I_g}\right)$$ M_{cre} = 23071 kip·in

$$f_{cpe} = \frac{P_e}{A_g} + \frac{P_e \cdot e \cdot y_{gb}}{I_g}$$ f_{cpe} = 2.00 ksi

V_{cg} = 6.2 kip

Shear capacity is minimum of web-shear and flexure-shear capacities V_c = 99.8 kip

Carried Loads:

Number of point loads		1	.
Applied point load maginitude	P =	360	kip
Applied point load location measured from the face of the girder	a =	148.5	in

for x < the first center of bearing: $V_u = -w \cdot x$

for x < the second center of bearing: $V_u = R_a - w \cdot x$ R_a = 244.9 kip

for x > the second center of bearing: $V_u = R_a + R_b - w \cdot x$ V_u = 251.1 kip

Shear capacity due to transverse reinforcement

cot(θ) used in calculating V_s $\cot\theta = 1 + 3 \cdot \frac{f_{pc}}{\sqrt{f_c'}}$ cot(θ) = 1.61

$V_s = \frac{A_v \cdot f_y \cdot d_v \cdot \cot\theta}{}$ θ = 28.0

$$V_s = \frac{\quad}{s}$$

V_s = 77.6 kip

$V_n < 0.25 \cdot f'_c \cdot b_w \cdot d_v + V_p =$ 458.77 kip

V_n = 177.4 kip

The following calculations are used to determine the nominal shear capacity based on the AASHTO 2010 LRFD manual for a prestressed, I-shaped girder. The General Procedure outlined in section 5.8.3.4.3 was used.

Length of girder	L_g =	341.75	in
First bearing pad center		7.75	in
Second bearing pad center		300.75	in
Span length	L =	293	in
Concrete compressive strength	f'_c =	7	ksi
Width of the girder web	b_w =	6	in
Height of deck	h_d =	9	in
Height of girder	h_g =	45	in
Jacking force	P_j =	732.15	kip
Width of the deck	b_d =	28.5	in
Girder centroid from the bottom	y_{gb} =	22.34	in
Girder centroid from the bottom for the net section	y_{ngb} =	22.58	in
Area of the girder	A_g =	624	in^2
	A_n =	616.1	in^2
Self weight of the girder	w_g =	0.056	kip/in
Self weight of the deck (assuming 150 lb/ft^3 for the self weight of concrete)	w_d =	0.022	kip/in
Strand area		0.2227	in^2
Strand diameter	d_s =	0.6	in
Area of draped prestressing steel	A_{psd} =	1.34	in^2
Area of straight prestressing steel	A_{pss} =	4.45	in^2
Area of prestressing steel	A_{ps} =	5.79	in^2
Centroid of draped strands at girder end	$y_{d,end}$ =	40.0	in
Centroid of draped strands at hold down point	$y_{d,hp}$ =	7.0	in
Centroid of the area of the straight strands	y_s =	3.00	in
Distance to hold down point	L_{hp} =	204	in
Angle of draped strands	α =	9.27	deg.
Eccentricity of the resultant of the prestress force at the location of interest "x"	e =	17.02	in
Moment of inertia for the girder	I_g =	167050	in^4
Net moment of inertia for the girder	I_n =	164212	in^4
Transformed moment of inertia for the composite girder	I_{Tc} =	285967	in^4
Centroid of the transformed composite section	y_{Tcb} =	29.32	in

Transverse reinforcement yield stress	f_y =	67.0	ksi
Transverse reinforcement spacing	s =	8	in

Prestress losses:

Seating loss	SL =	2.82	ksi
Elastic shortening losses	ES =	18.9	ksi
Relaxation prior to release		0.5	ksi
Relaxation following release		0.168	ksi
Relaxation of prestressing steel	CR_s =	0.668	ksi
Shrinkage	SH =	7.45	ksi
Creep of concrete	CR_c =	7.5	ksi

f_{cir} is the stress at the center of gravity of the strands due to prestress force and the dead load of the beam at release calculated at the location of maximum moment.

f_{cds} is the stress at the center of gravity of the strands due to the dead load on the beam except that applied at the time of release.

Eccentricity of the strand force at the location of maximum moment due to dead load (L/2)	e_{hp} =	18.97	in
The prestressing force after release includes the elastic shortening losses	P_i =	603.49	kip
Maximum moment due to self weight of girder at release (full length)	M_{maxi} =	817.1	kip·in

$$f_{cir} = \frac{P_i}{A_n} + \frac{P_i \cdot e^2}{I_n} - \frac{M_{max,i} \cdot e}{I_n}$$

= 0.97 ksi + 1.3 ksi - 0.09 ksi f_{cir} = 2.21 ksi

The maximum moment due to all dead load applied except that at the time of release $M_{max,d-i}$ = 225.1 kip·in

$$f_{cds} = \frac{M_{max,d-i} \cdot e}{I_n}$$ f_{cds} = 0.026 ksi

Total prestress losses $TL = ES + SH + CR_c + CR_s$+SL TL = 37.3 ksi

The effective prestress force after accounting for losses P_e= 516.2 kip

Shear Calculation:

The first portion of shear capacity which will be calculated is the V_{cw} portion, which accurately predicts the formation of web shear cracks in prestressed girders.

Web shear capacity $$V_{cw} = \left(0.06 \cdot \sqrt{f_c'} + 0.3 \cdot f_{pc}\right) \cdot b_w \cdot d_v + V_p$$

Determine the stress at the centroid of the composite section due to the prestress force and dead load

$$f_{pc} = \frac{L_t \cdot P_e}{A_g} - \frac{L_t \cdot P_e \cdot e \cdot (y_{Tcb} - y_{gb})}{I_g} + \frac{M_g \cdot (y_{Tcb} - y_{gb})}{I_g} + \frac{M_d \cdot (y_{Tcb} - y_{gb})}{I_g}$$

Location of interest measured from face of girder	x =	148.49	in
The moment due to the self weight of the girder at location x	M_g =	576.2	kip·in
The moment due to the self weight of the slab at location x	M_d =	229.2	kip·in
The moment due to live load at location x	M_L =	47023.9	kip·in
Development percentage where the total length is equal to 60 bar diameters	L_t =	1.00	.
	f_{pc} =	0.494	ksi
Depth of prestressing strand area	d =	48.00	in
Shear component due to the vertical component of the draped strand's effective prestress force	V_p =	18.1	kip
	V_{cw} =	97.66	kip
$d_v = d - \frac{a}{2}$	d_v =	43.20	in

Flexure shear capacity

$$V_{ci} = \max\left(0.02 \cdot \sqrt{f_c} \cdot b_w \cdot d_v + (V_g + V_d) + \frac{1.6 \cdot V_L \cdot M_{cre}}{1.6 \cdot M_L}, 0.06 \cdot \sqrt{f_c} \cdot b_w \cdot d_v\right)$$ V_{ci} = 171.4 kip

$$M_{cre} = \frac{I_{Tc}}{y_{Tcb}} \cdot \left(0.20 \cdot \sqrt{f_c} + f_{cpe} - \frac{M_g \cdot y_{gb}}{I_g}\right)$$ M_{cre} = 23936 kip·in

$$f_{cpe} = \frac{P_e}{A_g} + \frac{P_e \cdot e \cdot y_{gb}}{I_g}$$ f_{cpe} = 2.00 ksi

V_{cg} = 1.8 kip

Shear capacity is minimum of web-shear and flexure-shear capacities	V_c =	97.7	kip

Carried Loads:

Number of point loads		1	.
Applied point load maginitude	P =	643	kip
Applied point load location measured from the face of the girder	a =	148.5	in

for x < the first center of bearing: $V_u = -w \cdot x$

for x < the second center of bearing: $V_u = R_a - w \cdot x$ R_a = 334.1 kip

for x > the second center of bearing: $V_u = R_a + R_b - w \cdot x$ V_u = 334.4 kip

Shear capacity due to transverse reinforcement

cot(θ) used in calculating V_s $\cot\theta = 1 + 3 \cdot \frac{f_{pc}}{f_c'}$ cot(θ) = 1.56

$$V_s = \frac{A_v \cdot f_y \cdot d_v \cdot \cot\theta}{s}$$

$\sqrt{f'_c}$

$V_n < 0.25 \cdot f'_c \cdot b_w \cdot d_v + V_p =$ 471.74 kip

θ =	31.2	kip
V_s =	225.8	kip
V_n =	323.5	

The following calculations are used to determine the nominal shear capacity based on the AASHTO 2010 LRFD manual for a prestressed, I-shaped girder. The General Procedure outlined in section 5.8.3.4.3 was used.

Length of girder	L_g =	300.25	in
First bearing pad center		8	in
Second bearing pad center		254	in
Span length	L =	246	in
Concrete compressive strength	f'_c =	6.9	ksi
Width of the girder web	b_w =	6	in
Height of deck	h_d =	9	in
Height of girder	h_g =	36	in
Jacking force	P_j =	424.9	kip
Width of the deck	b_d =	28.5	in
Girder centroid from the bottom	y_{gb} =	17.97	in
Girder centroid from the bottom for the net section	y_{ngb} =	18.16	in
Area of the girder	A_g =	570	in^2
	A_n =	562.1	in^2
Self weight of the girder	w_g =	0.051	kip/in
Self weight of the deck (assuming 150 lb/ft^3 for the self weight of concrete)	w_d =	0.022	kip/in
Strand area		0.2227	in^2
Strand diameter	d_s =	0.6	in
Area of draped prestressing steel	A_{psd} =	1.34	in^2
Area of straight prestressing steel	A_{pss} =	2.67	in^2
Area of prestressing steel	A_{ps} =	4.01	in^2
Centroid of draped strands at girder end	$y_{d,end}$ =	29.0	in
Centroid of draped strands at hold down point	$y_{d,hp}$ =	5.0	in
Centroid of the area of the straight strands	y_s =	3.00	in
Distance to hold down point	L_{hp} =	222	in
Angle of draped strands	α =	6.19	deg.
Eccentricity of the resultant of the prestress force at the location of interest "x"	e =	10.73	in
Moment of inertia for the girder	I_g =	93351.373	in^4
Net moment of inertia for the girder	I_n =	91767.365	in^4
Transformed moment of inertia for the composite girder	I_{Tc} =	178419	in^4
Centroid of the transformed composite section	y_{cb} =	24.48	in

Transverse reinforcement yield stress	f_y =	70 ksi
Transverse reinforcement spacing	s =	8 in

Prestress losses:

Seating loss	SL =	2.82 ksi
Elastic shortening losses	ES =	10.3 ksi
Relaxaion prior to release		0.3 ksi
Relaxation following release		0.12 ksi
Relaxation of prestressing steel	CR_s =	0.420 ksi
Shrinkage	SH =	4.75 ksi
Creep of concrete	CR_c =	4.75 ksi

f_{cir} is the stress at the center of gravity of the strands due to prestress force and the dead load of the beam at release calculated at the location of maximum moment.

f_{cds} is the stress at the center of gravity of the strands due to the dead load on the beam except that applied at the time of release.

Eccentricity of the strand force at the location of maximum moment due to dead load (L/2)	e_{hp} =	14.87 in
The prestressing force after release includes the elastic shortening losses	P_i =	371.10 kip
Maximum moment due to self weight of girder at release (full length)	M_{maxi} =	576.2 kip·in

$$f_{cir} = \frac{P_i}{A_n} + \frac{P_i \cdot e^2}{I_n} - \frac{M_{max,i} \cdot e}{I_n}$$

= 0.65 ksi + 0.88 ksi - 0.09 ksi	f_{cir} =	1.46 ksi
The maximum moment due to all dead load applied except that at the time of release	$M_{max,d-i}$ =	150.3 kip·in

$$f_{cds} = \frac{M_{max,d-i} \cdot e}{I_n}$$

f_{cds} = 0.024 ksi

Total prestress losses	$TL = ES + SH + CR_c + CR_s + SL$	TL =	23.0 ksi
The effective prestress force after accounting for losses		P_e =	332.5 kip

Shear Calculation:

The first portion of shear capacity which will be calculated is the V_{cw} portion, which accurately predicts the formation of web shear cracks in prestressed girders.

Web shear capacity $$V_{cw} = \left(0.06 \cdot \sqrt{f_c'} + 0.3 \cdot f_{pc}\right) \cdot b_w \cdot d_v + V_p$$

Determine the stress at the centroid of the composite section due to the prestress force and dead load

$$f_{pc} = \frac{L_t \cdot P_e}{A_g} - \frac{L_t \cdot P_e \cdot e \cdot (y_{Tcb} - y_{gb})}{I_g} + \frac{M_g \cdot (y_{Tcb} - y_{gb})}{I_g} + \frac{M_d \cdot (y_{Tcb} - y_{gb})}{I_g}$$

Location of interest measured from face of girder	x =	119.99	in
The moment due to the self weight of the girder at location x	M_g =	357.9	kip·in
The moment due to the self weight of the slab at location x	M_d =	155.8	kip·in
The moment due to live load at location x	M_L =	34039.5	kip·in
Development percentage where the total length is equal to 60 bar diameters	L_t =	1.00	.
	f_{pc} =	0.371	ksi
Depth of prestressing strand area	d =	37.66	in
Shear component due to the vertical component of the draped strand's effective prestress force	V_p =	13.5	kip
	V_{cw} =	68.88	kip
$d_v = d - \frac{a}{2}$	d_v =	34.37	in

Flexure shear capacity

$$V_{ci} = \max\left(0.02 \cdot \sqrt{f_c} \cdot b_w \cdot d_v + (V_g + V_d) + \frac{1.6 \cdot V_L \cdot M_{cre}}{1.6 \cdot M_L}, 0.06 \cdot \sqrt{f_c} \cdot b_w \cdot d_v\right)$$

V_{ci} = 114.3 kip

$$M_{cre} = \frac{I_{Tc}}{y_{Tcb}} \cdot \left(0.20 \cdot \sqrt{f_c} + f_{cpe} - \frac{M_g \cdot y_{gb}}{I_g}\right)$$

M_{cre} = 12586 kip·in

$$f_{cpe} = \frac{P_e}{A_g} + \frac{P_e \cdot e \cdot y_{gb}}{I_g}$$

f_{cpe} = 1.27 ksi

V_{cg} = 2.2 kip

Shear capacity is minimum of web-shear and flexure-shear capacities	V_c =	68.9	kip

Carried Loads:

Number of point loads		1	.
Applied point load maginitude	P =	558	kip
Applied point load location measured from the face of the girder	a =	120	in

for x < the first center of bearing: $V_u = -w \cdot x$

for x < the second center of bearing: $V_u = R_a - w \cdot x$

for x > the second center of bearing: $V_u = R_a + R_b - w \cdot x$

	R_a =	304.0	kip
	V_u =	304.4	kip

Shear capacity due to transverse reinforcement

cot(θ) used in calculating V_s $\quad \cot\theta = 1 + 3 \cdot \frac{f_{pc}}{\sqrt{f'_c}}$ $\quad$ cot(θ) = 1.42

$\sqrt{f'c}$

$$V_s = \frac{A_v \cdot f_y \cdot d_v \cdot \cot\theta}{s}$$

$$V_n < 0.25 \cdot f'_c \cdot b_w \cdot d_v + V_p = \quad 369.14 \text{ kip}$$

θ =	36.5	
V_s =	171.2	kip
V_n =	240.1	kip

Appendix C Shear Testing Photographs

This appendix documents the photographs that were taken throughout the girder tests while the tests were paused to observe and mark damage. This section of the appendix includes photos taken during the test which were not included in the body of the report. The numbers written next to the crack lines represent the magnitude of the load applied by the displacement-controlled actuator. This is the actuator located at midspan for the 36M_18F test and is the universal testing system for the web-shear tests.

C.1 Photographs during 36M_18F Test

Figure C-1: Failure end setup for 36M_18F test.

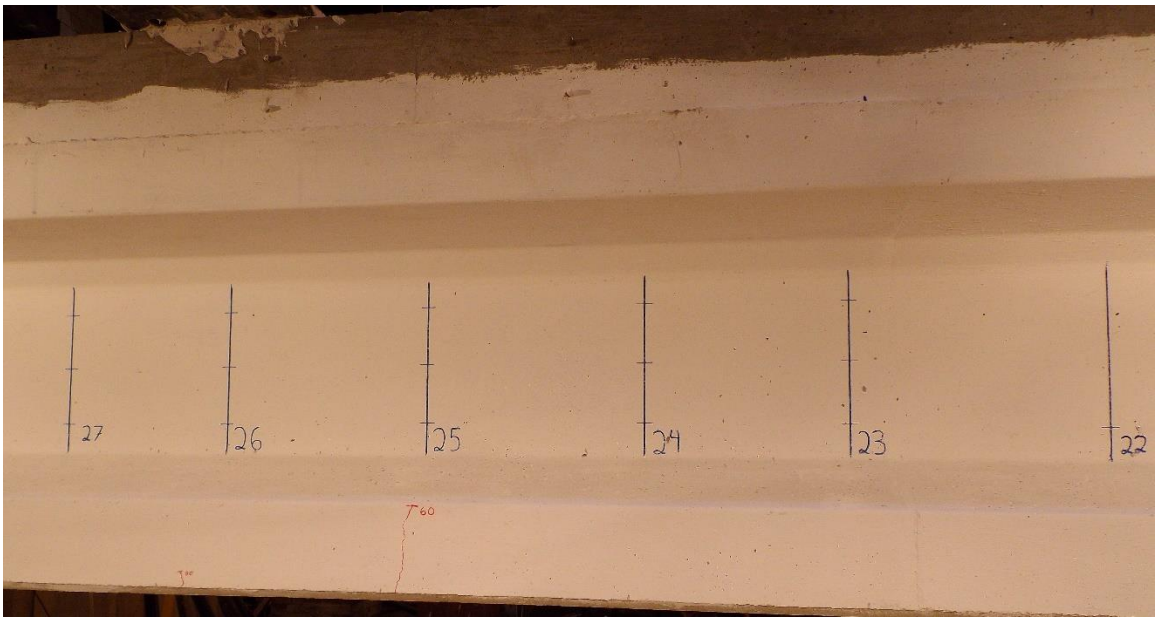

Figure C-2: Observed cracking in failure region of 36M_18F test with 90 kips applied load.

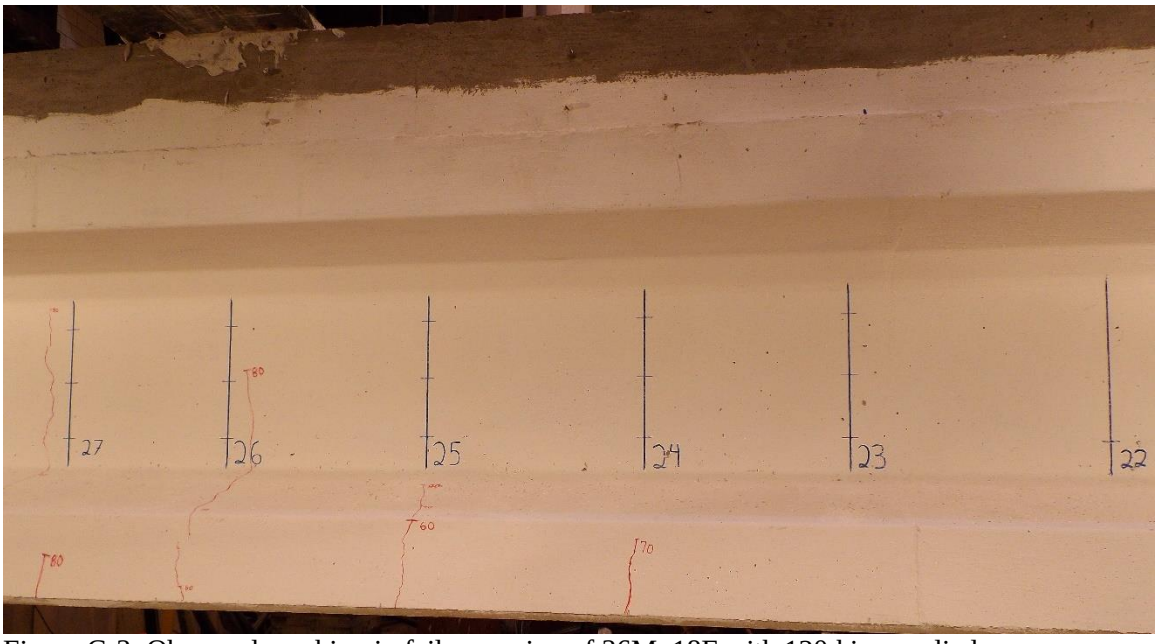

Figure C-3: Observed cracking in failure region of 36M_18F with 120 kips applied

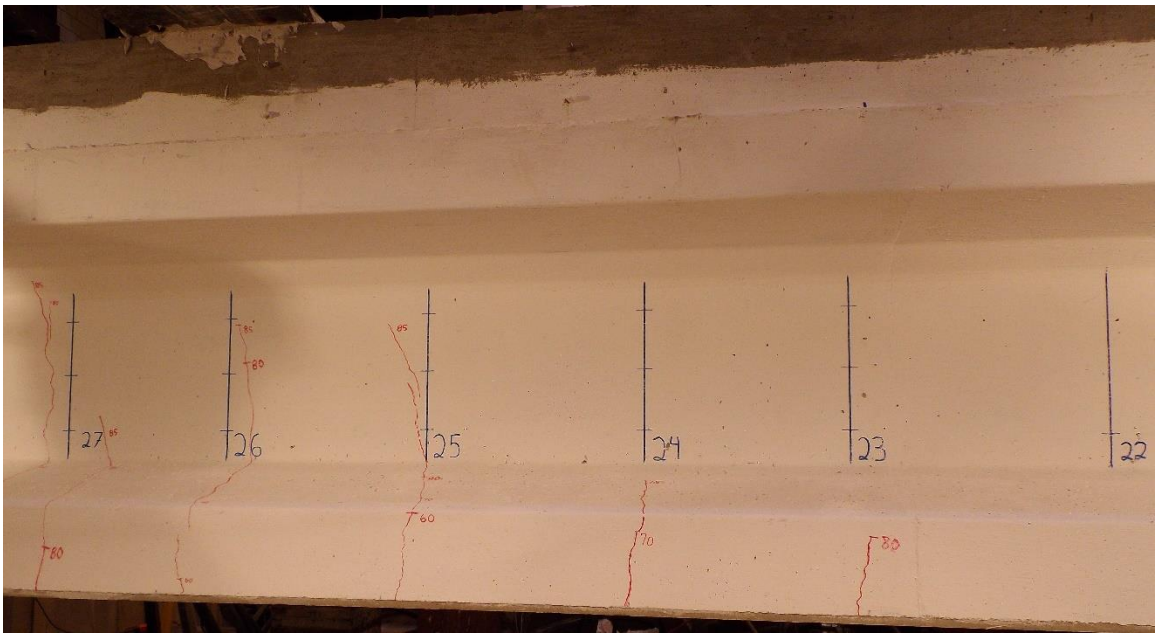

Figure C-4: Observed cracking in failure region of 36M_18F with 127.5 kips applied.

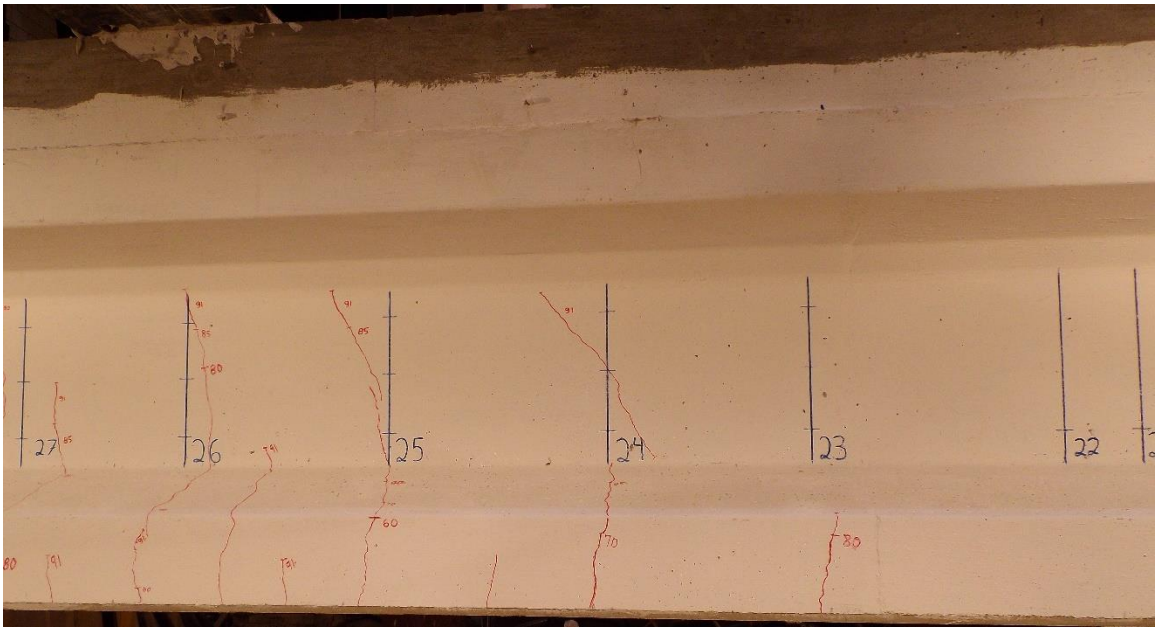

Figure C-5: Observed cracking in failure region of 36M_18F with 136.5 kips applied.

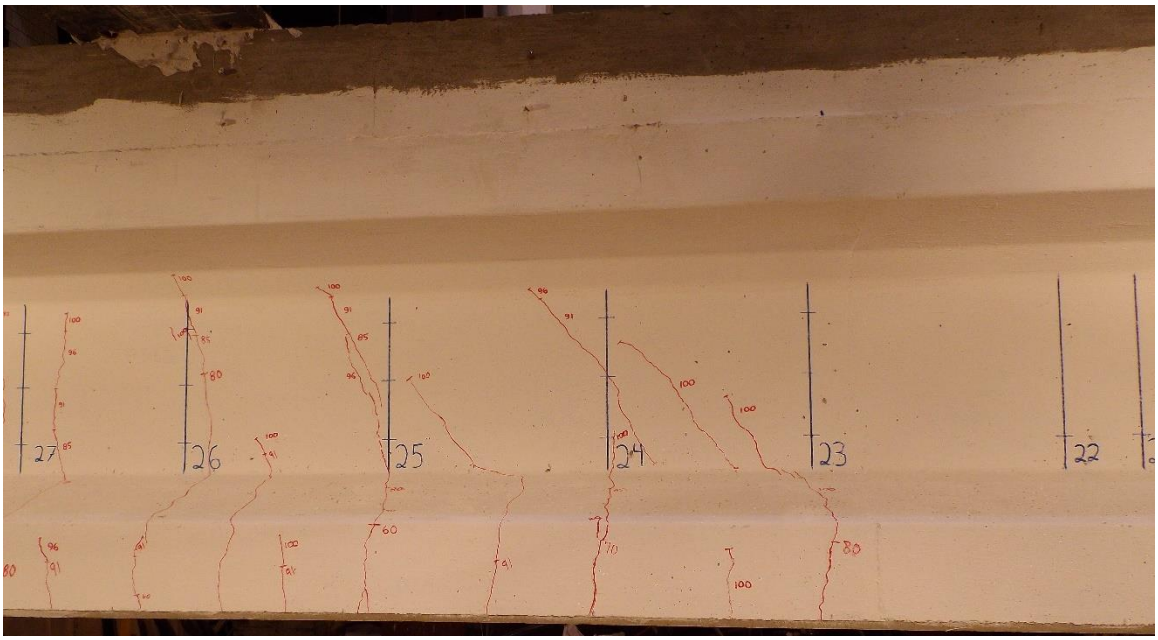

Figure C-6: Observed cracking in failure region of 36M_18F with 150 kips applied.

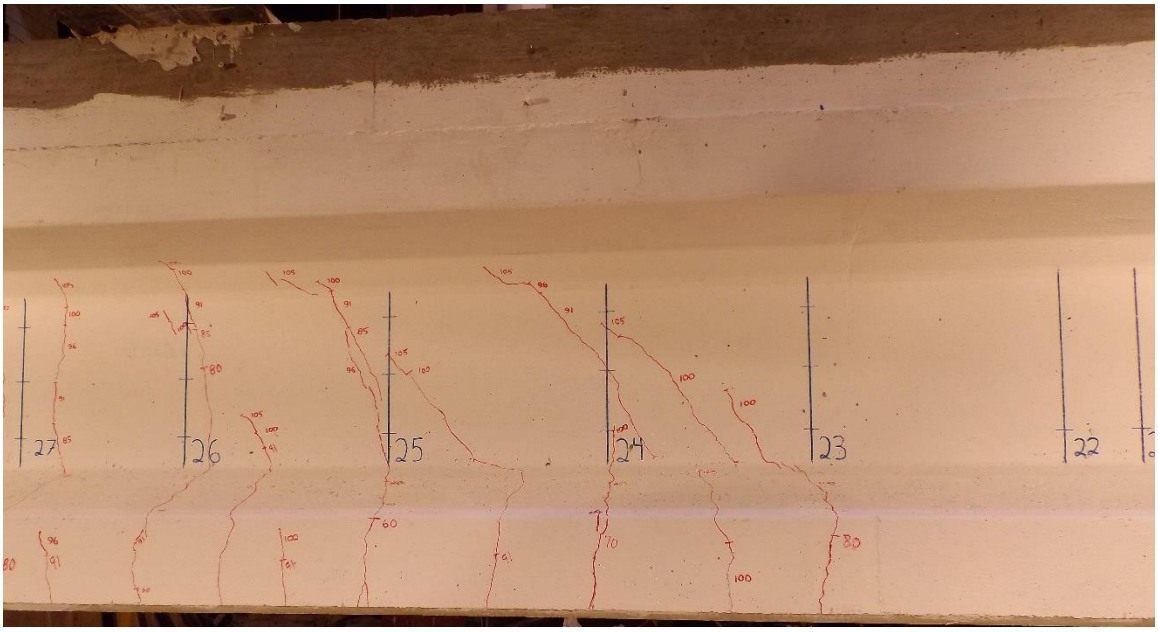

Figure C-7: Observed cracking in failure region of 36M_18F with 157.5 kips applied.

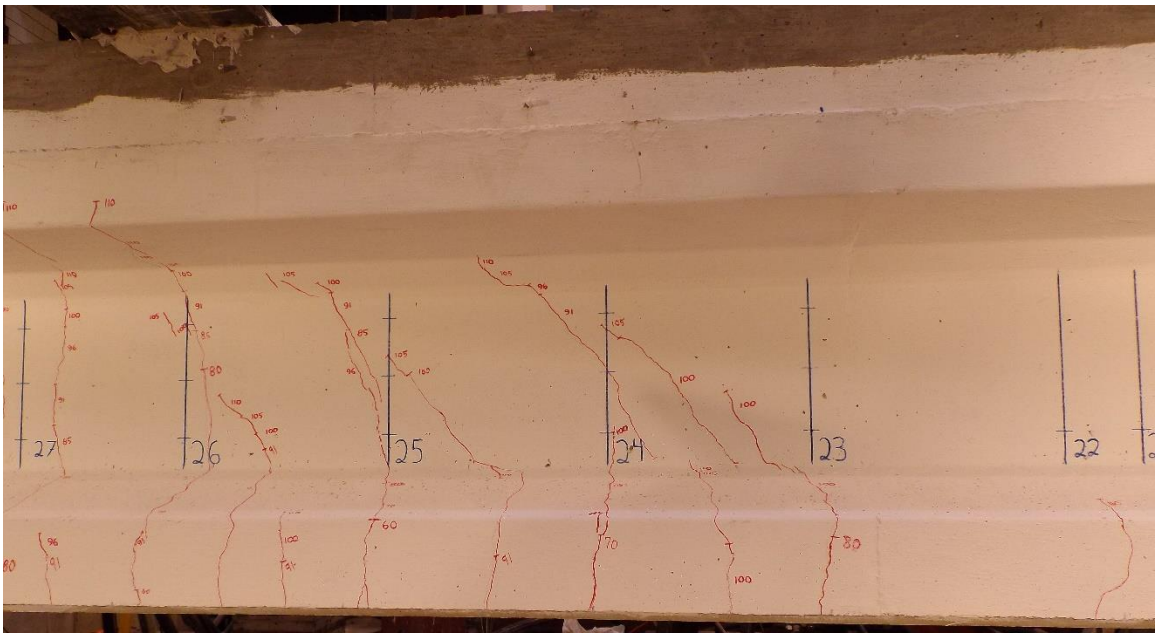

Figure C-8: Observed cracking in failure region of 36M_18F with 165 kips applied.

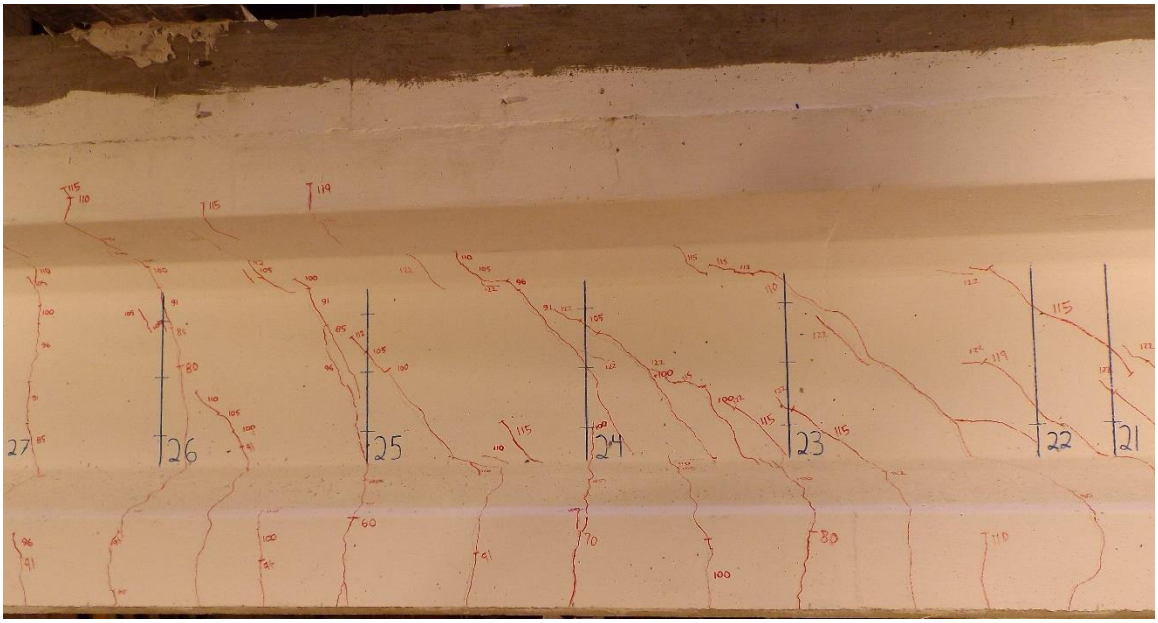

Figure C-9: Observed cracking in failure region of 36M_18F with 172.5 kips applied.

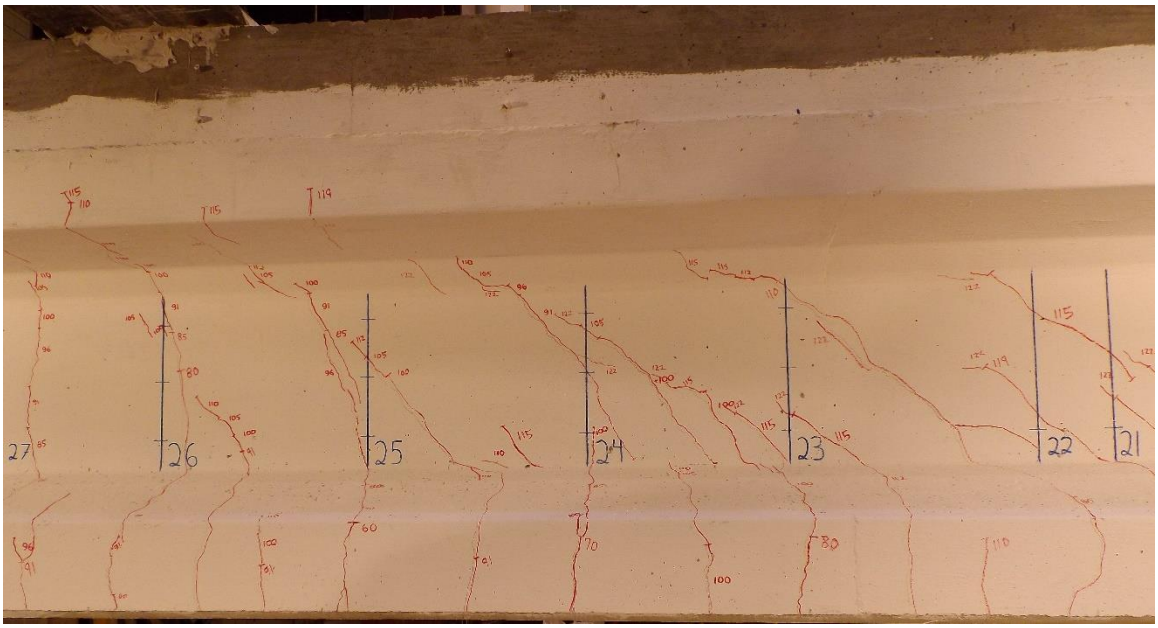

Figure C-10: Observed cracking in failure region of 36M_18F with 178.5 kips applied.

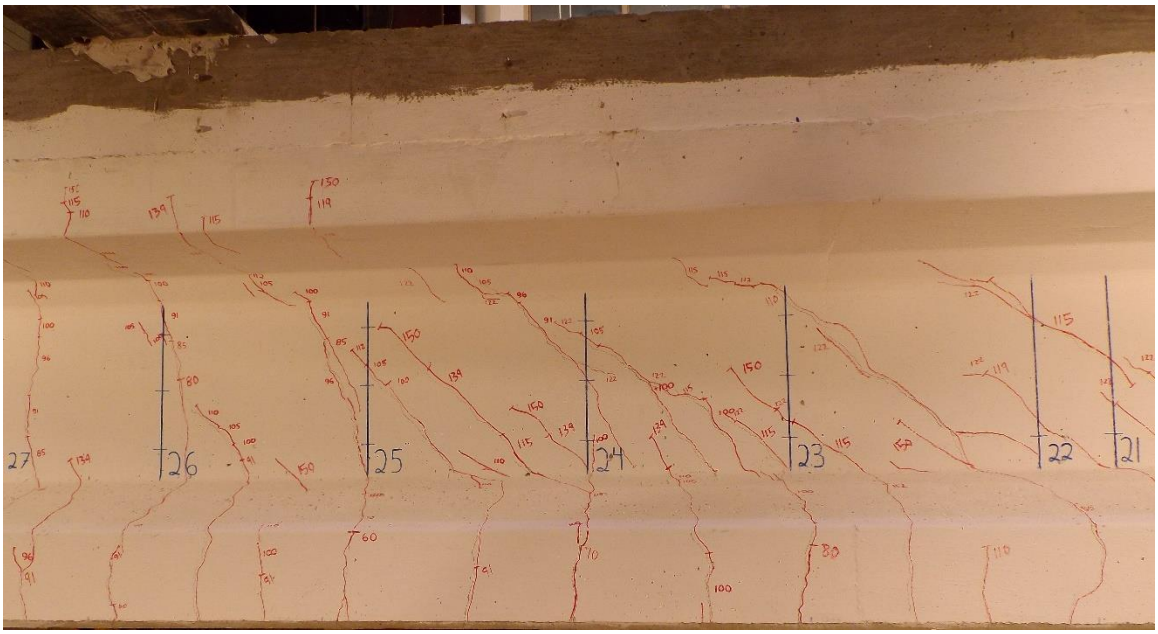

Figure C-11: Observed cracking in failure region of 36M_18F with 208.5 kips applied.

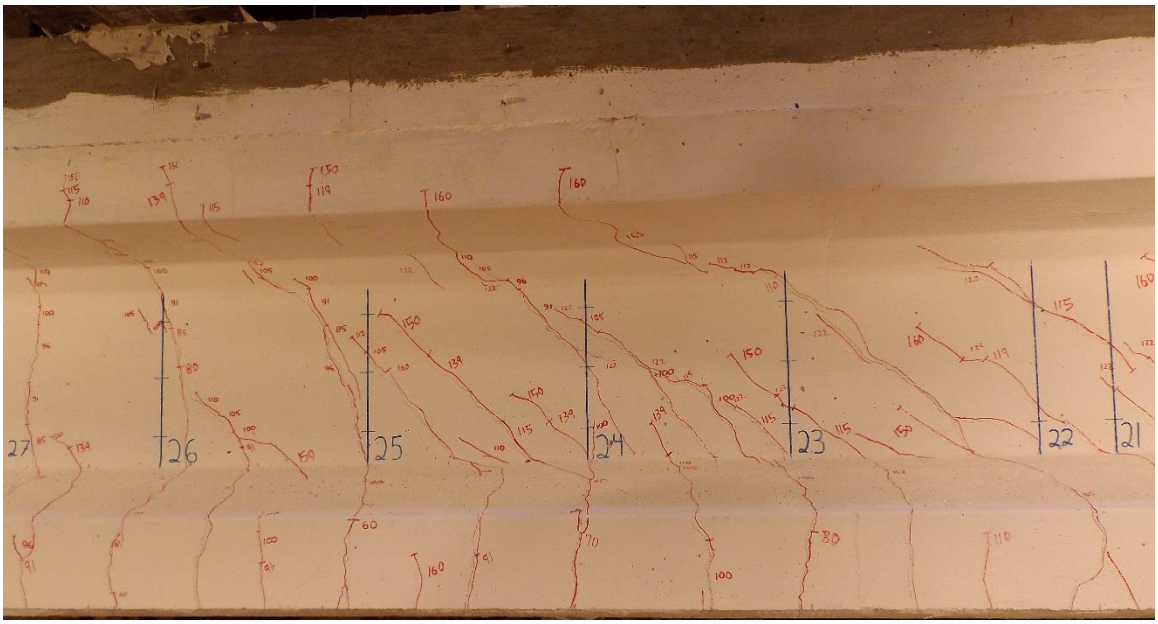

Figure C-12: Observed cracking in failure region of 36M_18F with 225 kips applied.

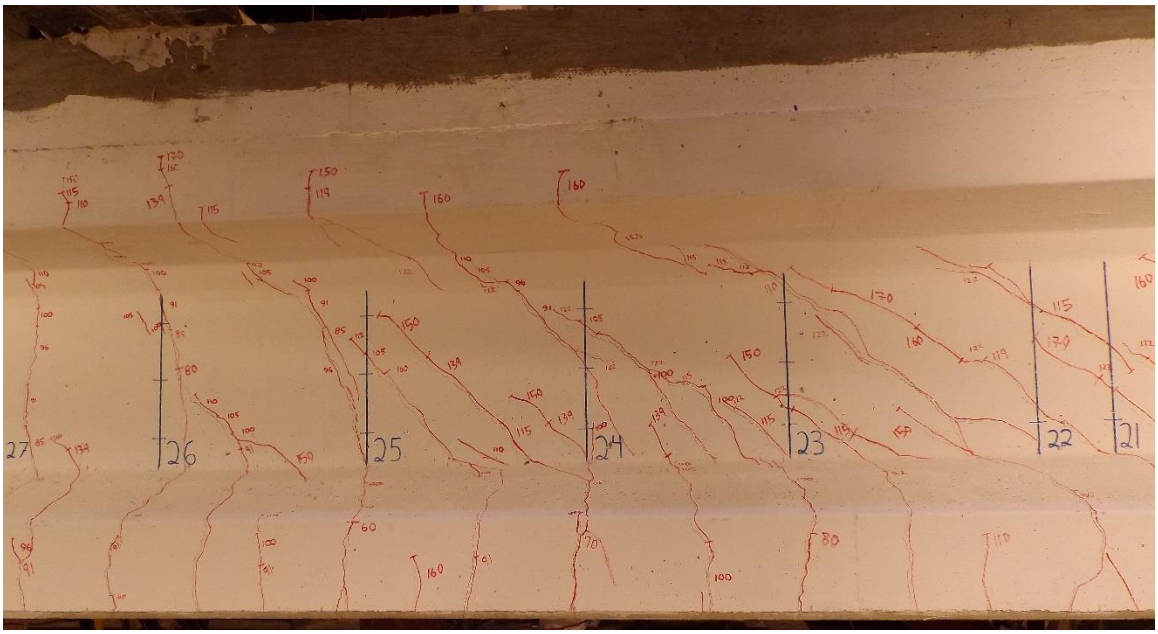

Figure C-13: Observed cracking in failure region of 36M_18F with 240 kips applied.

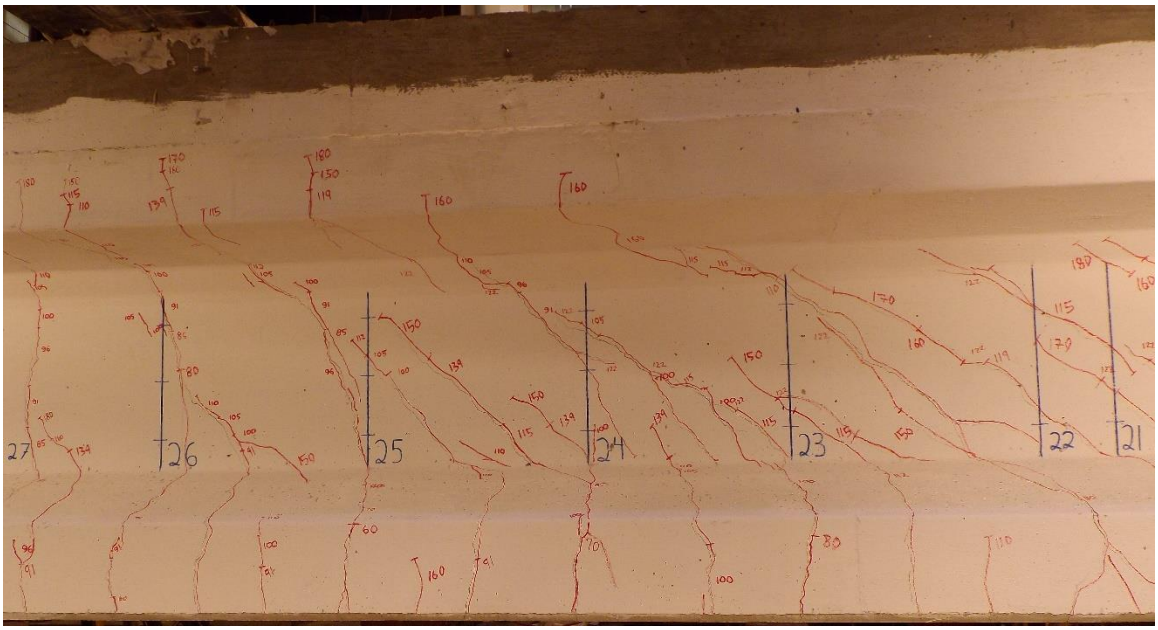

Figure C-14: Observed cracking in failure region of 36M_18F with 270 kips applied.

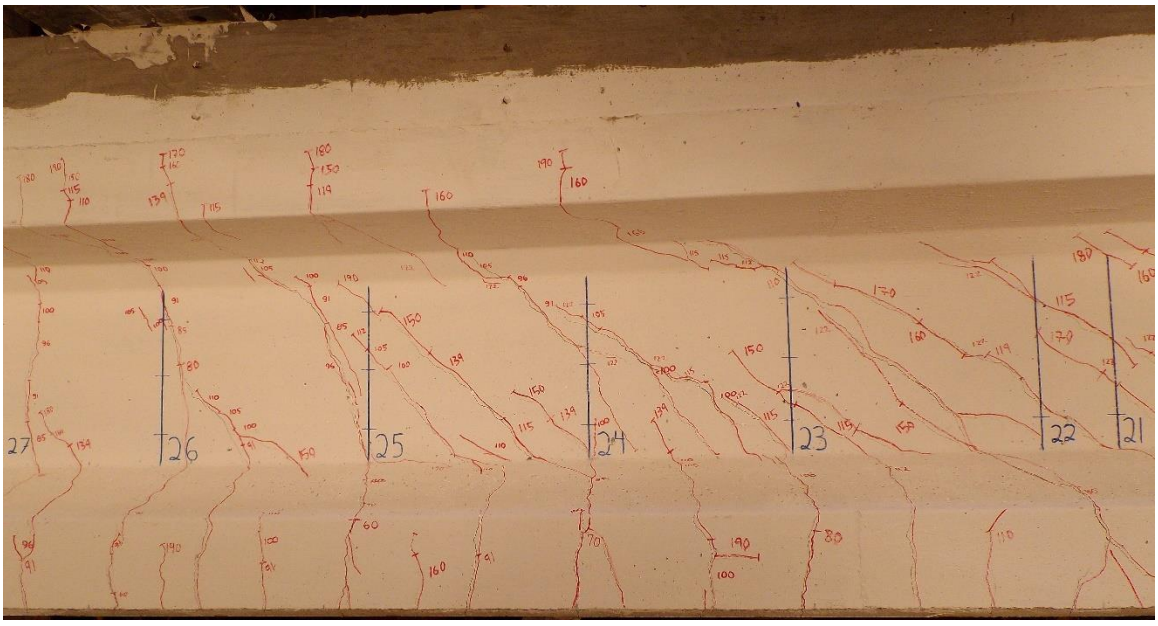

Figure C-15: Observed cracking in failure region of 36M_18F with 285 kips applied.

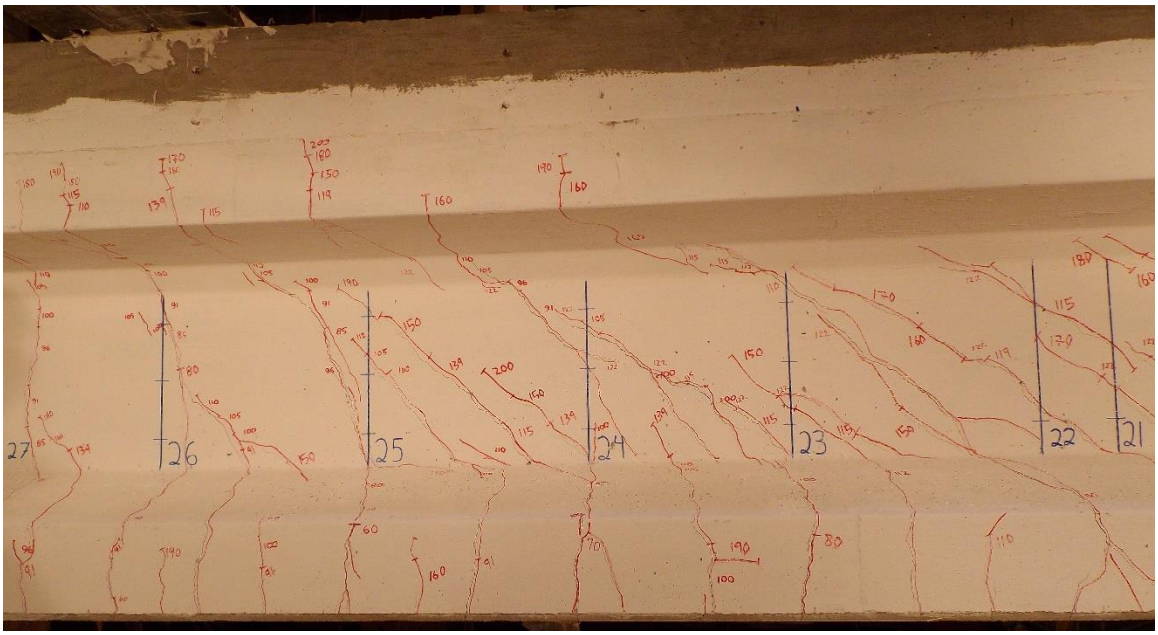

Figure C-16: Observed cracking in failure region of 36M_18F test with 324 kips applied.

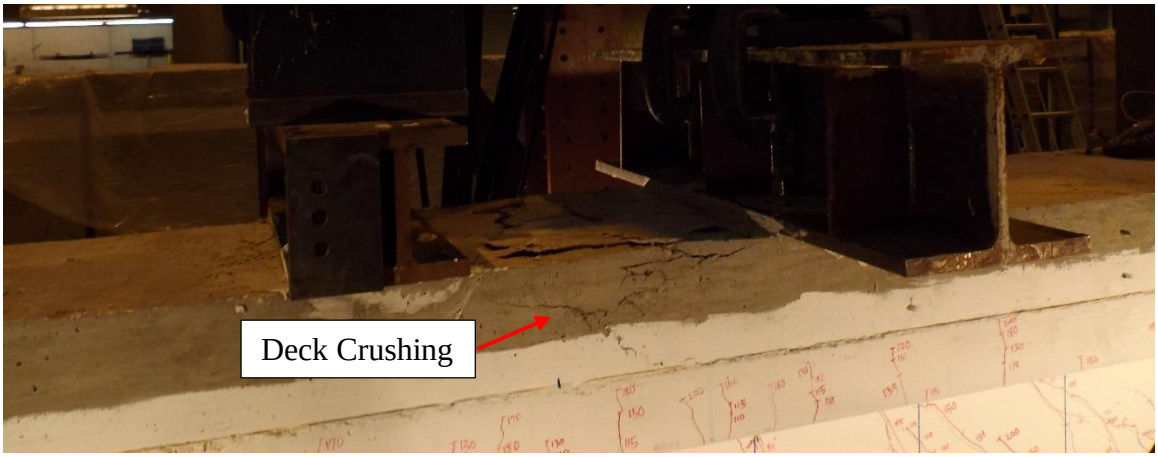

Figure C-17: Observed deck crushing during 36M_18F test.

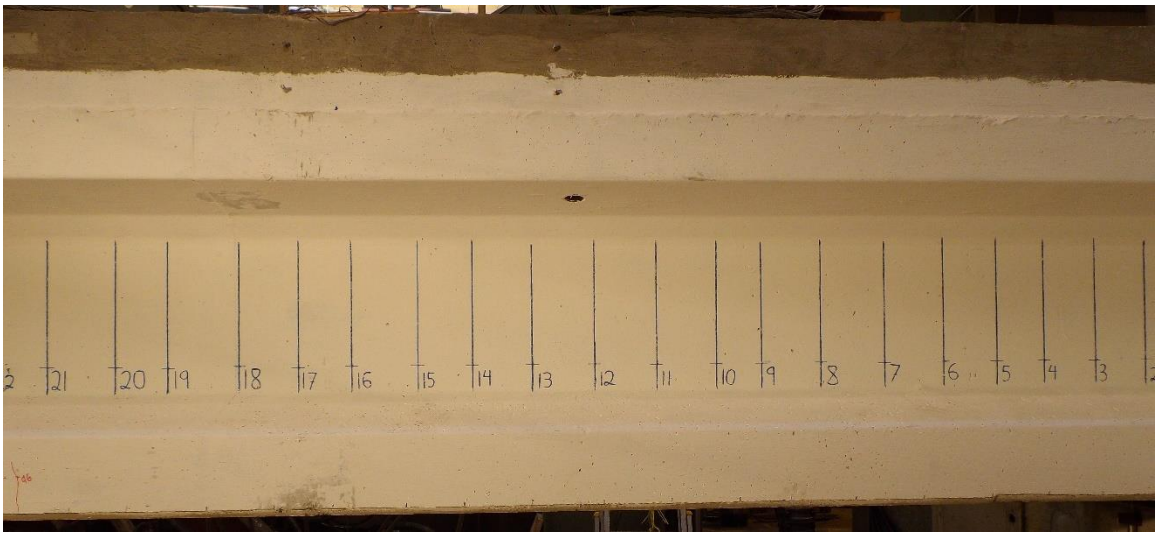

Figure C-18: Observed cracking in web-shear controlled region of 36M_18F test with 136.5 kips applied.

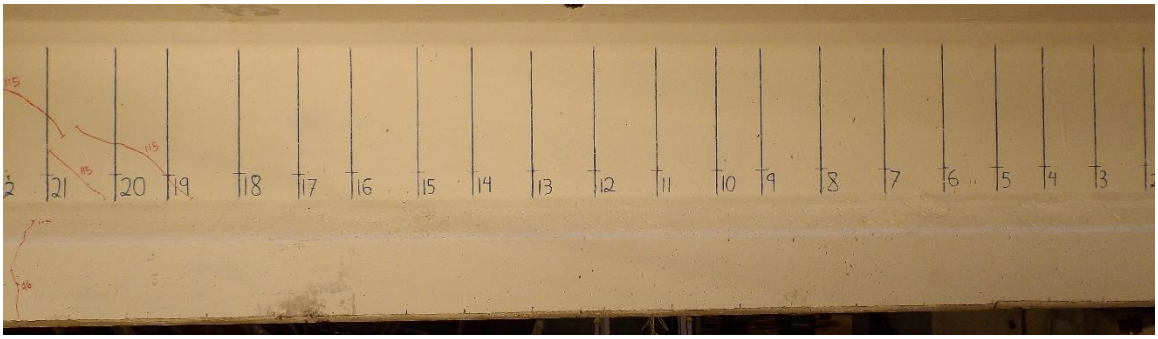

Figure C-19: Observed cracking in web-shear controlled region of 36M_18F test with 172.5 kips applied.

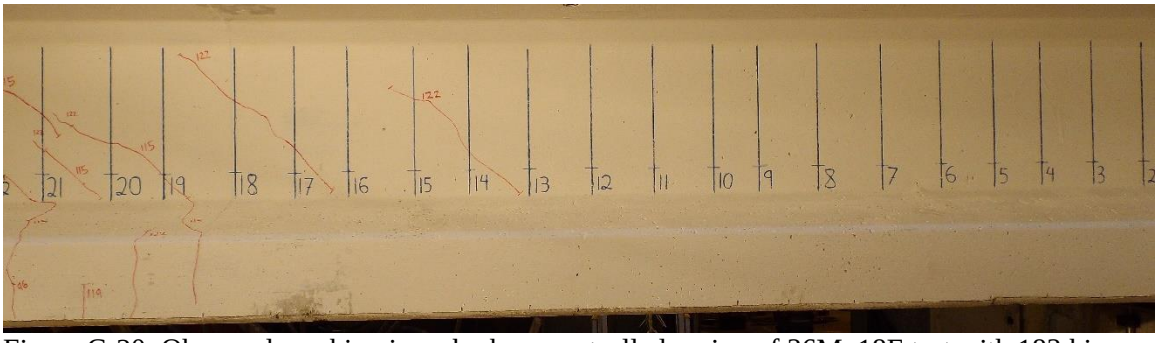

Figure C-20: Observed cracking in web-shear controlled region of 36M_18F test with 183 kips applied.

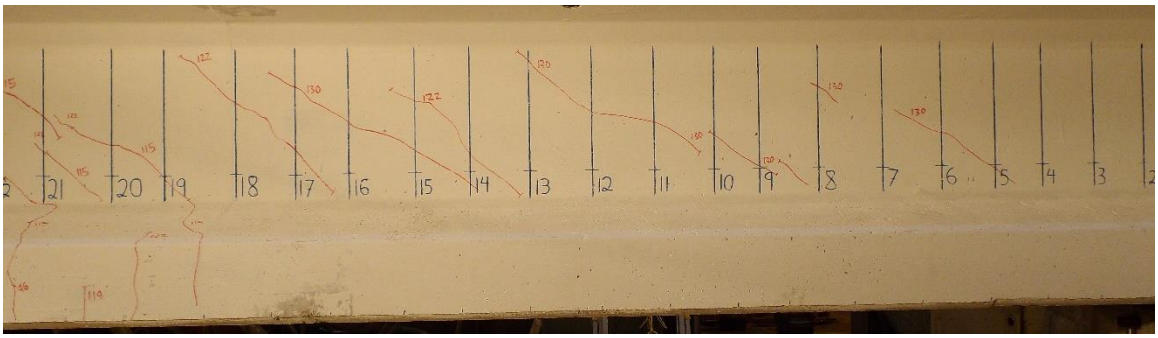

Figure C-21: Observed cracking in web-shear controlled region of 36M_18F test with 195 kips applied.

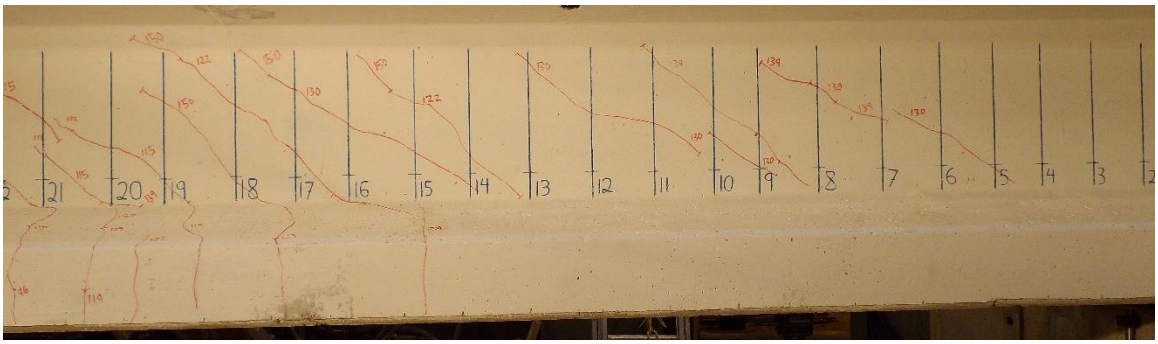

Figure C-22: Observed cracking in web-shear controlled region of 36M_18F test with 225 kips applied.

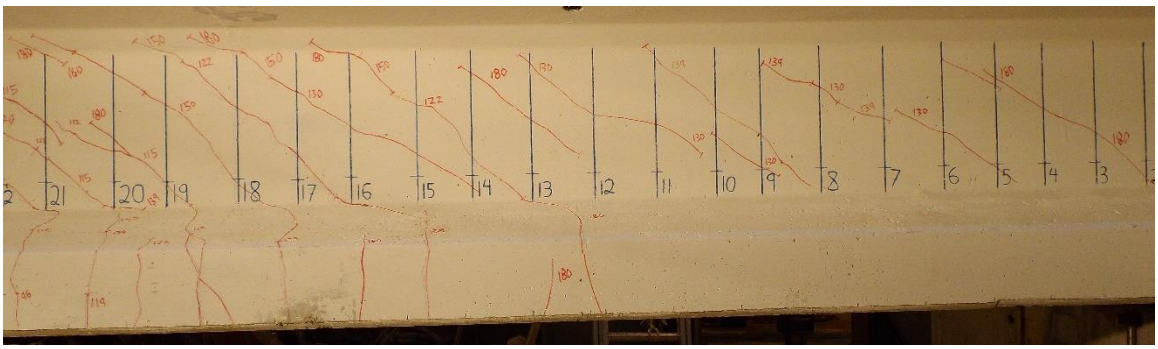

Figure C-23: Observed cracking in web-shear controlled region of 36M_18F test with 270 kips applied.

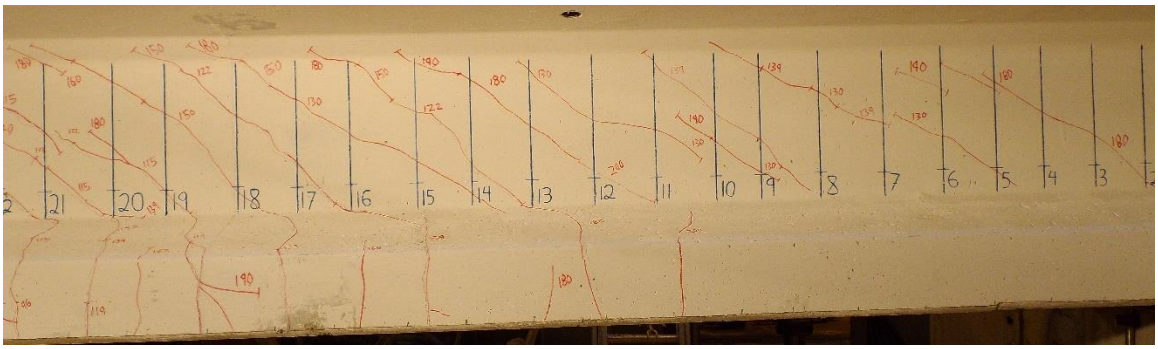

Figure C-24: Observed cracking in web-shear controlled region of 36M_18F test with 324 kips applied.

C.2 Photographs during 45M_24W Test

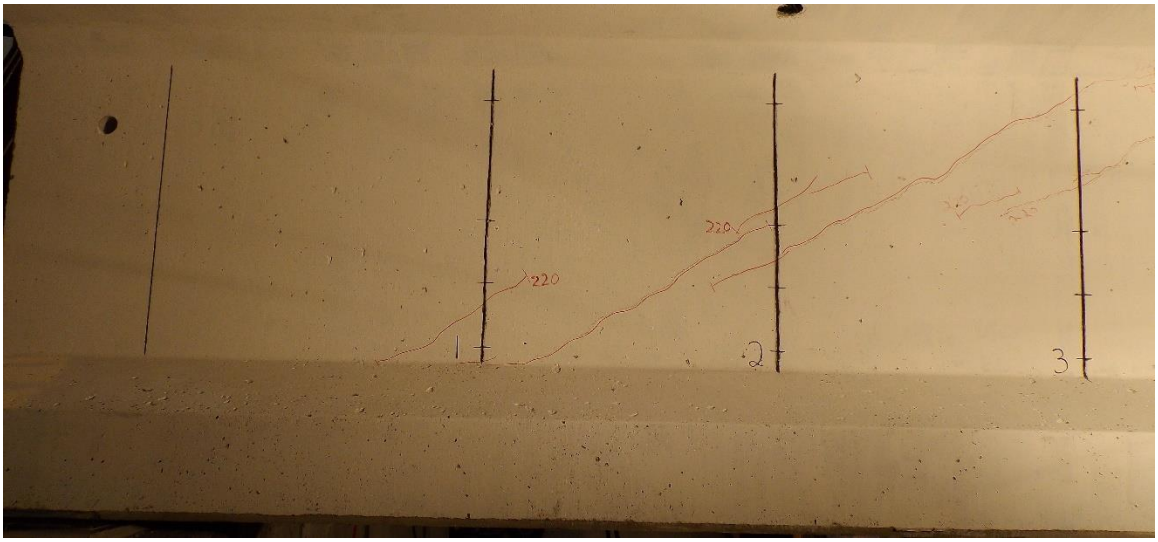

Figure C-25: Observed cracking in failure region of 45M_24W with 220 kips applied.

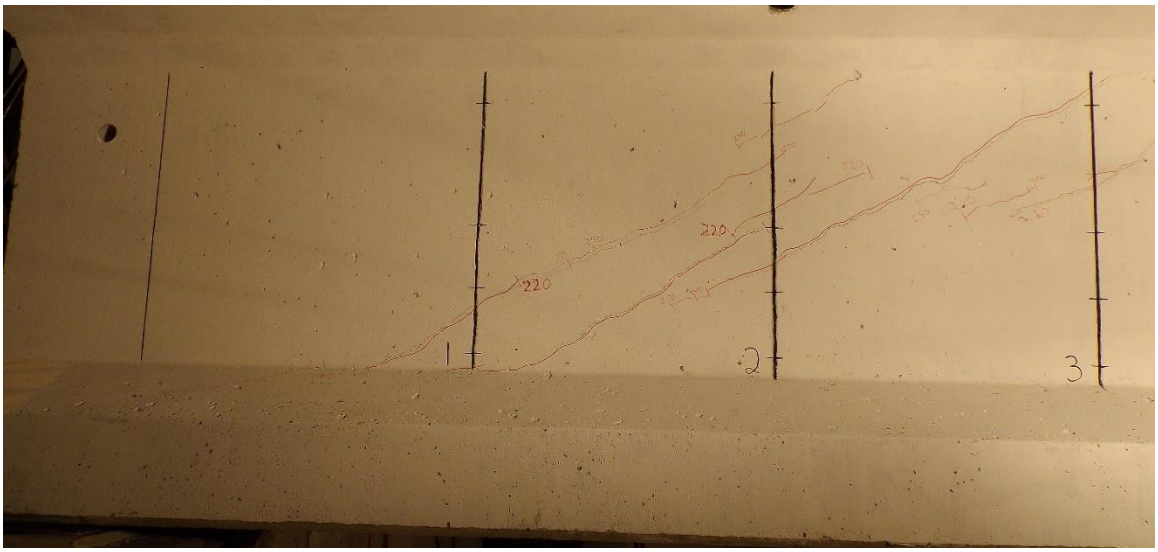

Figure C-26: Observed cracking in failure region of 45M_24W with 250 kips applied.

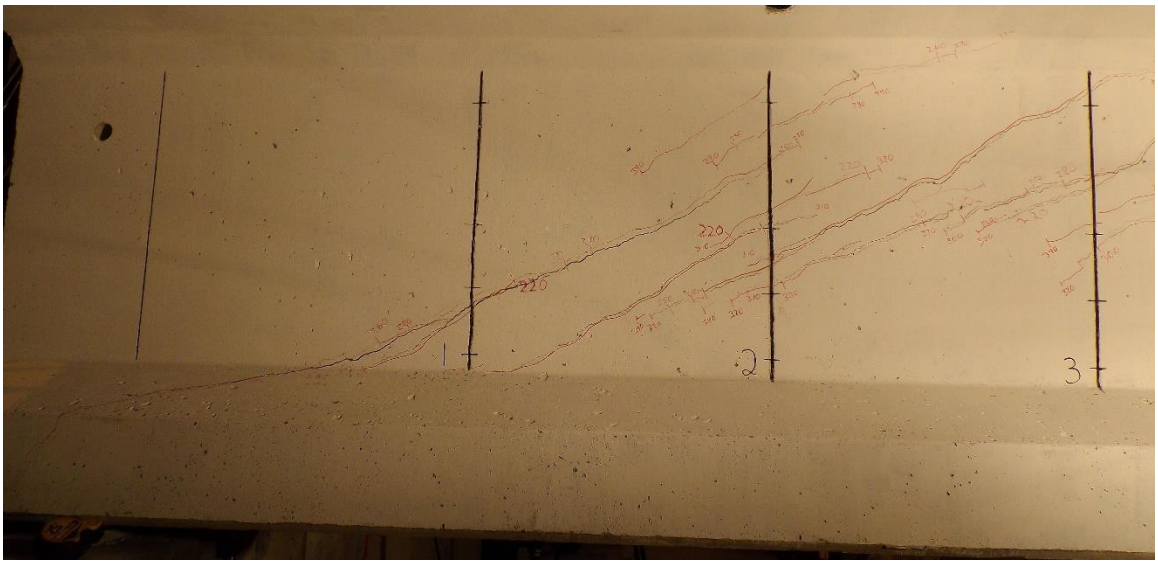

Figure C-27: Observed cracking in failure region of 45M_24W with 340 kips applied.

C.3 Photographs during 45M_8W Test

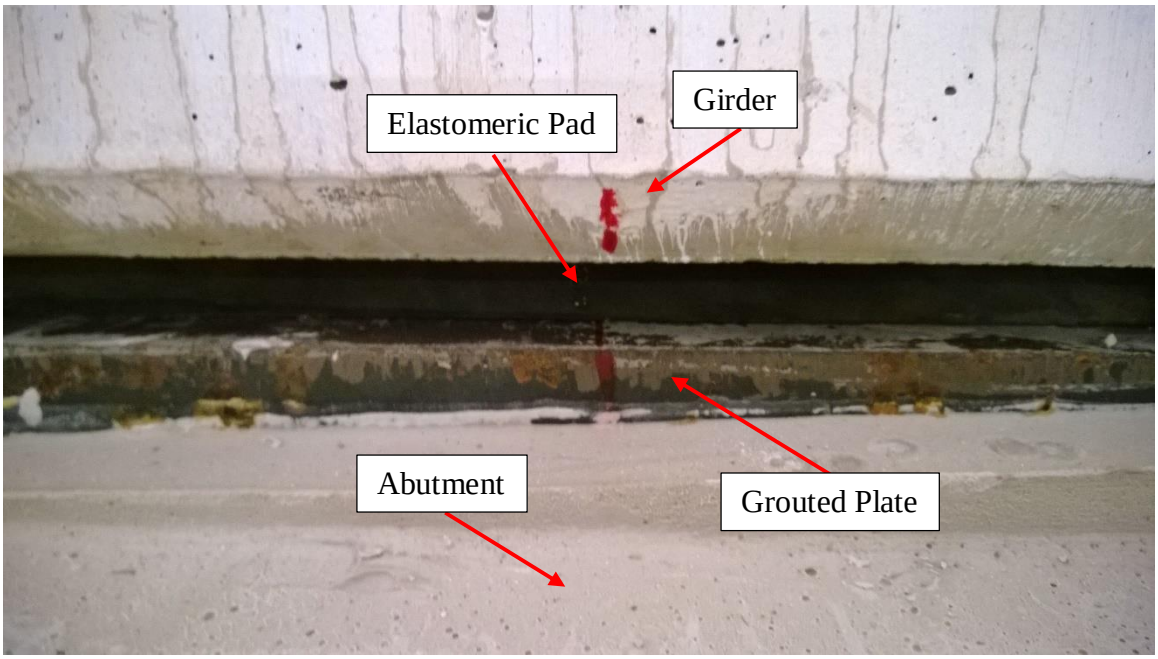

Figure C-28: Typical bearing placement shown here during the 45M_8W test.

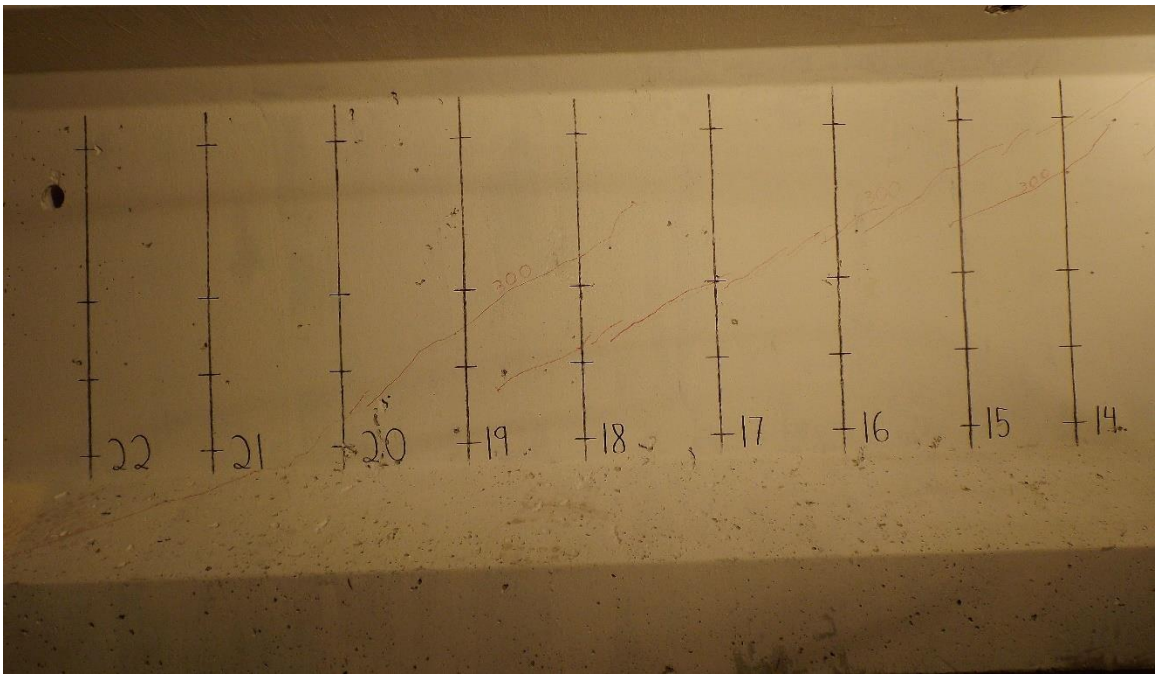

Figure C-29: Observed cracking in failure region of 45M_8W with 300 kips applied.

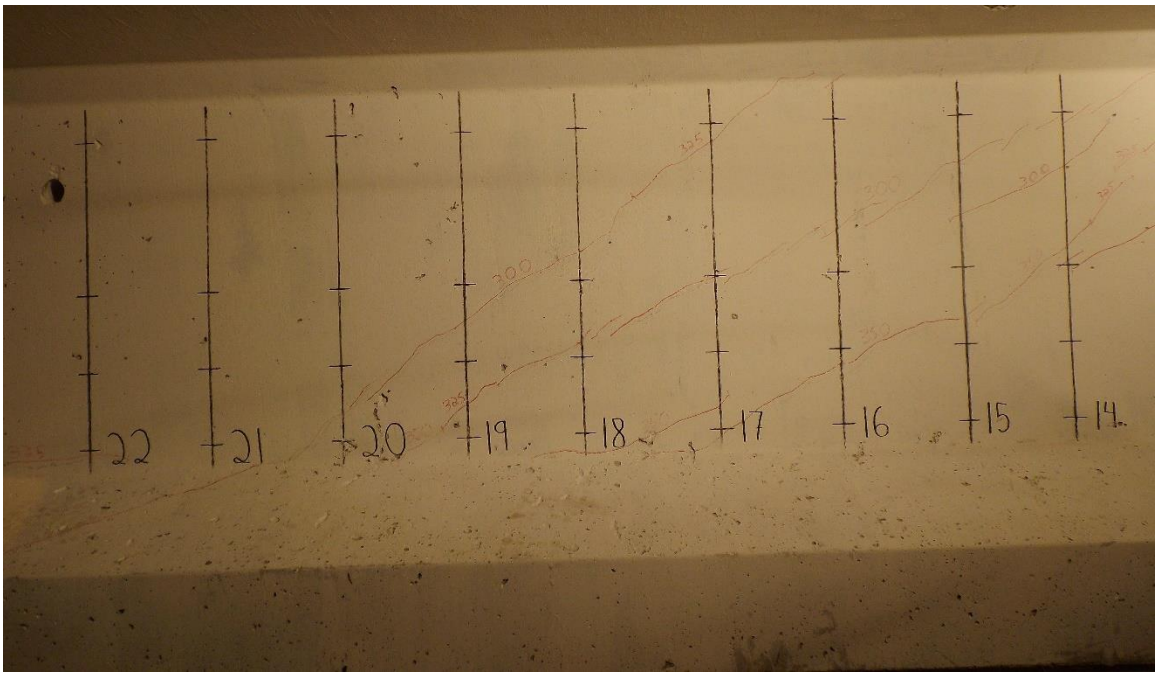

Figure C-30: Observed cracking in failure region of 45M_8W with 350 kips applied.

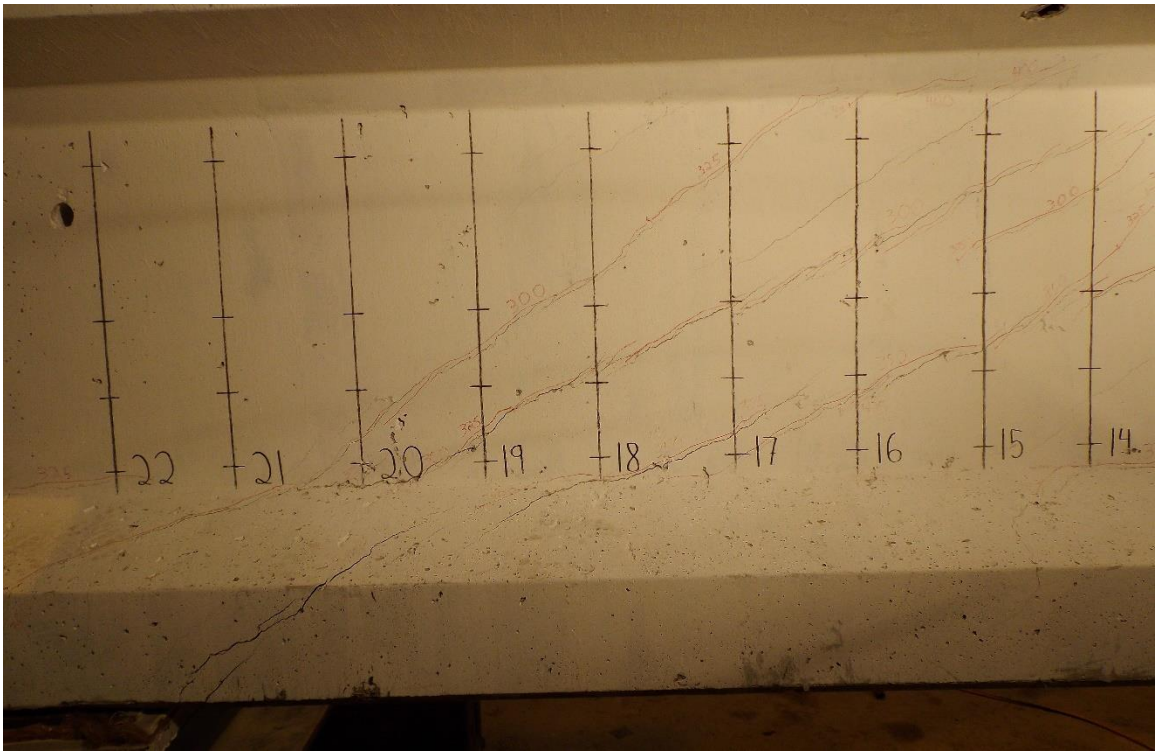

Figure C-31: Observed cracking in failure region of 45M_8W with 643 kips applied.

C.4 Photographs during 36M_8W Test

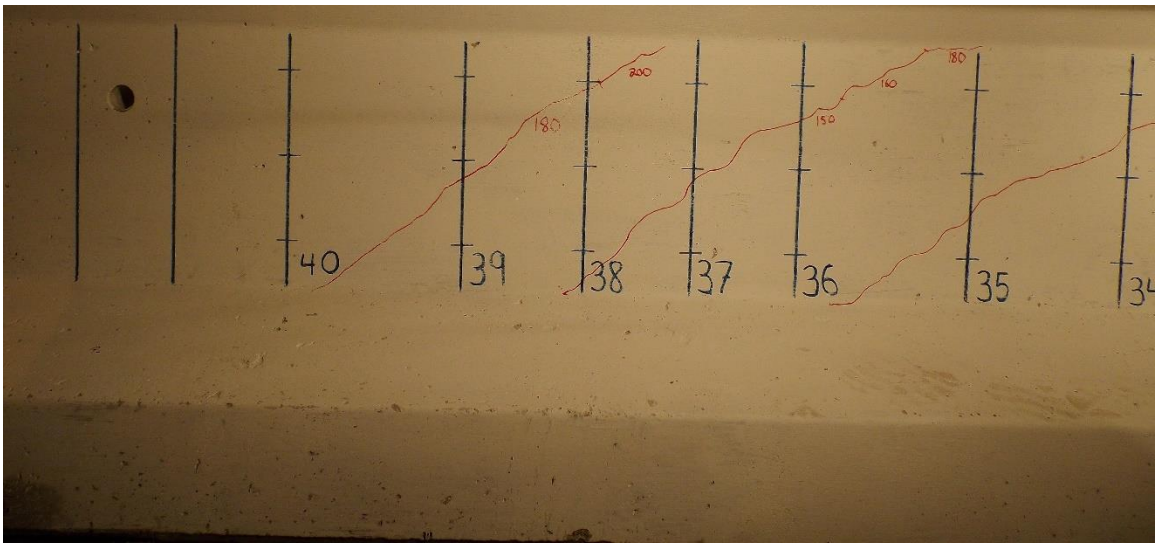

Figure C-32: Residual shear cracks at start of 36M_8W test.

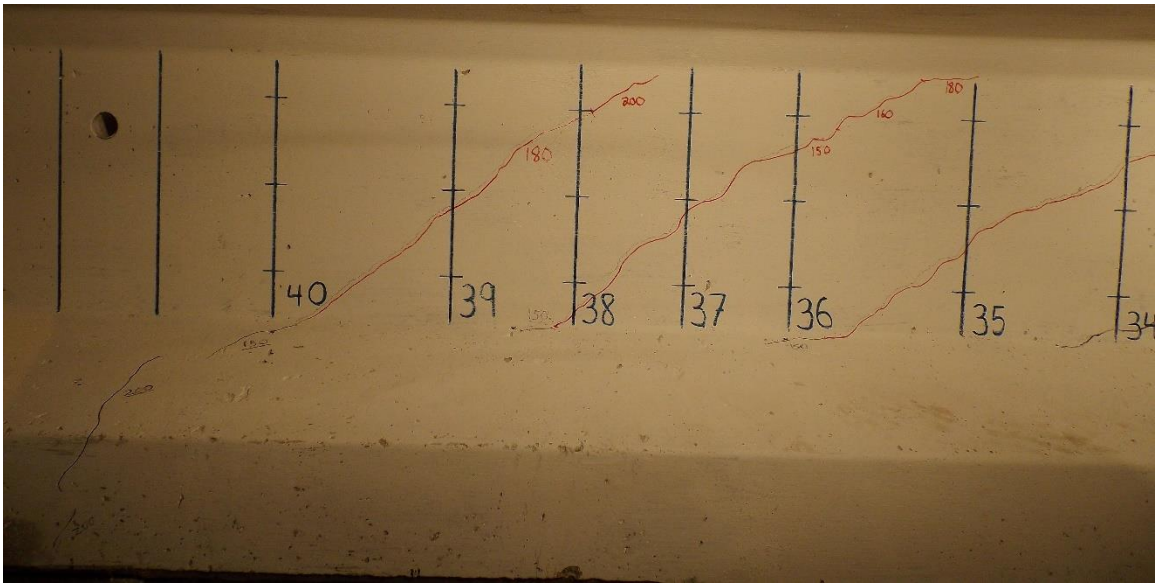

Figure C-33: Observed cracking in failure region of 36M_8W with 200 kips applied.

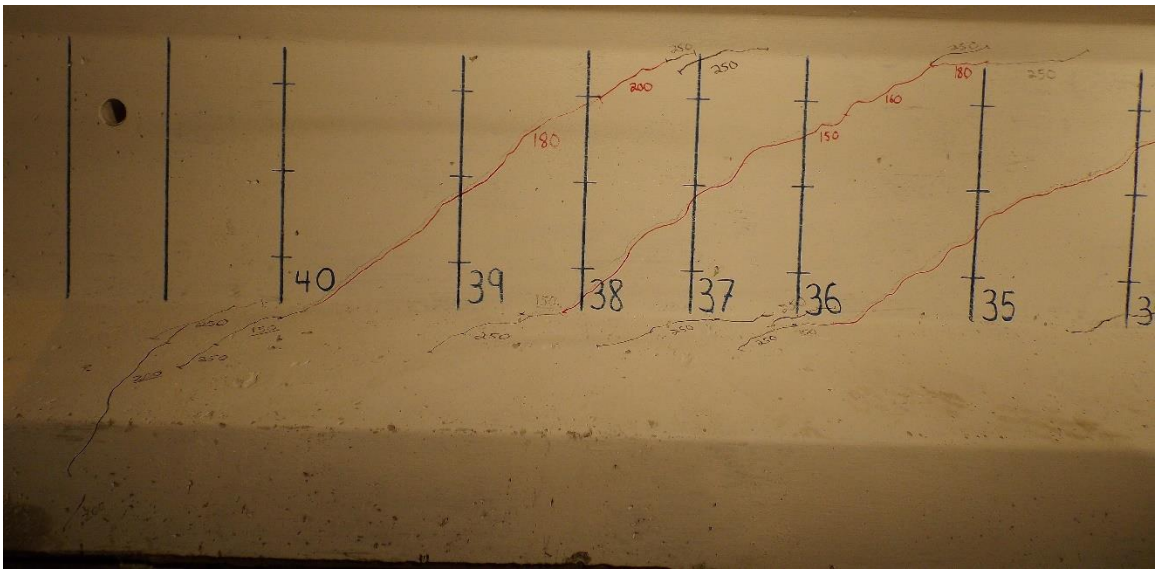

Figure C-34: Observed cracking in failure region of 36M_8W with 250 kips applied.

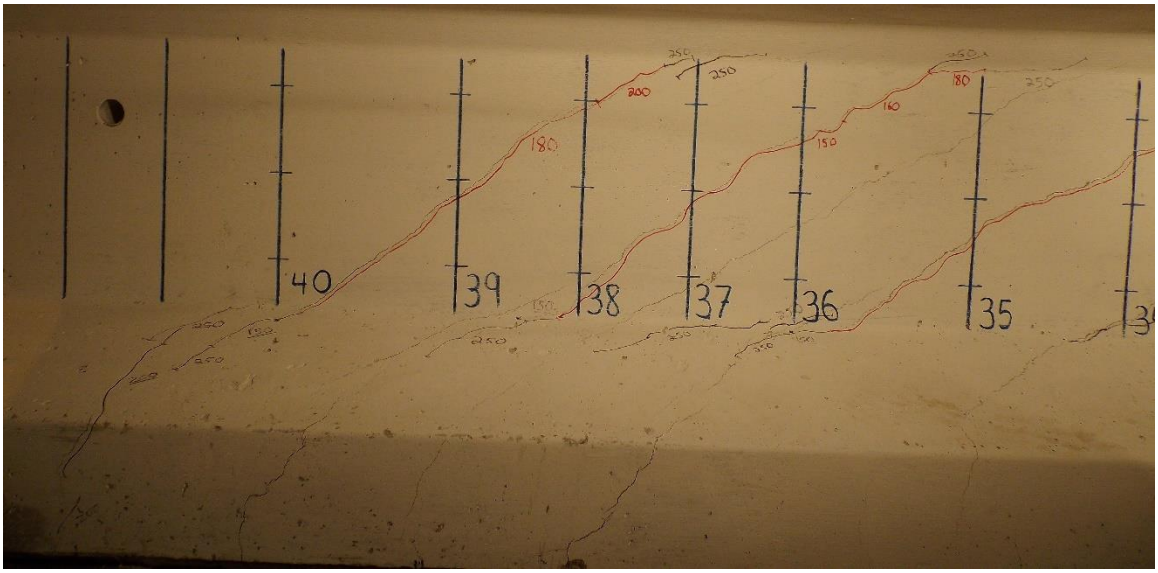

Figure C-35: Observed cracking in failure region of 36M_8W with 450 kips applied.

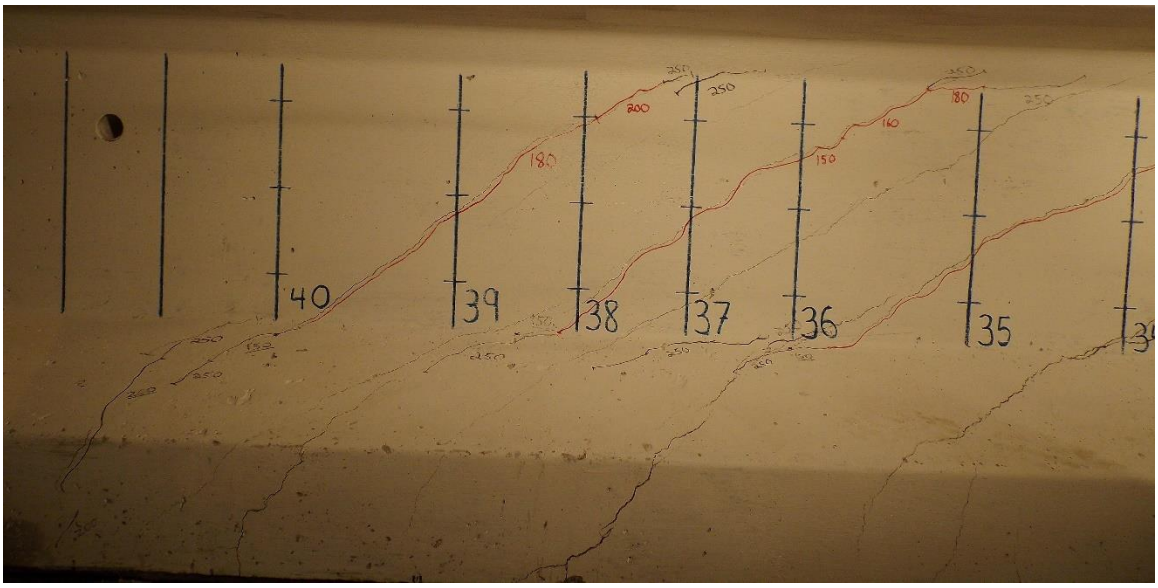

Figure C-36: Observed cracking in failure region of 36M_8W with 500 kips applied.

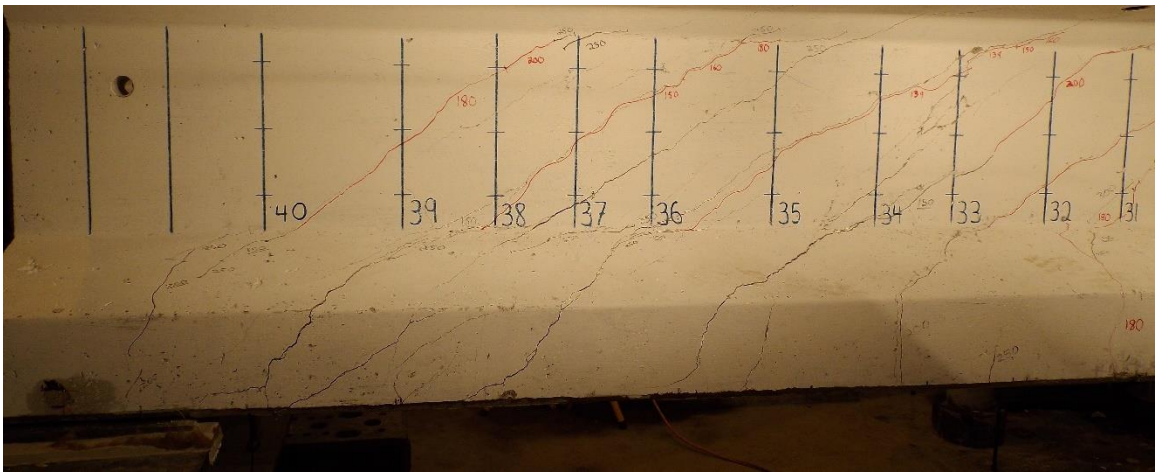

Figure C-37: Observed cracking in failure region of 36M_8W with 558 kips applied


Figure C-38: Deck crushing observed during 36M_8W test.

Appendix D Strain Measurements throughout Testing

The following plots show the applied shear force vs strain measurements for the individual stirrups in each of the girder tests. The naming convention used for gage locations was Girder type (i.e., 36M or 45M), Stirrup number (i.e., 1-22 for the 45M and 1-40 for the 36M), Gage location (i.e., A-E for the 45M and B, M, T, or S for the 36M) such that the gage applied to the bottom of the fifth stirrup in the 45M girder would be named 45M_5_A. This information can be used to determine the shear force levels at which the strain gages indicated yielding, as well as the maximum strains measured in the stirrups during the test. The proximity of the stirrups to cracks tended to influence the strain measurements such that larger strains may be expected to have been realized in the stirrups if the gages were not located near a crack.

D.1 Plots for 36M_18F Test

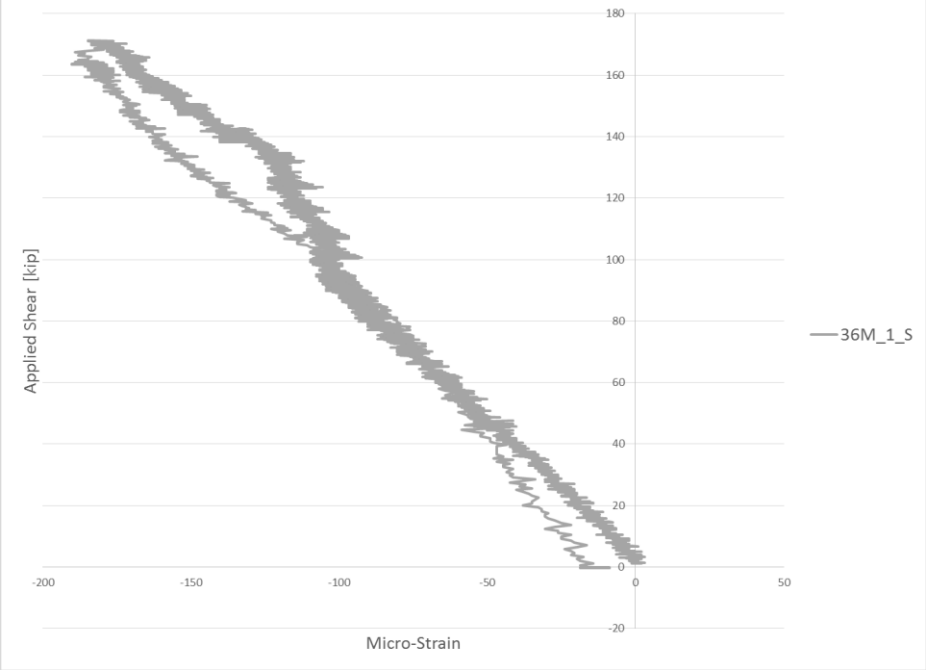

Figure D-1: Applied shear vs strain measurements for Stirrup 1 of the 36M_18F test.

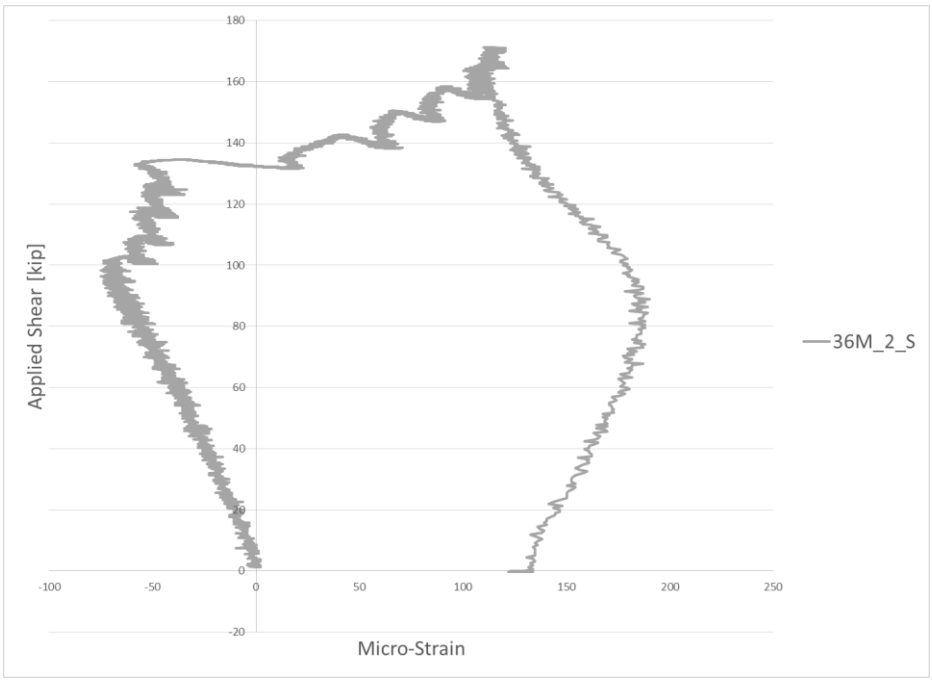

Figure D-2: Applied shear vs strain measurements for Stirrup 2 of the 36M_18F test.

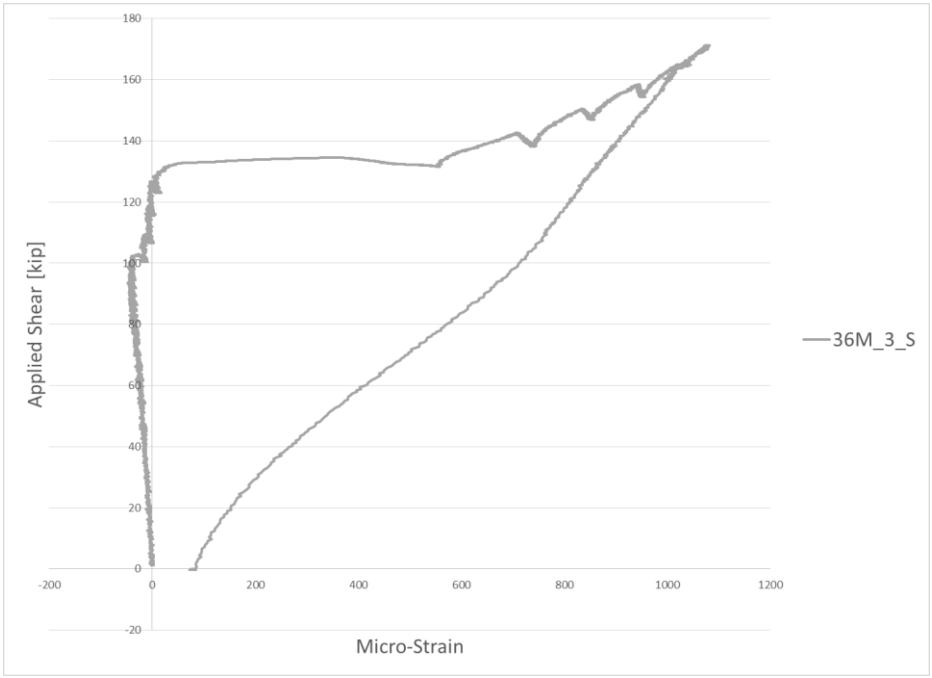

Figure D-3: Applied shear vs strain measurements for Stirrup 3 of the 36M_18F test.

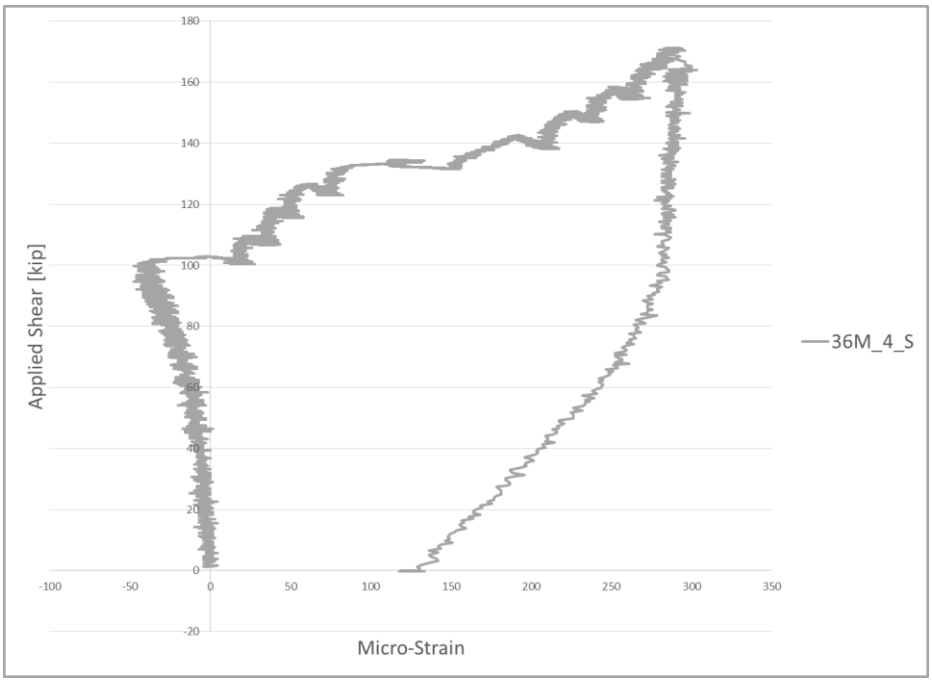

Figure D-4: Applied shear vs strain measurements for Stirrup 4 of the 36M_18F test.

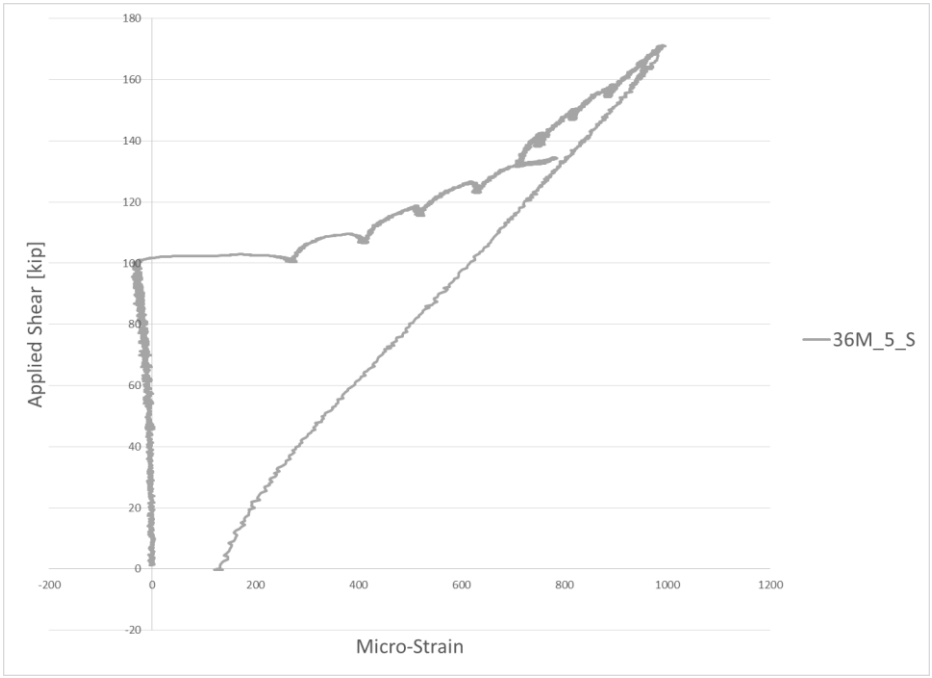

Figure D-5: Applied shear vs strain measurements for Stirrup 5 of the 36M_18F test.

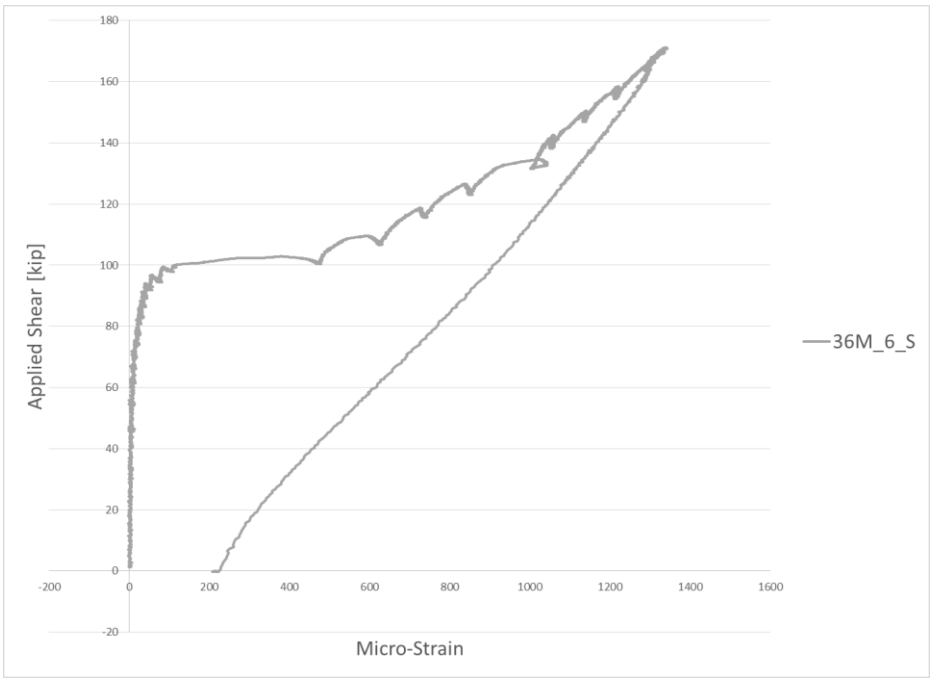

Figure D-6: Applied shear vs strain measurements for Stirrup 6 of the 36M_18F test.

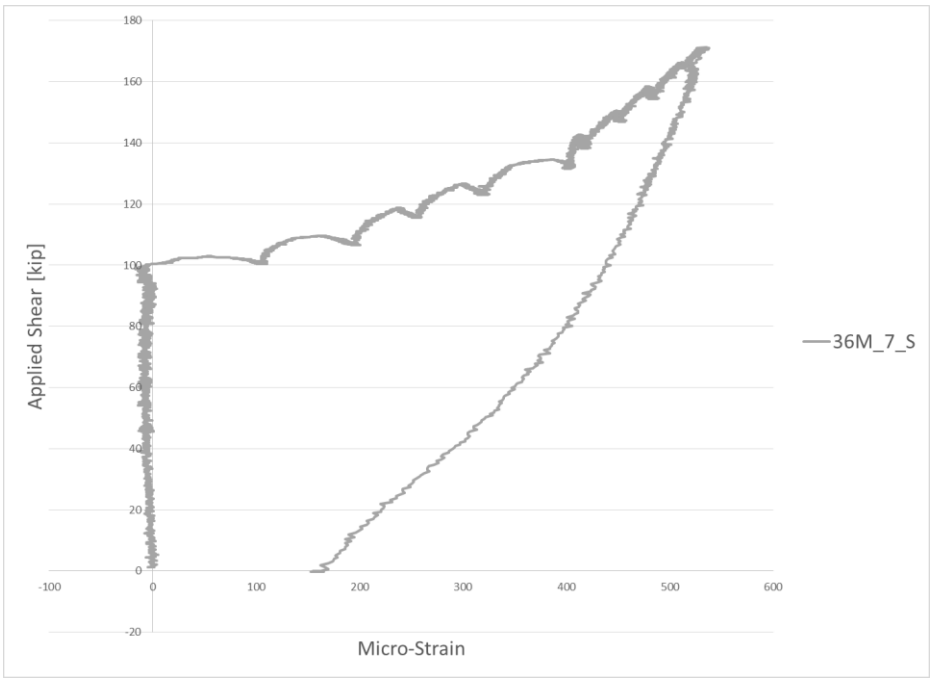

Figure D-7: Applied shear vs strain measurements for Stirrup 7 of the 36M_18F test.

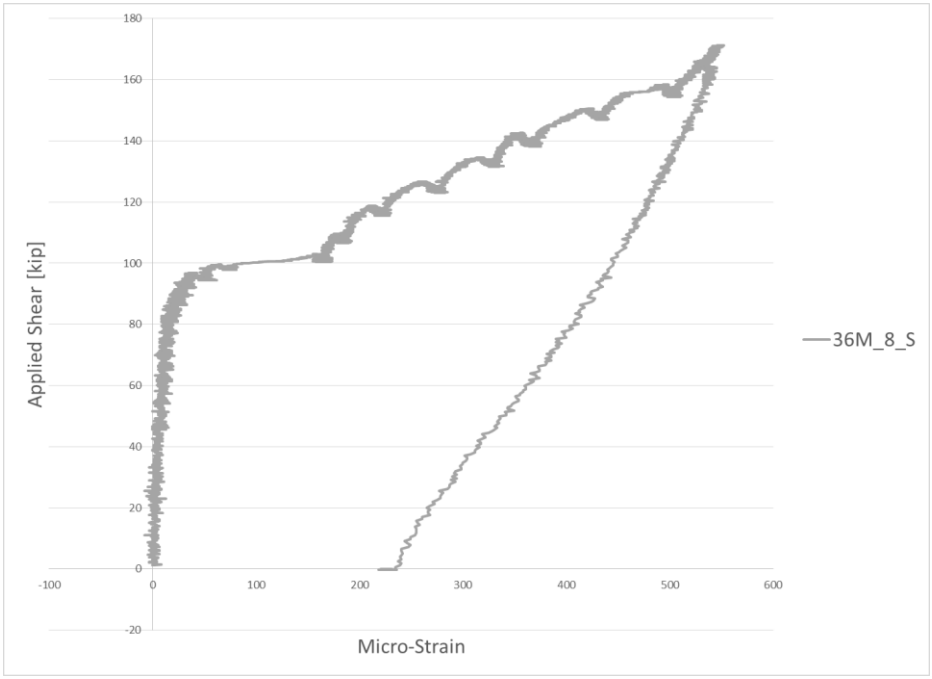

Figure D-8: Applied shear vs strain measurements for Stirrup 8 of the 36M_18F test.

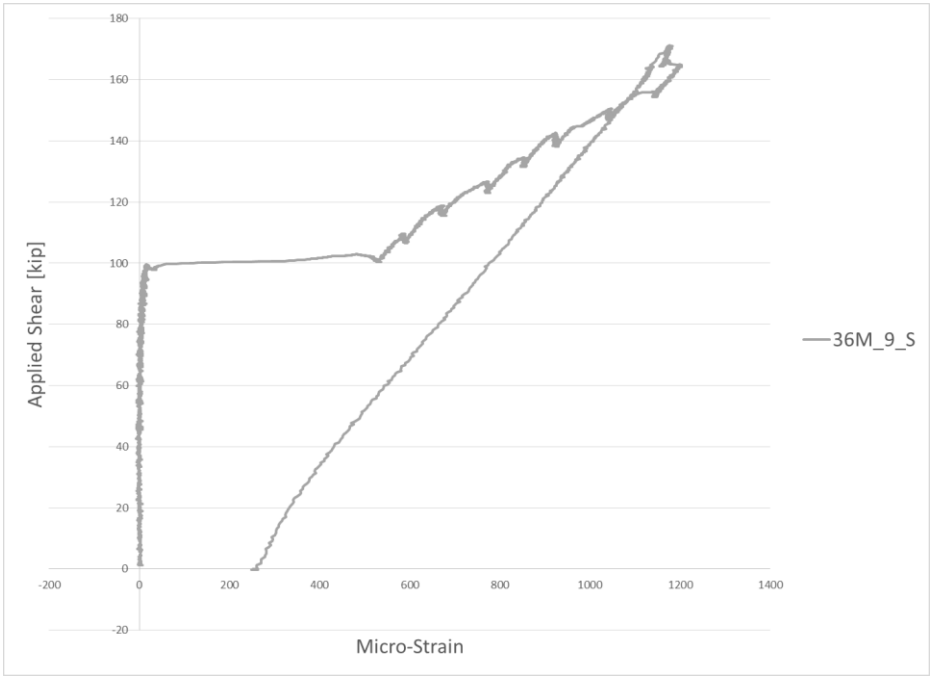

Figure D-9: Applied shear vs strain measurements for Stirrup 9 of the 36M_18F test.

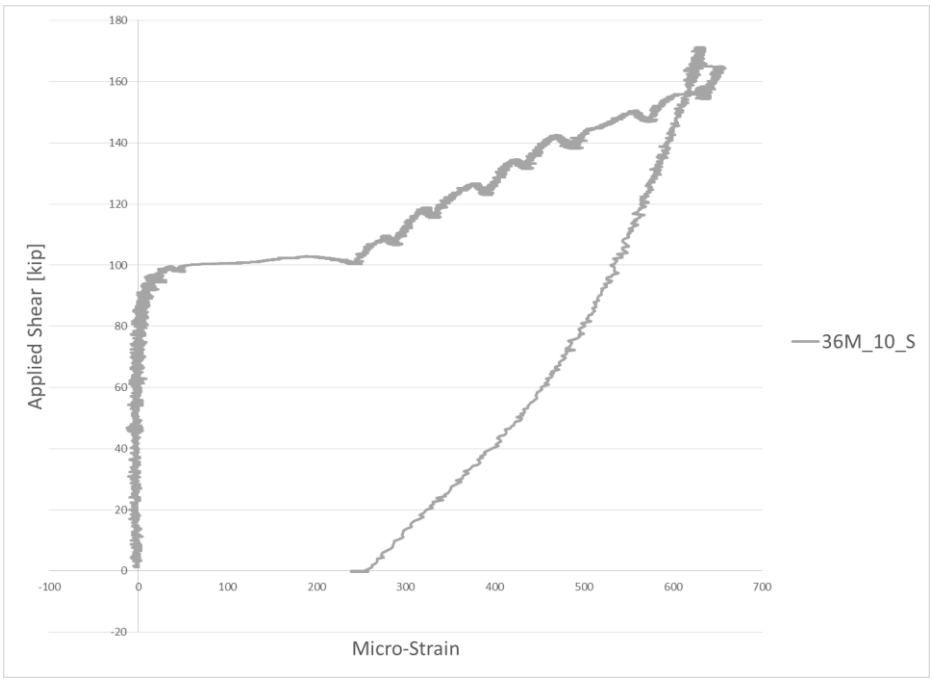

Figure D-10: Applied shear vs strain measurements for Stirrup 10 of the 36M_18F test.

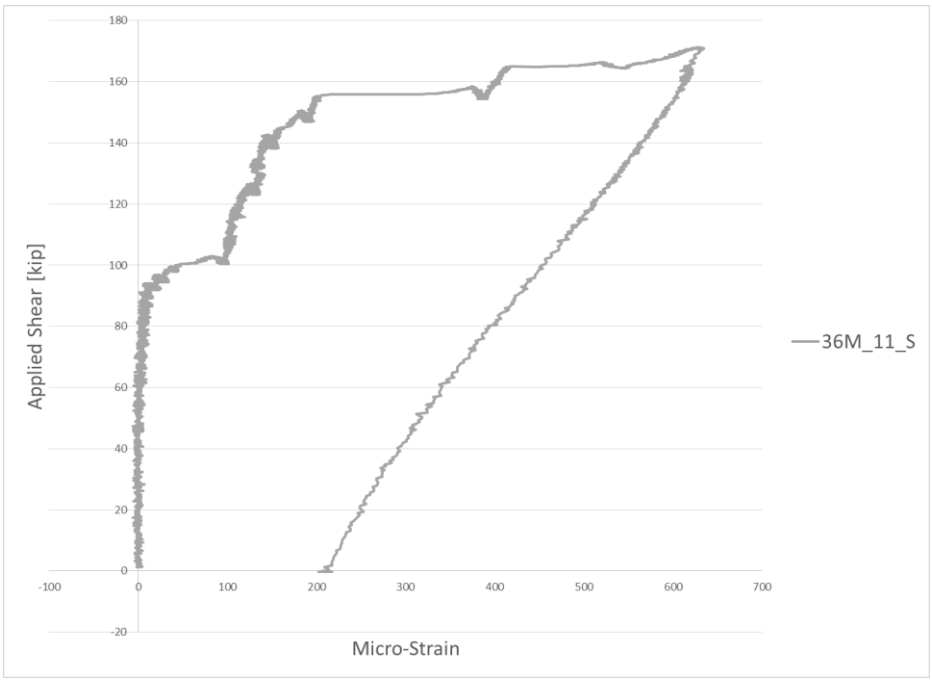

Figure D-11: Applied shear vs strain measurements for Stirrup 11 of the 36M_18F test.

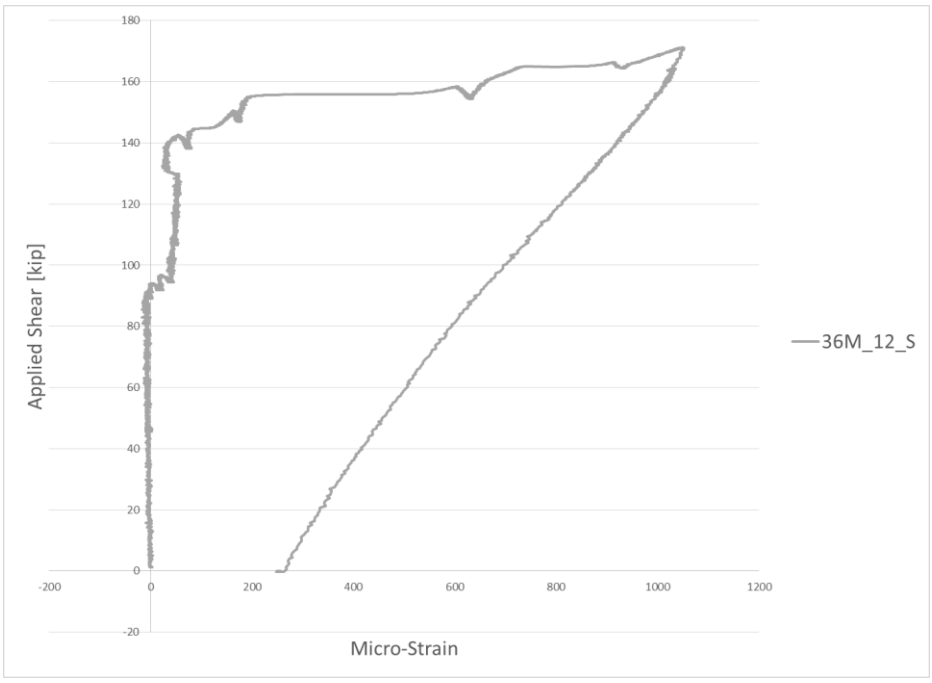

Figure D-12: Applied shear vs strain measurements for Stirrup 12 of the 36M_18F test.

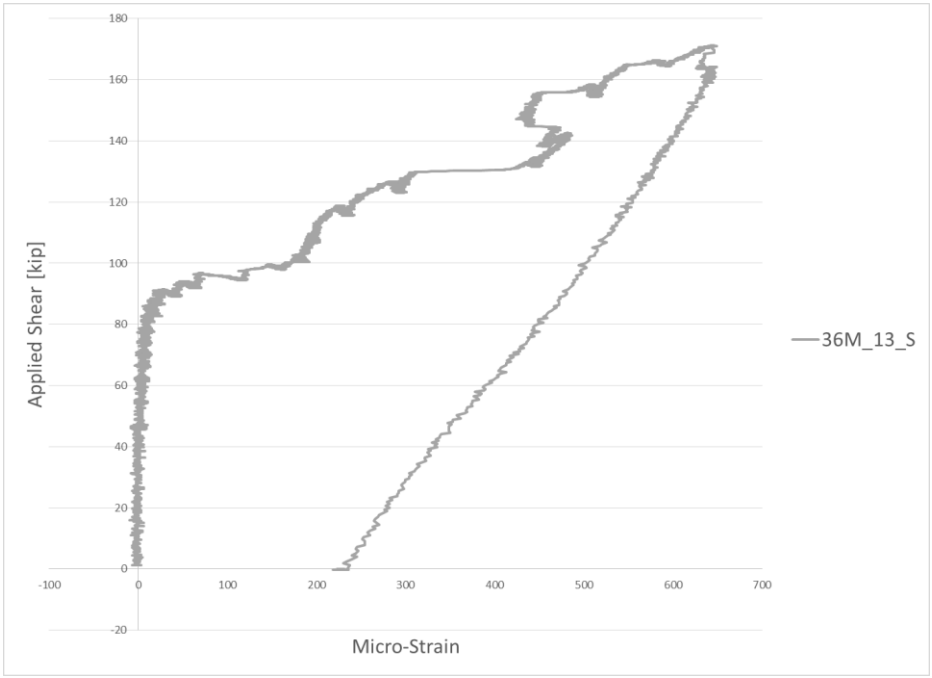

Figure D-13: Applied shear vs strain measurements for Stirrup 13 of the 36M_18F test.

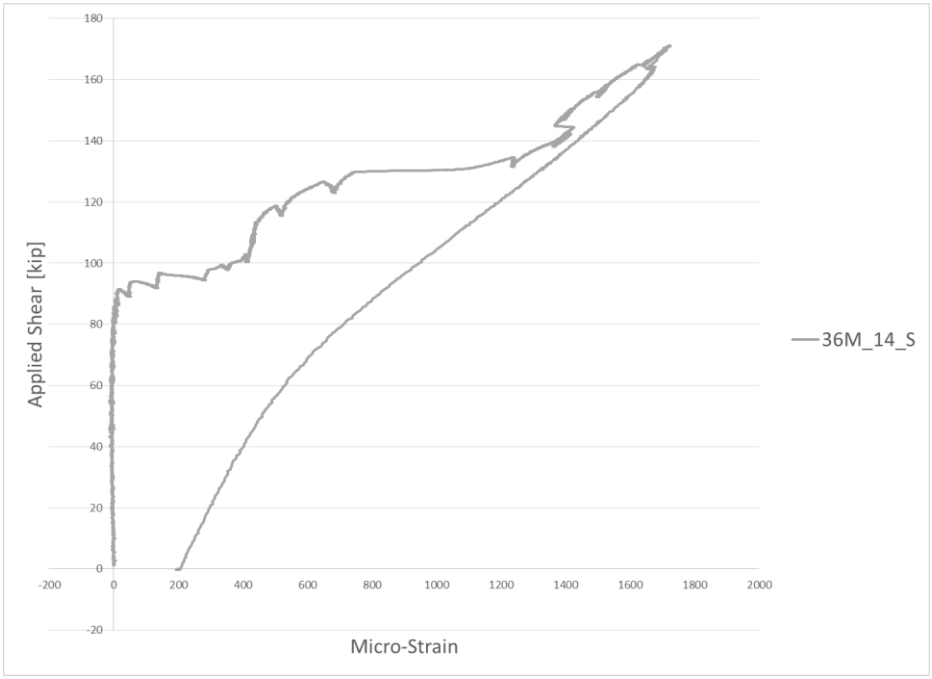

Figure D-14: Applied shear vs strain measurements for Stirrup 14 of the 36M_18F test.

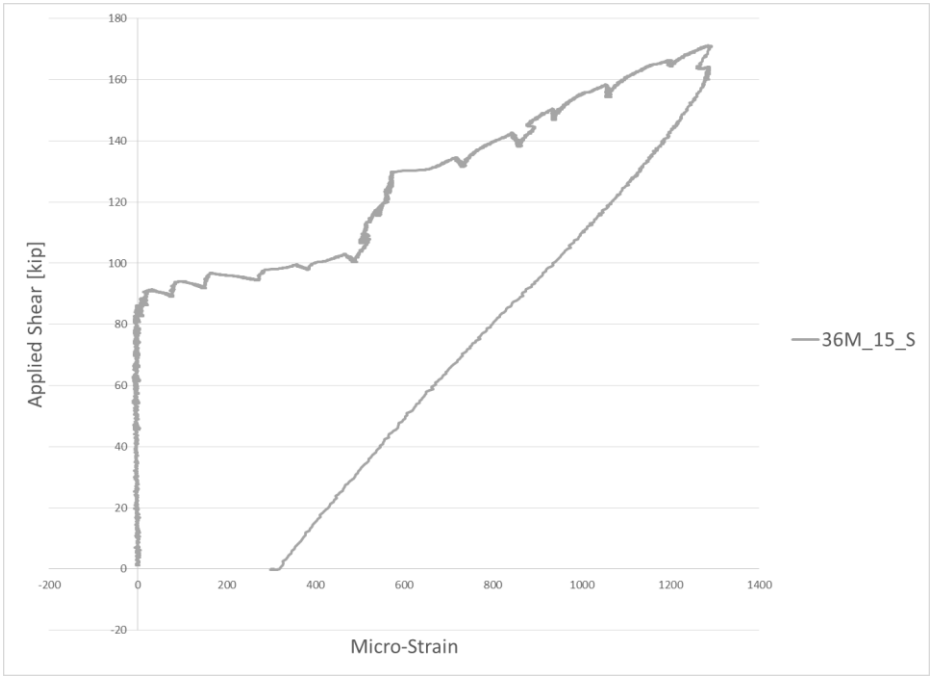

Figure D-15: Applied shear vs strain measurements for Stirrup 15 of the 36M_18F test.

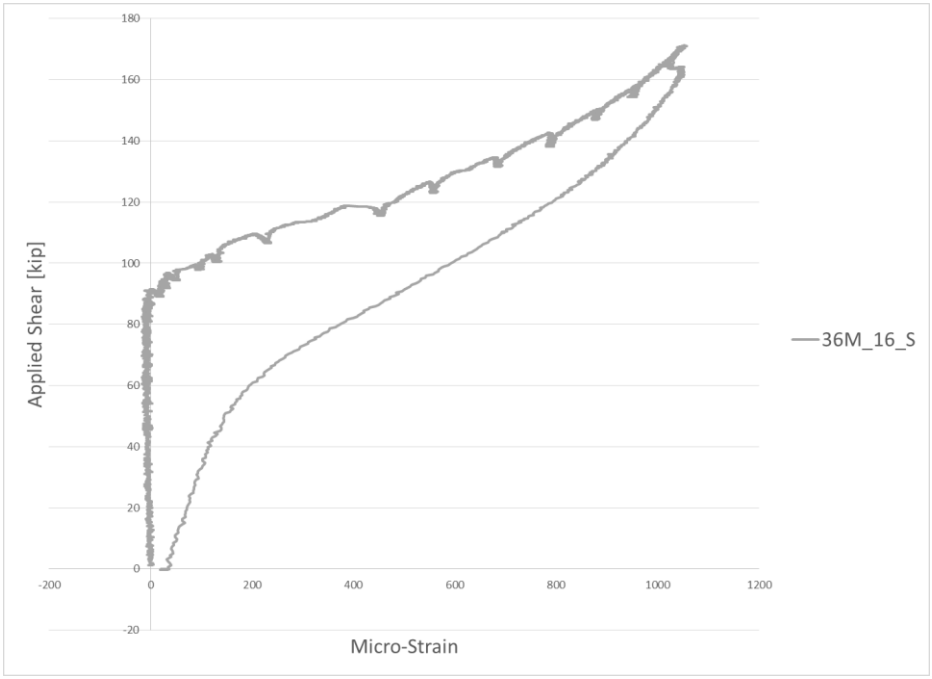

Figure D-16: Applied shear vs strain measurements for Stirrup 16 of the 36M_18F test.

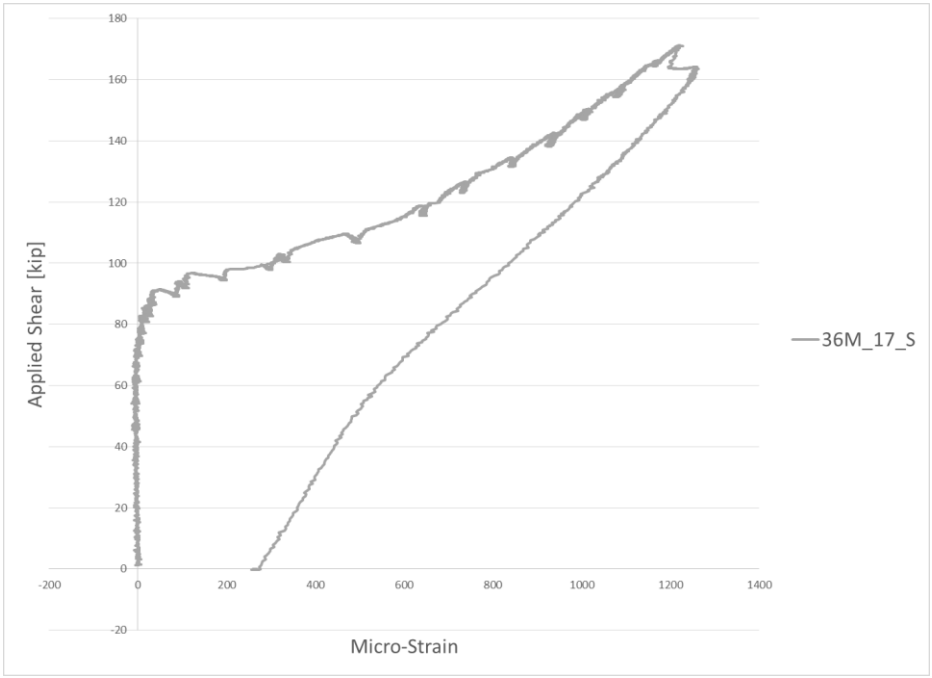

Figure D-17: Applied shear vs strain measurements for Stirrup 17 of the 36M_18F test.

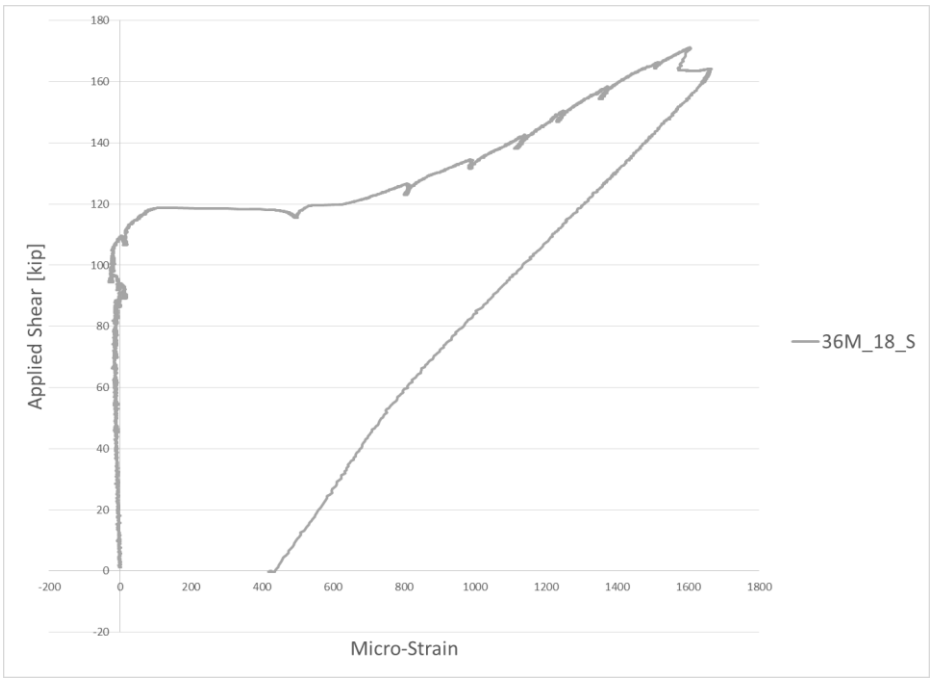

Figure D-18: Applied shear vs strain measurements for Stirrup 18 of the 36M_18F test.

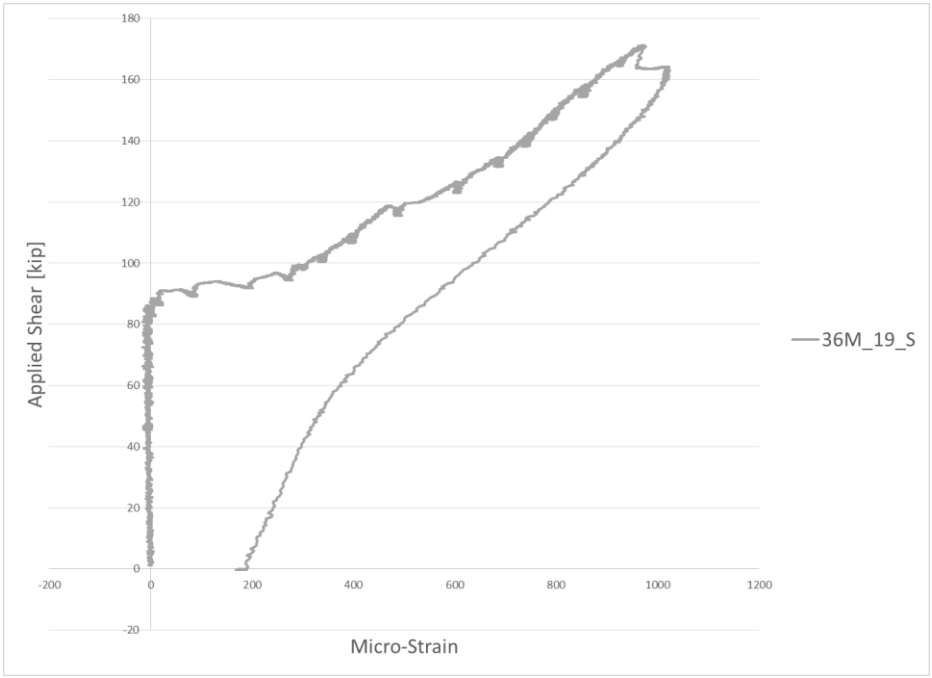

Figure D-19: Applied shear vs strain measurements for Stirrup 19 of the 36M_18F test.

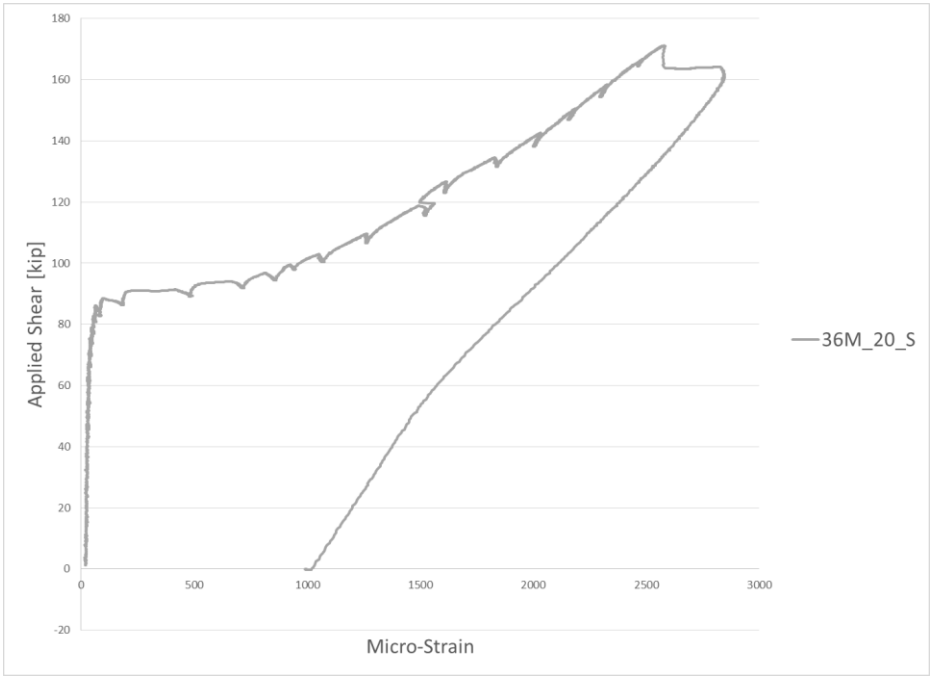

Figure D-20: Applied shear vs strain measurements for Stirrup 20 of the 36M_18F test.

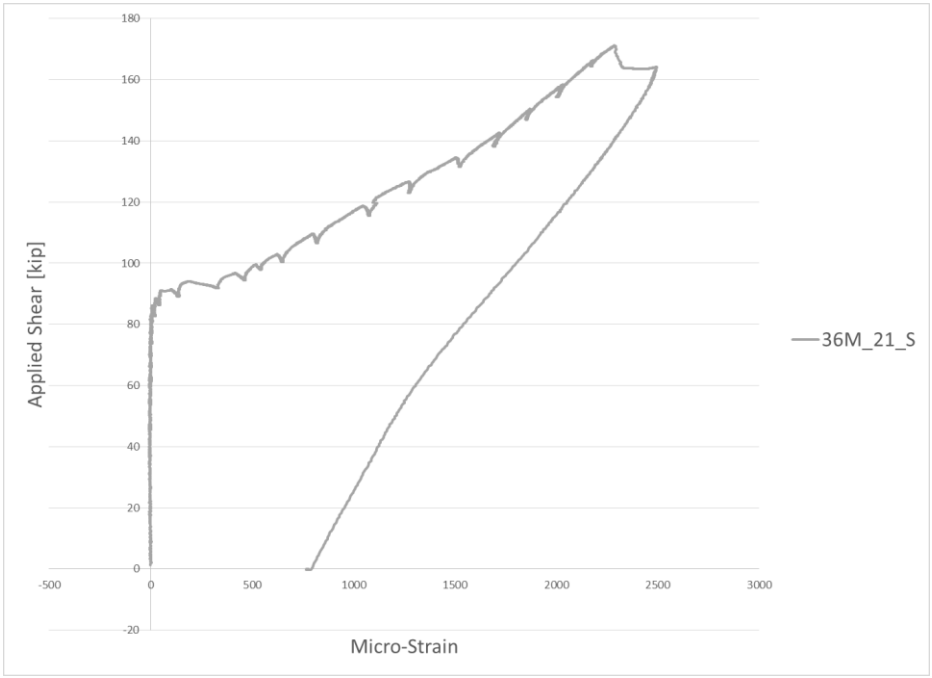

Figure D-21: Applied shear vs strain measurements for Stirrup 21 of the 36M_18F test.

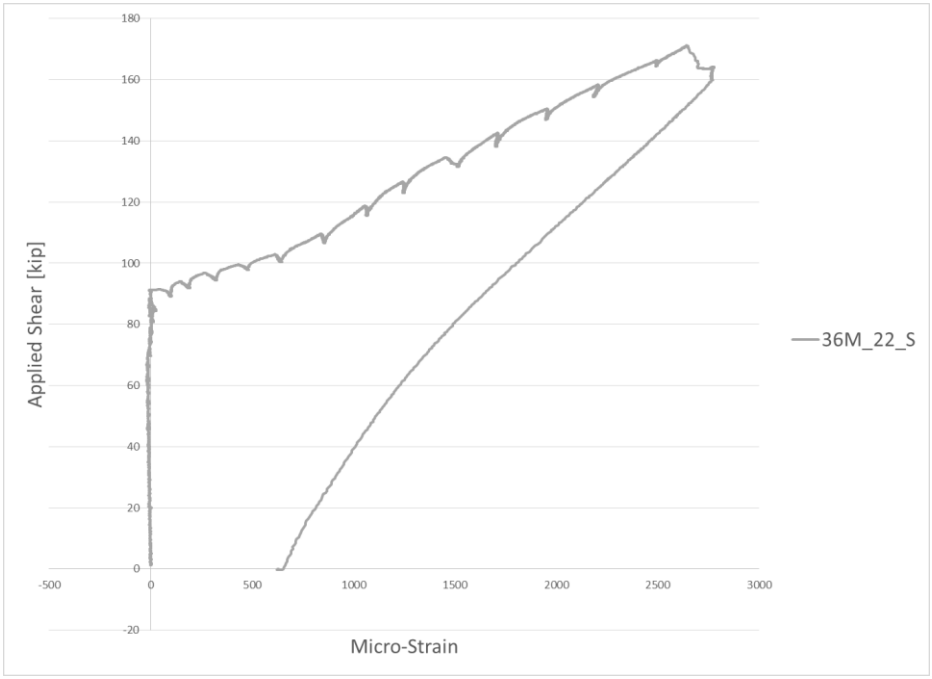

Figure D-22: Applied shear vs strain measurements for Stirrup 22 of the 36M_18F test.

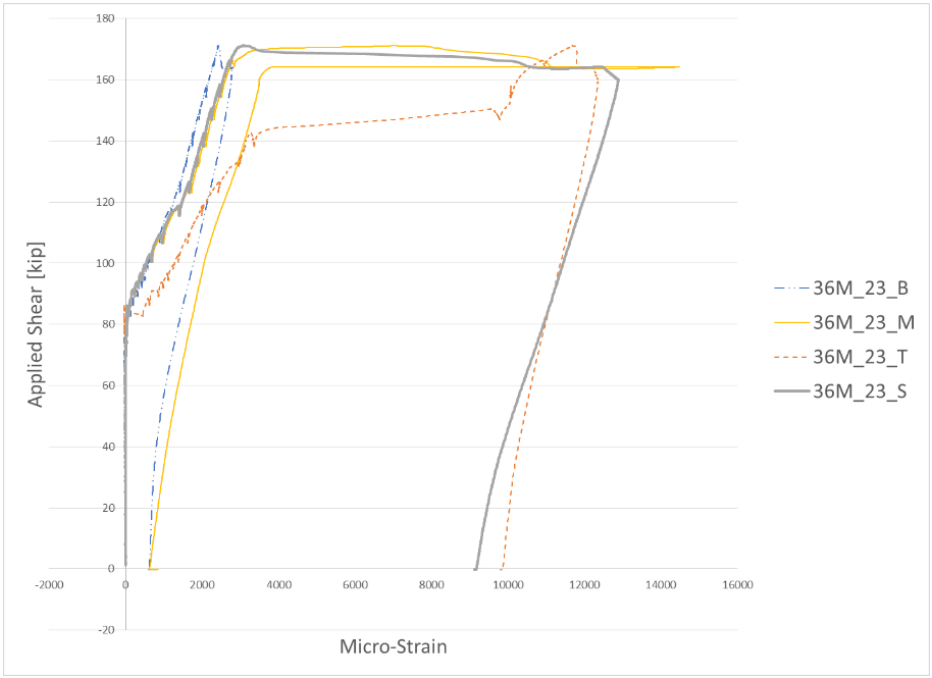

Figure D-23: Applied shear vs strain measurements for Stirrup 23 of the 36M_18F test.

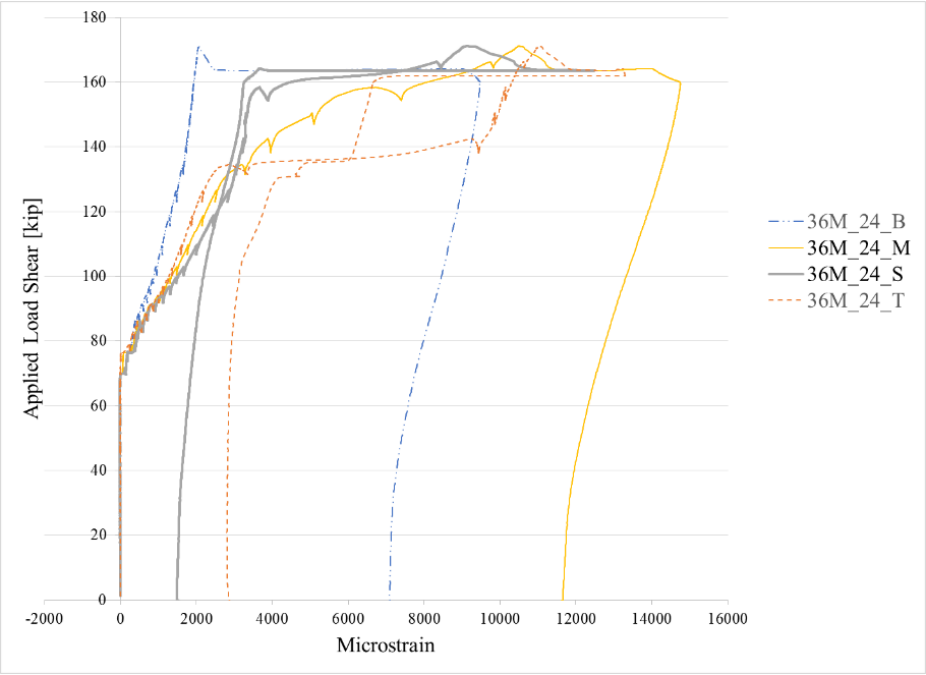

Figure D-24: Applied shear vs strain measurements for Stirrup 24 of the 36M_18F test.

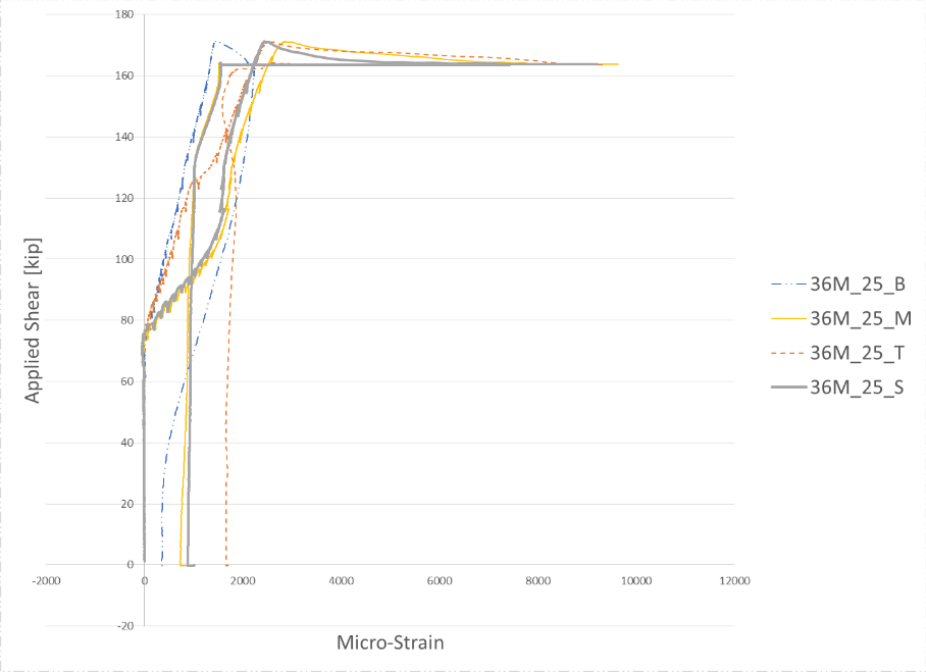

Figure D-25: Applied shear vs strain measurements for Stirrup 25 of the 36M_18F test.

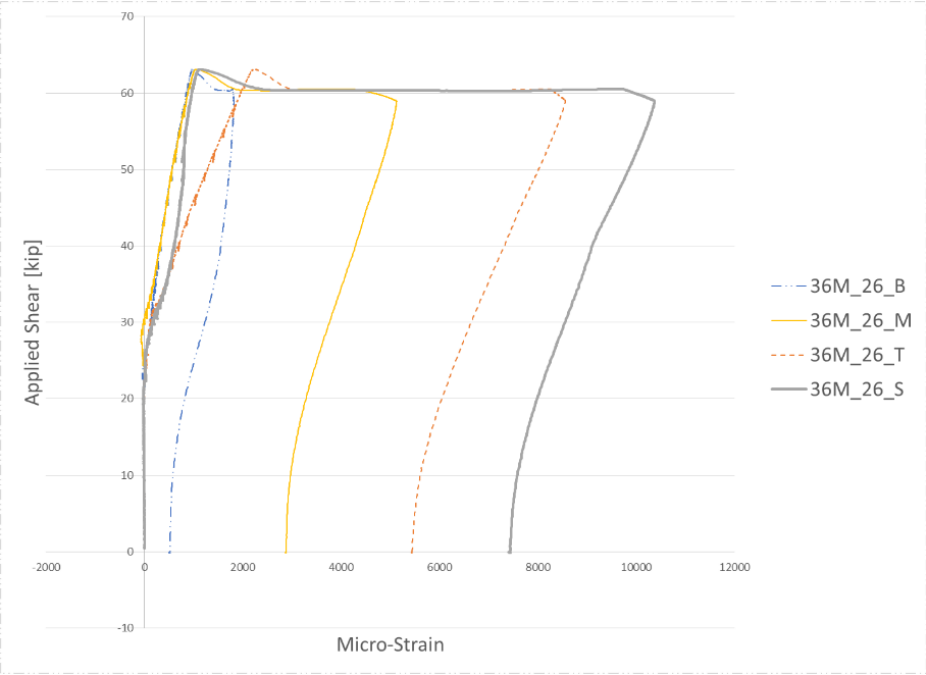

Figure D-26: Applied shear vs strain measurements for Stirrup 26 of the 36M_18F test.

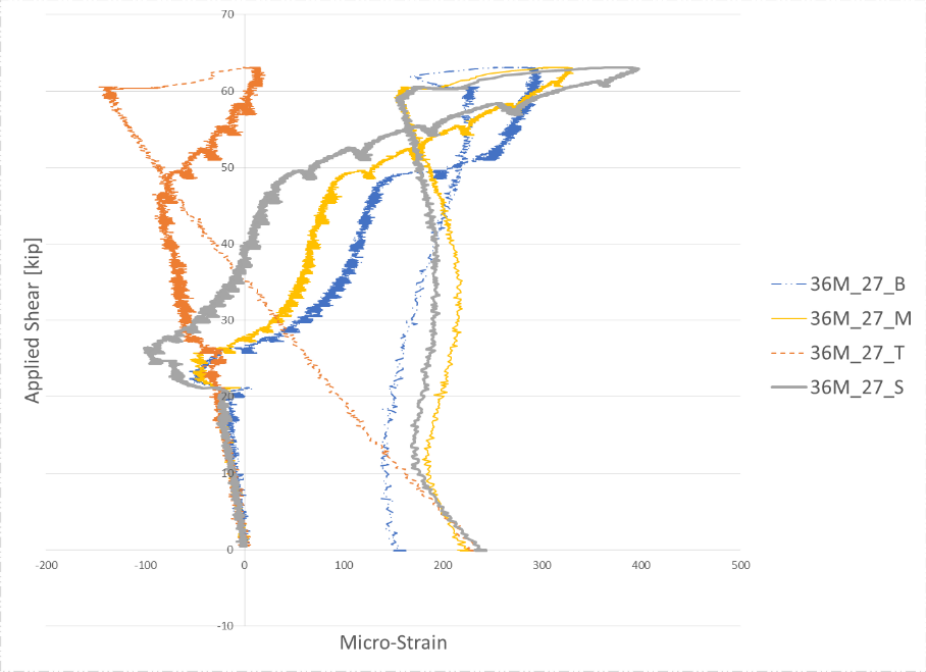

Figure D-27: Applied shear vs strain measurements for Stirrup 27 of the 36M_18F test.

D.2 Plots for 45M_24W Test

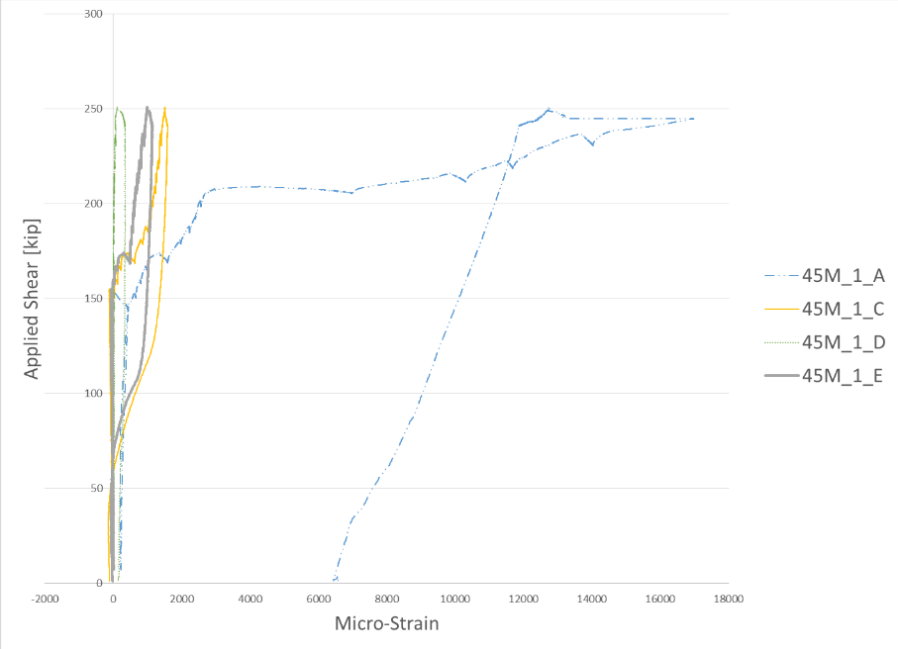

Figure D-28: Applied shear vs strain measurements for Stirrup 1 of the 45M_24W test.

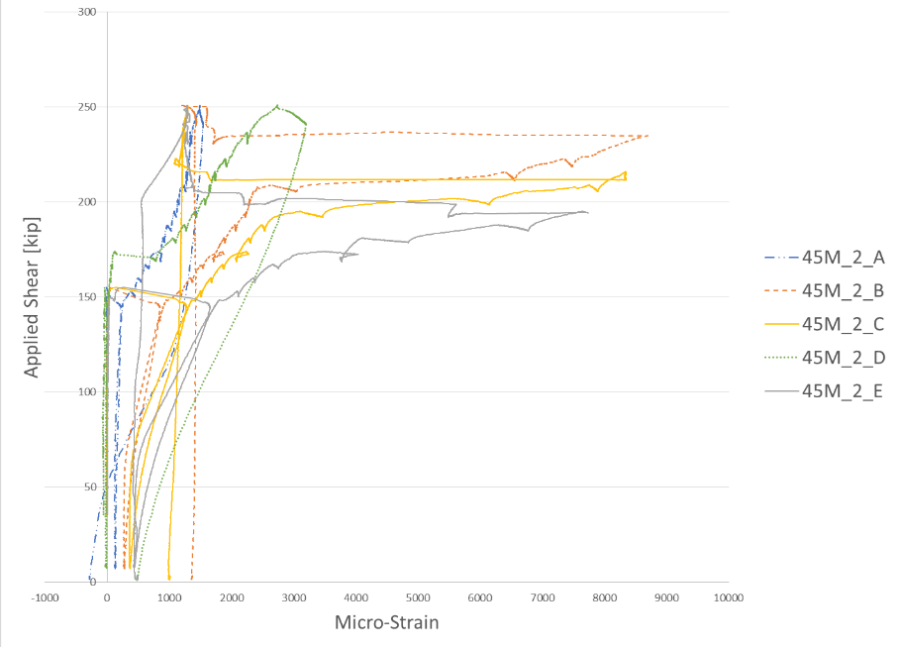

Figure D-29: Applied shear vs strain measurements for Stirrup 2 of the 45M_24W test.

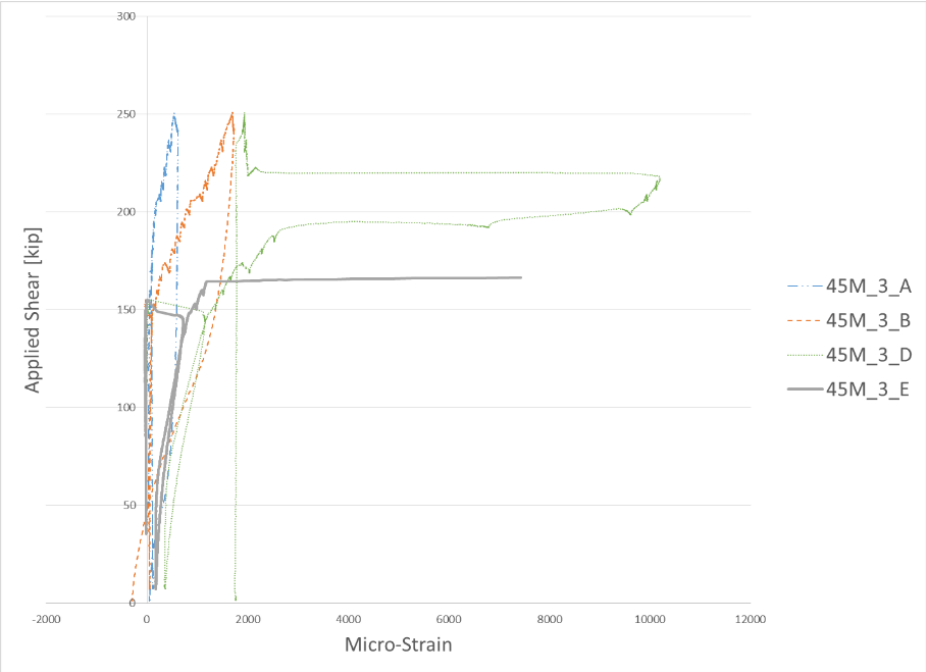

Figure D-30: Applied shear vs strain measurements for Stirrup 3 of the 45M_24W test.

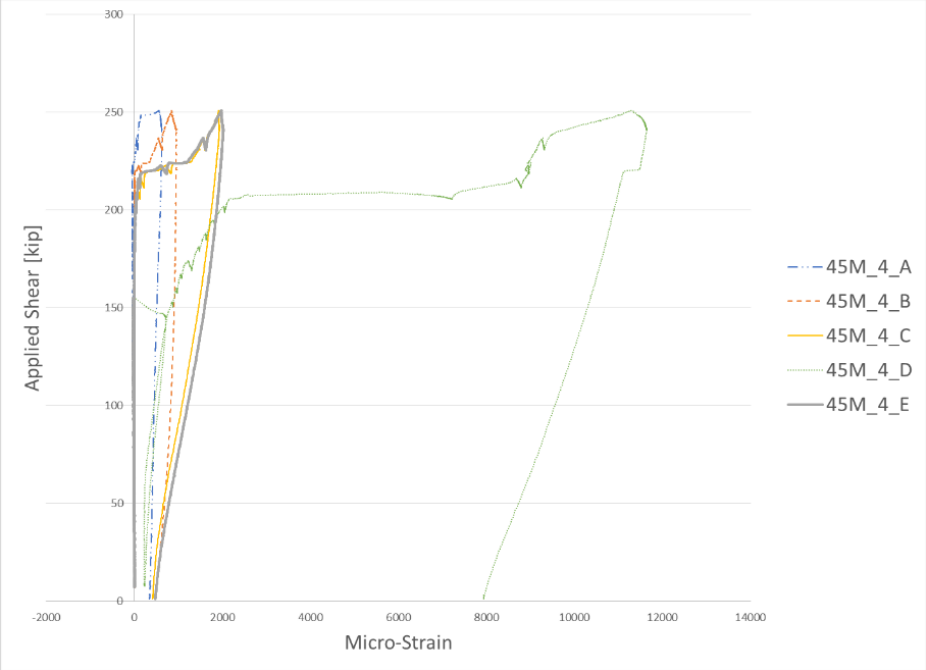

Figure D-31: Applied shear vs strain measurements for Stirrup 4 of the 45M_24W test.

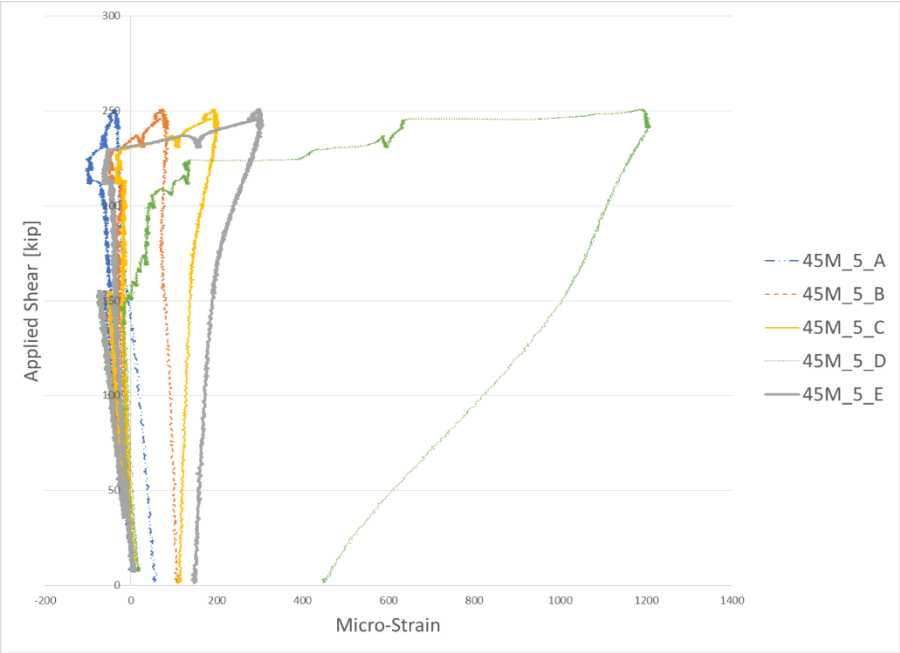

Figure D-32: Applied shear vs strain measurements for Stirrup 5 of the 45M_24W test.

D.3 Plots for 45M_8W Test

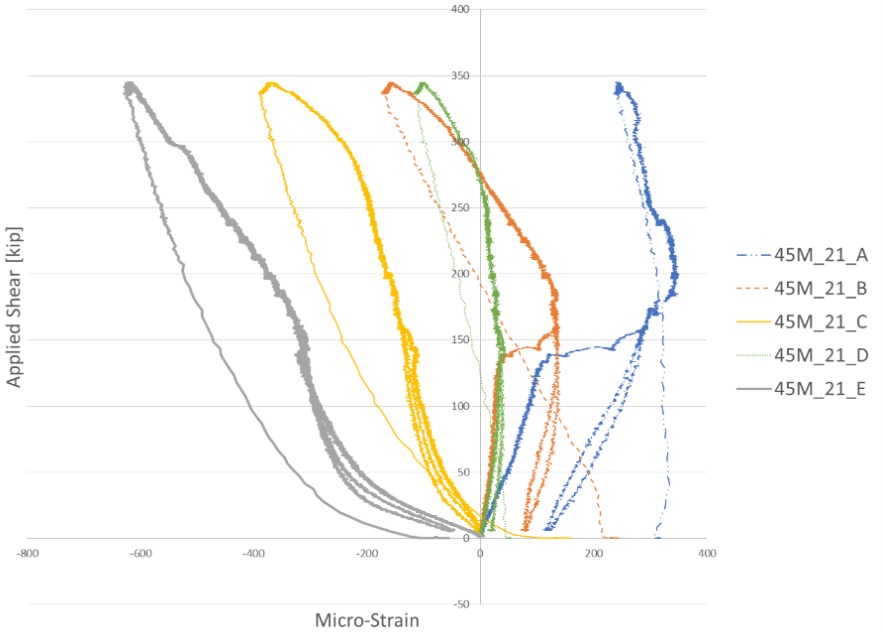

Figure D-33: Applied shear vs strain measurements for Stirrup 21 of the 45M_8W test.

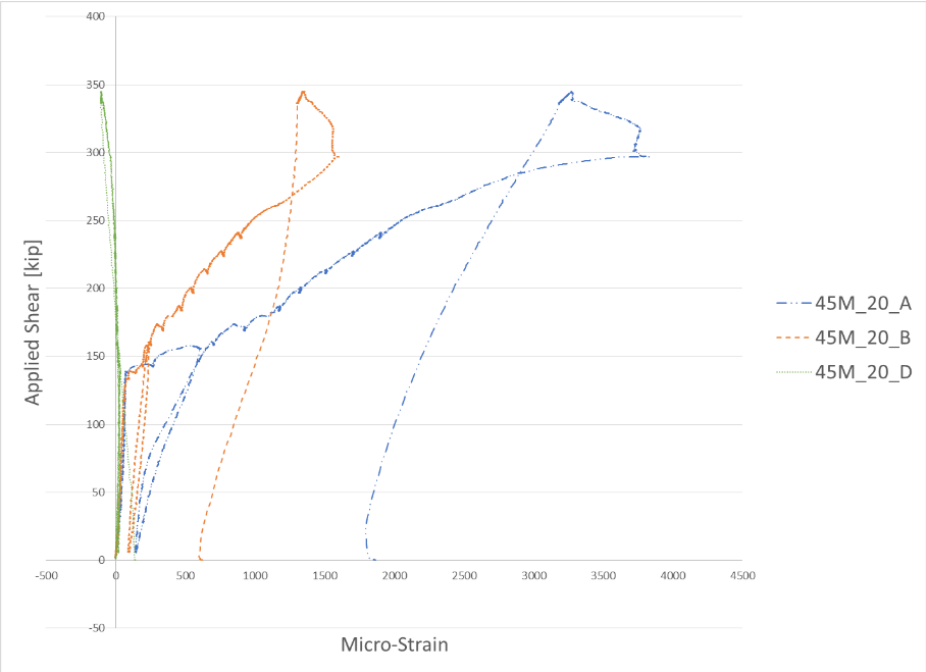

Figure D-34: Applied shear vs strain measurements for Stirrup 20 of the 45M_8W test.

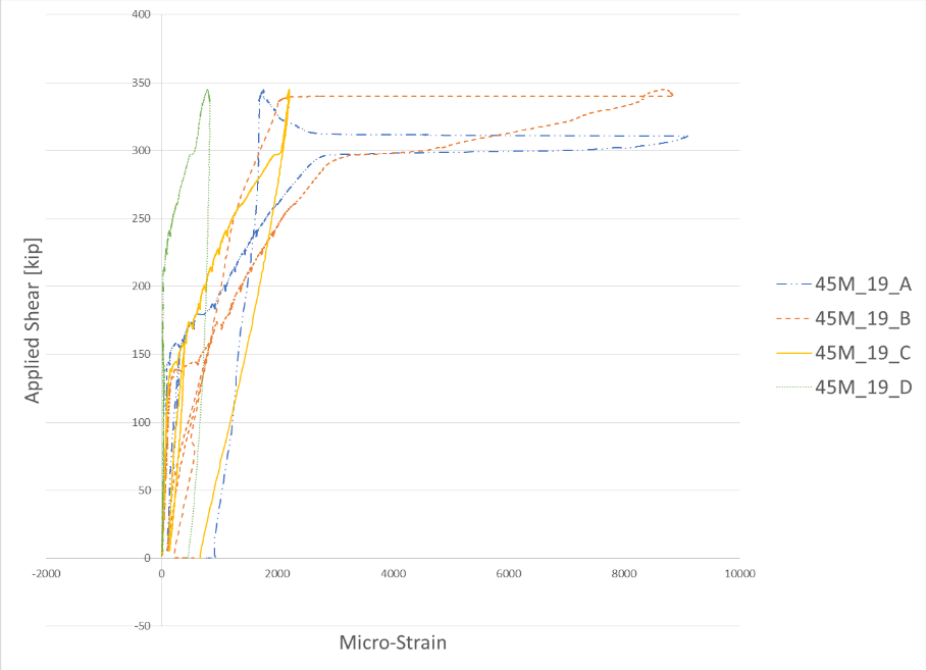

Figure D-35: Applied shear vs strain measurements for Stirrup 19 of the 45M_8W test.

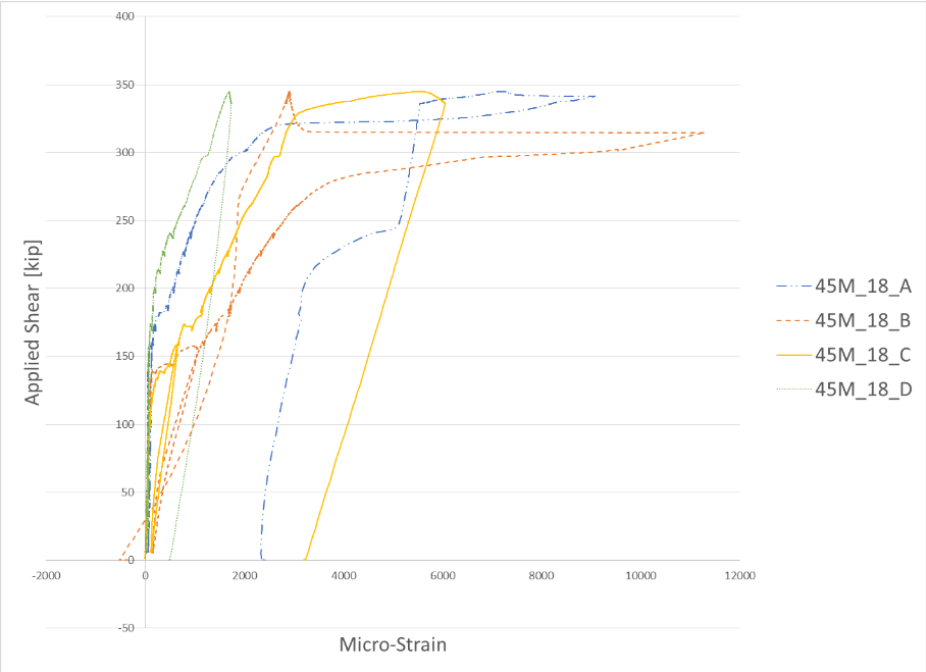

Figure D-36: Applied shear vs strain measurements for Stirrup 18 of the 45M_8W test.

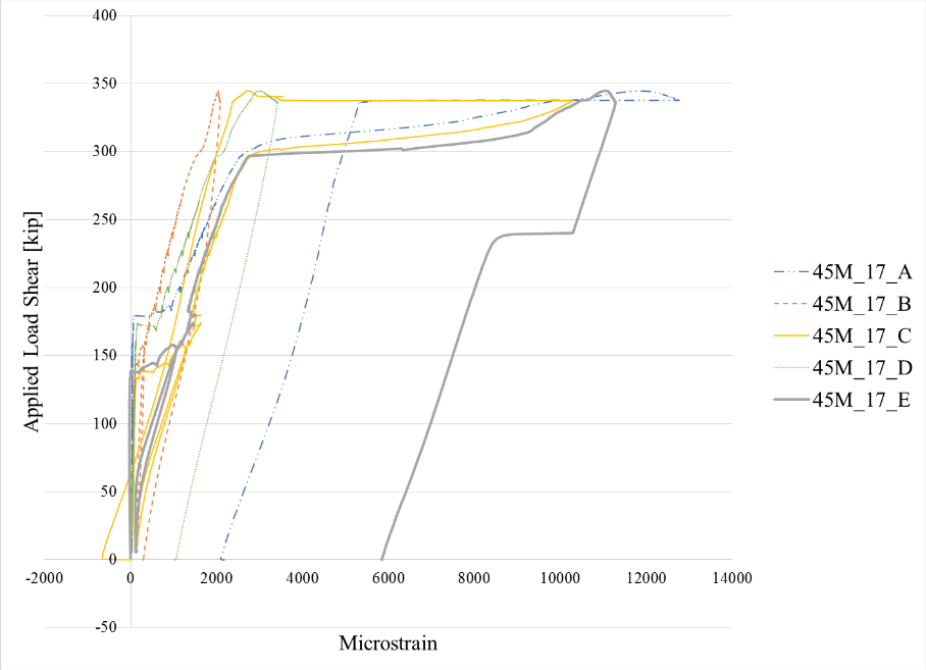

Figure D-37: Applied shear vs strain measurements for Stirrup 17 of the 45M_8W test.

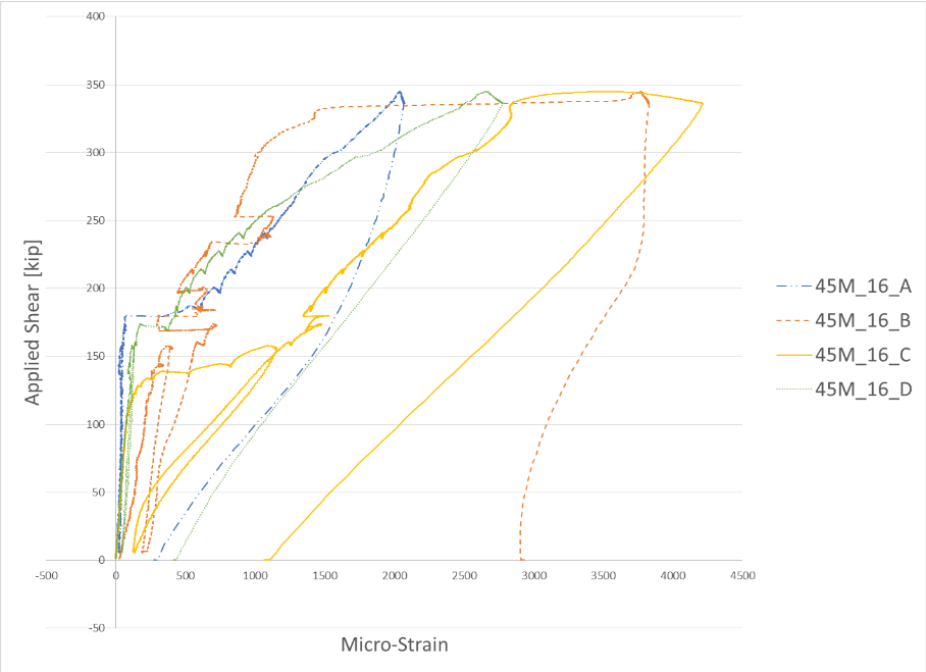

Figure D-38: Applied shear vs strain measurements for Stirrup 16 of the 45M_8W test.

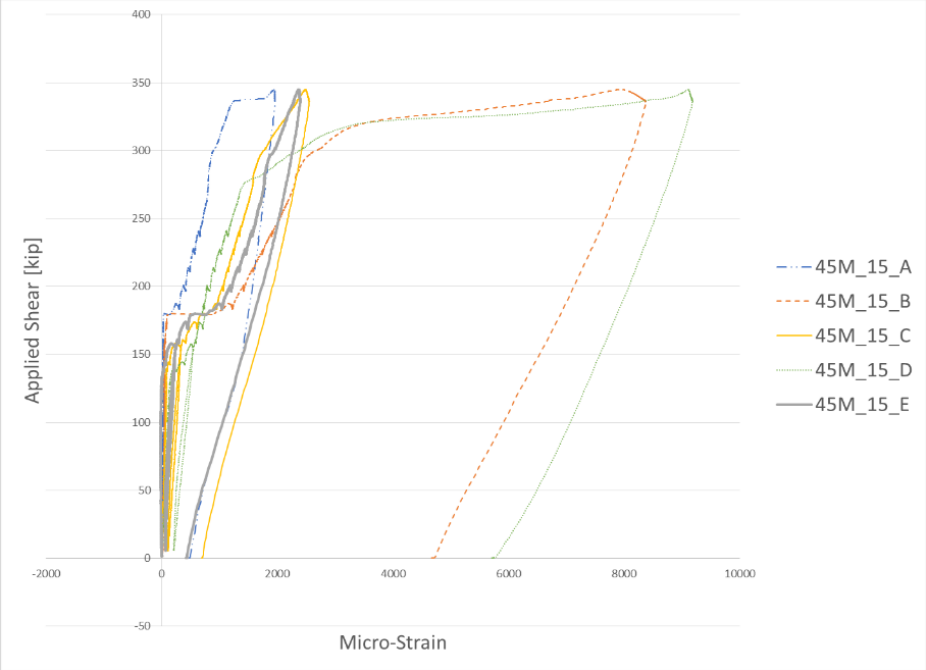

Figure D-39: Applied shear vs strain measurements for Stirrup 15 of the 45M_8W test.

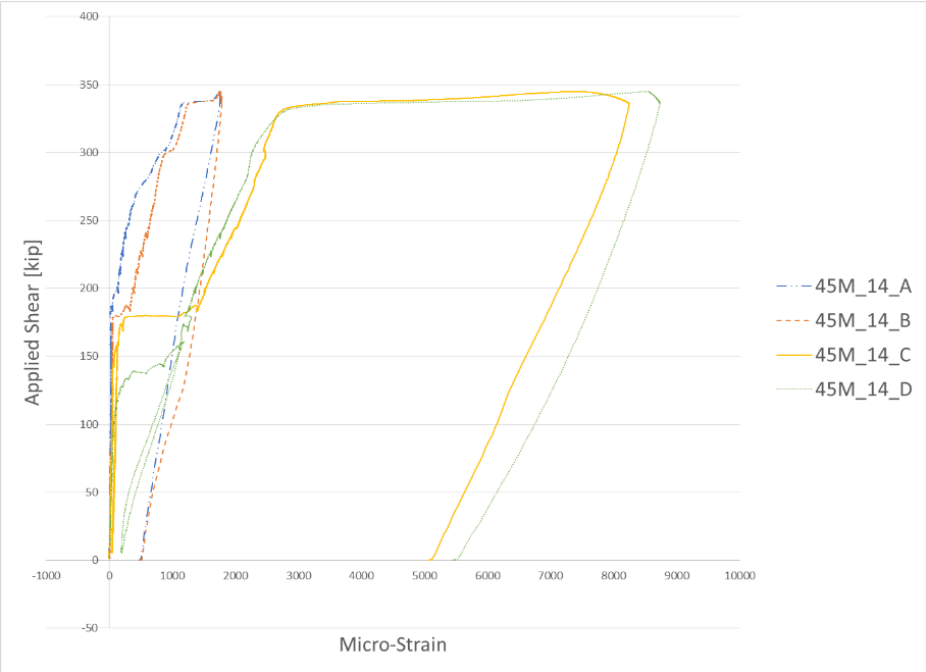

Figure D-40: Applied shear vs strain measurements for Stirrup 14 of the 45M_8W test.

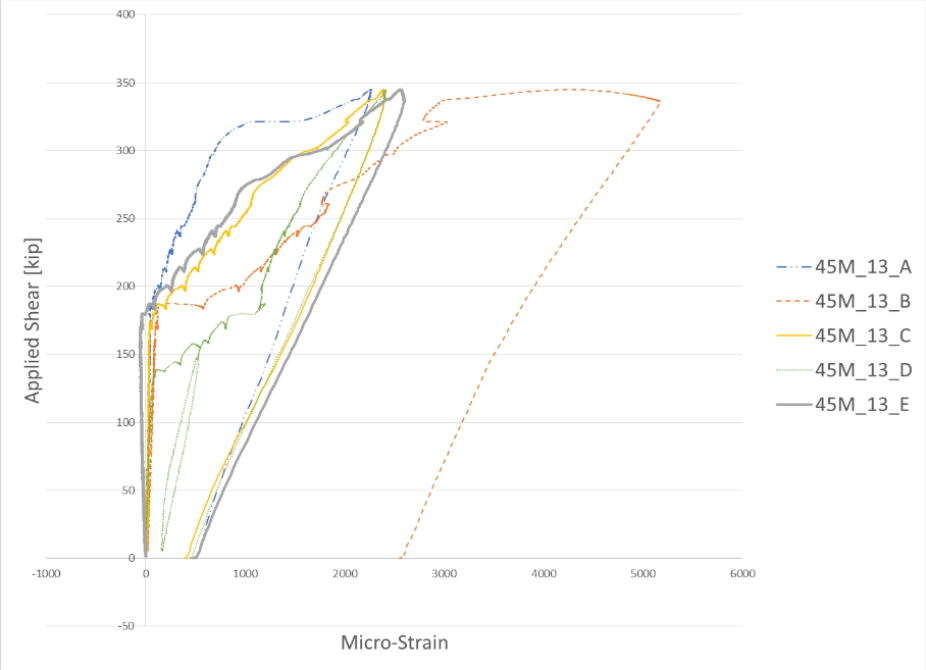

Figure D-41: Applied shear vs strain measurements for Stirrup 13 of the 45M_8W test.

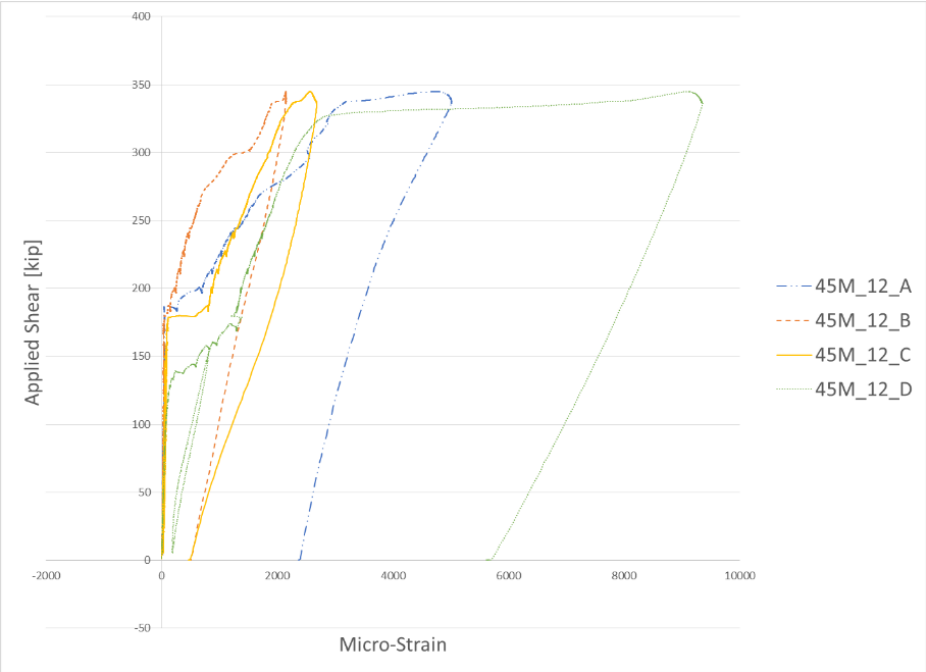

Figure D-42: Applied shear vs strain measurements for Stirrup 12 of the 45M_8W test.

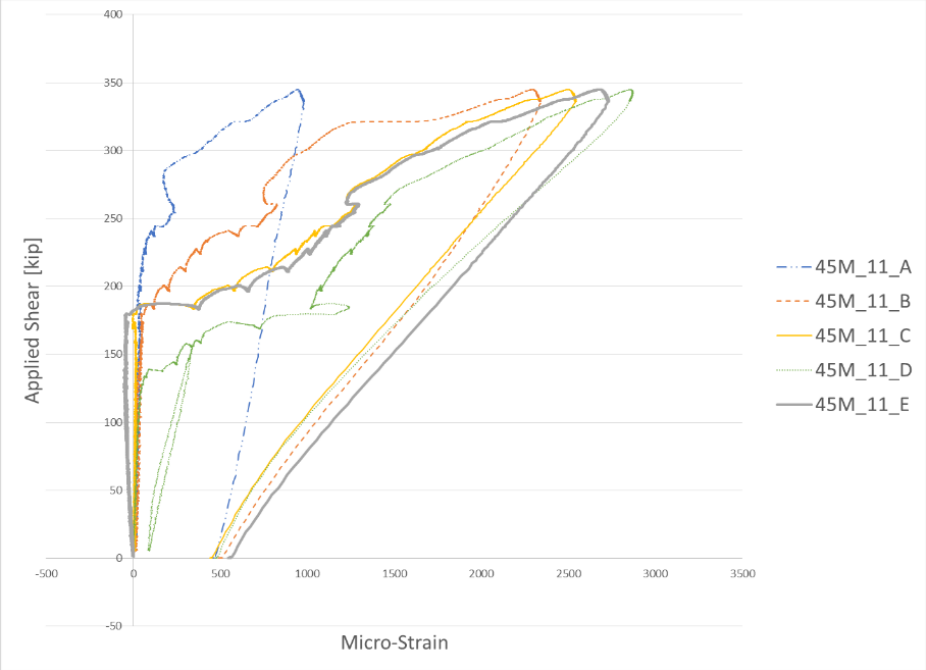

Figure D-43: Applied shear vs strain measurements for Stirrup 11 of the 45M_8W test.

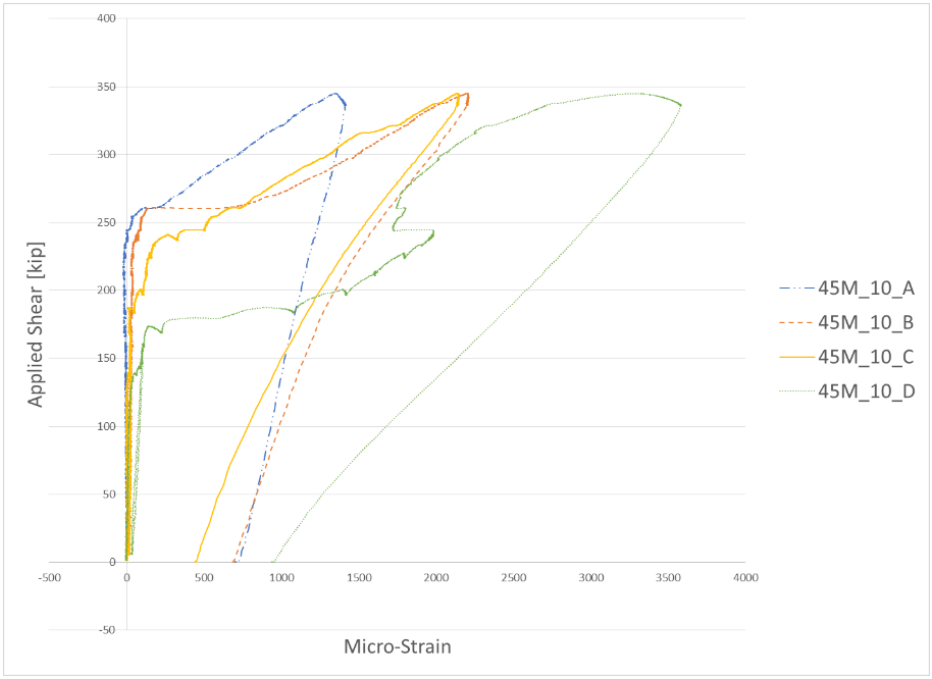

Figure D-44: Applied shear vs strain measurements for Stirrup 10 of the 45M_8W test.

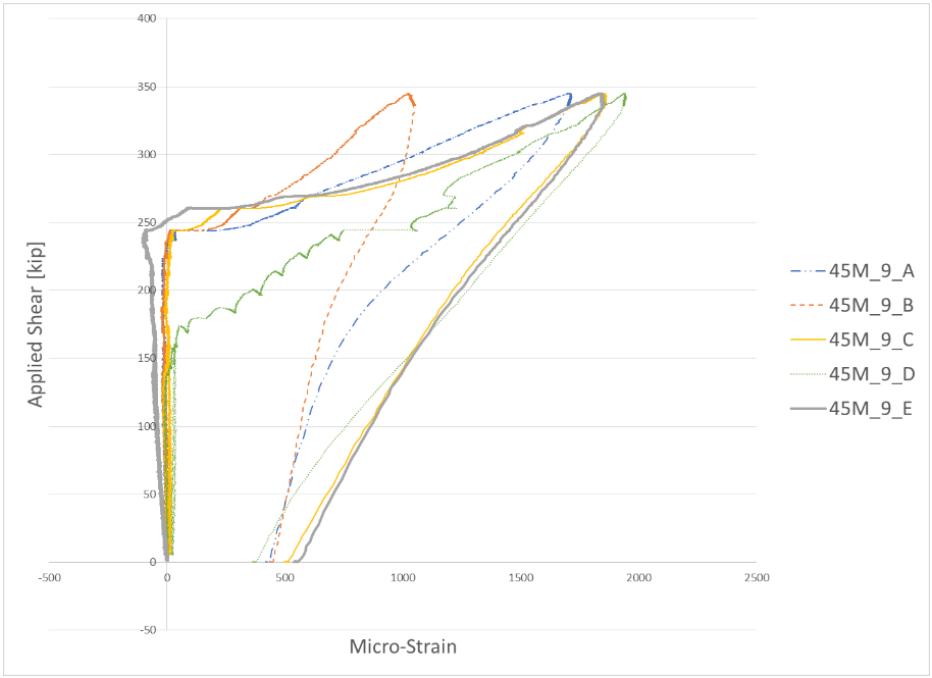

Figure D-45: Applied shear vs strain measurements for Stirrup 9 of the 45M_8W test.

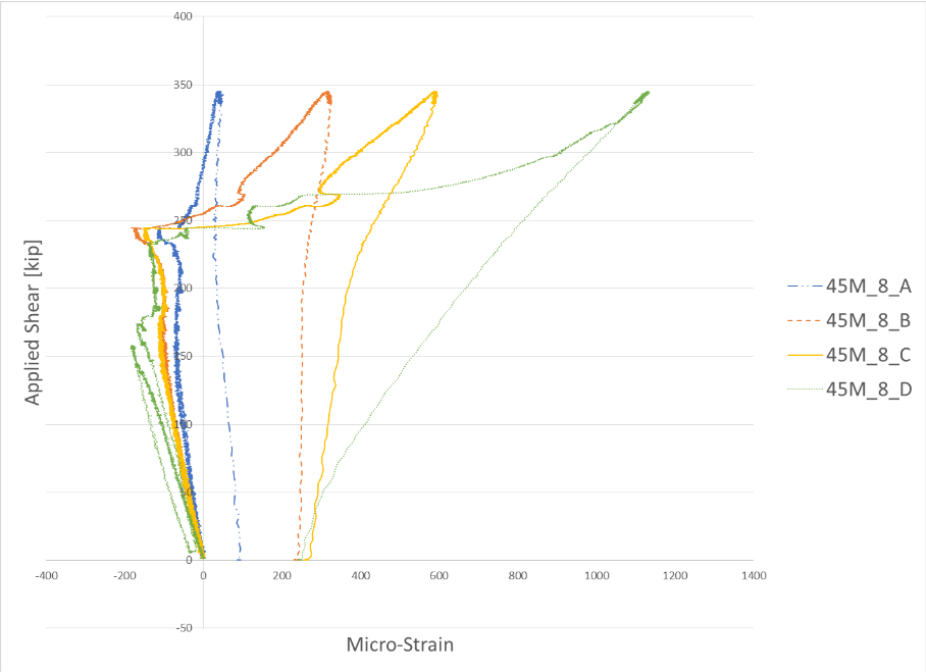

Figure D-46: Applied shear vs strain measurements for Stirrup 8 of the 45M_8W test.

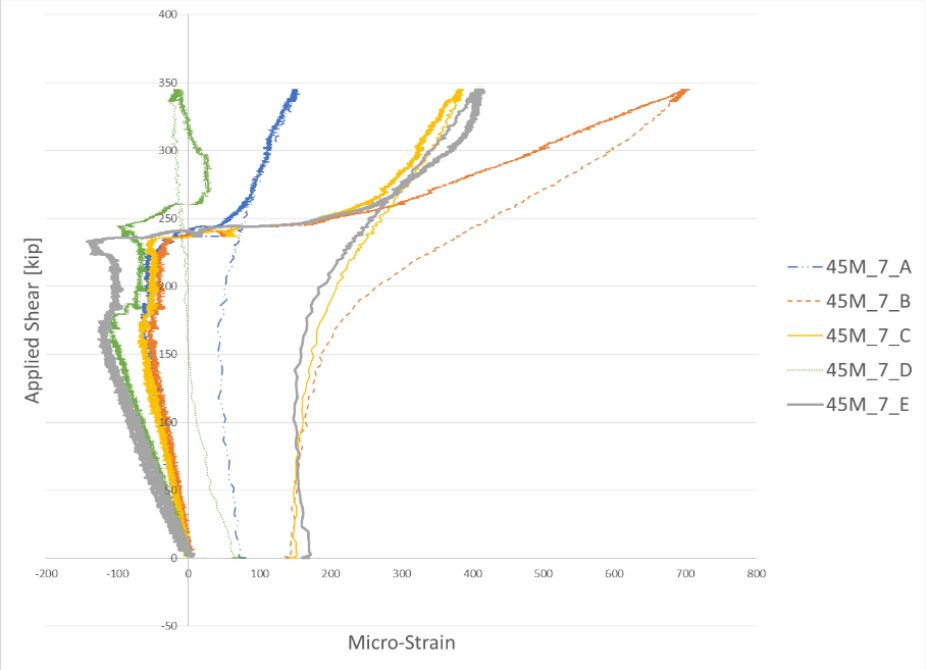

Figure D-47: Applied shear vs strain measurements for Stirrup 7 of the 45M_8W test.

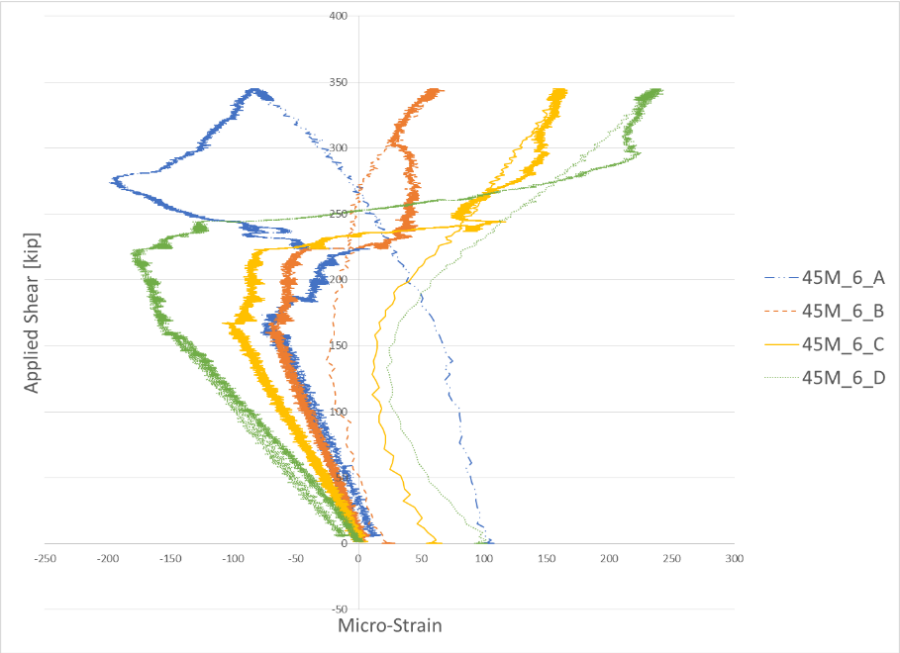

Figure D-48: Applied shear vs strain measurements for Stirrup 6 of the 45M_8W test.

D.4 Plots for 36M_8W Test

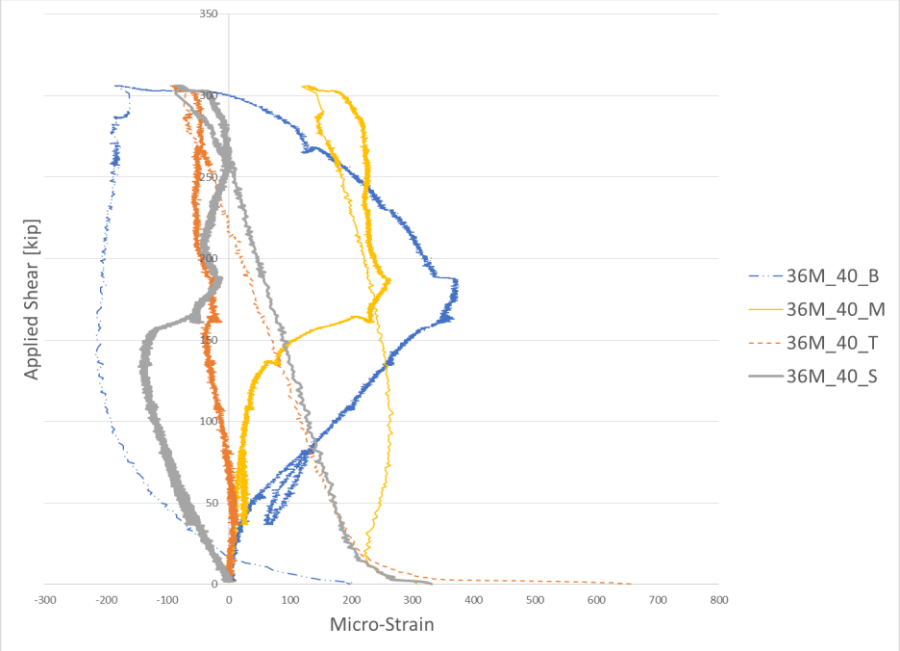

Figure D-49: Applied shear vs strain measurements for Stirrup 40 of the 36M_8W test.

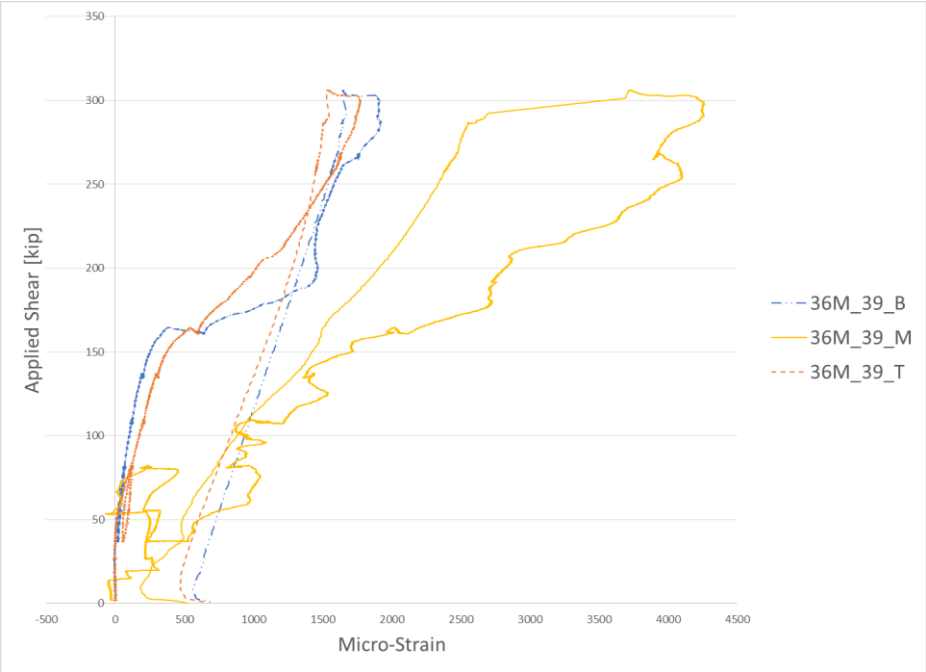

Figure D-50: Applied shear vs strain measurements for Stirrup 39 of the 36M_8W test.

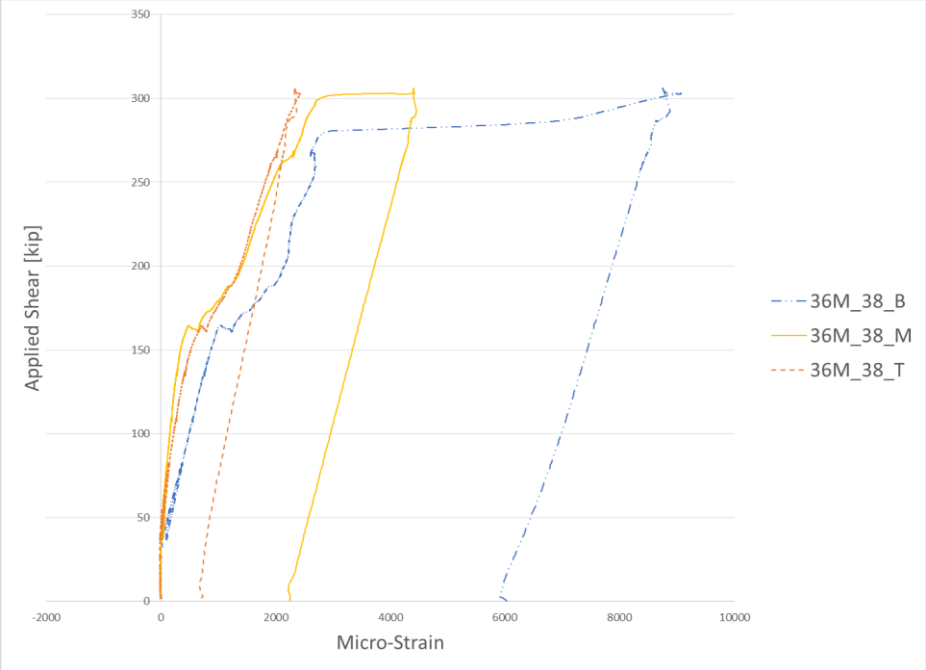

Figure D-51: Applied shear vs strain measurements for Stirrup 38 of the 36M_8W test.

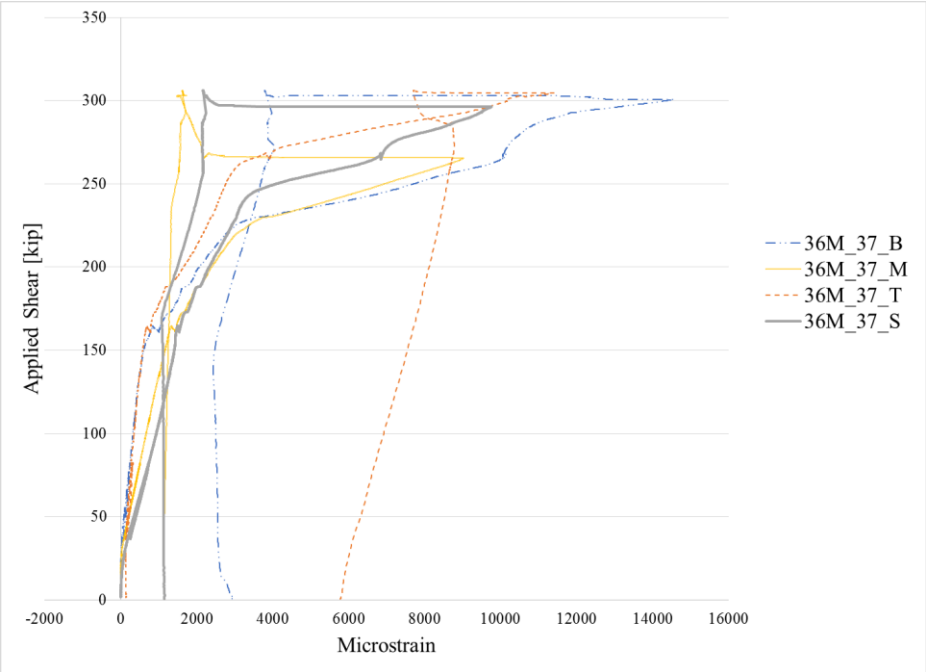

Figure D-52: Applied shear vs strain measurements for Stirrup 37 of the 36M_8W test.

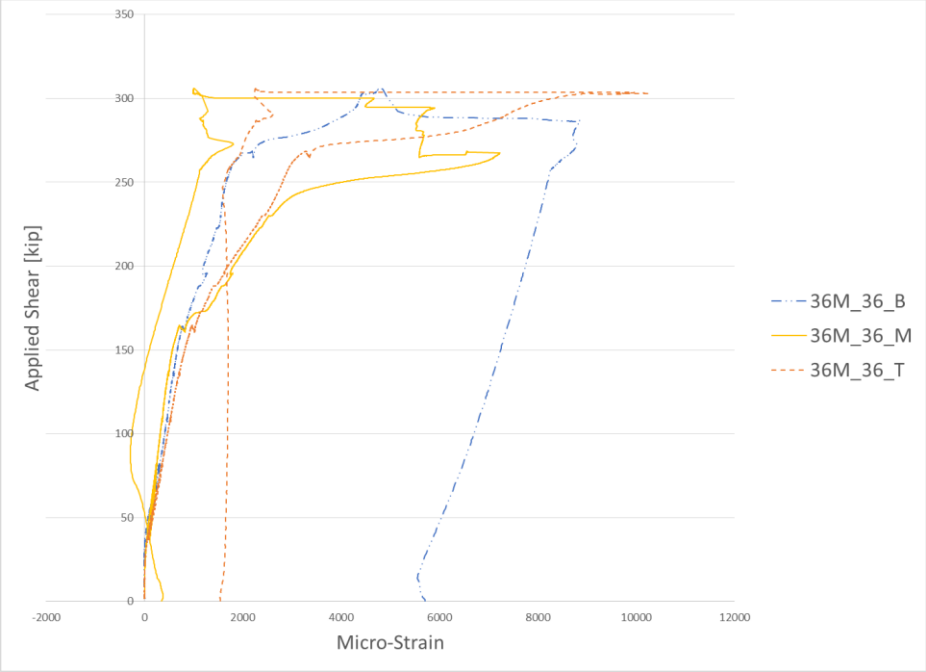

Figure D-53: Applied shear vs strain measurements for Stirrup 36 of the 36M_8W test.

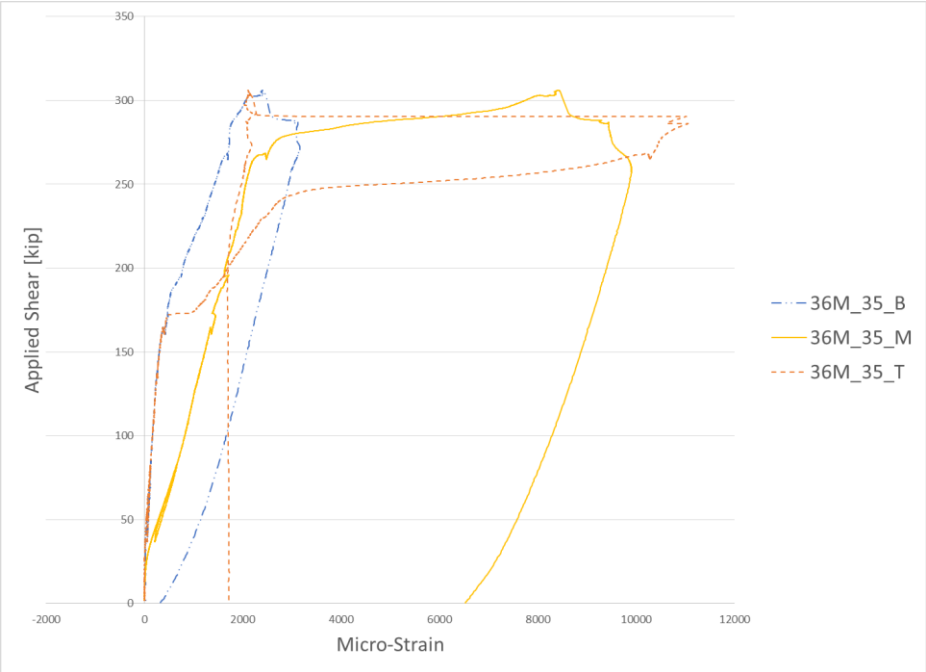

Figure D-54: Applied shear vs strain measurements for Stirrup 35 of the 36M_8W test.

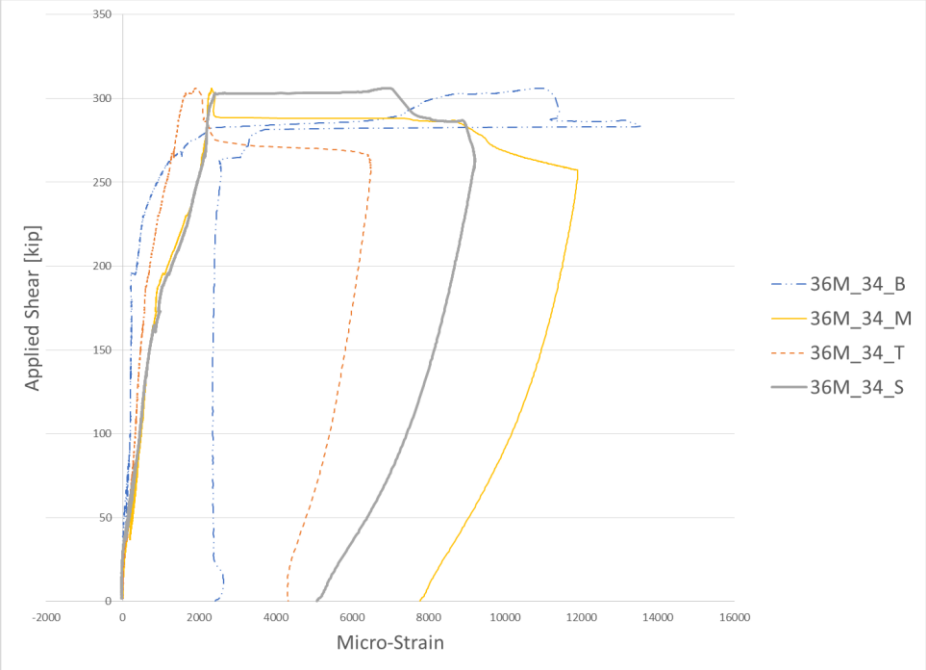

Figure D-55: Applied shear vs strain measurements for Stirrup 34 of the 36M_8W test.

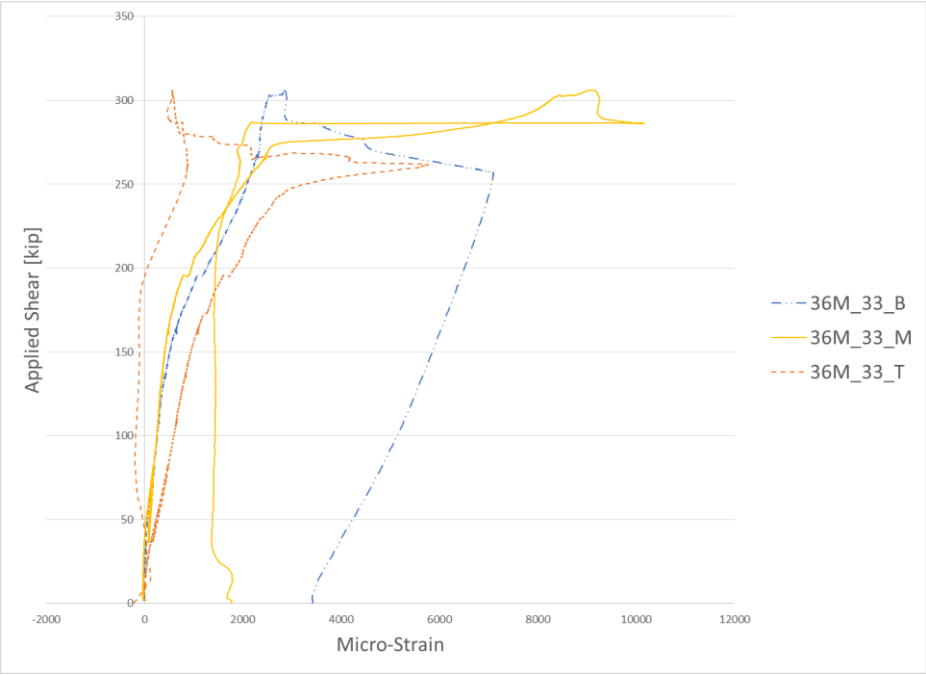

Figure D-56: Applied shear vs strain measurements for Stirrup 33 of the 36M_8W test.

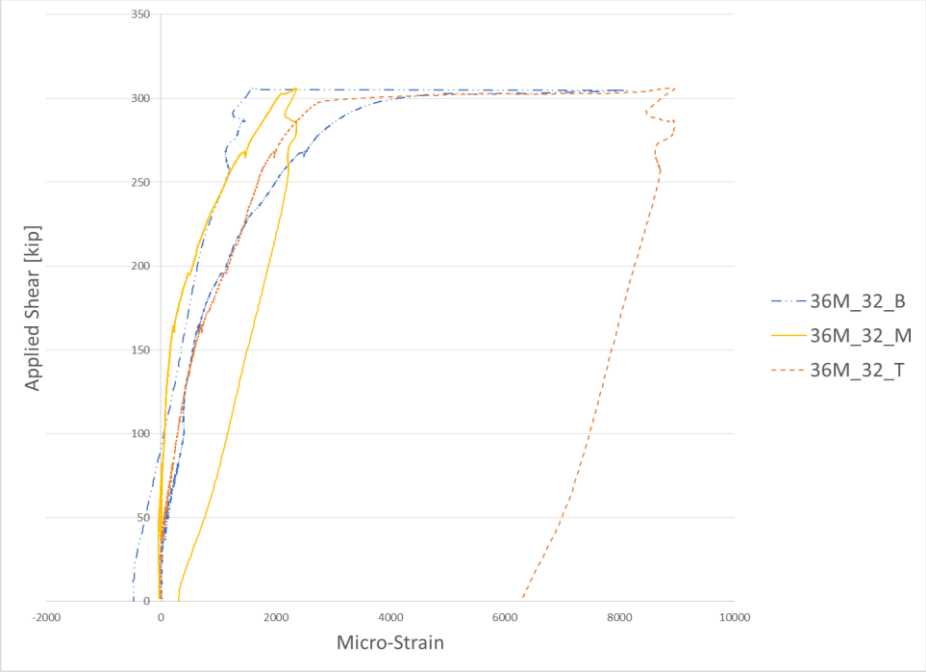

Figure D-57: Applied shear vs strain measurements for Stirrup 32 of the 36M_8W test.

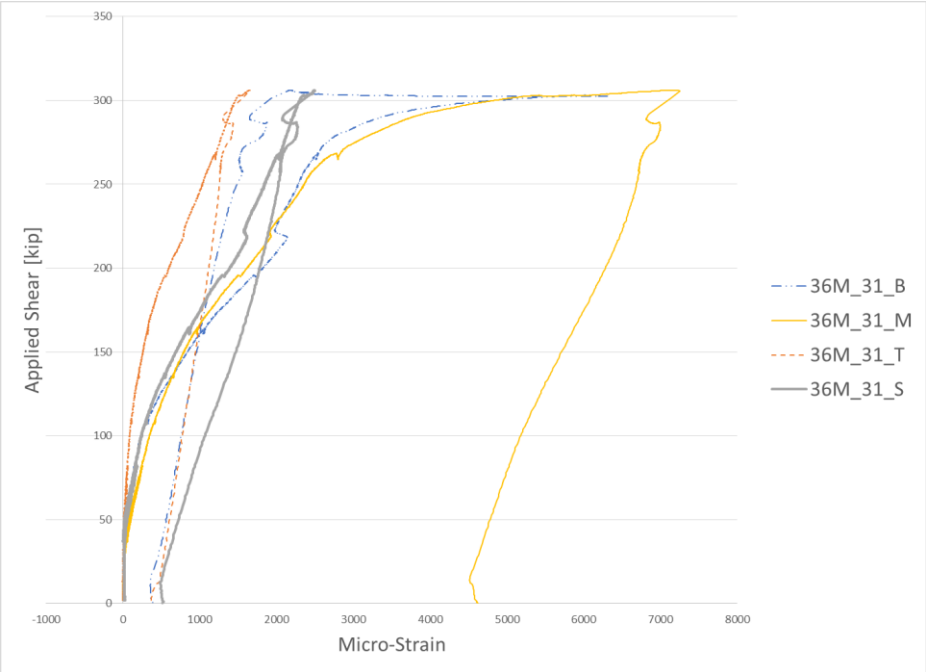

Figure D-58: Applied shear vs strain measurements for Stirrup 31 of the 36M_8W test.

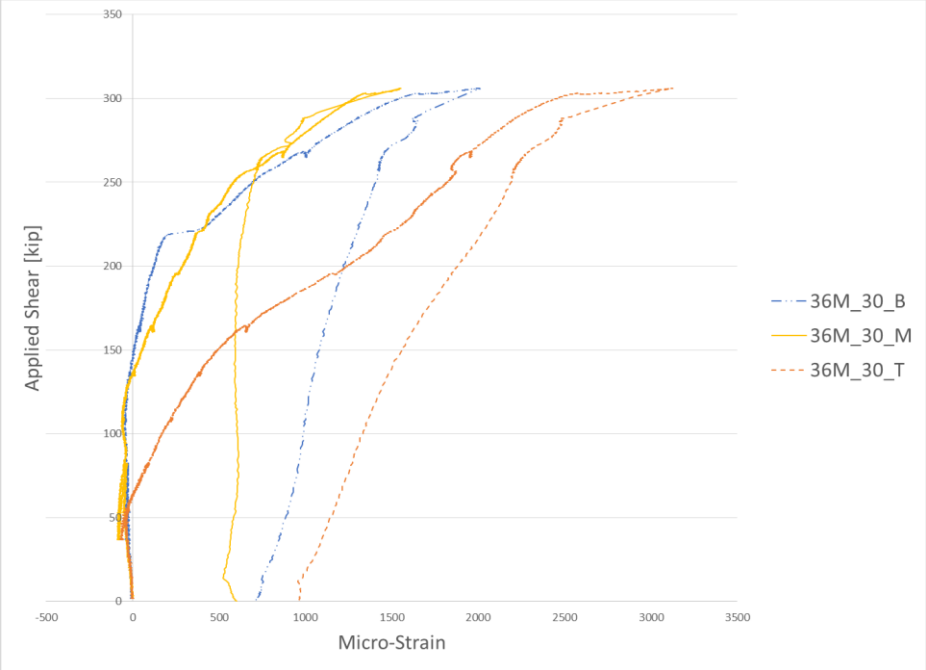

Figure D-59: Applied shear vs strain measurements for Stirrup 30 of the 36M_8W test.

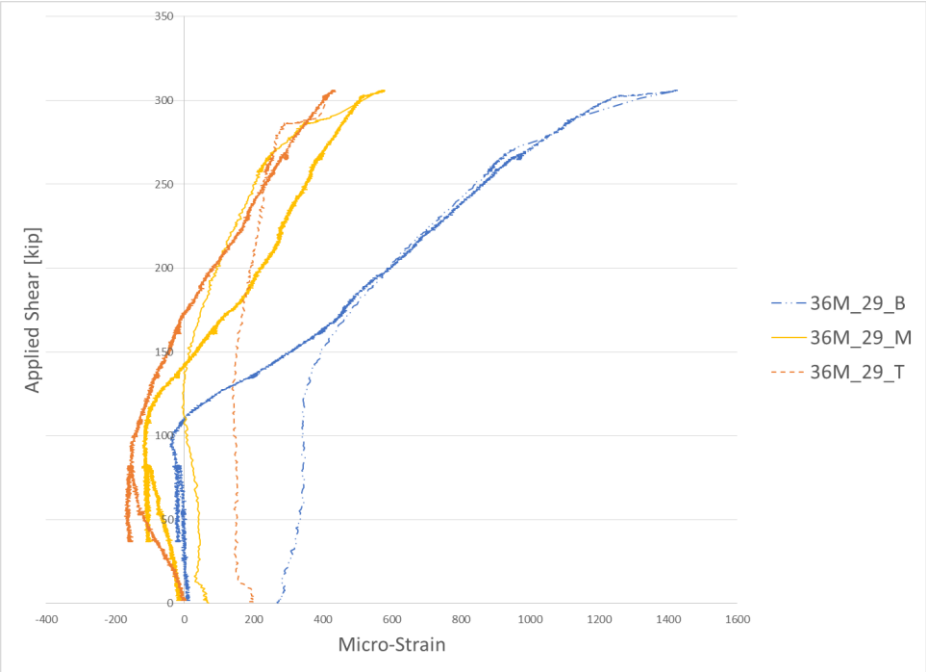

Figure D-60: Applied shear vs strain measurements for Stirrup 29 of the 36M_8W test.

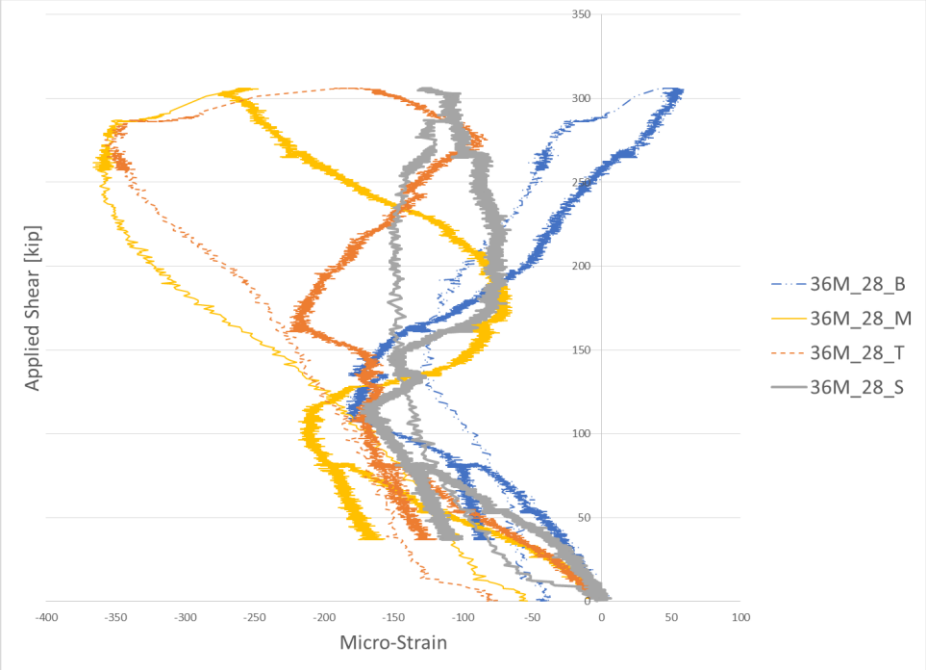

Figure D-61: Applied shear vs strain measurements for Stirrup 28 of the 36M_8W test.